STATIC PILE-SOIL-PILE INTERACTION IN OFFSHORE PILE GROUPS

by

Anjum Rashid Chaudhry

A thesis submitted for the Degree
of Doctor of Philosophy at the
University of Oxford

Brasenose College

Michaelmas Term 1994

ABSTRACT

STATIC PILE-SOIL-PILE INTERACTION IN OFFSHORE PILE GROUPS

A. R. Chaudhry
Brasenose College, University of Oxford

A thesis submitted for the Degree of Doctor of Philosophy

Michaelmas Term 1994

This thesis is a theoretical study, using both finite element and boundary element methods, of the behaviour of single-piles and pile groups under vertical and lateral loading. It offers an improved understanding of the soil-structure interaction that occurs in pile groups, particularly closely spaced piles subjected to lateral loads. The potential of a two-dimensional idealisation of what is a three-dimensional problem is demonstrated by achieving real insight into the complex nature of pile-soil and pile-soil-pile interaction in pile groups.

A new load transfer mechanism is presented for a rigid, axially loaded vertical pile. From this an improvement is then derived to the analytical solution for pile head settlement given by Randolph and Wroth (1978). The improved mechanism has the further merit that it can be applied also to solutions for flexible piles and pile groups.

The improved analytical solution is further adapted in the development of two correcting layers specifically for vertically loaded piles to model infinite boundaries in the finite element model. The correcting layers help in establishing superiority of the finite element method over the boundary element method.

To model pile-soil interaction, a purely cohesive interface element is developed and then validated by performing various two-dimensional test problems, including stability analysis of flat surface footings. Footing-soil interface tension is successfully modelled in this way - an outcome that entails a significant modification to the Hansen (1970) bearing capacity solution. Stability analysis is also carried out of conical footings using a three-dimensional finite element model: the results help to explain the applicability of the existing bearing capacity theories to conical footings.

The ultimate lateral soil reaction is determined and various pile loading stages are investigated through parametric studies. Study of the stage immediately following pile installation (i.e. the

consolidation stage) highlights the need to develop an effective stress analysis for laterally loaded piles. Pile-soil interaction is studied using the cohesive interface element presented earlier, which proves to be quite successful in smoothing out the stress discontinuities around the pile.

A new material model for frictional soils is presented, and validated by using it to model an extension test: it captures well post-peak behaviour and takes care of the effects of dilation on the response of laterally loaded piles.

Finally, mechanisms of interaction in closely spaced pile groups are studied. Simple analytical expressions are derived which quantify the effects of interaction. A new method of analysis is presented for single-piles and pile groups which offers a considerable degree of reliability without having to do either impossibly expensive full scale field tests or prohibitively expensive full three-dimensional analysis using the currently available computers.

References

Hansen, J.B. (1970)
"*A revised and extended formula for bearing capacity*",
Danish Geotechnical Institute, Copenhagen, Bull. No. 28: pp 38-46

Randolph, M.F. and Wroth, C.P. (1978)
"*Analysis of deformation of vertically loaded piles*",
Proc. ASCE, Journal of the Geotechnical Engineering Division, 104 (GT12): pp 1465-1488

ACKNOWLEDGEMENTS

Many thanks and praise are due first of all and above all to my Creator who made this thesis possible despite all the hurdles and constraints in the way of its completion: `If Allah helps you, none can overcome you' (Qura'n, 3.160).

I acknowledge with gratitude the support I have received as an ICI-scholar: my thanks to ICI (UK), the Foreign and Commonwealth Office and Oxford University, who jointly administered this award. I am grateful also to the High Commission for Pakistan in London for making a grant from the Dr Wali Mohammad Trust; to the Mott MacDonald Group (Consulting Engineers) for their travel grant; to the Sir Ernest Trust (Mountbatten Memorial Grant), the Sir Richard Stapley Educational Trust; and to the Professional Classes Aid Council for their very valuable (and much needed) financial assistance during the final year of my studies.

Sincere thanks go to the late Professor C.P. Wroth for his encouragement and advice in the early stages of this research: the privilege of studying under him will always remain a memorable part of my education.

I am grateful to Professor G.T. Houlsby for his assistance and inspiration to complete this work. I acknowledge especially his allowing me to use the following: OXMESH - finite element mesh generation and 2CAN - data contouring programs.

Special thanks to my supervisors, Dr H.J. Burd and Dr M.S. Williams, for their constant help, and patience throughout my study years at Oxford, especially while I got used to a new country and a new language. I am indebted to Dr H.J. Burd for allowing me to use his finite element program OXFEM and arranging for me to use the commercial finite element package ABAQUS. I would also like to thank him for his financial help through paid work for "Edmund Hambly Limited".

My moral tutor Dr R.W. Daniel and Dr G.C. Sills helped me with consistently positive, constructive criticism of my work: my warmest thanks.

Because it is not possible to mention everyone individually, may I express a `global' appreciation to all members of the Civil Engineering Group for providing a lively environment to work in, and for moral support when needed.

Last but not least, I should like to thank Dr Z.J. Qureshi, Dr A.L. Bello and Mr M. Appabai: none of them are engineers; their help was as friends who made themselves available whenever needed. I cannot express my appreciation better than in the Arabic of *jazākum Allāhu khairan*, being certain they will understand perfectly.

CONTENTS

NOMENCLATURE

Additional symbols and occasional alternative usage of the symbols below are defined where they occur in the text.

A	Cross-sectional area of the pile
A_c	Circumferential area of a pile element
A_p	Plan contact area of a partially penetrated spudcan
$[B]$	Matrix relating nodal velocities
B	Footing width
B'	Effective footing width
B_p	Penetrated diameter of a spudcan
C_L	Centre line
c	Cohesion at the interface
d	Pile diameter
D_p	Penetration depth of a spudcan
$[D]$	Material stiffness matrix
$[D]^E$	Elastic material stiffness matrix
$[D]^P$	Plastic material stiffness matrix
$[D]^{EP}$	Elasto-plastic material stiffness matrix
EI	Bending stiffness
E_p/E_s	Flexibility ratio

e	Void ratio
$[f^s]$	Soil flexibility matrix
$f(\underset{\sim}{\sigma})$	Yield function
G	Shear modulus
H	Horizontal/lateral load
H_p	Peak lateral resistance
$g(\underset{\sim}{\sigma})$	Plastic potential
I_D	Relative density
I_1, I_2, I_3	Stress invariants
I_r	Rigidity index
I_R	Relative dilatancy index
$[J]$	Jacobian matrix
K	Bulk modulus
$[K]$	Stiffness matrix
K_p	Coefficient of passive earth pressure
k	Coefficient of subgrade reaction
K_o	Coefficient earth pressure at rest
k_s	Interface element shear stiffness
k_n	Interface element normal stiffness
l	Length of the pile
l_c	Critical length
l_e	Length of a pile element
l_i	Length of an interface element

M	Bending moment
$[N]$	Shape function matrix
N_c	Bearing capacity factor due to cohesion
N_γ	Bearing capacity factor due to self-weight
P_{ult}	Ultimate bearing capacity of a plane strain footing
P_z	Axial load at depth z
$\underset{\sim}{P}$	Vector of applied loads
p	Volumetric stress
p_u	Ultimate lateral soil resistance
q	Deviatoric stress
R	External radius
r_m	Magical radius
r_o	Pile radius
s_u	Undrained shear strength of clay
s	Centre-to-centre pile spacing
t	Load transfer
u	Pile head deflection
$\underset{\sim}{U}$	Vector of nodal velocities
u_r	Relative tangential velocity
v_r	Relative normal velocity
V	Vertical load
V_M	Ultimate vertical load capacity of the spudcan
w	Pile head settlement

$\underset{\sim}{X}$	Vector of global nodal co-ordinates
y	Lateral deflection
z	Depth below ground surface
α	Isoparametric reference co-ordinate
α_{kj}	Interaction Factor between piles k,j
β	Angle of applied loading
ε_1, ε_2, ε_3	Principal strains
ε_v	Volumetric strain
$\acute{\gamma}$	Soil effective unit weight
Γ	Specific volume at a reference pressure p_a
λ	Slope of the Critical State Line
$\bar{\delta}$	Displacement of a single isolated pile under unit horizontal load
δ_k	Lateral displacement of pile k
η	Depth factor
θ	Load spread angle through the soil under the pile base
ϕ_{cv}	Critical state friction angle
ϕ_{mc}	Mohr-Coulomb friction angle
ϕ_p	The angle of peak friction
ϕ_{tc}	Triaxial compression friction angle
ψ	Dilation angle
ψ_{max}	The angle of maximum dilation
ψ_{tc}	Triaxial compression dilation angle
ν	Poisson's ratio

Ω	Cone angle
σ, τ	Normal stress, Shear stress
σ_1, σ_2, σ_3	Principal stresses

CHAPTER 1

INTRODUCTION

1.1 Introduction

For just over three decades now, with rapidly advancing technology and ever-increasing energy demands, oil and gas exploration and extraction activity have been moving from shallow water to deep offshore waters. Most of the offshore oil extraction platforms are pile-supported steel structures known as 'template' or 'jacket' structures. These consist of a space frame with legs through which the piles are driven into the sea-bed. Once driven to the required depth, the piles are cut off at the head of the template and a prefabricated deck section is placed on the piles at an elevation above the crests of anticipated storm waves. For deep water applications, the template or jacket structure is modified. In the modified form, called a 'tower structure', the deck rests on four large-diameter columns, each in turn supported by several closely spaced piles in a circular group. Such pile groups or deep foundations are subject to severe environmental loads (wind, wave action and current loading) in addition to gravity loads from the weight of the structure acting vertically.

Other offshore structures include concrete gravity platforms and mobile jackup rigs. Gravity structures have flat circular bases directly resting on the seabed. These structures achieve stability through their own weight. Mobile jackup rigs have either flat circular footings or conical shaped with a protruding tip at the centre (commonly known as spudcan footings). These footings are referred to as shallow foundations.

Environmental loads act laterally and produce horizontal and moment loads. A significant

proportion of these loads is cyclic in nature (see Figure 1.1). The pile-soil interaction in deep foundations and footing-soil interaction in shallow foundations, arising due to cyclic loads is an intricate phenomenon and is beyond the scope of this thesis. We will be dealing with static loads only.

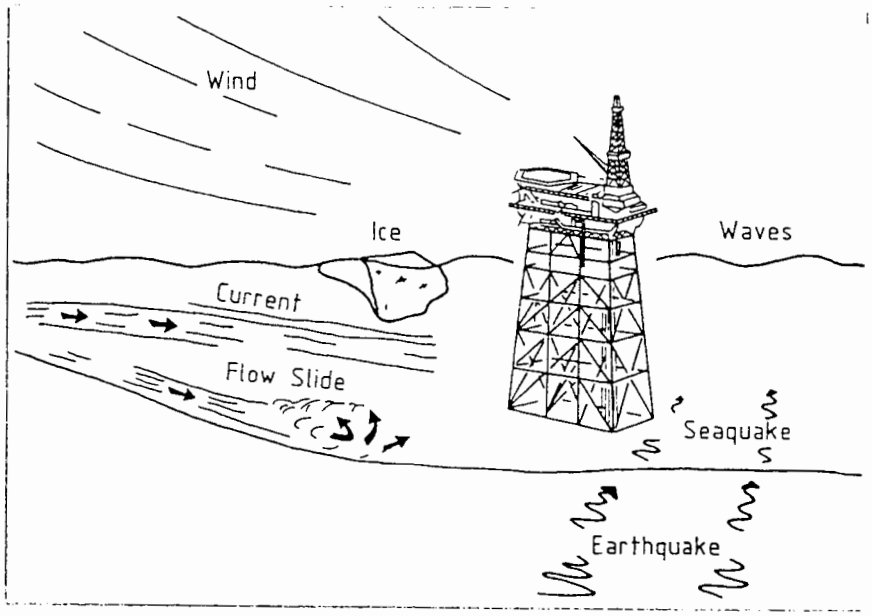

Figure 1.1: Environmental loads on a template platform (after Selnes (1982))

1.2 Description of the problem

Generally, onshore pile groups are subjected to vertical loads but often there are situations, when a significant lateral load is also experienced by these pile groups e.g. bridge abutment piles located adjacent to surcharge loads on alluvial soils (Springman (1984),(1989)). The magnitude of vertical and lateral loads carried by onshore pile groups is substantially lower compared to that supported by offshore pile groups. It is essential therefore to calculate the lateral response of piles, as well as their axial response, in order to design for the stability and safety of the overall structure. Similarly, the behaviour of shallow foundations under storm

loading conditions is also critical for the safety of a platform/rig. In this thesis, the axial and lateral behaviour of closely spaced pile groups, and the behaviour of flat and spudcan footings under combined (horizontal, vertical and moment loading) is discussed both in soft clays and in sands. An undrained material behaviour or the 'total stress approach' is adopted for clays, and the fully drained material behaviour or the 'effective stress approach' is considered for sands.

The behaviour of a pile in a group is affected by the spacing between the neighbouring piles. If the piles are wide apart (in the case of onshore pile groups), the displacement of a pile may have an insignificant influence of the movement of another pile in its neighbourhood. On the contrary, if the piles are closely spaced (as in the case of offshore pile groups), neighbouring piles interact with each other through the soil medium. In this situation, interactive effects will cause an increase in displacement of a pile in such a group. Before studying the behaviour of a pile affected by interaction, we shall study what happens to the soil when a single isolated pile is loaded vertically or displaced laterally.

The resistance to deflection which a laterally loaded single-pile develops is a non-linear function of the relative displacement between it and the soil. There is an increase in lateral stresses in the soil near the pile which decay rapidly in magnitude with radial distance. There is an annular region or a zone of high stresses close to the pile in which the soil gets yielded. For closely spaced piles within groups, these yielded zones of the soil around individual piles overlap, forming larger yielded zones in the soil surrounding the pile group (see Figure 1.2). The interaction arising due to overlapping of these yielded zones results in a larger deflection for the group before a level of lateral resistance is reached equivalent to that for a single-pile.

In order to develop a method for the analysis of pile groups, it is first necessary to obtain estimates of the reduction in lateral resistance of the soil which result from the overlapping of the yielded zones in the soil around the group. Once a reasonable estimate is obtained, then

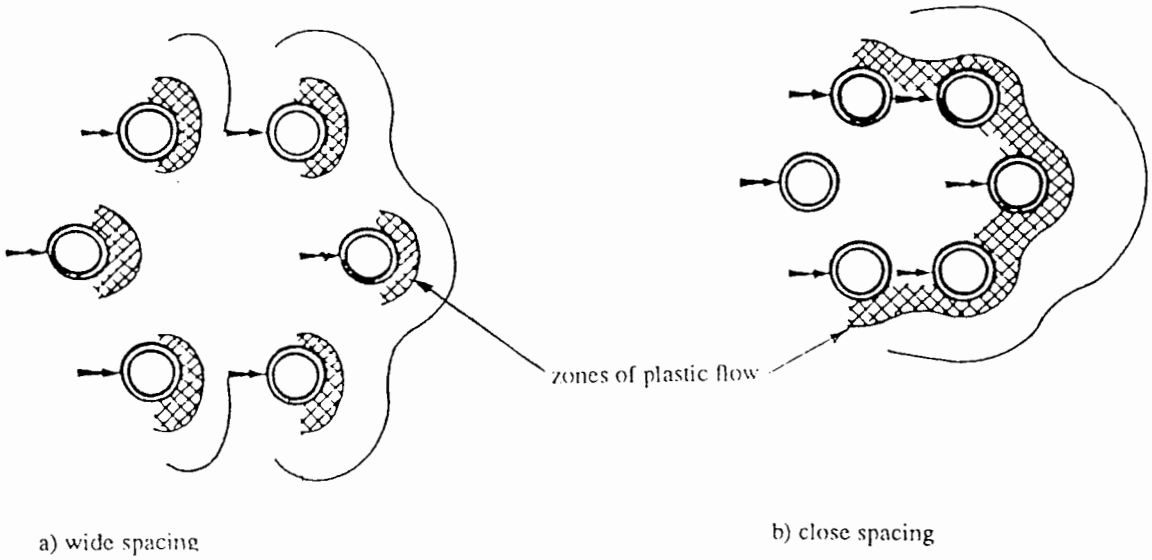

Figure 1.2: Schematic illustration of pile group under lateral loading (after Bogard and Matlock (1983))

the analysis of pile groups can be performed using the conventional methods of analysis developed for single-piles, provided the structural restraints are identical for each pile in the group, i.e. all piles in the group respond equally to the applied load.

1.3 Objective of this study

The phenomenon of overlapping yielded zones (see Figure 1.2 (b)) in offshore pile groups is very complex. It is difficult to model it accurately unless we have a suitable soil model capable of representing real non-linear soil behaviour. The objective of this study is to explore the most appropriate method of analysis equipped with a suitable, simple and realistic soil model, i.e. one able to predict the response of a pile group in a way that mimics actual response in the field. The larger goal is to develop a method of predicting lateral response which is reliable enough to be applied in the design of routine pile foundations. In the case of shallow foundations, the objective is to examine how the soil-structure interaction affects

the stability of these foundations.

1.4 Structure of the study

Previous research related to this problem has been based on various analysis procedures and techniques which, for one reason or another, are unsatisfactory. A critical review of the methods currently in practice with reference to the relevant literature is presented in Chapter 2.

Chapter 3 discusses analytical methods and compares two numerical methods, namely the integral equation method and the finite element method for investigating the response of a single vertical pile under axial loading. The problem is deliberately chosen to show how its axial symmetry can be exploited by simplifying it to two dimensions. The discussion also shows that, in the design of an offshore pile foundation, the precise determination of axial capacity and response is as important as the lateral load capacity and lateral response, and that both need to be considered together.

The comparison of the numerical methods clearly demonstrates the superiority of the finite element method over the integral equation/ quasi boundary element method for problems that can be idealised into two-dimensional problems and when elasto-plastic soil behaviour is an important consideration. The preferability of the finite element method is reinforced by presenting a computationally economical approach for carrying out the finite element calculations. The finite element method is therefore adopted in all the subsequent chapters.

Chapters 4, 5, 6 and 7 are devoted to study of the lateral loading of single-piles and pile groups.

Chapter 4 is concerned with the modelling of incompatibility in the displacements which occur at the pile-soil interface where two different materials meet at the common boundary. For this purpose, a purely cohesive interface element is developed. Its ability to model the interface behaviour is demonstrated by using it in two two-dimensional test problems. One of these problems is concerned with the calculation of the ultimate bearing capacity and stability analysis of a flat surface footing.

It is important to understand the problem of a single-pile under lateral loading before moving on to the more complex problem of a pile group. Therefore, Chapter 5 provides this necessary preliminary investigation before the study of pile group behaviour in Chapter 6. It demonstrates that a two-dimensional idealisation for laterally loaded piles is quite appropriate to study their behaviour. Each of the three soil loading stages, namely pile installation, subsequent consolidation of soil around the pile, and the application of foundation loads, is studied. The lateral capacity of a single-pile is found to be enhanced by almost 35% due to consolidation of soil around the pile. It seems appropriate to consider the effect of consolidation in the analysis of laterally loaded piles as previously suggested by Burland (1973) for axially loaded vertical piles. Finally, the interface element is shown to be quite successful in smoothing out the stress discontinuities around the pile and to be quite effective, therefore, in modelling the pile-soil interaction.

Chapter 6 considers the behaviour of pile groups subjected to lateral loading and, in the absence of a complete three-dimensional finite element analysis, presents a new approach for the analysis of laterally loaded pile groups. It combines a two-dimensional finite element

analysis with a standard *p-y* curve analysis for predicting the pile head response.

Following the study of pile-soil interaction in cohesive soils presented in Chapter 5, a new material model to represent the constitutive behaviour of frictional soils is presented in Chapter 7. The validity of the model is tested by predicting the results of an extension test. It captures the post-peak behaviour successfully and models variation of dilation as the analysis proceeds. In this way, effects of dilation on the ultimate response of laterally loaded piles are duly taken into account.

Following the brief discussion, in Chapter 4, of the ultimate bearing capacity of a flat footing, Chapter 8 considers the ultimate bearing capacity of the conical or spudcan footing now widely in use in offshore situations. The importance of being able to predict the load such footings can support, and the need (in the context of this thesis) to see how three-dimensional finite element analysis can be applied to carry out the required calculations, are both self-evident.

Chapter 9 presents an overview and an assessment of the arguments and discussions in the preceding chapters. Conclusions are drawn and immediate relevant further research is proposed.

CHAPTER 2

ANALYTICAL AND NUMERICAL METHODS: A REVIEW OF THE RELEVANT LITERATURE

In this chapter, a review of the existing analytical and numerical methods for the prediction of both axial and lateral response of single-piles and pile groups is presented. The discussion first covers analytical methods (Section 2.1), then numerical methods for linear elastic models of soil behaviour (Section 2.2), and, finally, numerical methods for non-linear elastic (Section 2.3) and elasto-plastic constitutive soil behaviour (Sections 2.4 and 2.5).

2.1 Analytical methods

Vertical loads

The problem of vertical displacement (settlement) of a single-pile under axial loading is statically indeterminate: no exact analytical solution is available as the actual stress distribution along the pile is unknown. However, Randolph and Wroth (1978) produced an approximate analytical solution for a rigid pile by considering separately the load sustained by the pile shaft and the load sustained by the pile base. They assumed a uniform shear stress distribution along the pile shaft, and the normal stresses beneath the pile base as those of arising from a rigid punch at the surface of an elastic half space. In the case of a rigid pile, the pile head load-settlement ratio is determined by a simple analytical expression without it being necessary to evaluate the exact distribution of shear stress along the pile. The analytical

expression involves an empirically determined parameter 'r_m' - the radial distance at which the vertical displacements are zero. (This parameter will be discussed in detail in Chapter 3 and a new analysis proposed which is thought to be an improvement on the Randolph and Wroth solution.)

In the same paper, Randolph and Wroth also produced modified solutions to take account of pile compressibility and radial and vertical inhomogeneity of the soil. In these solutions, a careful choice of the values of soil shear moduli is very important to get sensible results. In another paper, Randolph and Wroth (1979a) applied their analytical approach in the analysis of two-pile groups and presented simple expressions for the elastic interaction between the piles. The interaction is quantified as interaction factors. These interaction factors, which depend on the spacing between the piles, were then used in the analysis of groups of piles symmetrically placed around a pitch circle, where each pile responded identically. They also suggested modifications in the analysis of pile groups when piles are not subjected to the same load, for example under a rigid pile cap. (The computer program PIGLET developed by Randolph (1980), one frequently used by practising engineers, is based on the approximate analytical solution for single-piles and the simple expressions for interaction between piles. The soil is modelled as an elastic material with a linear variation of stiffness with depth. Piles may be raked in any direction, and effect of not only axial but also lateral and torsional loading can be analysed.) The solutions given by Randolph and Wroth (1978, 1979a) are excellent for idealised linear-elastic soil behaviour (i.e. it does not consider soil non-linearity, soil yielding and soil plasticity); it works very well for most practical situations where piles are installed at spacings wide enough for the interactions among the piles to remain in an elastic regime and the principle of superposition to remain valid. However, in the case of closely spaced piles, especially in an offshore environment, this principle is not applicable.

Lateral loads

In the case of lateral loading of piles, the problem is not as simple as for vertical loading in

that no simple analysis has yet proved possible. The horizontal pressure distribution along the pile is unknown as the behaviour of a pile is flexible under lateral loading. (In the case of a vertically loaded pile, it is the shear stress distribution which is unknown.) However, for purely cohesive materials, a simplified distribution of soil pressure was suggested by Broms (1964a) for short, intermediate and long piles. According to Broms, the soil pressure is zero from ground surface to a depth of 1.5d and, below this depth, a constant $9S_u$ regardless of the shape of the pile and the nature of the pile-soil interface. Where S_u is the undrained shear strength of the soil. The value of $9S_u$ was largely empirical and no theoretical justification was attempted. Broms (1964a) also pointed out that the ultimate lateral soil pressure which develops along a laterally loaded pile in a cohesive soil can be calculated by means of the theory of plasticity below a depth of approximately 3d, assuming that plane strain conditions hold, that the soil is weightless, and that failure of soil takes place along plane or spiral slip surfaces.

Reese (1975) presented two simple expressions for the determination of the ultimate lateral soil pressure $p_{us}{}^c$ at any depth z below the surface:

$$p_{us}{}^c = p_u/d = \left(3 + \frac{\gamma z}{S_u} + \frac{0.5z}{d}\right) S_u \qquad \text{for shallow depths}$$

and

$$p_{us}{}^c = 9S_u \qquad \text{for greater depths}$$

where

p_u = the ultimate lateral soil resistance,

d = diameter of the pile and γ = soil unit weight (bulk).

The expressions given above seems to suggest that the ultimate lateral soil resistance, p_u, in a purely cohesive soil increases from a value of $3S_u d$ at the ground surface to $9S_u d$ down to

a depth of about 3d and remains constant for greater depths.

Later, Randolph and Houlsby (1984) showed that the ultimate lateral soil resistance is very much dependent upon the pile-soil interface. Using the method of characteristics, they produced exact analytical solutions for the ultimate lateral soil resistance which develops in front of a laterally loaded rigid circular disc - $11.94S_u d$ for a completely rough pile-soil interface, and $9.14S_u d$ for a smooth interface.

Similarly, for sands, Broms (1964b) suggested a triangular distribution of passive pressure along the front of a laterally loaded pile ignoring the active pressure at the back of the pile. The passive pressure being equal to 3 times the Rankine passive pressure:

$$p_{us}^{\phi} = 3\gamma' z K_p$$

where

γ' = effective soil unit weight

$K_p = (1+\sin\phi')/(1-\sin\phi')$

ϕ' = angle of internal friction (effective stress)

For the more general case, Hansen (1961a) suggested the following simplified expression for the determination of the ultimate lateral soil pressure $p_{us}^{c-\phi}$ at any depth z below the surface:

$$p_{us}^{c-\phi} = \gamma z K_q + S_u K_c$$

where

K_c, K_q = factors that are functions of ϕ and $\frac{z}{d}$

ϕ = friction angle

For a purely cohesive soil, the factor K_q is zero and the overburden pressure has no effect

on p_u.

For any assumed pressure distribution, such as a uniform or a linear variation, the combination of the ultimate horizontal load and moment to cause failure of a relatively slender short floating pile with negligible base resistance, can be calculated using a simple statical approach given by Poulos and Davis (1980). For a general distribution of soil pressure, a trial and error procedure is recommended by Hansen (1961a). The analysis procedure was extended by Poulos (1976) for the case of a pile near a slope. This type of analysis neither provides any information about the ultimate lateral pile head displacements at failure nor can be applied to pile groups.

A pile can also be analysed as a transversely loaded beam carrying some axial load with different end restraints. The surrounding soil is treated as a series of elastic springs attached to the pile at a number of discrete points which divide the pile into a series of inter-connected beam-column elements. This soil representation is after Winkler (1867) (see Scott (1981)) and the analogy derives from the analysis of a beam on an elastic foundation carried out by Hetenyi (1946), who produced closed form solutions for various loading conditions and end restraints. The stiffness of the soil springs is referred to as the coefficient of subgrade reaction k of the soil. It is computed by assuming it to be equal to that of a strip footing founded on the surface of a semi-infinite, ideal elastic medium. Since the pile is surrounded on all sides by the elastic medium, this assumption gives a lower value for the coefficient of subgrade reaction than the actual one. It may be kept constant or variable along the length of the pile. The lateral deflections calculated using this analysis procedure therefore yield only a conservative estimate, as was pointed out by Broms (1964a). Further, the soil springs are attached only to the front of the pile, neglecting completely soil behaviour at the back of the pile. In any case, modelling the soil as a spring cannot truly represent a soil continuum - indeed, it completely ignores soil continuity. As Schofield and Wroth (1968) pointed out, a three-dimensional soil continuum cannot be represented by three-orthogonal coil springs. The basic Winkler soil model was refined by Vlasov and Leontiev (1966) who added a tension

layer at the surface of the spring series, causing the springs to interact with each other and behave like an elastic continuum. In the same paper, Vlasov and Leontiev also gave consistent closed form solutions, but these solutions cannot be extended to pile groups.

For long flexible piles, Broms (1964a) and, later, Randolph (1981), showed that the subgrade reaction analysis of a long flexible pile of bending rigidity EI embedded in soil with coefficient of subgrade reaction k, yields a critical length of pile beyond which the pile behaves as if infinitely long and then the length of the pile does not influence the deformation at the loaded end. This critical length l_c may be expressed as $l_c \approx 4[EI/k]^{\frac{1}{4}}$. It follows from this, that the whole length of the pile does not need to be considered in the subgrade reaction analysis. For piles that are longer than their critical length, the solutions of Hetenyi (1946), for a pile loaded by a lateral load H and bending moment M, yield expressions for the deflection u and rotation θ at the loaded end given by:

$$u = \sqrt{2}\frac{H}{k}\left(\frac{l_c}{4}\right)^{-1} + \frac{M}{k}\left(\frac{l_c}{4}\right)^{-2}$$

$$\theta = \frac{H}{k}\left(\frac{l_c}{4}\right)^{-2} + \sqrt{2}\frac{M}{k}\left(\frac{l_c}{4}\right)^{-3}$$

In some cases analytical methods are not very attractive - not only because there is no information on lateral deflections (Hansen (1961a)), but also because of their cumbersome solution procedures (Vlasov and Leontiev (1966)). Moreover, these methods cannot be extended to pile groups. In this thesis, therefore, preference is given to numerical methods. However, the numerical solutions are validated against the analytical solutions, wherever possible.

2.2 Numerical methods (linear-elastic soil behaviour)

Vertical loads

In the absence of adequate analytical solutions, various theoretical/numerical methods have been developed over the years and are currently in use to predict the axial response of a single-pile. These methods can be classified into two groups:

a) Methods which model the soil as a series of non-linear springs.
b) Methods that treat the soil as a continuum.

The methods which belong to group (a) are presented in Section 2.3. However, an approximate analysis based on Winkler (1867) soil model is presented by Scott (1981). It is assumed that a series of elastic soil springs are connected to the pile shaft along the length of the pile and a spring below its tip. The stiffness of these springs is carefully chosen such that the results obtained from the approximate analysis match with the elastic continuum methods given by Poulos and Davis (1968) for rigid piles and Mattes and Poulos (1969) for flexible piles.

The elastic continuum methods of group (b) are: the integral equation method, presented initially by Poulos and Davis (1968) and later by Randolph (1977); the boundary element method proposed by Butterfield and Banerjee (1971); more recently, the infinite layer method of Guo *et al.* (1987), in which a rigorous approach is presented to model a layered soil medium for the analysis of a single-pile and Cheung *et al.* (1988) for pile groups; and finally, the finite element method adopted by, among others, Ottaviani (1975), Randolph (1977) and Baguelin and Frank (1980).
All of these methods may be used to obtain solutions for linear elastic soil behaviour. However, all these methods except the finite element method (see below), suffer from the

disadvantage that they cannot be readily extended to more complicated constitutive models. Although some recent refinements of these methods take account of soil non-linearity and soil plasticity, they have serious limitations when it comes to dealing with soil inhomogeneity (vertical and horizontal), and the further drawback of slowness of the numerical calculations. (Elastic continuum methods are explored in Chapter 3 and a new approach is there presented to make the finite element analyses more economical.)

It is difficult in the finite element method to model an infinite domain. Usually the boundaries in a finite element mesh are set at sufficiently large distances for the boundary effects to become negligible, at least beyond the theoretical extent of the collapse mechanism, as studied by Bell (1991). However, Brocklehurst (1993), following this approach in his study of a two-layer soil system, observed some sizeable errors in the finite element results due to the close proximity of the mesh boundaries, and had to shift them further away to obtain acceptable results. This difficulty of fixing boundaries in a finite element model had been dealt with in the past either by the use of special elements (infinite elements) described by Bettess (1977), Medina (1981) and more recently by Chen and Poulos (1993), or by combining the finite element formulation with a boundary element formulation (Zienkiewicz *et al.* (1977). (Chapter 3 takes a different approach, in which a correcting layer is used to model the infinite boundaries. This approach is similar to the one described by Burd and Houlsby (1990) for a large strain cavity expansion problem.)

Lateral loads

Various attempts have been made in the past to calculate the lateral deflection of piles under working loads. The methods used to predict the lateral response can also be classified into two groups, as described above. One of the earliest analysis procedures belongs to group type (a) and is known as the subgrade reaction method (see above, Section 2.1). The analytical solutions given by Hetenyi (1946) can also be obtained using numerical methods. One such

method, proposed by Poulos and Davis (1980), employs finite difference numerical technique to solve the beam column differential equation. It is easy to incorporate a spring coefficient which varies linearly with depth. Again, the method is not applicable to analysis of groups of piles.

Poulos (1971a) also proposed an elastic solution, known as the Integral Equation Method (IEM), based on Mindlin's solution for a point load in an homogeneous, isotropic elastic half space. This method belongs to group type (b) and employs a semi-analytical approach in which the pile is assumed to be a thin rectangular strip of the same rigidity as the actual pile. The pile response is calculated by integrating Mindlin's equation over the corresponding rectangular area of the soil. The method can be extended to study group behaviour (Poulos 1971b)) but the amount of computational work involved is substantially reduced by the introduction of interaction factors. These factors take into account the additional movement of an individual pile attributable to the movements of neighbouring piles in its group. However, subsequent extension of the method to deal with a layered soil profile introduces a degree of approximation into the solution because of the choice of an equivalent shear modulus. The accuracy of the solution is further affected by the manner in which the pile is discretised. Evangelista and Viggiani (1976) reported that the use of varying size elements along the pile gives improved accuracy over the solutions given by Poulos (1971a). For piles of large flexibility, the solutions are strongly dependent upon the length of the elements near the top of the pile. (A similar trend in the use of the integral equation method for the settlement analysis of a vertical pile, is reported in Chapter 3 below.) However, the cylindrical pile idealisation proposed by Randolph (1977), rather than the rectangular strip idealisation by Poulos (1971a) showed close conformity with finite element analysis results.

Randolph (1981) suggested algebraic expressions which allow the behaviour of the flexible piles under lateral loading to be calculated in terms of fundamental soil properties. The expressions are based on the results of finite element studies for the response of a laterally loaded cylindrical pile embedded in elastic soil with stiffness varying linearly with depth. Randolph performed a special type of finite element analyses in which he applied non-

symmetrical loading to the axi-symmetric geometry of the circular pile. This type of analysis is computationally economical compared to a three-dimensional finite element analysis: it remains to be further explored using more refined soil models, and for the analysis of pile groups. Earlier, in a similar study, Kuhlemeyer (1979) presented his finite element results fitted with simple power law relationships. Randolph (1981), in addition to the algebraic expressions, also suggested an approximate analysis procedure (without the aid of a computer) for a flexible pile under lateral loading embedded in a soil with a linearly varying soil modulus with depth, and having zero value at ground level. Due to the very low soil stiffness around the upper part of the pile shaft, he suggested that limiting soil pressure will be reached at large pile deformations. Therefore, the deformation of the pile in this region may be calculated by treating the pile as a simple cantilever. For the lower part of the pile shaft, i.e. below this failed region, a single pair of algebraic expressions gives the deformations at the transition point between the failed and the un-failed regions. Both free-headed or fixed-headed piles can be analysed in this way. Later, Randolph and Houlsby (1984) presented a more rational approach: they suggested expressions for the limiting soil reaction, for the two modes of failure i.e., wedge type of failure near the surface, and the failure at depth which takes place due to the flow of material round the pile. The analytical expressions for the latter type of failure give limiting soil reaction per unit length of pile, assuming plane strain conditions. But it is difficult to obtain such expressions for pile groups. Also, the lateral deflections still remain unknown. (A numerical method, the finite element method, is used in Chapters 5, 6 and 7 to determine lateral deflection of single-piles and pile groups.)

An extension of the integral equation method mentioned above is the boundary element method presented by Butterfield and Banerjee (1971), in which soil continuum and pile are treated as two separate domains whose boundaries are discretised into a finite number of elements. A set of fictitious tractions are assumed at the pile-soil interface. Butterfield and Banerjee (1971) showed that these fictitious tractions are identical to the real ones for pile slenderness ratio greater than five. Each boundary element is associated with unknown

tractions and displacements. Some of these are known over parts of the boundary, the rest of them are computed using point-force singular solutions as proposed by Kelvin (Sir W. Thomson, Cambridge and Dublin Math. J. (1848)) or Mindlin (1936). Once these boundary values are obtained, the displacements and tractions at any point inside the domain, satisfying the boundary conditions at the soil-pile interface, are computed using the boundary integral equation, which is the basis of the boundary element method. This method has also been used to evaluate pile group behaviour. It has the advantage over finite element analysis that only the boundaries need to be discretised and the singular solutions used in the analysis automatically satisfy the boundary conditions at the free surface and at infinity. The number of equations needed to be solved is thereby reduced, making the method computationally efficient. Various computer programs based on the boundary element method are currently in use. The Department of Transport's computer program PGROUP was developed by Banerjee and Driscoll (1976). It is capable of handling pile groups of any geometrical shape subjected to combined horizontal, vertical and moment static loading. It has since been upgraded to include a soil model with a linearly increasing modulus following the work of Banerjee and Davies (1978). Banerjee and Davies (1978) described a non-linear method of analysis in which volume cells were introduced into the soil domain to handle soil yielding. In this analysis procedure the boundary element method loses its inherent computational efficiency over the finite element method i.e. loses the merit of a smaller system of algebraic equations than is needed in the finite element method. Another computer program DEFPIG, less rigorous than PGROUP, written by Poulos (1980), is based upon a simplified boundary element approach for a single-pile analysis and the calculation of the interaction factors for two equally loaded identical piles. Soil non-linearity is modelled by limiting the stresses at the pile-soil interface, while soil inhomogeneity is approximated by an averaging procedure using the point load solutions of Mindlin (1936). The PIGLET computer program (mentioned earlier, Section 2.1, and developed by Randolph (1980)) is based on analytical solutions that are either derived theoretically or fitted to the finite element results to give the response of single-piles. Pile-soil-pile interaction is based on interaction factors determined from

expressions fitted to the results of the finite element analyses. The interaction-factor approach used in DEFPIG and PIGLET for pile-soil-pile interaction gives loads and bending moments only at the pile heads, not their distributions along the piles. Limitations of the elastic approach to pile interaction under lateral loading have been revealed from model pile tests carried out on a centrifuge by Barton (1982). These tests show that the leading piles of groups embedded in sand carry a higher proportion of overall applied load than the trailing piles. For pairs of piles at close spacing (s/d=2) , where s is the centre-to-centre pile spacing, Barton found that applied load was shared 60% to the front piles and 40% to the rear piles. In contrast Matlock *et al.* (1980) reported results of tests on pile groups in clay, where a uniform sharing of the applied load was found. Clearly, the adequacy of the elastic approach will depend on a number of factors such as the load level, soil type, and most importantly pile spacing. Despite the limitations, these two programs are widely used since (apart from there being no viable alternative) they provide conservative solutions to most in-land in-service foundations. Springman (1989) developed a computer program SINPILE (some parts of the underlying theory are adapted from PIGLET) to predict the bending moment and deflection of piles subjected to active lateral loading by soil. The program was further upgraded into an interactive version SIMPLE. This program analyses a group of two vertical piles which are connected with a stiff cap i.e. under similar lateral loading conditions. More recently a spreadsheet program SLAP has been presented by Randolph and Springman (1991) for the analysis of pile response due to external loads and soil movements.

2.3 Numerical methods (for non-linear elastic soil behaviour)

Vertical loads

As real soils seldom obey Hooke's law, the methods that fall within group type (a) (see above, Section 2.2) take account of non-linear soil behaviour. The earliest, the load transfer

method, given by Coyle and Reese (1966), involves an iterative analysis procedure. The procedure relies on curves which relate the ratio of load transfer to soil shear strength versus pile displacement along the length of the pile. The curves are constructed from data obtained from the field or laboratory-instrumented piles. The pile is divided into a number of small segments. An initial guess is made for the movement of the segment at the bottom. Then, with the help of the appropriate load transfer curve, an iterative procedure is followed to obtain the load acting on the segment. From this information about the load and the movement of the bottom segment, the analysis then proceeds upwards, segment by segment, to the top of the pile. Thus, various initial movements at the bottom pile segment are used to construct the load displacement curve at the pile head. Clearly, such load transfer methods ignore continuity of the soil medium and cannot be applied to pile groups. Moreover, in order to obtain load transfer curves on site, considerably more instrumentation is required than for a normal pile load test. Also, as soil conditions vary, horizontally as well as vertically, extrapolation of test data from one site to another may not always be entirely satisfactory. The load transfer method was refined by Kraft *et al.* (1981) who suggested the use of theoretical expressions for the data obtained from field tests on instrumented piles to determine curves relating load transfer t to vertical pile movement z at various points along the pile. These t–z curves were then used as non-linear supporting soil springs in an analysis of the load settlement behaviour of the pile using the finite difference numerical technique. Randolph (1981) developed a computer program RATZ, based on the load transfer method.

A hybrid approach, which is a combination of load transfer method and the integral equation method (mentioned earlier Section 2.2), is used to predict the settlement of vertically loaded pile groups. In this approach, the soil behaviour of individual piles is modelled using load transfer curves and the pile-soil-pile interaction is determined using Mindlin's (1936) solution which is the basis for the integral equation method. Among others, Chow (1986) has demonstrated the success of this approach by presenting a close match between the predicted results and the measured results from the field load tests.

Lateral loads

The subgrade reaction method for the analysis of laterally loaded piles is improved by introducing non-linear reaction-deflection *p-y* curves in the analysis. These curves are derived from actual field measurements which represent non-linear stiffness of soil springs. The method is generally known as the *p-y* curve method, developed by Reese and co-workers (1974,1975), who obtained a finite difference solution to the following equilibrium equation for a beam on an elastic foundation:

$$EI\frac{d^4y}{dz^4} + P_z\frac{d^2y}{dz^2} - p = 0$$

where

y = lateral movement

EI = bending rigidity

z = depth

p = soil reaction per unit length

P_z = axial load at depth z

The finite difference form of the equation and a full description of the resulting equations after applying the boundary conditions were presented by Reese (1977) who also described a computer program that solves these equations. The solution requires input of a series of *p-y* curves at various depths along the pile. Essentially, an iterative solution procedure is adopted

as the curves are non-linear: for each iteration the values of the lateral soil reaction are updated from the corresponding *p-y* curves by considering the calculated deflections in the previous iteration until convergence is achieved. The iterative procedure is also needed in order to have compatible deflections at various levels along the length of the pile.

Design procedures for constructing *p-y* curves from the results of field measurements on full size instrumented piles have been developed by Matlock (1970) for soft clays, by Reese *et al.* (1974) for sands, and again by Reese *et al.* (1975) for stiff clays. To construct these curves, the ultimate lateral soil reaction per unit length of the pile is required in order to work out soil stiffness before and after the yielding of soil. There is no consideration of the soil flow rule and plasticity. In a unified approach, presented by Sullivan *et al.* (1980), the linear and non-linear parts of the curves are given by two different empirical relations, slightly different from those proposed by Matlock (1970). These involve the selection of two empirical parameters based on intuition and engineering judgement.

The limitations of the *p-y* curve method are:

1) Difficulties exist in choosing appropriate *p-y* curves for a given combination of pile size and soil type.

2) Replacement of the soil continuum by discrete springs restricts the extension of the analysis to pile groups since interaction between the neighbouring piles may not be taken into account, when constructing the *p-y* curves.

Although a fairly successful guess of the initial displacement field is important to obtain a convergent solution. However, algorithms can be derived which give a convergent solution.

An improvement was suggested by Georgiadis and Butterfield (1982) which introduces a

shear coupling between the springs. The coupled spring model, known as a Pasternak foundation model (Pasternak (1954)), was originally developed for single-piles. Attempts to extend it to the analysis of pile groups have not enjoyed any significant success.

O'Neill *et al.* (1977) proposed a hybrid model in which the response of a single-pile is evaluated using *p-y* curves, and the interaction between the piles through the soil is found using Mindlin's (1936) solution. An iterative solution procedure was adopted to respond to the non-linearity of the *p-y* curves. Later, a similar approach for the analysis of offshore battered pile groups was presented by Poulos (1980). He considered piles of equal length and uniform diameter. Leung and Chow (1987) studied pile interaction effects using a hybrid approach. Beam finite elements for piles and Mindlin's equation for an elastic continuum were used to model pile-soil-pile interactions. They demonstrated that their method compares well with the commonly used interaction factor approach for pile groups in a homogeneous elastic half space. They also modelled field studies made on two offshore pile groups (five-pile and ten-pile) by Matlock *et al.* (1980). However, for the ten-pile group, their method tended to over-predict the load carried by the piles when compared with field test results - perhaps because of the overlapping of plastic zones around the individual piles. Closely spaced group interaction cannot therefore be modelled using Leung and Chow's method. More work is needed to investigate the over-predictive effect further.

A computer program is given in the textbook by Smith and Griffiths (1988) implementing Leung and Chow's method. Two other widely used computer programs are SPLICE developed by Clausen *et al.* (1984) and the W. S. Atkins program SPLINTER. A third, more recent program, FUGROUP developed by Aldridge and Erbrich (1990), eliminates the inconsistency in using a constant shear modulus across a layer boundary as computations are made independent of the shear modulus.

Muqtadir and Desai (1986) described a finite element analysis of a group of battered piles in which they used a hyperbolic soil model (Duncan and Chang (1970)) for sands to incorporate

material non-linearity. They adopted a non-linear incremental method for the solution of equilibrium equations. The load is divided into small increments and tangent stiffness defined by a hyperbolic formula, computed after each increment, and used for the succeeding increment. Although a hyperbolic soil model does not reflect the failure behaviour of the soils, it does model pre-peak behaviour of both loose and dense sands and also of clays.

2.4 Numerical methods (for elasto-plastic soil behaviour)

The methods so far described cover linear and non-linear elastic soil behaviour. Kooijman and Vermeer (1988) presented a quasi three-dimensional pile foundation analysis in which, instead of using *p-y* curves, they employed a two-dimensional finite element analysis for an elasto-plastic soil behaviour to calculate lateral soil stiffnesses i.e. theoretical *p-y* curves using finite element analysis. These *p-y* curves take account of interaction between neighbouring piles. This analysis is based on the assumption that the shear strains in the soil along the vertical plane of the pile-soil model are zero, whereas the horizontal layers of the soil are modelled as plane stress slices. This assumption has not been checked and needs numerical experimentation to test its validity. The analysis was later extended to cover pile group response by Kooijman (1989).

A three-dimensional finite element analysis for pile group response is computationally expensive. Lane and Griffiths (1988) carried out such an analysis economically for a laterally loaded single-pile using a finite element harmonic analysis. The analysis utilises the advantage of axial symmetry to perform two-dimensional modelling of the three-dimensional problem with non-symmetric loading applied in the third dimension in the form of Fourier harmonic terms. (This analysis is similar to the analyses done by Kuhlemeyer (1979) and Randolph (1981) except that the soil is modelled as an elasto-visco-plastic material.) The technique is an efficient way of handling large three-dimensional problems by reducing computer storage requirements and running time. Brown and Shie (1990a) performed a realistic three-

dimensional analysis using a commercial finite element-code, ABAQUS. They modelled the gap formation and slippage between the soil and pile near the pile head using interface elements. Two elasto-plastic soil models, the von Mises yield criterion (Calladine (1985)) for undrained clays and the extended Drucker-Prager plasticity model (Drucker and Prager (1952)) for sands, were used. Brown and Shie (1990a) reported numerical problems in using the latter soil model for purely frictional soils. They managed to eliminate the difficulty by specifying a small value of cohesion in the model. The finite element model boundaries were chosen to pass through the pile centre-line and through the soil midway between the piles. The results were processed to construct *p-y* curves and a close match with the experimental curves was shown. The analysis does not strictly correspond to that for a single-pile as the mesh boundaries are chosen in such a way that the presence of neighbouring piles are bound to contaminate the finite element results. A similar type of model for the behaviour of a pile group has also been presented by Brown and Shie (1990b).

Use of the elasto-plastic boundary element method to study pile group behaviour has not been actively considered by researchers working in this area. The one reported study, by Banerjee and Davies (1980), contains very little detail on the actual methods used to incorporate plastic behaviour in the boundary element method. It is thought (for the reason stated earlier, Section 2.2) that this is not a worthwhile method to pursue.

2.5 Plane strain solutions for laterally loaded piles

In addition to the numerical solutions described above, plane strain analytical solutions for laterally loaded piles have been derived which provide more quantitative information about pile and soil behaviour. Baguelin *et al.* (1977) presented an analytical solution for a circular disc (two dimensional plane strain model) displaced laterally in an elastic soil. In their analysis, they justified plane strain conditions to hold near the pile because the displacements of the various sections of the pile are not arbitrarily independent but vary in a highly

continuous manner, since the pile's radius of curvature is always very large with respect to its diameter.

The displacement of the pile section caused by a lateral loading, given by Baguelin *et al.* (1977) solution, depends on the choice of outer radius R of a two-dimensional model. The solution has an ambiguity that for a realistic value of R to be infinity, the displacement of the pile section in turn tends to infinity, which is unrealistic. It was therefore necessary for them to determine the value of R for the two-dimensional model used in their theoretical study, such that the analytical solution would give realistic displacement values. They carried out a peculiar analysis in which deformation fields from the two-dimensional analysis and a simplified three dimensional analysis were matched. The analysis is based on the assumption that there is an annular zone of radius r_a in which deformation field follows the law of plane strain and outside this zone the behaviour of soil is three-dimensional. For the annular zone, strains were calculated by differentiating the analytical solution with respect to r. For the outside the zone, they considered a simplified three-dimensional problem of a vertical axis, loaded horizontally in a semi-infinite elastic solid. The three-dimensional strains were calculated using Mindlin's (1936) solution for a point source. The distribution of load along the axis was calculated from the theory of subgrade reaction discussed earlier in Section 2.1. For short piles, a constant soil stiffness with depth and for long piles, variable stiffness along the length of the pile was assumed. Using a trial and error procedure, several load distributions were tried and the value of R was chosen in such a way that the displacement at r_a, as calculated by the two- and three-dimensional models was the same. The influence of the pile section (square pile), disturbance of the soil around the pile due to pile installation, and plastic yielding of the soil in undrained behaviour, based on Tresca's yield criterion (Calladine (1985)), were studied using finite element method. Graphs were produced to calculate the corresponding corrective terms to be applied to the analytical solution. Baguelin *et al.* (1977) show that such influences are confined to within two pile diameters of the circular disc. The analytical solution raises doubts about the question of modelling soil

behaviour as linear elastic, under lateral loading in a two-dimensional model.

Randolph, Carter and Wroth (1979) studied the effects of pile installation and subsequent consolidation on the performance of driven piles in clay. They modelled pile installation as an undrained expansion of a cylindrical cavity. The assumption is valid for deep penetrations when the soil predominantly displaces radially. They considered a work hardening elasto-plastic material behaviour based on the Modified Cam-Clay model (Roscoe and Burland (1968)). The excess pore pressures generated in this process were subsequently assumed to dissipate by means of outward radial flow of pore water. Analyses of the stress changes due to the expansion of the cylindrical cavity and the subsequent consolidation of the soil with the dissipation of pore water pressure were presented by Carter, Randolph and Wroth (1979). Randolph, Carter and Wroth (1979) carried out a parametric study and gave the effects of past stress history of the soil on the stress changes due to pile installation. In another paper, Randolph and Wroth (1979b), produced an analytical solution for the consolidation of the soil around a driven pile. They considered an elastic soil behaviour under plane strain conditions in the derivation of their solution. The solution gives pore pressure and stress changes in the soil around an impermeable rigid pile, starting from an initial pore pressure distribution due to the expansion of a cylindrical cavity in an ideally elastic, perfectly plastic material. The resulting logarithmic variation of excess pore pressure with radius is considered to be close to that generated around a pile as a result of driving.

These useful studies are related to axial loading of single-piles. No such study has been done for the case of lateral loading of piles. That is why the main emphasis in this thesis is on laterally loaded piles and pile groups (Chapters 4, 5, 6 and 7).

When a pile is loaded laterally, two types of soil behaviour are expected, one near the surface close to the pile head where a wedge type of failure is assumed, and the other at some depth from the surface where the soil is assumed to flow around the pile at failure. In an offshore pile foundation, the latter type of failure is more likely to occur than the former. As described earlier, Randolph and Houlsby (1984) carried out a plane strain analysis of the problem using the method of characteristics. The soil was modelled as a perfectly plastic cohesive material.

They presented an exact solution (i.e., one in which both upper and lower bound closed form solutions match) for the ultimate lateral resistance of the soil. It was found that if the load was non-dimensionalised with respect to the soil strength, the load factor varied between $(6+\pi)$ for a perfectly smooth pile and $(4\sqrt{2} + 2\pi)$ for a perfectly rough pile. The solution provides information about the size of the expected plastic zone in the soil. A limitation of the method, however, is that no information is obtained on the displacements needed to reach the limit load. An understanding of pile-soil-pile interaction phenomena is greatly helped by determining the ultimate lateral resistance of a soil in a pile group subjected to an external load under undrained conditions. (A detailed study done on these lines is presented in Chapters 5 and 6.)

2.6 Summary

Elastic methods are widely used to model the behaviour of inland/onshore pile foundations. Non-linear methods, which mainly rely on empirical curves based on limited field data, are used for offshore pile foundations. For closely spaced pile groups in soft clay, the use of these methods requires great care as it is difficult to predict the effects of interaction on pile group response. The interactions are highly non-linear due to the overlapping plastic zones around the individual piles. However, for the case of vertically loaded pile groups, the plastic zones around the individual piles are not as large in size as in the case of laterally loaded piles. There is less likelihood that these zones will overlap. The hybrid method presented by Chow (1986) based on elastic interaction amongst the piles seems quite suitable to predict the response of vertically loaded pile groups. The use of the boundary element and finite element methods enables the effects of various soil models to be studied. Application of the boundary element method to study the elasto-plastic soil-structure interaction has not so far been very well explored. Current finite element approaches to the problem are computationally uneconomical, especially for group behaviour. For that reason, a simplified approach for the

analysis of laterally loaded piles and pile groups similar to that developed by Kooijman and Vermeer (1988) is proposed in Chapter 6, in which the ultimate capacity of a single-pile or a pile group is determined using plane strain finite element analysis as a first step. This predicts ultimate behaviour more accurately, more or less eliminating the degree of uncertainty. It therefore helps in optimising foundation design. Then, as a second step, theoretical *p-y* curves are determined from a single plane strain finite element analysis of single-piles or pile groups along their lengths and used as input to non-linear beam-column equations (see above, Section 2.3) to determine the pile-head displacements. Although the method is not ideally successful at modelling field tests (see Chapter 6), because of its simplification of the three-dimensional nature of the problem, it is nevertheless, in the absence of a complete three-dimensional analysis, and for other reasons to be explained below, the best method available.

CHAPTER 3

ELASTIC ANALYSIS OF A SINGLE-PILE UNDER AXIAL LOADING

3.1 Introduction

This chapter proposes a new analytical method for calculating the pile head settlement of a rigid pile. An approximate analytical solution is derived. Its validity is checked using the integral equation method (IEM). The new analytical method is further adapted in the development of a correcting layer approach to model the infinite boundaries in the finite element analysis of a single-pile. The correcting layer approach is computationally economical to perform the finite element calculations. The response of a single flexible pile under static axial loading is analysed using the finite element method (FEM) and the IEM and the results obtained are compared. The ability of the correcting layer approach to model the infinite boundaries is demonstrated by achieving a close agreement in the results from both of these methods.

Figure 3.1 shows a pile driven into a linear elastic homogeneous soil. The following conditions are assumed: there is a perfect bond at the pile-soil boundary (i.e. no relative slip); and there are no shear stresses acting at the pile base-soil interface (i.e. there is a smooth pile base).

The aim of this simplification of the initial conditions before the analyses are undertaken is to focus exclusively on the problem of determining, from the methods currently in use, the numerical method best suited to the analysis of single-piles. Two out of the various numerical

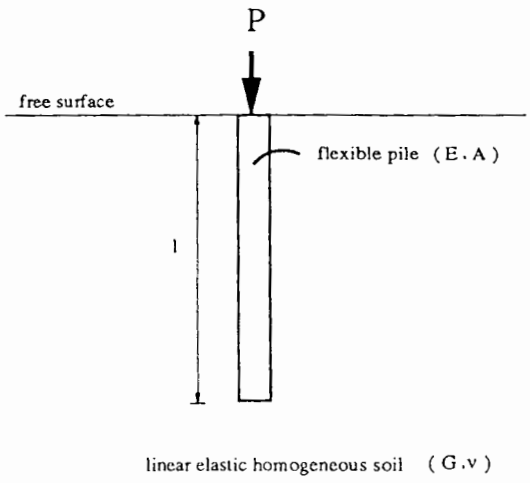

Figure 3.1: A single-pile under axial loading

methods described in the preceding chapter, namely the IEM (also known as quasi-boundary element method) and the FEM, are used in the analysis following.

A computer program was developed to perform the integral equation analysis for a single vertical pile under axial loading in an ideal linear elastic homogeneous soil medium. The numerical formulation of the analysis, presented in Section 3.2 is in some part adapted from an early work by Randolph and Wroth (1978). In this paper they carried out both the finite element and the integral equation analyses for an underreamed pile, and compared the results. Since the FEM requires fixed boundaries to analyse a problem unlike the IEM which does not require any, they artificially introduced a fixed boundary in their integral equation formulation at the same depth below the pile base where they had a fixed boundary in their finite element analysis in order to make a satisfactory comparison, adopting the rigid layer model described in Butterfield and Banerjee (1971). In this model fictitious stresses are introduced over the layer to give zero overall vertical displacements at that depth. Randolph and Wroth (1978) used this model to test their finite element formulation.

The principal aim here is to model infinite boundaries in the finite element analyses while

keeping the integral equation analysis as simple as possible. However, Section 3.3 goes on to describe the possibility of extending this analysis into a general purpose two-dimensional elasto-plastic boundary element method, and the reasons why it is not pursued further in this thesis.

A new analytical method is proposed in Section 3.4 which provides an improved solution for the pile head settlement of a rigid single-pile in an ideally elastic soil medium. The method adopts a load transfer mechanism such that the solution does not have to rely on a fictitious radius, r_m, as in Randolph and Wroth's (1978) solution. The proposed method suggests further a correcting layer approach to model the infinite boundaries in the finite element analyses. The finite element analyses were carried out using the commercial package ABAQUS, and the results obtained are compared with the integral equation analysis described in Section 3.2. The computer program, performing the integral equation analysis, is significantly adapted from Randolph and Wroth (1978) in order to serve the particular conditions of this study. The effectiveness of the correcting layer approach is demonstrated by the close agreement achieved in the results from these two numerical methods (i.e. IEM and FEM).

The correcting layer approach also has the merit of achieving a very significant saving of computational effort in the finite element analyses by making meshes almost half the size they would otherwise have to be (Randolph and Wroth (1978); Baguelin and Frank (1980)). The saving naturally encourages the use of FEM to study the response of not only single-piles but also closely spaced offshore pile groups under vertical loading, whereas IEM is incapable of modelling the non-linear pile-soil and pile-soil-pile interactions.

3.2 Axi-symmetric quasi constant boundary element formulation

It is important to appreciate how the integral equation analysis presented here differs from that of Randolph and Wroth (1978) (see Figure 3.2 below). The pile shown in the figure is

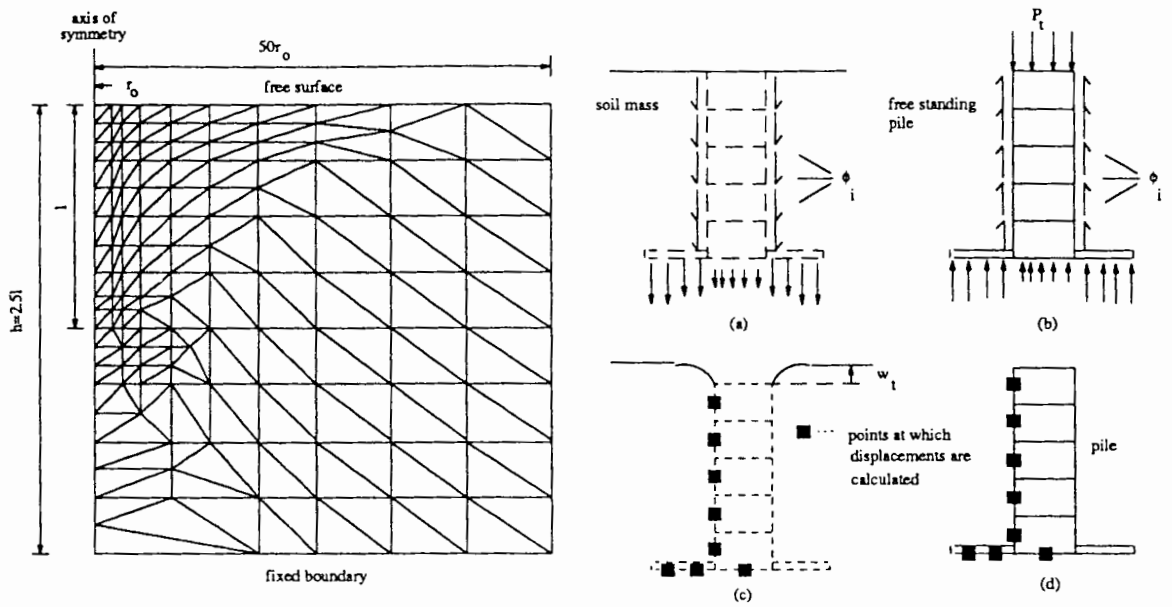

Figure 3.2: Finite element grid and schematic diagram of integral equation method (after Randolph and Wroth (1978))

underreamed. Various stages involved in the integral equation analysis of the pile are drawn next to the finite element mesh to model the same pile in the finite element analysis.

Randolph and Wroth (1978) were obliged to consider a rigid layer at some depth below the pile base in order to compare satisfactorily the results with the FEM. In the present analysis we need not worry about the rigid boundaries as these are taken care of by adopting the correcting layer approach being presented in Section 3.5 for the finite element analyses. It is worth remembering that use of the IEM is reliable only under linear elastic conditions and is not suited to more complex soil models which are required for detailed analysis. It is for this reason that the present integral equation formulation is kept simple, and a straight (i.e. not underreamed) pile is analysed, and the effect of a rigid layer is not considered.

The analysis is done using an axi-symmetric quasi-constant boundary element computer program specifically designed for elastic analysis of a single-pile under axial loading. The numerical formulation is based on the solution for a point load inside a semi-infinite homogeneous elastic half space derived by Mindlin (1936). The solution gives stresses and

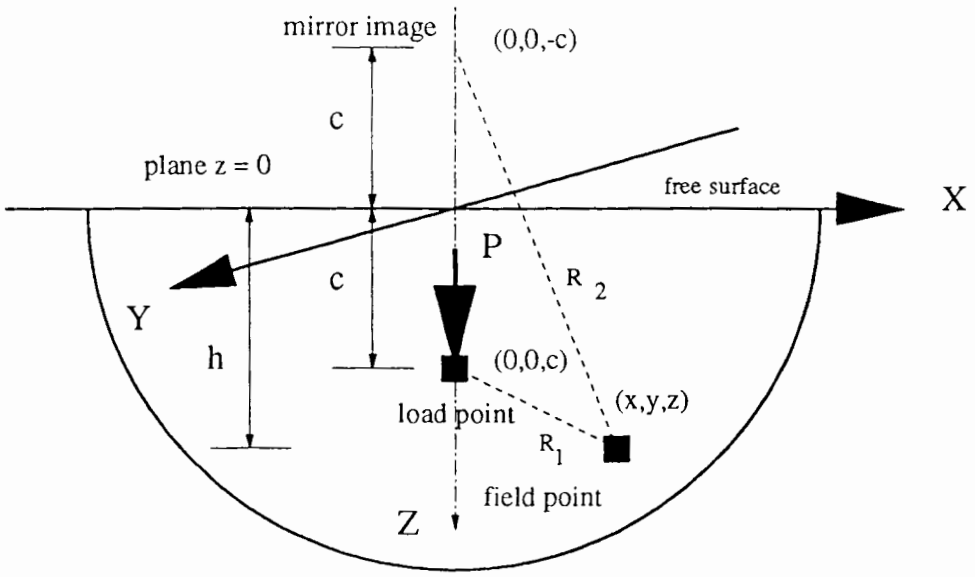

Figure 3.3: Force in the interior of a semi-infinite elastic half space (after Mindlin (1936))

displacements at a field point (x,y,z) due to a point load at coordinates $(0,0,+c)$ as shown in Figure 3.3.

The analysis is based on the following formulation. Figure 3.4(a) shows a cylindrical column of soil consisting of n elements. These are described as shaft elements. A set of shear stresses are imagined to be acting at the boundary of this column and vertical normal stress at its base. The shear stresses are assumed to be constant over each element of pile-soil interface which is discretised into a number of constant strain boundary elements. The greater the number of these elements, i.e. the finer the discretisation of the interface, the more accurate the solution will be. The other assumptions made in the analysis (as mentioned at the beginning of the chapter) are: a perfectly rough pile which makes a perfect bond with the soil, and which has a perfectly smooth base. The compatibility of radial displacements is not taken into account. Poulos and Davis (1968) reported that the radial stresses on the piles are only of the order of 0.5% of the shear stresses on the pile. Mattes (1969) found that the distribution of shear stresses and the settlement of the pile, considering both vertical and radial displacement

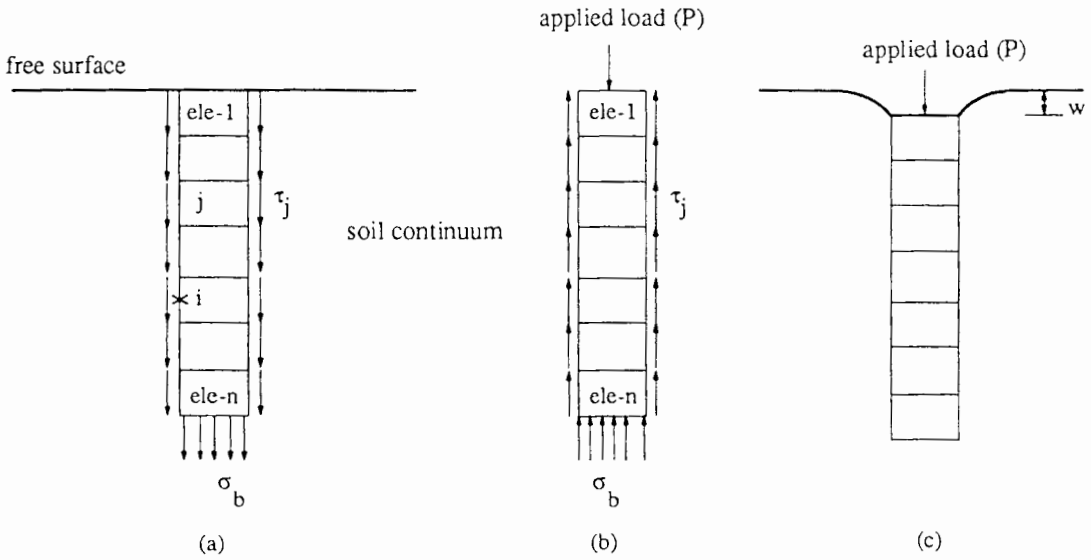

Figure 3.4: Schematic diagram of the integral equation method

compatibility, is almost identical to that obtained by considering vertical displacement compatibility only. Butterfield and Banerjee (1971) also found that the additional radial compatibility condition in the boundary element formulation did not affect the resulting vertical displacements for a given load.

Each shaft element exerts a constant shear stress on the soil. The stress exerted by j^{th} element is τ_j, while the base element exerts a normal stress σ_b on the soil underneath it. Making use of Mindlin's solution, the vertical displacement may be calculated at any point in the soil continuum by integrating the effects of all the stresses acting on the shaft elements. In particular, the displacement of the mid-point of each shaft element can be calculated. Though the discretisation suggests a linear variation of displacement within the element, but for the purpose of this part of the calculation, the value of displacement at the mid-point is assumed to apply.

For the pile in Figure 3.4(a), the displacement w_{ij}^s in a shaft element i due to the traction at element j is given by:

$$w_{ij}^{s} = f_{ij}\ \tau_j \tag{3.1}$$

where f_{ij} is an influence coefficient for the shaft element i, determined by integrating Mindlin's equation over the element j.

The total displacement w_i^s (at any depth) is the sum of individual displacements caused by the shear stresses acting on each of the n shaft elements and the normal stresses σ_b at the base elements. This can be expressed as:

$$w_i^{s} = \sum_{j=1}^{n} f_{ij}\ \tau_j + f_{ib}\ \sigma_b \tag{3.2}$$

where the subscript b represents the base element. The influence coefficient for shaft element i, determined by integrating Mindlin's equation over the base element is f_{ib}.

Similarly, the settlement w_b^s at the base is:

$$w_b^{s} = \sum_{j=1}^{n} f_{bj}\ \tau_j + f_{bb}\ \sigma_b \tag{3.3}$$

where f_{bj} and f_{bb} are the influence coefficients for the base element integrating Mindlin's equation over the shaft element j and the base element itself, respectively.

Combining equations (3.2) and (3.3), we can write the n+1 equations in matrix form as:

$$\underset{\sim}{w^s} = [f^s] \cdot \underset{\sim}{\tau} \tag{3.4}$$

where $\underset{\sim}{w^s}$ and $\underset{\sim}{\tau}$ are the vectors of displacements; shear and normal stresses in the shaft and base elements respectively as shown in Figure 3.4(a). The displacements and the stresses are linked together through the soil flexibility matrix $[f^s]$.

The pile is discretised into exactly the same number of pile elements as the shaft elements. We will now establish a link between the displacements in the pile and the shear tractions by satisfying the compatibility condition that, at the pile-soil interface, displacement in the pile and the soil element will be the same. Figure 3.4(b) shows a free body diagram of the pile carrying a vertical load P and the fictitious soil tractions acting in the opposite direction. The applied loading will produce elastic shortening of the pile which is determined from the theory of elasticity, considering each pile element as a spring of axial stiffness $\kappa=EA/l_e$, where A is the cross-sectional area, E is the elastic modulus, and l_e is the length of the element. Each of these stiffnesses of the pile elements are assembled in a stiffness matrix $[K]$. The equilibrium of the pile can then be represented by the equation:

$$\underset{\sim}{P} - \underset{\sim}{\tau} A_c = [K] \cdot \underset{\sim}{w^p} \tag{3.5}$$

where $\underset{\sim}{P}$, $\underset{\sim}{\tau}$ and $\underset{\sim}{w^p}$ are the vectors of applied forces and the vector of pile displacements respectively, as shown in Figure 3.4(b). The circumferential area of a pile element is A_c.

Substituting equation (3.4) into equation (3.5), noting that $\underset{\sim}{w^s} = \underset{\sim}{w^p}$, and then rearranging,

gives equation (3.6) for the n shear tractions and a normal base pressure:

$$\underset{\sim}{\tau A_c} = [F] \cdot \underset{\sim}{P} \tag{3.6}$$

where the matrix $[F]$ is the inverse of the matrix $[K.f^s+I]$.

Shear tractions obtained from equation (3.6) are then substituted back into equation (3.4) in order to find vertical displacements along the length of the pile. Figure 3.4(c) shows the pile head settlement of the actual pile under an axial load, installed in place of the imaginary pile initially assumed in the soil medium.

The main part of the program is the evaluation of the influence coefficients for the soil flexibility matrix $[f^s]$ which relate the displacements at points on the eventual pile-soil interface to the stresses acting over the interface (details can be found in Poulos and Davis (1980) and are given for completeness in the appendix at the end of the chapter). The non-singular integration for the off-diagonal terms of $[f^s]$ is carried out analytically in the vertical direction (shaft elements) and radial direction (base elements) in the manner described by Poulos and Davis (1968). The circumferential integration is done using Simpson's rule with an angular step size of (π/50) radians. The integration, both analytical and numerical, required for the evaluation of the leading diagonal coefficients of the flexibility matrix $[f^s]$, needs special attention and has been carried out as suggested in Randolph (1977). These coefficients relate the displacement of the same point at which the load is assumed to be acting i.e. when $i=j$ in Figure 3.4. The analytical integration is carried out in two parts leaving a tiny gap equivalent in size to a very small fraction (.01%) of the pile radius, at the centre of the element. The numerical integration is performed at intervals of (π/60) radians over the

majority of the pile circumference but with a much finer step length in the vicinity of the singularity. This scheme excludes from the integration a square region of the side, 0.0001 times the pile radius, thus eliminating the point singularity (see Figure 3.5). For the numerical integration of the base elements, intervals of $(\pi/50)$ are used.

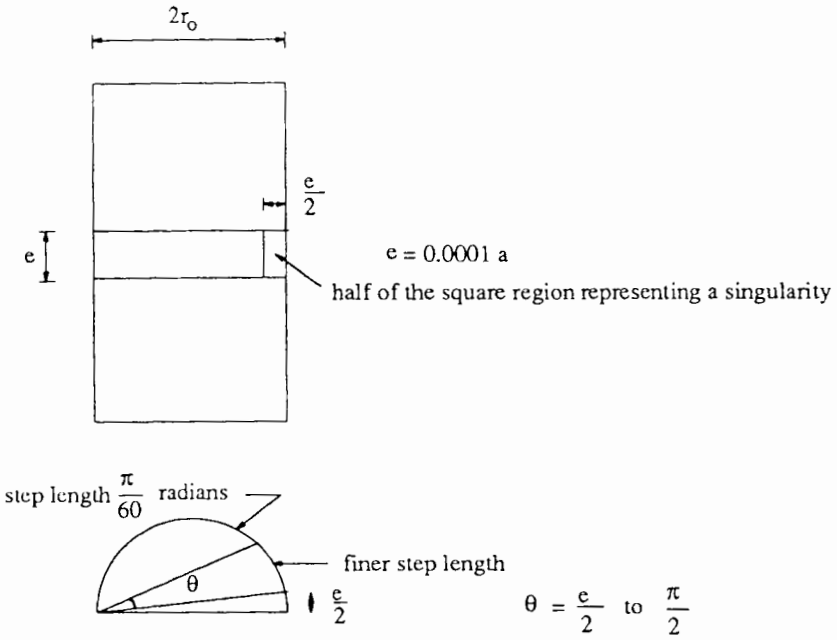

Figure 3.5: Typical pile element showing square region excluded from the numerical integration

The results obtained from the integral equation analysis are shown in Figures 3.6 and 3.7. These figures show the distribution of shear stresses along the length of the pile both for the case of a flexible pile and a rigid pile. Results from the integral equation analyses done by Mattes and Poulos (1969) for a flexible pile and Poulos and Davis (1968) for a rigid pile are also plotted in these figures. The results match well with the results of the present integral equation analysis. (E_p/E_s is the relative pile-soil stiffness or flexibility ratio.)

3.3 Two-dimensional elasto-plastic boundary element method

There is a body of opinion that holds that the boundary integral equation method can be satisfactorily extended to enable better soil modelling. This would mean that Randolph and

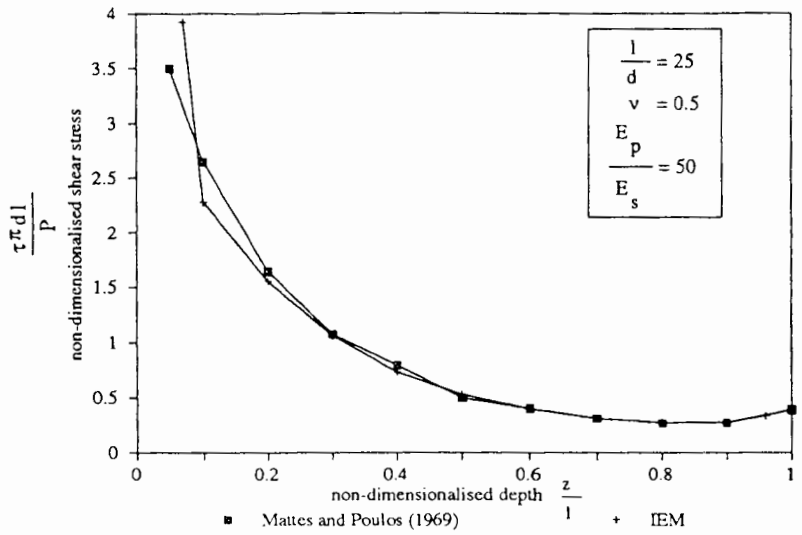

Figure 3.6: Shear stress distribution along the length of a flexible pile

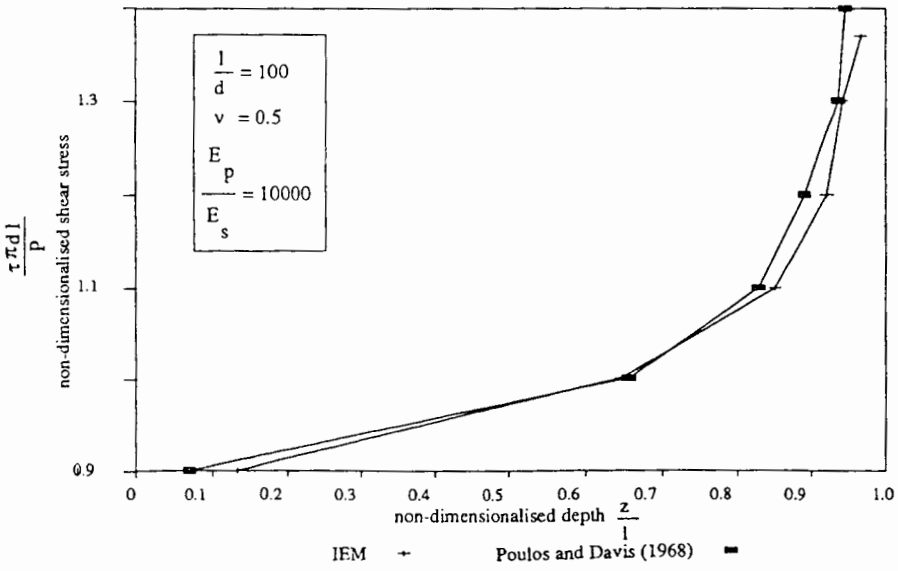

Figure 3.7: Shear stress distribution along the length of a rigid pile

Wroth's (1978) integral equation formulation is not limited to ideal linear elastic soil

conditions but adaptable to elasto-plastic soil modelling by extending it to the boundary element method. But, as we shall see, the adaptation of this method is computationally expensive and yields results no better than the finite element method.

The boundary element method forms a flexibility matrix which has to be inverted and the resulting stiffness matrix is fully populated. Therefore the numerical solution procedures are applied to the whole matrix. The finite element method is based on direct assembly of the stiffness matrix which is symmetric and banded in nature. The advantage of having a banded matrix allows the use of efficient Gaussian elimination solution schemes. The boundary element method is based on singular solutions which require superposition and work well with elasticity. These solutions are irrelevant to non-linearity. The finite element method can be readily extended to non-linearity. It is difficult to model infinite boundaries in the finite element method whereas, in the boundary element method, the condition of infinite boundaries is automatically satisfied. (A correcting layer approach to model infinite boundaries in the finite element method is presented in the following Section 3.5.)

Swedlow and Cruse (1971) presented a modified boundary element formulation in which they introduced fictitious body forces in such a way as to satisfy the yield and flow equations of plasticity. The resulting new equation, no longer a boundary integral equation, was presented in an incremental form to take account of material non-linearity. The algorithm required surface integrals as well as area integrals due to the discretisation of expected plastic zones in the body of the soil layer into a number of cell elements. Later, Telles *et al.* (1981) outlined a procedure to incorporate plasticity, which is the same as the finite element method, but entailing rather complex computer coding. The numerical procedure for the solution of the resulting system of algebraic equations cannot be made any more efficient because the stiffness matrix obtained is very sparse and non-symmetric. The fact that the size of the stiffness matrix will be much smaller than the one arising in the finite element method does not make any substantial difference to the problem under consideration here. In both methods, an almost similar mesh is required since, in the elasto-plastic boundary element method, in addition to the surface discretisation, domain discretisation of the expected plastic zones

around the pile is also necessary. By contrast, a carefully graded finite element mesh, having large finite elements outside the expected high stress concentration areas, results in nearly the same size stiffness matrix as that which arises in the boundary element method which is also non-symmetric and sparse. The disadvantage of having to handle a larger stiffness matrix in the finite element method, compared to the boundary element method, for most geotechnical problems, is outweighed by the efficient numerical solution procedure of the resulting algebraic equations, especially when dealing with non-linear problems. Moreover, numerical evaluation of the terms of the stiffness matrix in the boundary element method is not straightforward. For example, in order to eliminate the singularity in a triangular element, the number of integration points near the singularity is increased and each element is subdivided into a number of sub-elements. Although these sub-elements do not create any additional nodes in the final system of equations, this procedure does make the computer coding quite complex and cumbersome. There are, besides, other problems like anisotropies, radial and vertical inhomogeneities in the soil medium, which remain to be resolved. All of these reservations combine to discourage the pursuit of the elasto-plastic boundary element method.

3.4 Analytical methods for the analysis of rigid single-piles

Study of the incorporation of an elasto-plastic soil model in the boundary element method proves that the method to be less efficient as compared to the finite element method. There is no significant advantage in using an elasto-plastic boundary element method, not only because of the inefficient performance of the numerical computations involved in the method, but also because the element discretisation of the problem is more or less the same as that required in a finite element model. On the other hand, in the finite element method, the condition of infinite boundaries is not automatically satisfied as is the case in the boundary element method.

In this section, we describe a new analytical method for the analysis of a rigid single-pile under axial loading. The method is a development of an early work of Randolph and Wroth

(1978).

The analytical solution given by Randolph and Wroth (1978) for the analysis of a rigid single-pile under axial loading is based on the idea of a magical radius r_m where the displacements become zero. This parameter was artificially introduced to ensure analytical tractability. The new method, described in Section 3.4.2 adopts a load transfer mechanism which eliminates the need to have a magical radius r_m and provides an improved analytical solution. Also, we will see later that the method is further adapted in the development of two correcting layers around the finite element mesh of a single-pile to model infinite boundaries in the finite element analysis. The success of modelling infinite boundaries using correcting layers is demonstrated for a single-pile but it can equally be applied to closely spaced pile groups assuming a pile group to be of an equivalent large diameter single-pile. In order to explain the work involved in the development of the new analytical method, it is necessary to describe some of the early work on the analysis of a rigid single-pile, and, more particularly, the work of Randolph and Wroth (1978).

3.4.1 Simplified analysis of a rigid single-pile (after Randolph and Wroth (1978))

The analysis is based on the separation of loads carried by the pile shaft and the base. The approach to the analysis is shown in Figure 3.8(a), where the soil has been divided into an upper and a lower layer by a horizontal plane AB, at the level of the base of the pile. It is assumed that the upper layer of the soil will be deformed exclusively by the load shed by the pile shaft and that the lower layer of the soil will be deformed exclusively by the pile base load. Figure 3.8(b) shows the separate deformation patterns anticipated. The plane AB has been "exploded" to A_1B_1 and A_2B_2. The deformation patterns along A_1B_1 and A_2B_2 will not be compatible and this will lead to some interaction between the upper and lower soil layers. The deformations in the soil around the shaft are modelled as shearing of concentric soil cylinders.

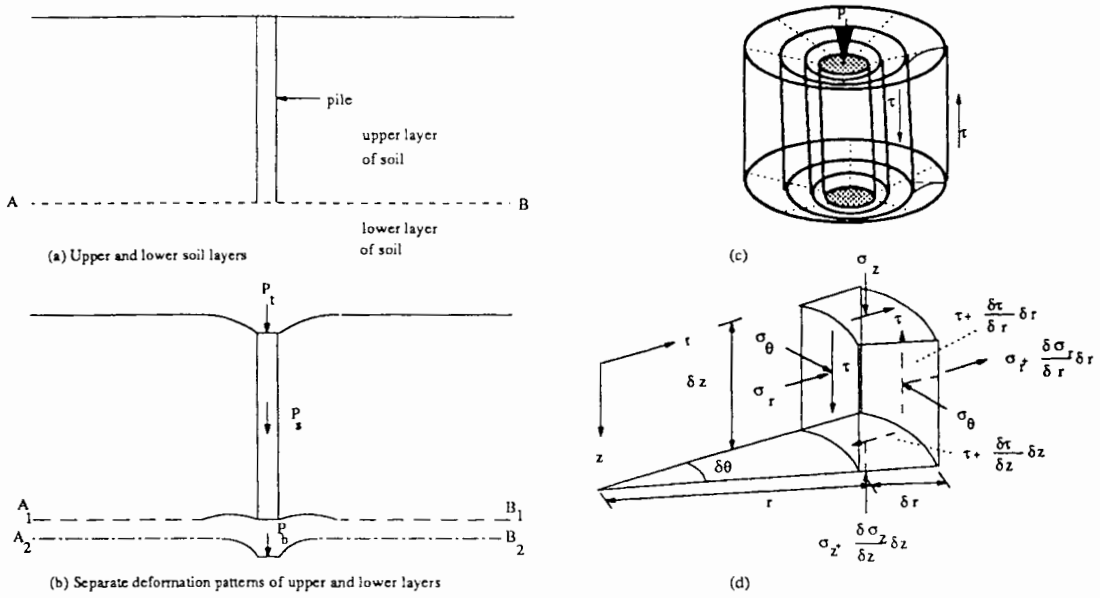

Figure 3.8: Analysis of pile by separation of loads carried by shaft and base (after Randolph and Wroth (1978))

When the pile is loaded, the increase in shear stress, τ, in the vicinity of the pile shaft, will be much greater than the increase in vertical stress, σ_z. Therefore, the vertical equilibrium of an element of soil shown in Figure 3.8(d) can be expressed as:

$$\frac{\partial}{\partial r}(r\tau) \simeq 0 \qquad (3.7a)$$

ignoring the $(\partial\sigma_z/\partial z)$ term. If the shear stress τ_o at the pile face $r = r_o$, the above expression can be integrated to show that the shear stresses around the pile decrease in inverse proportion to the radius, such that $\tau r \simeq \tau_o r_o$ is approximately constant. (This relationship is valid only under the assumption that the soil around the pile shaft will deform independently from the rest of the soil below the level of the pile base i.e. the deformations in the soil, around the shaft and below the base, will remain confined within distinct horizontal boundaries. This seems to be an unrealistic assumption.) Using the elasticity theory, the shear strain will be:

$$\gamma = \frac{\tau}{G} = \frac{\partial u}{\partial z} + \frac{\partial w}{\partial r}$$

in which u and w are the radial and vertical displacements of the soil respectively, and G is the soil shear modulus. The primary displacement will be vertical, and thus, ignoring $\partial u/\partial z$, integration of the vertical strains results in the following approximate expression for the displacement of the pile shaft:

$$w_s \approx \frac{\tau_0 r_0}{G} \int_{r_0}^{\infty} \frac{dr}{r} \tag{3.7b}$$

where, w_s is the settlement of the pile shaft; τ is the shear stress at any radius r from the axis of the pile; τ_o is the constant shear stress at the pile shaft; and r_o is the radius of the pile.

Equation 3.7b gives infinite displacements for a rigid pile which is physically untrue. This ambiguity is a direct result of the improper assumption (the soil around the pile being separated into two distinct layers which deform independent of each other) made in the analysis. To avoid this ambiguity Randolph and Wroth (1978) suggested that there is some magical radius r_m at which the displacements become negligible, and that, therefore, the settlement of the pile shaft, w_s, is given by:

$$w_s = \frac{\tau_o r_o}{G} \ln\left(\frac{r_m}{r_o}\right) \tag{3.8}$$

or

$$w_s = \zeta \frac{\tau_o r_o}{G}$$

where

$$\zeta = \ln\left(\frac{r_m}{r_o}\right).$$

The parameter, r_m, is determined empirically and as we shall see in the next section, theoretically r_m does not have a unique value but varies with the depth of the pile. Randolph and Wroth (1978) adopted a constant value of r_m and suggested an empirical relationship to determine this value by matching the analytical solution with the results of their integral equation analysis.

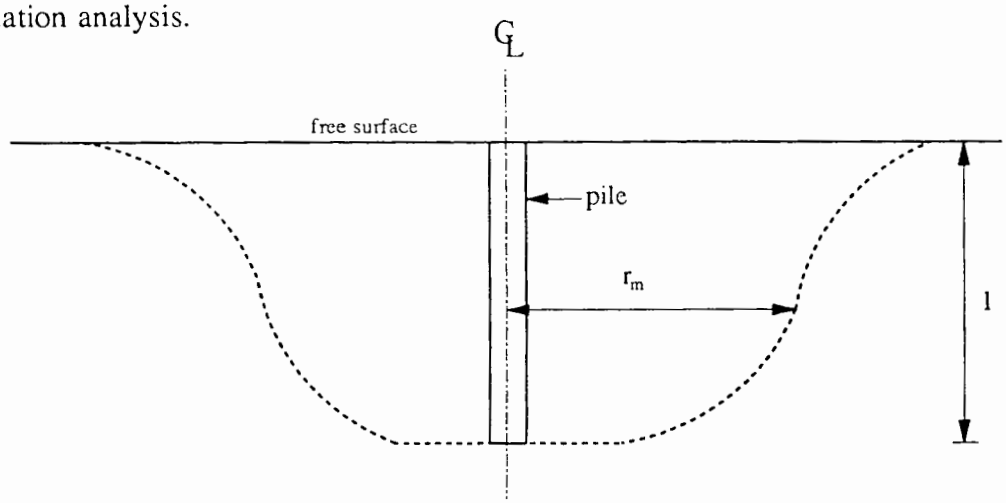

Figure 3.9: Hypothetical variation of limit of influence of pile (after Randolph and Wroth (1978))

3.4.1.1 Effect of lower layer of soil on upper layer

The deformations in the lower layer are assumed to be those arising from a rigid surface punch (the solution was given by Boussinesq (1876) for a smooth base with non-uniform pressure distribution at the base-soil interface (see Poulos and Davis (1974)). At some large distance from the pile the base will appear as a point load, and thus the deformations of A_2B_2

will decrease approximately inversely with r. The deformation of A_2B_2 (Figure 3.8(b)) will decrease more rapidly than the logarithmic variation implied in equation (3.7b). Thus, the lower layer will act as a restraint to the deformation of the upper layer, causing vertical stress σ_z increments in it, and contradicting to the assumption made in deriving equation (3.8). Undoubtedly these stress increments die out at the free surface but, in order to satisfy the equilibrium equation, an additional non-zero $(\partial\sigma_z/\partial z)$ term has to be included. This means that the shear stresses decrease, more rapidly than initially assumed, with radial distance along the depth of the pile; similarly, the radius r_m, will not be constant but also decrease with depth, as shown in Figure 3.9.

The assumption that the deformations in the soil below the level of the pile base will be the same as arising in a soil beneath a rigid punch seems to suggest that the value of r_m will depend not only on the length of the pile l but also on Poisson's ratio ν of the soil. This assumption brings another ambiguity in equation (3.8) that we cannot have a unique solution for the settlement of a rigid pile. However, to avoid this problem Randolph and Wroth (1978) ignored the variation of r_m with depth, and suggested an average value of $2.5l(1-\nu)$.

3.4.1.2 Modelling the base of the pile

Randolph and Wroth (1978) treated the base of a pile as a rigid punch. Since the available analytical solution corresponds to a rigid punch at the surface of an elastic half space, they introduced a depth factor, η in order to take account of stiffening effect of the soil above the level of the loaded area. The load settlement behaviour was described as (Timoshenko and Goodier (1970)):

$$w_b = \frac{P_b(1-\nu)}{4r_o G}\eta$$

where w_b is the displacement of the pile base.

The depth factor is the ratio of the stiffness of a rigid punch at the surface of an elastic half space to its stiffness at some depth below the surface.

Pile base can be modelled as either of these two possible ways. It can be treated as a rigid circular footing at the bottom of an open borehole or a loaded rigid circular area embedded in a soil mass at a depth, h. The appropriate model to consider is a loaded rigid circular area embedded at a depth h. A study conducted by Butterfield and Banerjee (1971) based on this model shows that the limiting value for the depth factor is 0.6. Randolph and Wroth (1978) suggested that this factor would be greater than 0.85 or close to unity for a straight (i.e., not underreamed) pile. They argued that there will be no stiffening effect of the soil above the level of the loaded area because the upper layer of soil is already being deformed by the action of shear stresses along the pile shaft. The pile is not capable of absorbing any of the load at its base (as would be a column of soil) since it is the means by which the load is transmitted to the base. In other words they considered the base of the pile as a loaded rigid circular area at the bottom of an open borehole. This seems to be a conservative approach. The load-settlement ratio was finally given by (adding together the contribution of the pile shaft and the base):

$$\frac{P_t}{Gr_o w_t} = \frac{P_b}{Gr_o w_b} + \frac{P_s}{Gr_o w_s} = \frac{4}{\eta(1-\nu)} + \frac{2\pi l}{\zeta r_o}$$

where P_t is the sum of the contributions from the pile base P_b and the pile shaft P_s.

The difficulty in the choice of a proper model for the pile base only arises when we consider two distinct soil layers, around the pile, deforming independently and interacting at a common boundary. In the new analytical method, explained in the following section, we do not have to worry about the choice of a model for the pile base.

3.4.2 Simplified analysis of a rigid single-pile: (proposed new method)

In this section a new analytical method is described. The soil is not considered to deform separately in two distinct horizontal layers. A pyramidal load transfer is assumed below the pile base which eliminates the need to consider the so-called magical radius r_m (at which the displacement are assumed to be zero). The outer boundaries of the soil are taken out to infinity. This load transfer mechanism is depicted in Figure 3.10.

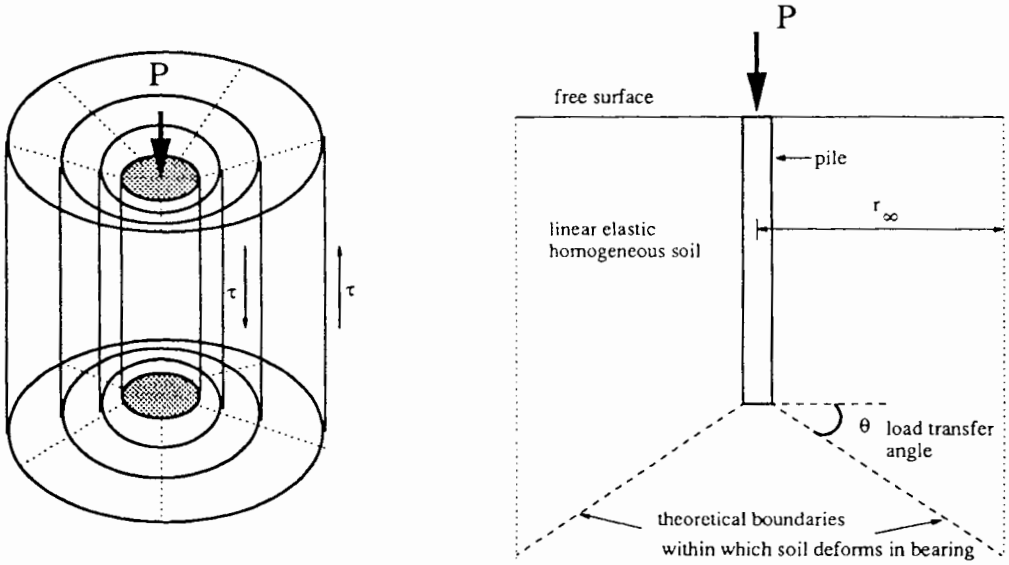

Figure 3.10: Load transfer mechanism adopted in the development of new analytical method

The load transfer line marks the boundary between the soil deforming due to shearing of concentric cylinders of varying depth (unlike constant depth as in Randolph and Wroth's (1978) analytical approach) around the pile shaft and the soil deforming in bearing below the level of the pile shaft. This boundary is not fixed but varies with the assumed load spread angle. Consider a vertical pile embedded in a linear elastic soil medium as shown in Figure 3.11. Due to axial symmetry, only half of the pile and the surrounding soil needs to be shown. Zone *A* will deform in shear and if we assume that loading of the pile generates uniform shear stresses along the boundary *XY* at a radial distance r_1 from the centre line, and the soil continues to an infinite radius to the right, beyond *XY*, where the shear stresses will

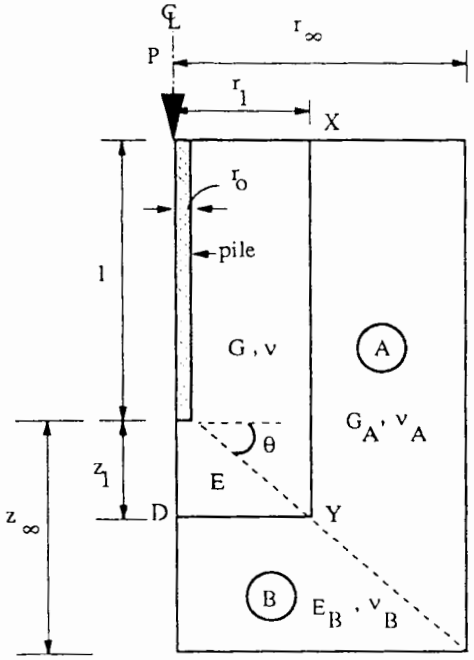

Figure 3.11: Zones of soil deforming in shear and bearing around a pile

be zero, it is possible to estimate vertical deformation at X as follows:

From the geometry of the problem, integration of the approximate equilibrium equation (3.7a) gives the shear stress τ at radius r, to be:

$$\tau = \frac{\tau_1 r_1 (l+(r_1-r_0)\tan\theta)}{r(l+(r-r_0)\tan\theta)}$$

where θ is the load transfer angle.

Applying the condition of elasticity, the vertical displacement at point X can be expressed in this integral form:

$$w_X = \int_{r_1}^{\infty} \frac{\tau}{G}\, dr.$$

Evaluating the integral analytically, the following expression is obtained for the vertical settlement of point X:

$$w_X \propto \frac{\tau_1 r_1 (l - r_0 \tan\theta + r_1 \tan\theta)}{G} \left[\frac{\tan\theta}{l\cot\theta - r_0} \cdot \ln \frac{r_1 + l\cot\theta - r_0}{r_1} \right] \tag{3.9}$$

where equation (3.9) represents an elaborated form of the new improved solution for the calculation of settlement of a rigid pile shaft. If the point X (see Figure 3.11) is located on the pile shaft i.e. $r_1 = r_o$ and $\tau_1 = \tau_o$ in equation (3.9), then once again we obtain equation (3.8) for the vertical displacement of a pile shaft with the following improvement:

$$\zeta = \frac{l}{l - r_o} \ln\left(\frac{l}{r_o}\right) \text{ for } \theta = 45°.$$

The improvement suggests that the vertical displacement of a pile shaft depends on the logarithm of the *slenderness ratio* of the pile and is not dependent on the empirically determined magical radius r_m.

Now consider a pyramidal load transfer beneath the pile base as shown in Figure 3.11. Zone B under the pile base will deform in bearing. If we assume a uniform normal stress σ, at a depth z_1, below the pile base, then, considering the geometry of the problem and satisfying the equilibrium condition, the vertical normal stress at any depth z, can be approximately written as:

$$\sigma(z) \propto \frac{\sigma r^2_1}{(r_1 + (z - z_1)\cot\theta)^2}.$$

(It is important to note that the above expression does not require any choice of model for the pile base as was needed in the earlier work presented by Randolph and Wroth (1978).) The settlement of point D, assuming soil of infinite extent, can be estimated by evaluating the following integral expression:

$$w_D \approx \int_{z_1}^{\infty} \frac{\sigma(z)}{E} dz$$

where E is the stiffness (Young's modulus) of the soil underneath the pile base.

The analytical evaluation of this integral gives an approximate stiffness of the zone B:

$$w_D = \frac{\sigma r_1}{E \cot\theta}. \qquad (3.10)$$

The vertical settlement of the pile shaft (equation (3.9)) and the pile base (equation (3.10)) will be the same for the conditions assumed above that the pile is rigid, point X lies on the pile-soil interface and D lies at the centre of the pile base. If we keep to our assumption that $r_1 = r_o$ and $\sigma = \sigma_o$ then adding the contribution of load carried by the pile shaft and the base from equations (3.9) and (3.10), the pile head load-settlement ratio can be written as given below:

$$\frac{P}{G r_o w} = \frac{2\pi l}{\zeta r_o} + 2\pi(1+\nu) \qquad \text{for } \theta = 45°.$$

3.4.3 Comparison of results

Load-settlement versus slenderness ratios for rigid and flexible piles are plotted in Figures

3.12 and 3.13, along with the results obtained from Randolph and Wroth's (1978) analytical solution and Poulos and Davis's (1980) integral equation method.

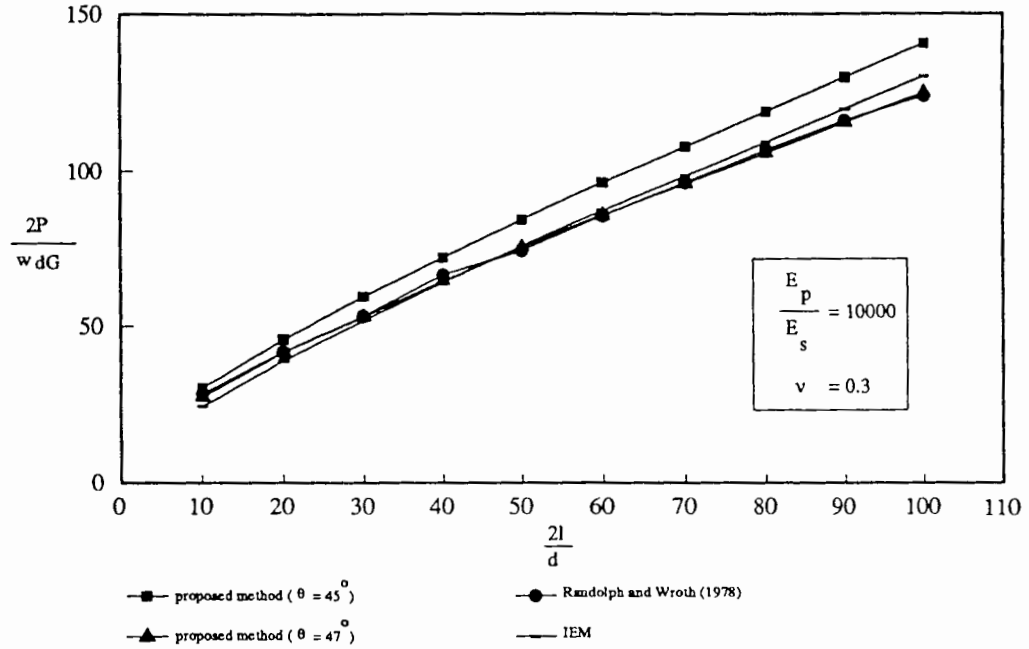

Figure 3.12: Load-settlement ratios for rigid piles

Figures 3.12 and 3.13 show that the assumed load spread angle of 45°, in the present analysis, provides a stiffer pile response compared to the one obtained from Randolph and Wroth's (1978) solution, for rigid and flexible piles. As mentioned in Section 3.4.1.2, perhaps Randolph and Wroth's solution (1978) is conservative due to the model they have adopted for the pile base. (However, the assumed load spread angle can be adjusted to give a less stiff response. A load spread angle of 47 ° provides an exact match with the Randolph and Wroth's (1978) solution for the rigid piles. It is therefore seen that Randolph and Wroth's (1978) approach is a special case of the above analysis.) Nevertheless, for the case of flexible piles, the results from the present analysis match well with Poulos and Davis (1980) results.

In the following Sections 3.5.1 and 3.5.2, the development of two correcting layers to be used in the finite element analyses, one around the pile shaft and the other below the pile base, is explained. The properties of the two correcting layers are derived using the above analytical

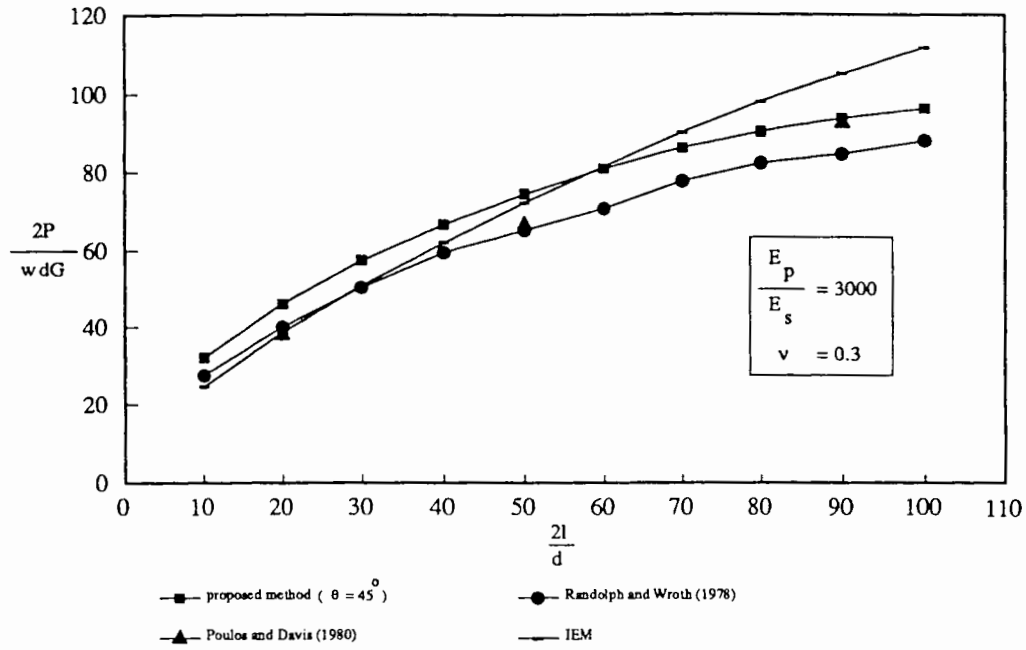

Figure 3.13: Load-settlement ratios for flexible piles

approach. Section 3.5.3 shows how successfully the correcting layers model the infinite boundaries in the finite element analyses.

3.5 Finite element analysis using correcting layer approach

In this section, the results obtained from the integral equation analysis are compared with the finite element analysis results. The finite element analysis has a problem of fixed boundaries which effect the results. We can reduce the effect of boundaries by having softer layers (correcting layers) adjacent to the boundaries. Although in this case it is difficult to derive exact expressions for material properties in the softer layers but it is possible to use the proposed analytical method to obtain approximate values of reduced stiffness which are thought to reduce the effect of rigid boundaries.

The comparison of results given in Section 3.5.3 shows that two correcting layers, one around the pile shaft and the other below the pile base, successfully model the infinite boundaries in

the finite element analyses.

3.5.1 Development of the correcting layer around the pile shaft

Let us consider again the vertical pile embedded in a linear elastic soil medium as shown in Figure 3.14. Due to axial symmetry, only half of the pile and the surrounding soil needs to be shown. We know that Zone *A* of an infinite extent will deform in shear and the vertical settlement of point *X* can be approximately written as:

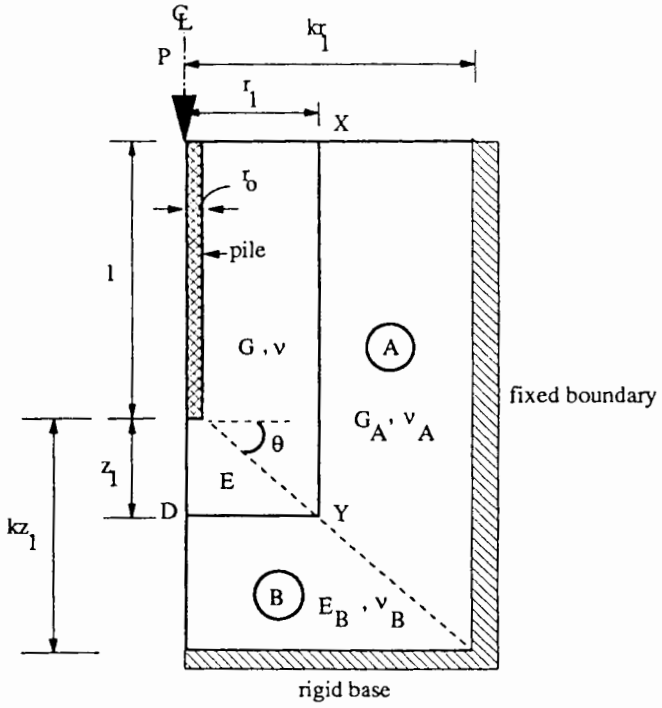

Figure 3.14: Shaft and base correcting layers

$$w_X \simeq \frac{\tau_1 r_1 (l - r_0\tan\theta + r_1\tan\theta)}{G}\left[\frac{\tan\theta}{l\cot\theta - r_0} \cdot \ln\frac{r_1 + l\cot\theta - r_0}{r_1}\right] \tag{3.9}$$

Now if the value of shear modulus G is modified, making the zone A more flexible than the rest of the soil, the outer (zero displacement) boundary moves closer from infinity to a distance kr_1 from the centre of the pile. In other words displacements dampen out quickly by making the zone softer. This modification leads to a new integral expression for the vertical displacement of point X:

$$w_X = \int_{r_1}^{kr_1} \frac{\tau}{G_A} \cdot dr.$$

Analytical evaluation of this integral gives:

$$w_X = \frac{\tau_1 r_1 (l - r_0 \tan\theta + r_1 \tan\theta)}{G_A} \left[\frac{\tan\theta}{l\cot\theta - r_0} \cdot \ln \frac{k(r_1 + l\cot\theta - r_0)}{kr_1 + l\cot\theta - r_0} \right]. \qquad (3.11)$$

Theoretically, w_X from equations (3.9) and (3.11) must be equal as both the equations represent the same definite integral having an upper limit, a radius where displacements are zero. If that is so, the value of shear modulus for the zone A can be obtained from the following expression:

$$G_A = G \cdot \ln \frac{k(r_1 + l\cot\theta - r_0)}{kr_1 + l\cot\theta - r_0} \left[\ln \frac{r_1 + l\cot\theta - r_0}{r_1} \right]^{-1}.$$

For an assumed value of k, values of G_A and ν_A can be obtained from the above expression.

There are three finite element meshes used in the analyses presented in Section 3.5.3. Typical values of G, G_A, ν_A for the smallest mesh are 250000 kPa, 79800 kPa, 0.25, respectively, with a load spread angle of $\theta = 45^o$, $k = 2$, $\frac{l}{r_o} = 40$ and $r_1 = 10r_o$.

3.5.2 Correcting layer under the pile base

Figure 3.15 shows a pyramidal load transfer beneath the pile base. Zone B under the pile base will deform in bearing and we know that the settlement of point D assuming soil of infinite extent can be estimated by the following expression:

$$w_D = \frac{\sigma r_1}{E\cot\theta}. \tag{3.10}$$

If the elastic modulus for the layer B is now modified by making it softer, as we did for zone A, the boundary at infinity moves to a distance kz_1 from the base of the pile and the displacement of point D can be expressed in the integral form as given below:

$$w_D = \int_{z_1}^{kz_1} \frac{\sigma(z)}{E_B} dz.$$

The analytical evaluation of the integral yields:

$$w_D = \frac{\sigma r_1}{E_B \cot\theta}\left[1 - \frac{r_1}{r_1 + (k-1)z_1\cot\theta}\right] \qquad (3.12)$$

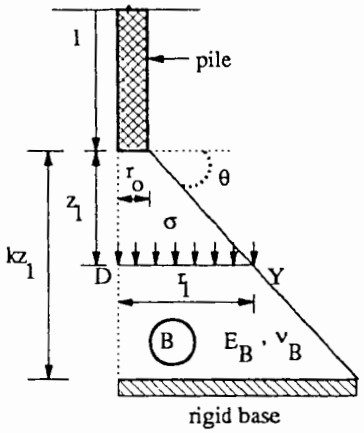

Figure 3.15: Base correcting layer

Now if we equate w_D from equations (3.10)and (3.12) the modulus for the base correcting layer can be found from this expression:

$$E_B = E\left[1 - \frac{r_1}{r_1 + (k-1)z_1\cot\theta}\right].$$

Again by choosing a reasonable value of k the values for the modulus can be obtained, from the above expression, for the base correcting layer. For the three finite element meshes used in the analyses described in Section 3.5.3, the typical values of E, E_B, ν_B for the smallest

mesh are 745000 kPa, 352400 kPa, 0.49, respectively, with a load spread angle of $\theta = 45^{o}$, $k = 2$, $\frac{l}{r_o} = 40$ and $r_1 = 10r_o$.

3.5.3 Finite element analysis results

Figure 3.16 shows an axi-symmetric finite element mesh. The pile, the soil and the correcting layers are modelled with 182 eight-noded quadrilateral elements (CAX8) included in the element library of ABAQUS (version 4.6 from Hibbitt, Karlsson and Sorensen, Inc., Providence, Rhode Island), the commercial finite element package used for this analysis. The rigidity index G/s_u is equal to $5*10^3$ and a Poisson's ratio of 0.49 is used for the soil i.e. an undrained or total stress analysis is performed. The mesh is quite coarse which will affect the accuracy of the finite element results. As we said at the beginning, our main emphasis here is to select a suitable method for the analysis of axially loaded piles - detailed discussion of mesh refinements is omitted for that reason. The present analysis is not intended to inspect the possibility of slippage at the interface therefore pile-soil boundary has not been modelled using zero thickness interface elements (see e.g. Cheung *et al.* (1991)). Although, interface elements are helpful in obtaining stresses at the pile-soil boundary, a simple way of extracting shear stresses at the pile-soil boundary described by Burd (1986) has been adopted. In this method only the force at the midside node is used to determine the shear stress at the element boundary. The total shearing force acting on the element side is3/2 of the midside nodal force of the element and calculation of shear stress on the element boundary becomes quite straightforward

In the present axi-symmetric finite element analysis, the shear stresses and the vertical displacements down the pile are compared with those obtained by the integral equation method. The results correspond reasonably well and are shown in Figures 3.17 and 3.18. Various mesh sizes are shown in brackets at the bottom of these figures. The shear stresses

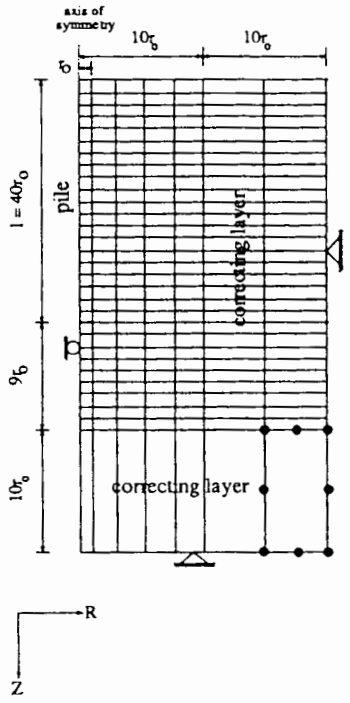

Figure 3.16: Finite element mesh with two correcting layers

obtained using these methods agree quite well with each other except near the top and bottom of the pile. This suggests that a more refined discretisation of soil-pile boundary in those areas is required in both the integral equation method and the finite element method. The trend in question was also noted by Evangelista and Viggiani (1976) who reported that the accuracy of the results from the integral equation method improves by varying the size of the pile-soil boundary discretisation down the pile. For the displacements, on the other hand, no similar close agreement is observed. The discrepancy within the displacements arises from the coarse discretisation of the meshes, the inherent approximations involved in these methods and the approximate analysis used for obtaining the properties of the correcting layers.

Figure 3.18 shows that, for larger mesh dimensions, the agreement between the results of the integral equation method and the finite element method is much closer than for the smaller mesh dimensions. As we can see from Sections 3.5.1 and 3.5.2 that the properties of the base correcting layer depend on the choice of load spread angle. The gap between the results from the integral equation method and the finite element analysis using correcting layers will

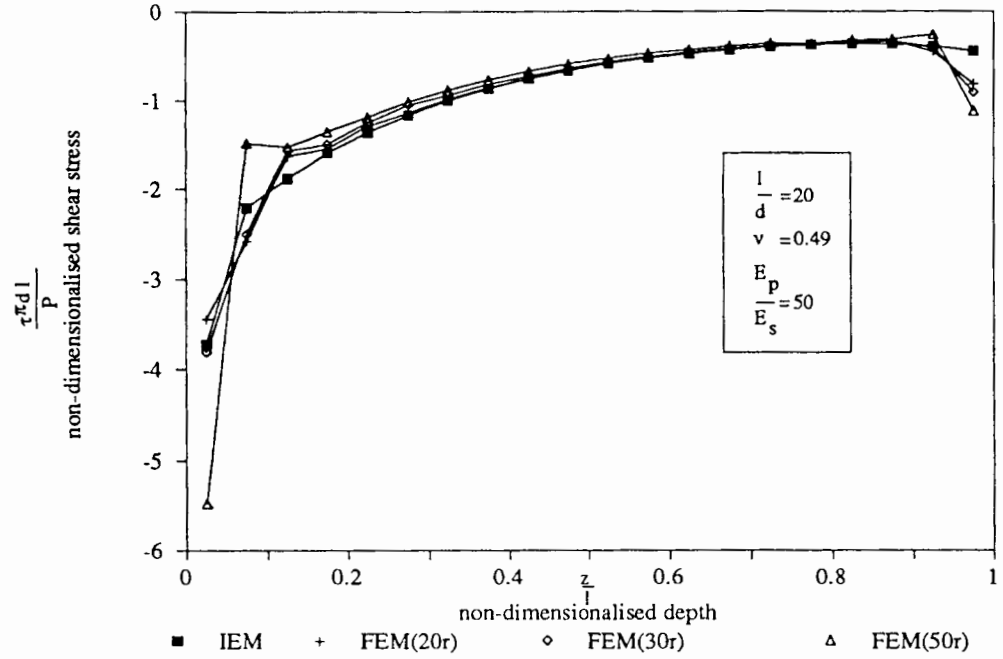

Figure 3.17: Shear stress distribution along the length of a flexible pile

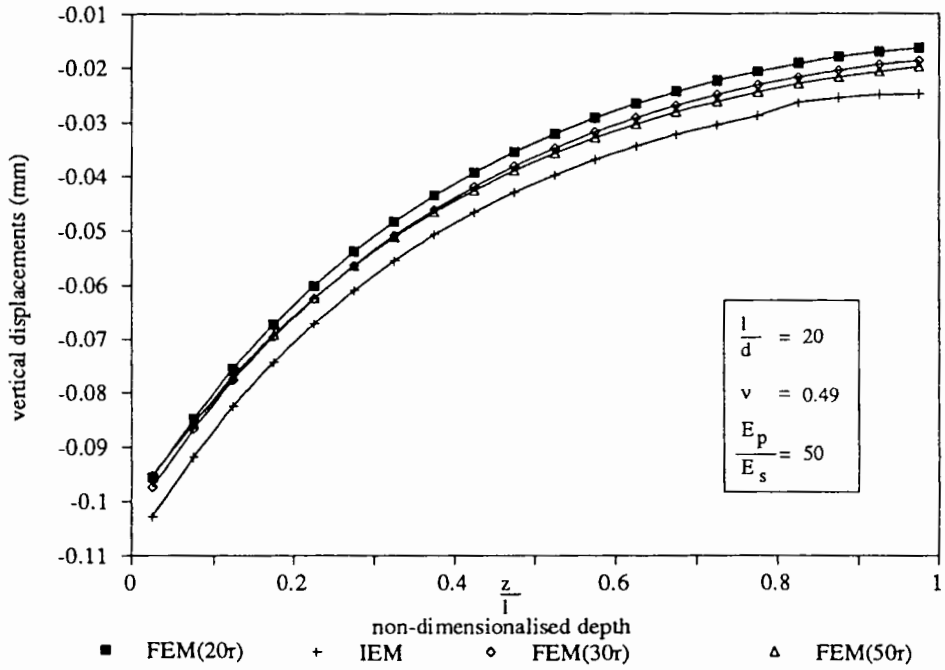

Figure 3.18: Vertical displacement profile of a flexible pile

diminish, giving an excellent match between the two curves if a load spread angle of 47

degrees is chosen. However, some discrepancy between these two sets of results will remain. This is not unexpected as the integral equation method and the development of correcting layers are based on different underlying assumptions. With the revised properties of the base correcting layer i.e. using a load spread angle of 47°, even the smallest mesh is sufficient to obtain results of reasonable accuracy - the difference between the results from these methods (shown in Figures 3.17 and 3.18) is almost the same as we can see in Figures 3.12 and 3.13. This proves that the correcting layer approach significantly reduces the problem size in a finite element analysis. In the particular problem here described, the mesh dimensions are less than half of those previously adopted (e.g., Randolph (1977); Baguelin and Frank (1980)). A trend opposite to that shown in Figure 3.17 can be observed in Figure 3.18. This is due in part to the reasons given above, and in part to improper modelling of the pile-soil boundary.

3.6 Conclusions

The validity of the integral equation method (or the quasi boundary element method) for the analysis of pile foundations is conditional on the assumption that the piles are embedded in a linear elastic soil medium, and spaced widely enough for each pile to be outside the radius of influence of its neighbour. The pile-soil interactions are assumed to be elastic and considered only at the pile cap level. However, in closely spaced pile groups or even for a single-pile, the condition of elastic interactions no longer apply, and therefore linear elasticity is not suitable to model the soil behaviour. It follows that the semi-analytical approach given by Randolph and Wroth (1978), (1979a) for the behaviour of a single-pile and pile groups is no longer satisfactory. A more refined constitutive soil model is required for the real life situation. One possible extension of the boundary element method to incorporate plasticity is tested in this chapter. However, as we have seen, such an extension makes the method inefficient: it loses the advantage of requiring only the boundary discretisation of the domain (whereas FEM always requires discretisation of both surface and interior of the domain), and it therefore loses the merit of a smaller system of algebraic equations than is needed in the

finite element method. The algorithm to incorporate plasticity and the overall solution procedure becomes similar to that of the finite element method which is already well established. Moreover, the architecture of a boundary element computer program is not conceptually as easy as the one for the finite element method. In addition, strong numerical singularities arise in the formulation of the boundary element method which restrict its further development. For all these reasons, the choice has to be the finite element method. The correcting layer approach for the modelling of infinite boundaries in the finite element mesh for the analysis of a single vertical pile under axial loading is quite successful. It not only models the infinite boundaries quite well but also helps to reduce the overall size of the problem significantly (for comparison see Figures 3.2 and 3.16). The analysis of pile groups can therefore be computationally much less expensive.

Finally, it is worth emphasising that, in an offshore environment, piles are subjected to not only vertical but also horizontal and moment loading. Proper interface analysis for vertical loading was deliberately omitted in this chapter as irrelevant for the simplified problem considered in the axi-symmetric two-dimensional finite element model.

APPENDIX 3A

Determination of influence coefficients

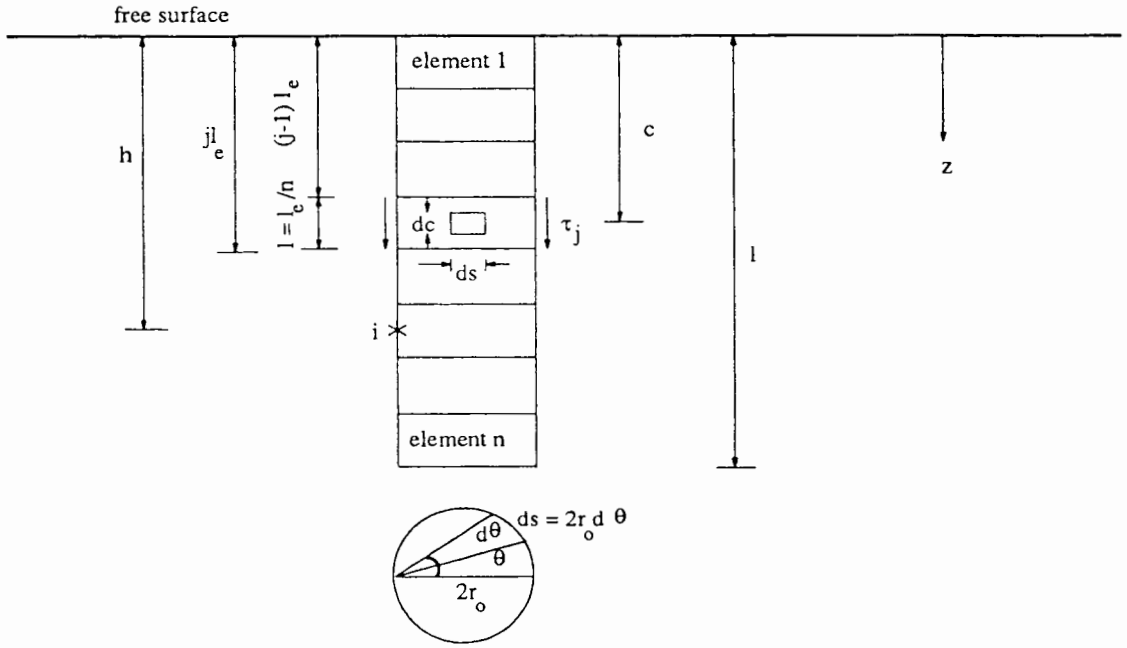

Figure 3A-1: Geometry of a typical pile

The geometry of a typical pile element is shown in Figure 3A-1. For the point i at the mid height of the i th element on the periphery of the pile of radius r_o, the influence factor for vertical displacement due to the uniform shear traction on the j th element is:

$$f_{ij} = 4r_o \int_{(j-1)l_e}^{jl_e} \int_{0}^{\pi/2} I_m \, d\theta \, dc \qquad (3A.1)$$

where

l_e = length of the pile element, and

I_m = influence factor for vertical displacement due to a vertical load, which is taken from Mindlin's equation, as follows:

$$I_m = \frac{1}{16\pi G(1-\nu)}\left(\frac{z^2_1}{R^3_1} + \frac{(3-4\nu)}{R_1} + \frac{(5-12\nu+8\nu^2)}{R_2} + \frac{((3-4\nu)z^2-2cz+2c^2)}{R^3_2} + \frac{6cz^2(z-c)}{R^5_2} + \frac{6cz^2(z-c)}{R^5_2}\right) \quad (3A.2)$$

where

$z = h+c$ (h and c are defined in Figure 3A-1.)

$z_1 = h-c$

$R_1^2 = 4r_o^2\cos^2\theta + z_1^2$

$R_2^2 = 4r_o^2\cos^2\theta + z^2$.

The integral with respect to c in equation (3A.1) is evaluated analytically and the integral with respect to θ is evaluated numerically using Simpson's rule.

The geometry of the pile base is shown in Figure 3A-2. For the element i on the shaft, the influence factor for vertical displacement due to uniform loading at the base is given as:

$$f_{ib} = \int_0^{2\pi}\int_0^{r_o} I_m r dr d\theta \quad (3A.3)$$

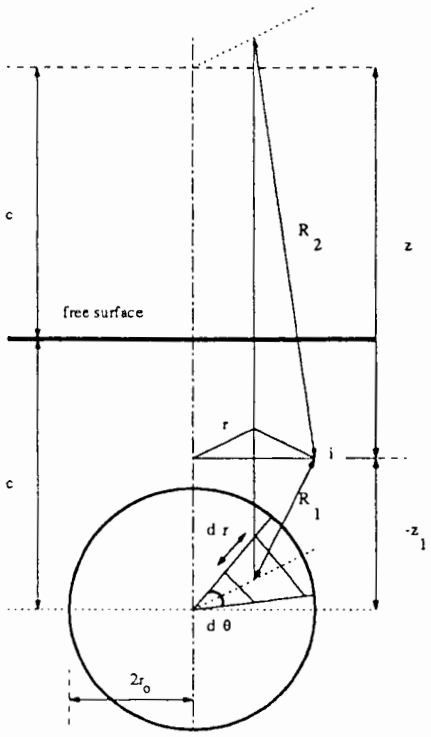

Figure 3A-2: Geometry for integration over circular area

where I_m is given by equation (3A.2), but now

$$c = l$$

$$R_2^2 = z^2 + r_o^2 + r^2 - 2r\, r_o \cos\theta$$

$$R_1^2 = z_1^2 + r_o^2 + r^2 - 2r\, r_o \cos\theta .$$

Again the integration with respect to r is carried out analytically and integration with respect to θ is evaluated by Simpson's rule.

The integral for the flexibility coefficient for the displacement at the centre of the base resulting from shear traction on a shaft element j is given by:

$$f_{bj} = 2\pi r_o \int_{(j-1)l_e}^{jl_e} I_m \, dc .$$

This integral can be evaluated analytically.

For the vertical displacement of the base associated with the stresses on the base itself, the integral for the flexibilty coefficient for the base is:

$$f_{bb} = \frac{\pi}{4} \cdot \frac{\pi}{r_o} \int_0^{r_e} I_m \, r dr$$

where

$c = l$

$R_2^2 = 4c^2 + r^2$

$R_1 = r$

$z_1 = 0.$

The analytical evaluation gives:

$$f_{bb} = \frac{\pi}{4} \cdot \frac{1}{16G(1-\nu)r_o} \left((3-4\nu)r_o + (5-12\nu+8\nu^2)(R-z) + \frac{(5-8\nu)}{2} z^2 \left(\frac{1}{z} - \frac{1}{R}\right) + \frac{z}{2} - \frac{z^4}{2R^3}\right)$$

where

$R^2 = (z^2 + r_o^2)$

CHAPTER 4

INTERFACE ANALYSIS

4.1 Introduction

In order to proceed with the detailed analysis of interactions between the pile and the soil, it is necessary to consider the interface between them. The main reason for carrying out an interface analysis is to model the possibility of loss of contact between them near the ground surface. Soil close to the pile under such a situation is highly constrained in front of the pile and stretched at the back of the pile where it has the tendency to break away from the pile. An additional advantage of having an interface element is to extract the stresses at the pile-soil interface, which are the key to the understanding how the problem is behaving. In Chapter 3, the objective was to select a suitable numerical method for the analysis of a single vertical pile under axial loading considering the simplest possible case. No attention was given to performing a complex interface analysis to extract the stresses at the pile-soil interface.

In this chapter, a purely cohesive interface element to model small relative slip and loss of contact at the back of the pile is developed and validated by verifying various test problems. It is also quite useful in extracting stresses at the interface. It is important to have suitable test problems where we have loss of contact between bodies of two dissimilar materials. One such problem considered in this chapter is a plane strain surface footing subjected to combined vertical and moment loading. The footing experiences an uplift force which causes a partial loss of footing contact with the ground surface. An approximate solution has been given by

Hansen (1970) which is modified to take account of the uplift force acting on the footing which arises due to the applied eccentric loading. The interface element has been successful in modelling the uplift force and the results match with the modified Hansen's (1970) solution. In the next chapter, the response of a single-pile under lateral loading in a purely elastic, cohesive material will be studied.

4.2 Background

In a finite element analysis, the interface between bodies of two dissimilar materials needs special attention. If, a perfect bonding is maintained between the bodies, an interface analysis is useful to extract stresses at the interface. But if, at some point in the loading history, the bond between the two contacting bodies breaks down then an interface analysis is necessary to model either slip between the two bonding surfaces, such as the rigid pile and the soil continuum shown in Figure 3.16 or in addition to slip, loss of contact as in the case of a laterally loaded pile. Conventional continuum elements have often proved inadequate in modelling relative slip and loss of contact between two bodies of dissimilar materials (see e.g. Gens *et al.* (1989) and Bell (1991)). Interface elements have been applied comparatively successfully. They have been applied, typically, to the problem of modelling jointed rock masses (Goodman *et al.* (1968)), or to the simulation of particular soil-structure interface behaviour in, e.g., piles (Zaman (1985)), footings (Bell (1991)) and two-layer soil systems separated by soil reinforcement (Brocklehurst (1993)).

Basically there are two types of analysis procedure to deal with the two bodies in contact with each other. One works on the constraint approach in which the two contacting bodies are treated independently and allowed to meet at the mutual boundary satisfying some contact constraints. It is quite a powerful method which does not allow interpenetration of the two contacting bodies. But it has the disadvantage that it does not automatically provide interface stresses i.e. there is no obvious way of storing the stresses at the interface. This approach

follows an iterative solution procedure e.g. as described by Katona (1983), who models the friction interface between the two contacting bodies as sequence of node pairs. The different states of the interface i.e. stick, slip and debonding are imposed through a constraint matrix. (Earlier, a similar model for the interface behaviour 'linkage elements' was presented by Frank *et al.* (1982) in which only the connections between opposite nodes are considered.) Moore and Booker (1989) and Kodikara and Moore (1991) adopted a similar approach to model circular tube-soil interface. They suggest using a non-linear frictional-adhesive zero-tension interface model at the boundary between the two separate bodies, rather than employing a discrete interface element. The technique they presented is capable of capturing large rotations and slipping as well as the occurrence or loss of contact at the interface. (However, large relative slip is not an important characteristic of the problem under consideration here, therefore, this model will not be pursued in this chapter.) The second type of procedure is based upon the stiffness approach, as described by Goodman *et al.* (1968), which falls more naturally into the finite element formulation. In Goodman *et al.* (1968), the interface element is said to have zero thickness, as also in the work of Gens *et al.* (1989) and Burd and Brocklehurst (1991). The relative displacements between opposite nodes become primary deformation variables instead of movements at the nodal points, and observe elastic or elasto-plastic constitutive behaviour. The interface element can also have a finite thickness, as proposed by Desai *et al.* (1984), who called it a 'thin layer element'. The element works more like a continuum element of small finite thickness. It represents a thin layer of material between two bodies and seems suitable for jointed rock masses. The element exhibits a non-linear elastic plastic behaviour. The values for the normal stiffness and the thickness of the interface are suggested, following parametric studies. The shear stiffness is determined from a laboratory direct shear test but no suggestions have been made for choosing cross coupling terms. The idea of a 'thin layer element' is derived from the early work presented by Zienkiewicz *et al.* (1970). They introduced quasi-continuum elements possessing a weakness plane in the direction of the interface plane. However, it has been reported by Ghaboussi *et al.* (1973) that numerical difficulties may arise from ill-conditioning of the stiffness matrix

due to very large off-diagonal terms or very small diagonal terms which are generated by these elements in certain cases. Within the stiffness approach, the most obvious way of modelling interfaces is to use standard continuum finite elements of small thickness. Griffiths (1985) demonstrated the suitability of a thin eight-noded quadratic element with an aspect ratio of up to 100, by analysing interface behaviour in various geotechnical problems. Griffiths reported that as the aspect ratio is increased to 1000, a much tighter tolerance for convergence is required than would be required in normal usage of elements other than interface elements. Finally, Herrmann (1978) presented an analysis procedure which combines the constraint and the stiffness approach.

For the problem being tackled here, the stiffness approach is obviously preferable to the constraint approach and to the combination of them proposed by Herrmann (1978). In the analysis which follows, a purely cohesive interface element is described. It is adapted from Goodman *et al.* (1968) for undrained clays, just as Burd and Brocklehurst (1991) adapted this approach for sands to study the interface stresses in a two-layer soil system. It will be used to study the pile-soil interface behaviour in clays under lateral loading in the next chapter.

4.3 Six-noded isoparametric interface element formulation

In this section, a zero thickness, six-noded isoparametric interface element which is kinematically compatible with a six-noded linear strain triangular element (used for the plane strain finite element analyses in Chapter 5) is described. The geometry of the parent element and the mapped element is shown as Figure 4A-1 in Appendix 4A. The element geometry consists of three pairs of nodes sharing the same coordinates. However, within each pair, the nodes have independent degrees-of-freedom. The corner nodes are numbered 1-4, 2-5 and the middle nodes carry node numbers 3-6 such that the difference between the bottom node number and the corresponding top node number is three. The bottom nodes of the interface elements are connected to the corresponding continuum nodes in the finite element meshes

shown in this chapter. As all the finite element analyses are displacement controlled, the imposed displacements are applied to the top interface nodes.

4.3.1 Kinematic equations

Although details about the kinematics of the element can be found elsewhere (Burd and Brocklehurst (1991)), the basic equations are repeated here for convenience. Figure 4.1(a) shows two coincident arbitrary points, a and b, lying on the element sides A and B. The vector of the global co-ordinates of the two points in the element is $\underset{\sim}{x}^T = [\, x_a \; y_a \; x_b \; y_b \,]$, and is related to the vector of global nodal co-ordinates $\underset{\sim}{X}$ by:

$$\underset{\sim}{x} = [N]\underset{\sim}{X} \tag{4.1}$$

where $[N]$, the shape function matrix, is a function of α. The elements of this matrix are given in Appendix 4A. (Note that the co-ordinates $(x_a \; y_a)$ are identical to $(x_b \; y_b)$.)

Similarly, the vector of relative velocities $\underset{\sim}{u_r}^T = [u_r \; v_r]$ is given by the matrix equation:

$$\underset{\sim}{u_r} = [B] \; \underset{\sim}{U} \tag{4.2}$$

where $[B]$ relates the vector of nodal velocities, $\underset{\sim}{U}$, to the vector of relative velocities at a point in the interface, $\underset{\sim}{u_r}$, and is given in Appendix 4A.

$f(\underset{\sim}{\sigma})$, defined by:

$$f(\underset{\sim}{\sigma}) = |\tau| + c = 0 \tag{4.5}$$

where c is the cohesion at the interface. The vector of stress is denoted by $\underset{\sim}{\sigma}$ and $|\tau|$ is the absolute value of shear stress. The dotted line in Figure 4.2 marks the tension cut-off, the stress at which we get a sudden loss of contact. This line is not part of the yield surface i.e. we can use the equations of plasticity everywhere on the yield surface and not on the dotted line. The plastic potential in this analysis is assumed to be identical to the yield function (i.e. plastic flow is fully associated):

$$g(\underset{\sim}{\sigma}) = |\tau| + c \tag{4.6}$$

where c is the cohesion of the interface.

An associated flow rule requires that the plastic potential is the same as the yield function (i.e. $g(\underset{\sim}{\sigma}) = f(\underset{\sim}{\sigma})$). Therefore, the plastic relative velocities will lie normal to the yield surface.

The vector of stress, $\underset{\sim}{\sigma}$, of an arbitrary point in the interface can be differentiated with respect to time (denoted by a superior dot), to give the stress rate vector, $\dot{\underset{\sim}{\sigma}}^T = [\dot{\tau}\ \dot{\sigma}]$. This is then related to the relative velocities, $\underset{\sim}{u_r}$, by the expression:

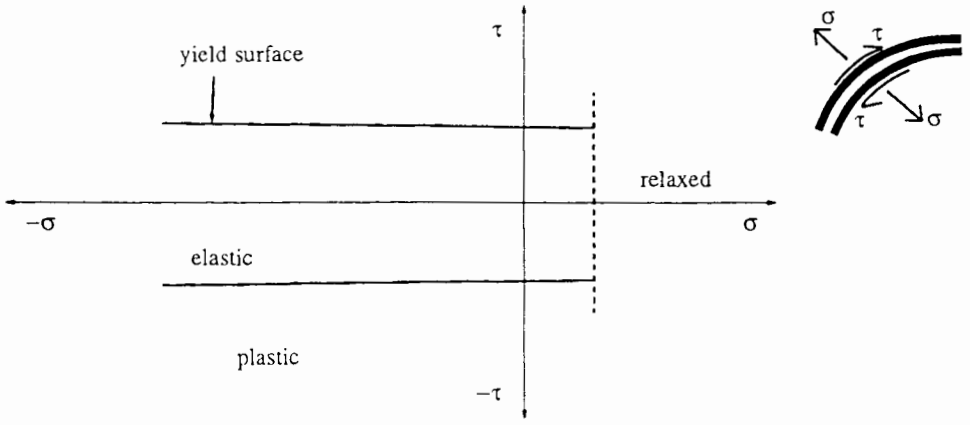

Figure 4.2: Yield surface with an allowable tension cutoff

$$\underset{\sim}{\sigma} = [D]^{EP} \underset{\sim}{u_r}$$

or substituting equation (4.2)

$$\underset{\sim}{\sigma} = [D]^{EP} [B] \underset{\sim}{U} \tag{4.7}$$

where $[D]^{EP}$ is the elasto-plastic material stiffness matrix and is expressed in terms of the elastic component of the material stiffness matrix $[D]^{E}$ and the plastic component $[D]^{P}$ thus:

$$[D]^{EP} = [D]^{E} + [D]^{P} \tag{4.8}$$

Note that the interface element relative velocities are analogous to strain in continuum mechanics.

The elastic material stiffness matrix is essentially the same as that proposed in the original work proposed by Goodman *et al.* (1968), which is given by:

$$[D]^E = \begin{bmatrix} k_s & 0 \\ 0 & k_n \end{bmatrix} \tag{4.9}$$

The parameters k_s and k_n represent, respectively, shear and normal stiffness of the interface.

The plastic material interface stiffness matrix is derived from the approach conventionally adopted for continuum elements (e.g. Burd (1986)) and is given by:

$$[D]^P = \frac{-[D]^E \left[\frac{\partial g}{\partial \underset{\sim}{\sigma}}\right]\left[\frac{\partial f}{\partial \underset{\sim}{\sigma}}\right]^T [D]^E}{\left[\frac{\partial f}{\partial \underset{\sim}{\sigma}}\right]^T [D]^E \left[\frac{\partial g}{\partial \underset{\sim}{\sigma}}\right]} \tag{4.10}$$

This equation (4.10) involves the assumptions that the relative velocities can be decomposed into elastic and plastic parts and that the stress rate is related to elastic relative velocities. The yield function, $f(\sigma)$, is given in equation (4.5), and the plastic potential $g(\sigma)$ in equation (4.6) is used to define the plastic relative velocities, using equations of the form:

$$u_r^P = \lambda \frac{\partial g}{\partial \tau} \tag{4.11}$$

$$v_r^P = \lambda \frac{\partial g}{\partial \sigma} \tag{4.12}$$

where λ is an undetermined multiplier.

Although it is possible to calculate $[D]^{EP}$ using the standard approach but following the experience of Brocklehurst (1993) it is kept equal to $[D]^{E}$ to make the calculations better conditioned i.e. a localised initial stress approach is adopted for this part of the finite element calculations.

4.3.3 Finite element equations

If a set of virtual velocities $\underset{\sim}{U}^{*}$ are applied to the nodes of the element, then by the principle of virtual work:

$$\underset{\sim}{U}^{*T}\,\underset{\sim}{P} = \int_{E} \underset{\sim}{u_r}^{*T}\underset{\sim}{\sigma}\, dA \tag{4.13}$$

where $\underset{\sim}{u_r}^{*}$ are the relative velocities compatible with the virtual nodal velocities, $\underset{\sim}{U}^{*}$ and $\underset{\sim}{P}$, is the vector of nodal forces which are in equilibrium with the stresses $\underset{\sim}{\sigma}^{T} = [\tau\ \sigma]$. The element surface area, dA, is given by:

$$dA = J\, d\alpha \tag{4.14}$$

where J is the Jacobian or transformation matrix (see Appendix 4A).

It follows, therefore, that the virtual work equation (4.13) can be re-written, substituting the relative velocities vector as given in equation (4.2), as:

$$\underset{\sim}{U}^{\bullet T}\ \underset{\sim}{P} = \int_E \underset{\sim}{U}^{\bullet T}[B]^T \underset{\sim}{\sigma}\ J\ d\alpha. \tag{4.15}$$

Since this expression must hold for arbitrary nodal velocities $\underset{\sim}{U}^{\bullet}$, it follows that:

$$\underset{\sim}{P} = \int_E [B]^T \underset{\sim}{\sigma}\ J\ d\alpha. \tag{4.16}$$

Equation (4.16) is differentiated with respect to time to give an expression for the nodal force rate, giving:

$$\dot{\underset{\sim}{P}} = \int_E [B]^T \dot{\sigma} J d\alpha. \tag{4.17}$$

The term in the integrand may be used to derive conventional infinitesimal displacement stiffness matrix (Zienkiewicz (1977)) by substituting equation (4.7) and writing $\dot{\underset{\sim}{\sigma}}$ in terms of nodal velocities, which gives:

$$\dot{\underset{\sim}{P}} = \int_E [B]^T\ \dot{\underset{\sim}{\sigma}}\ J\ d\alpha = \int_E [B]^T\ [D]\ [B]\ \underset{\sim}{U}\ J\ d\alpha \tag{4.18}$$

where $[D]$ will be either $[D]^E$ or $[D]^{EP}$ depending upon the state of stresses (elastic or plastic) during the analysis.

The nodal force rate (equation (4.17)) can therefore be simplified to:

$$\underset{\sim}{\dot{P}} = [K]\ \underset{\sim}{U} \tag{4.19}$$

where $[K]$ is the incremental stiffness matrix given by:

$$[K] = \int_E \left([B]^T\ [D]\ [B]\ J\right)\ d\alpha. \tag{4.20}$$

4.3.4 Stress update calculations

The finite element calculations are typically conducted as a series of steps for a particular prescribed displacement, or prescribed force, or a mixture of the two. At the end of each load step, corresponding to a finite time increment Δt, the updated normal and shear stresses associated with the calculated relative velocities are determined by a 'stress update procedure'. This gives the out-of-balance nodal forces that are needed for incremental solution procedure and provides a check on the general equilibrium of the system. The computed final stresses are characterised into different states according to their position in stress space relative to the failure envelope shown in Figure 4.3. The three possible states are denoted as Elastic, Plastic and Relaxed as indicated in Figure 4.3.

The length of the increment of time for each load step, Δt is normalised into a time interval of unity. At the start of a load step Δt=0; at the end Δt=1 In order to calculate Gauss point stresses at the end of a load step, the response of each Gauss point is assumed, initially, to be elastic, regardless of initial state. The relevant final stresses τ and σ, are calculated using the elastic material stiffness matrix $[D]^E$ in equation (4.9), giving:

$$\tau = \tau_o + k_s u_r \Delta t \tag{4.21}$$

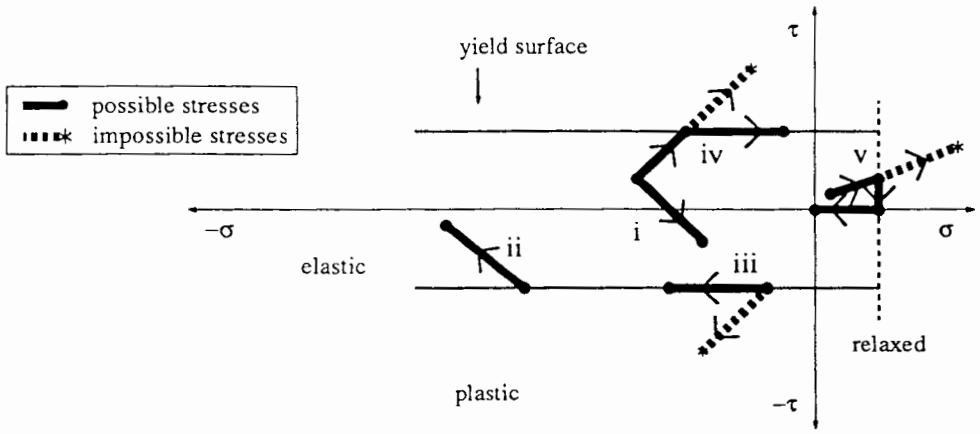

Figure 4.3: Yield surface and possible cases of constitutive behaviour

$$\sigma = \sigma_o + k_n v_r \Delta t \tag{4.22}$$

where τ_o and σ_o are the initial Gauss point stresses, and $\Delta t = 1$. This assumption of a purely elastic stress update is then checked to ensure that the final stresses, τ and σ, do not violate the failure conditions:

1) If $|\tau/c| > 1$ then the updated stress point has yielded and must be re-analysed plastically beyond the point at which the stress path intersects the yield surface.

2) If $\sigma \geq \sigma_t$ (σ_t is the allowable tension cut-off) then separation of the interface has occurred during the load step and the stress point is relaxed by setting the stresses to zero; i.e. $\sigma = \tau = 0$.

Given that the initial stress state is either elastic and lies inside the failure envelope, or plastic and lies on the failure envelope, or relaxed (see Figure 4.3), there are five possible cases of

constitutive behaviour:

Case i

The calculated stresses at the end of the assumed elastic step are correct.

Case ii

The Gauss point stress is initially on the failure envelope, but the final stresses are correct since the behaviour involves a purely elastic increment away from the yield surface.

Case iii

As in Case ii the initial Gauss point stress lies on the failure envelope, but in Case iii the assumed elastic increment produces stresses outside of the yield surface. The entire step, therefore, has to be re-analysed plastically using the elasto-plastic stiffness matrix $[D]^{EP}$ in equation (4.8).

$$\sigma = \sigma_o + k_n v_r \Delta t.$$

But shear stress will be:

$$\tau = |\tau_o|$$

though only when $\sigma < \sigma_t$. If $\sigma \geq \sigma_t$ then τ and σ are set equal to zero representing the separation of two contact bodies. If no separation is allowed, then $\sigma = \sigma_t$ and $\tau = |c|$.

Case iv

The initial point is elastic but the elastic updated stresses lie outside the yield surface. The proportion of the time increments, μ_1, μ_2, at which the stresses cross the yield surface, must be determined from the equations (4.21), (4.22) and the yield function equation (4.5):

$$\mu_1 = \frac{(|\tau| - |c|)}{k_s u_r} \tag{4.23}$$

when $\sigma < \sigma_t$. Otherwise, if $\sigma \geq \sigma_t$ then:

$$\mu_2 = \frac{(\sigma - \sigma_t)}{k_n v_r} \tag{4.24}$$

The elastic and plastic parts of the stress increment can then be calculated separately for the time increments $\mu\Delta t$ and $(1-\mu)\Delta t$, respectively. Where μ can be μ_1 or μ_2 depending upon the location of the point of intersection with the yield surface either left or right side of the origin in Figure 4.3. The yield stresses τ_y and σ_y, are calculated from the elastic equations:

$$\tau_y = \tau_o + k_s u_r \mu \Delta t \tag{4.25}$$

$$\sigma_y = \sigma_o + k_n v_r \mu \Delta t \tag{4.26}$$

and the final plastic stresses, given by the elasto-plastic material stiffness matrix $[D]^{EP}$, are:

$$\tau = \tau_y \tag{4.27}$$

where τ cannot be greater than $|c|$,

$$\sigma = \sigma_y + k_n v_r (1 - \mu)\Delta t \tag{4.28}$$

and where σ has always to be less than σ_t.

The proportion of time increment μ_2 is only considered when separation at the interface is not allowed, i.e. when the interface stresses are not set to zero. This arbitrary condition has been imposed in the test problem of two rigid blocks in Section 4.4 below to verify that the present formulation of the element works also when only tensile stress is applied.

Case v

The initial point is elastic but the elastic updated stresses lie outside the yield surface to the right side of the origin in Figure 4.3. The stresses in this case are set to zero to mark the separation of the interface.

A careful choice of a numerical integration scheme is important to evaluate the incremental element stiffness matrix of equation (4.20). It has been suggested that a Newton-Cotes integration scheme provides a better solution then a three point Gaussian quadrature scheme. Gens *et al.* (1989) investigated the application of one- and two-dimensional interface elements to model a pull-out test in which a reinforcement element is extracted from a surrounding material, they observed spurious oscillations of the shear stress when a Gaussian integration scheme was used but which did not appear when a Newton-Cotes scheme, where all of the

integration points lie at the element nodes, was adopted. However, Gens *et al.* also pointed out that the adoption of a Newton-Cotes integration scheme resulted in decreased accuracy in integrating polynomial expressions. Langen and Vermeer (1990) adopted this scheme in the pile penetration analysis in which they introduced internal interface elements near the corners of the pile base. They reported that although this technique proves to yield smoother stress results in the pile penetration analysis, bad results are still obtained near corners in the finite element mesh, as encountered in many problems of soil-structure interaction. Burd and Brocklehurst (1991) successfully adopted a three point Gaussian integration scheme in their study of the problem of soil reinforcement: no instability in the interface stresses was reported. Such stresses do not occur neither in the case of a reinforcement problem nor in the case of the problem being tackled here. Therefore, following the experience of Burd and Brocklehurst (1991), a three point Gaussian integration scheme is adopted to evaluate the incremental stiffness matrix. The numerical instability experienced by Gens *et al.* (1989) might be due to the generation of large shear stresses during a pull out test which is quite a severe test for an interface element.

4.4 Verification of the plane strain interface element

4.4.1 Two jointed solid blocks

The plane strain interface element formulation described in Section 4.3 is tested in this simple finite element problem which consists of two solid blocks, one sitting on the other and separated by the new interface element, as shown in Figure 4.4.

The lower block is fixed at the base and the upper block is free. Two loading conditions were tried: upper block sliding horizontally over the lower block and upper block being pulled away vertically from the lower block. These two loading situations are depicted in Figure 4.4. The two blocks were given very high strength compared to the interface strength so that

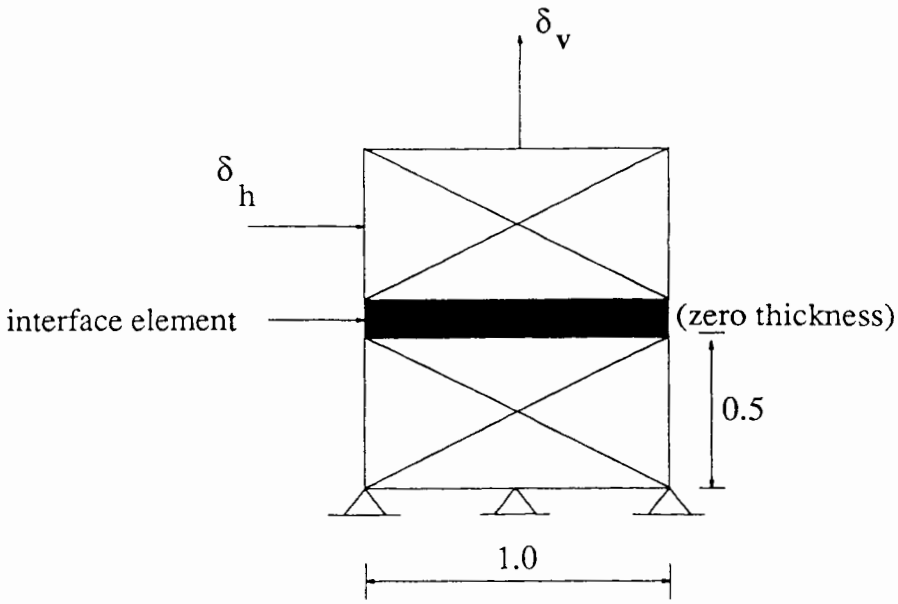

Figure 4.4: Two jointed solid blocks

yielding could only occur at the interface. Goodman *et al.* (1968) showed that the joint strength, c, and the interface stiffness values are independent of each other. Following his experience, in this problem, therefore, arbitrary values were set for the joint strength, c, the normal stiffness, k_n, and the shear stiffness, k_s, of the interface element. The results here are obtained through displacement controlled finite element analyses. The load displacement curves are shown in Figures 4.5 and 4.6.

The figures show that the elastic deformations in the element took place at the prescribed initial tangent stiffness values until the yielding occurred at the interface and the plastic deformations continued. The computed shear stresses are equal to the joint strength, c, and the normal stresses are equal to allowable tension, σ_t, at the interface. This shows that the computed stresses at the interface are consistent with the applied normal and shearing stresses.

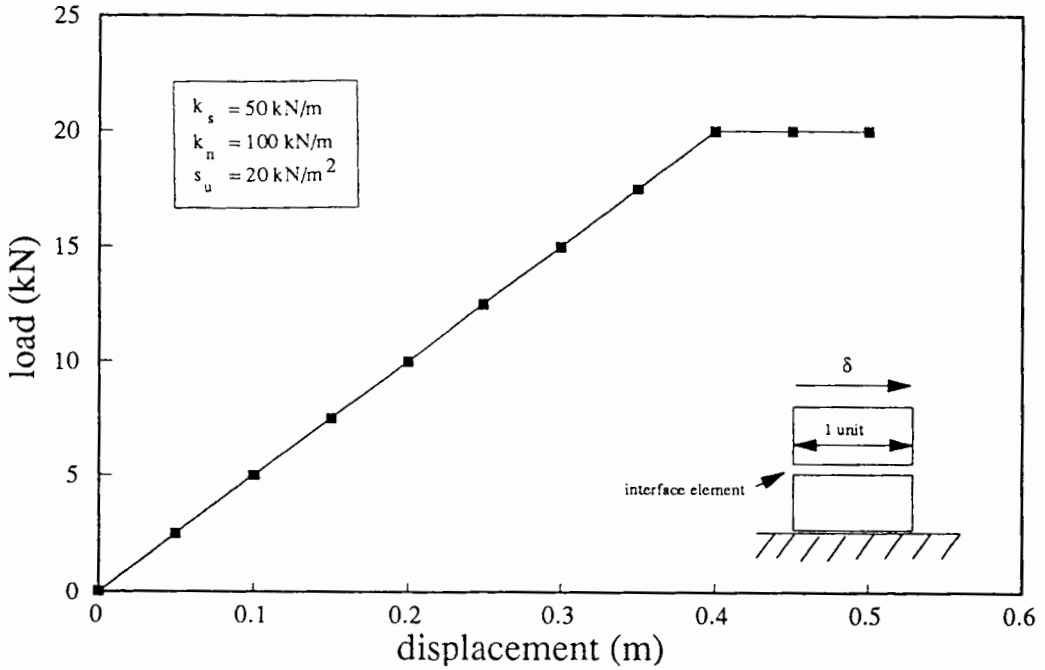

Figure 4.5: Interface stresses against relative displacement (shearing mode)

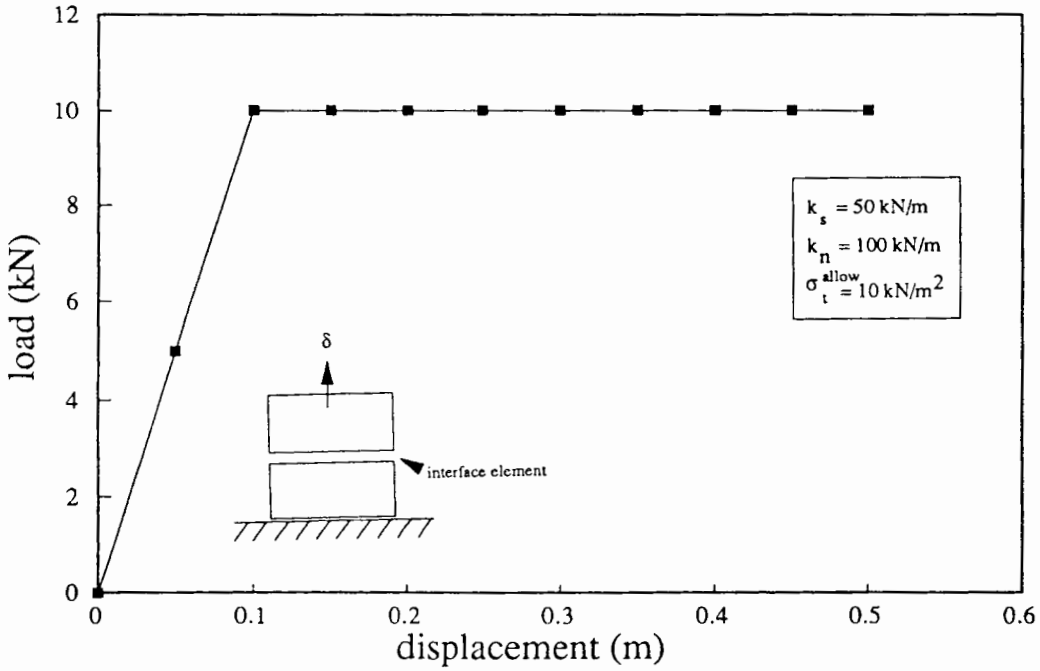

Figure 4.6: Interface stresses against relative displacement (tensile mode)

4.4.2 Plane strain footing subjected to moment and vertical loading

The ultimate vertical load carrying (bearing) capacity of a surface strip footing on a cohesive soil, in the absence of a moment loading is given by this plasticity solution based on Tresca's

yield criterion (Calladine (1985)):

$$\frac{P_{ult}}{s_u B} = \pi + 2$$

where P_{ult} is the ultimate bearing capacity, s_u is the undrained shear strength of the cohesive soil and B is width of the footing.

As the footing receives a moment loading in addition to the vertical loading, the ultimate bearing capacity of the footing is significantly reduced. There are no exact solutions available for this problem. Various models have been proposed e.g. Meyerhof (1953), Hansen (1970) and Vesic (1975) based on the concept of effective contact area of the footing, acknowledging the fact that tensile stresses develop between the footing and the soil and footing experiences a partial loss of contact when subjected to a moment loading. The effect of moment loading is considered by assuming the vertical load to be applied at some eccentricity from the centroid of the footing and the point of application of load coinciding with the centroid of the effective (reduced) contact area of the footing with the soil. It was thought to be a good test problem to validate the interface element by comparing the finite element analysis results with one of these existing analytical solutions. Hansen's (1970) solution, widely used by the offshore industry, is chosen for this comparison. This solution has been modified to take account of allowable uplift force acting on a strip footing subjected to moment and vertical loadings. The modified solution is used to validate the results obtained from the interface analysis described in Section 4.4.2.2.

4.4.2.1 Analytical solution (loss of footing contact)

This section presents a simple analytical model which is a development of the earlier model proposed by Hansen (1970) for a footing subjected to moment and vertical loading. We are modifying Hansen's (1970) equation to model the uplift force acting on a plane strain footing

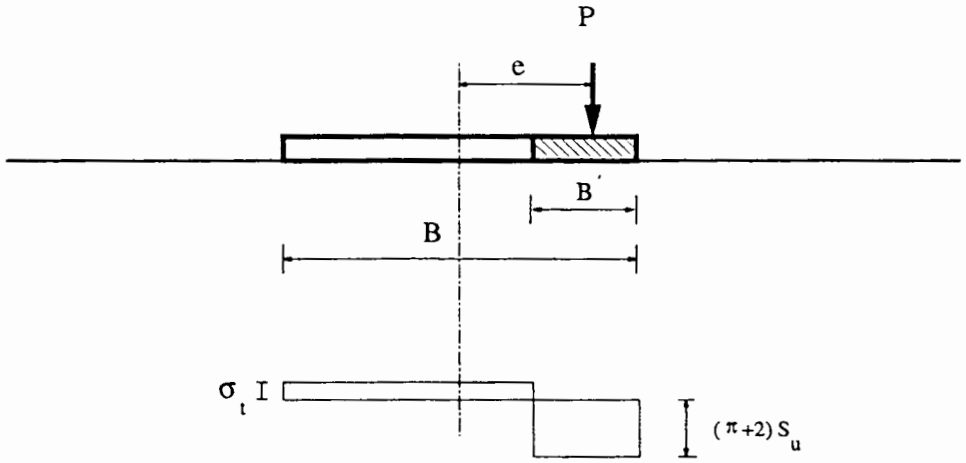

Figure 4.7: A strip footing resting on the surface of a clay layer

subjected to moment and vertical loadings. Consider a strip footing of width B subjected to eccentric loading, P, as shown in Figure 4.7. The shaded area represents the reduced effective contact area in compression. A small amount of tension cut-off stress, σ_t, is specified.

The vertical equilibrium of the footing can be expressed by the equation:

$$P + \sigma_t (B - \acute{B}) = (\pi + 2)s_u\acute{B} \tag{4.29}$$

The moment, M, applied to the footing due to the eccentricity, e, will be:

$$M = (\pi + 2)s_u\acute{B}\left(\frac{B - \acute{B}}{2}\right) + \sigma_t \acute{B}\left(\frac{B - \acute{B}}{2}\right) \tag{4.30}$$

From equation (4.29), the effective footing width under compression $\acute{B}$ can be written as:

$$\acute{B} = \frac{P + B\sigma_t}{(\pi + 2)s_u + \sigma_t} \tag{4.31}$$

substituting the value of $\acute{B}$ in equation (4.30), results in the following new equation:

$$\frac{2M}{B} = (P + P_t)\left(1 - \frac{P + P_t}{P_{ult} + P_t}\right) \tag{4.32}$$

where:

$$P_t = B\sigma_t$$

$$P_{ult} = (\pi + 2)s_u B.$$

This is a modified form of the Hansen's equation for eccentrically loaded footings which represents a parabola in the moment-vertical load space with the origin shifted to the left by an amount equal to the actual amount of tensile cut-off force (shown in Figure 4.13). If P_t is zero, equation (4.31) becomes Hansen's equation representing a parabola.

For any given values of tension cut-off σ_t and s_u, a combination of the moment and the vertical load can be determined by equation (4.32) and the width of loss of contact $(B - \acute{B})$ can be determined using equation (4.31).

4.4.2.2 Finite element analysis

In this section an interface analysis of a smooth strip footing on a clay layer is performed using the new interface element.

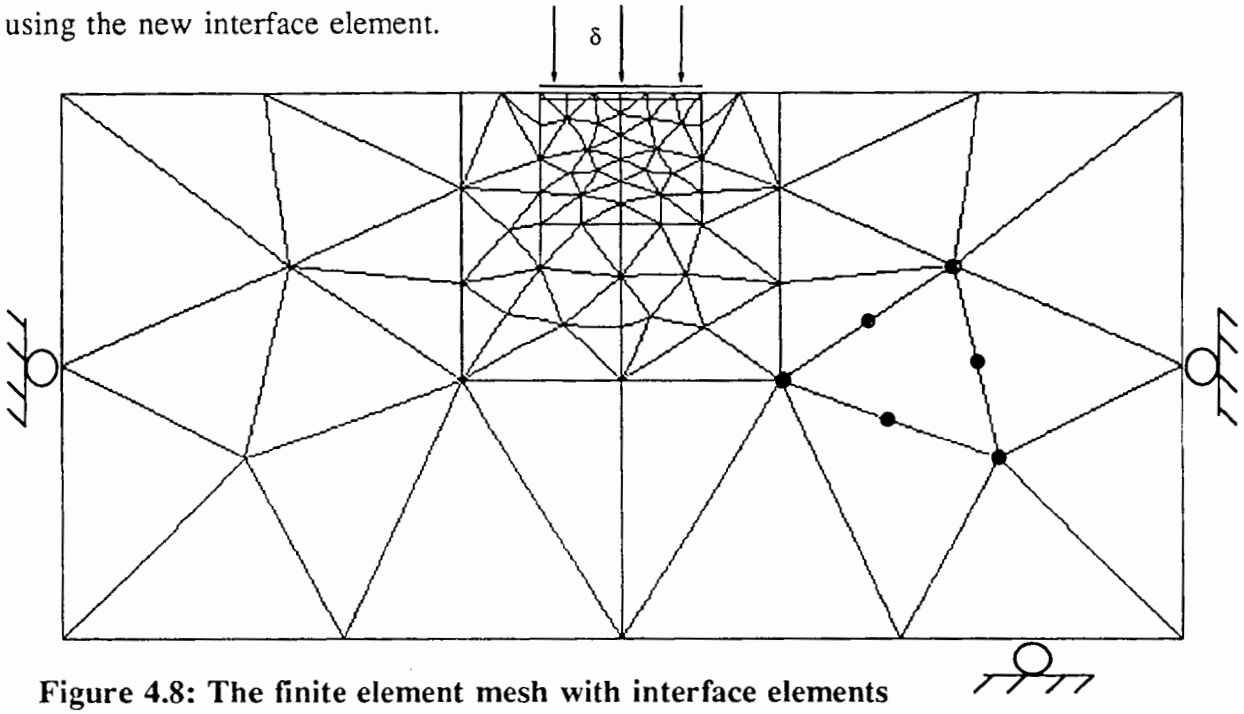

Figure 4.8: The finite element mesh with interface elements

Figure 4.8 shows the mesh with interface elements representing a strip footing which was first pushed vertically until the collapse load was achieved, it was then rotated to predict the reduction in vertical bearing capacity of the footing with the application of moment loading. The displacements are applied at the upper layer of nodes of the interface element. Generally, mesh dimensions for the prediction of vertical collapse loads accurately, are of the order of five times the width of the footing or, in the case of a circular footing, ten times its radius (Sloan (1981); Sloan and Randolph (1982); De Borst and Vermeer (1984)). In the present test problem the mesh dimensions are 30% smaller than usual as the aim is validation of the interface element rather than accuracy in the predicted collapse loads. The material properties used in the analysis are: rigidity index G/S_u = 50 and Poisson's ratio ν = 0.49.

Figure 4.9 shows the predicted vertical collapse load (without any moment loading) using the

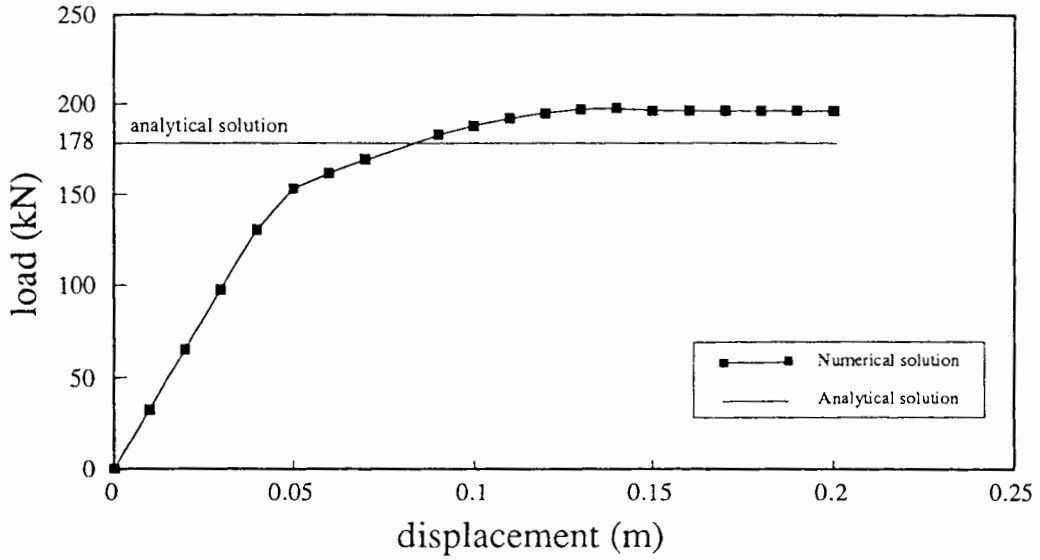

Figure 4.9: Load displacement curve with interface elements

mesh with interface elements shown in Figure 4.8. The mesh results in an over-prediction of the collapse load by just over 10%. The normal and shear stiffnesses of the interface were set to very high values to make sure that the interface should not yield before the continuum elements did. The values of the interface stiffness need to be chosen very carefully, taking into account the continuum material properties. The values of k_s and k_n cannot be too high or too low: too high results in ill-conditioning, too low leads to errors (Brocklehurst (1993)). The ratio of shear stiffness, G, to k_s has dimensions of length and represents the equivalent continuum thickness of the interface element when subjected to pure shear. For a rough footing base, the problem at hand, G/k_s should ideally be set to a very small dimension to represent a footing base that has no movement relative to the soil until the adhesive strength (joint strength) of the interface, c, taken to be the undrained shear strength of the continuum s_u, is exceeded. Bell (1991) found that if the values of G/k_s were too small, it caused numerical instability when non-linear behaviour is being modelled. To represent a zero thickness element in the direction normal to the interface, the normal interface stiffness k_n should be given a value such that the ratio E/k_n is also a very small value. The ratios G/k_s

and E/k_n in this analysis are chosen to be $0.6/l_i$ where l_i is the length of the interface element, in the light of the recommendations made by Brocklehurst (1993). The footing is given rigid body displacements vertically followed by rigid body rotations. As we do the rotation part we track the values of moment and vertical force. The first set of calculations involve pushing the footing down until we get complete failure and then rotating. We find that a failure envelope is traced out and this particular calculation must stop when the moment reaches the apex of the failure envelope. It is possible to explore other part of the curve by applying initial vertical loads less than the collapse load. Five load cases were tried and are shown in Figure 4.10. The results, for zero interface tension, are plotted in Figure 4.11. Hansen's (1970) solution is also shown for comparison purposes. Some over-prediction is expected because the discretisation of the mesh but generally the shape agrees quite well.

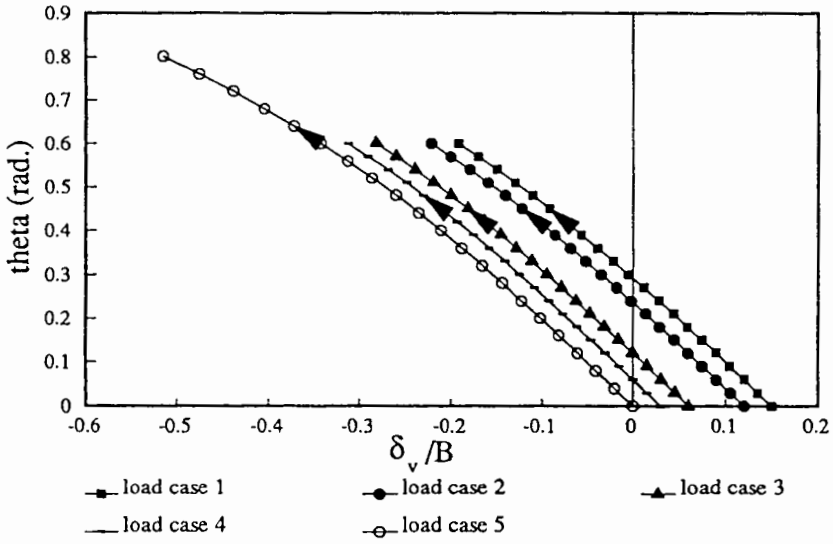

Figure 4.10: Applied footing displacements

Figure 4.12 shows interaction curves for moment versus vertical load. Both analytical and numerical results have been plotted. The figure shows that the footing-soil interface tension has negligible effect. There is a very small increase in the allowable moment carrying capacity of the footing.

Figure 4.13 shows that when a small tension is allowed at the footing-soil interface, the origin

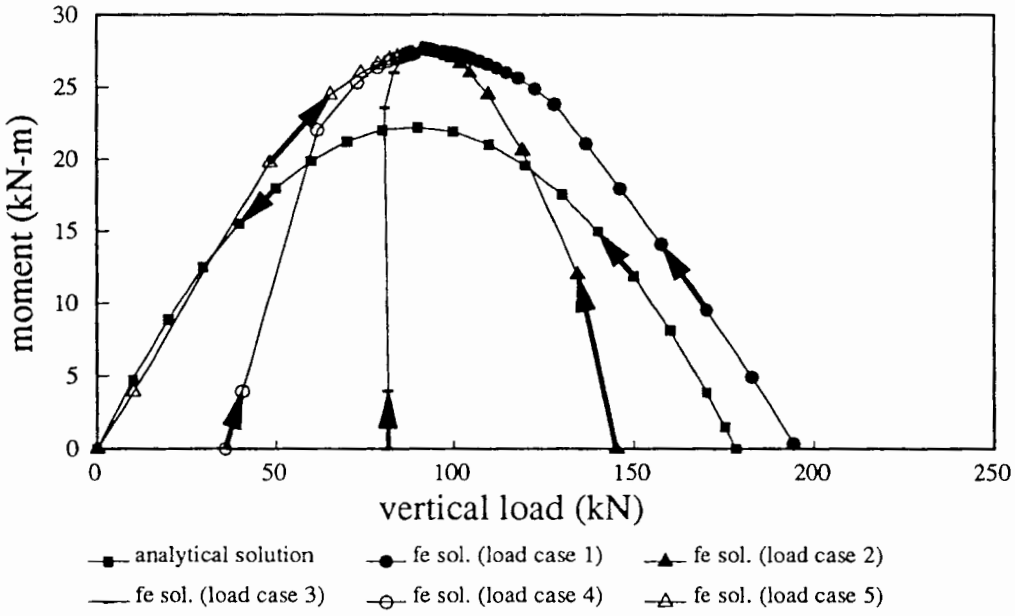

Figure 4.11: Moment - vertical load interaction curves with zero interface tension

of the parabola is shifted to the left by the actual amount of allowable uplift force specified in the analysis. The area of the footing under tension, eventually representing loss of contact, can be determined analytically for a strip footing (see Section 4.4.2.1). However, Bell (1991) produced contour plots of normal stresses showing areas where loss of contact took place in circular footings subjected to eccentric loading. The forces and moments are obtained either directly by the summation of elemental nodal forces or worked out by integrating the Gauss point stresses over the element.

The load cases shown in Figure 4.13 are the same as in Figure 4.11 except that load case 4 is not shown and in load case 5, an interface tension of 10kPa is assumed. For load cases 1-3, we use method 1 in which elemental nodal forces are summed up to get external forces and moments. For load case 5, two separate calculations are shown. These calculations correspond to method 1 and 2 respectively. In method 2, Gauss point stresses are integrated over the element to obtain external forces and moment. These two methods are carried out to compare two different ways of getting external forces and moments and to check on stress updating

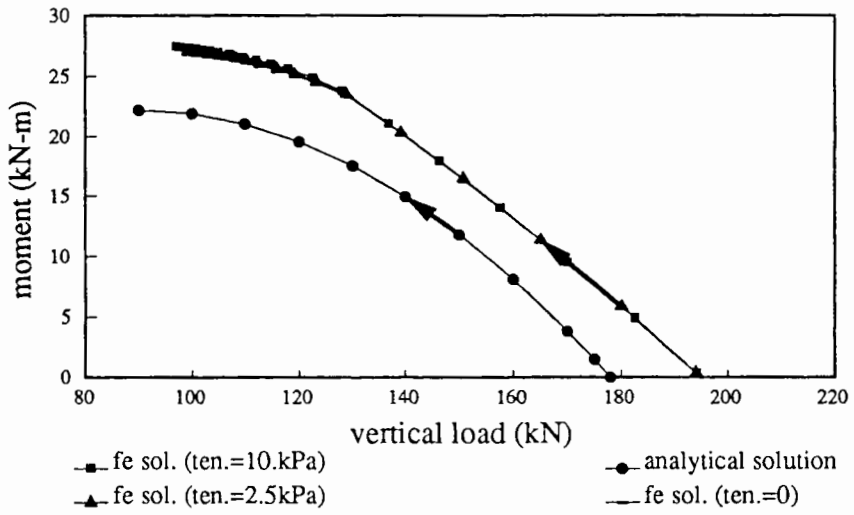

Figure 4.12: Moment - vertical load interaction curves showing the effect of interface tension

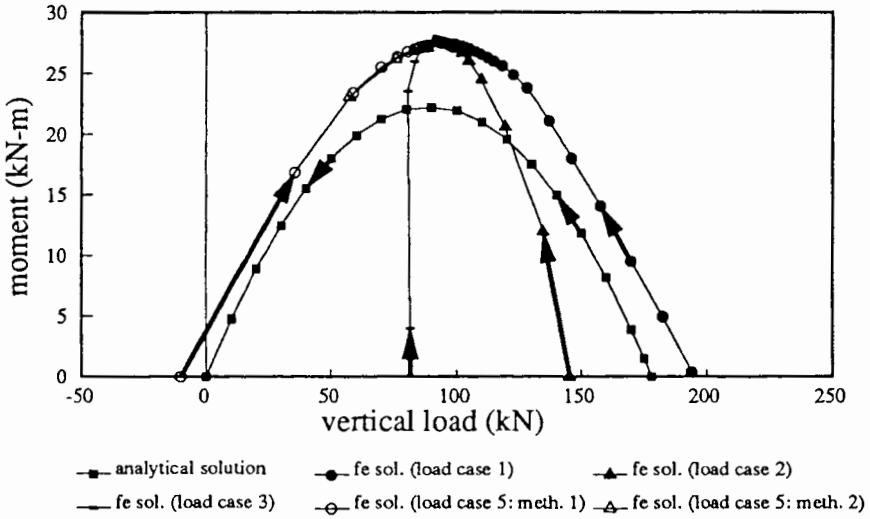

Figure 4.13: Moment - vertical load interaction curves (shifted)

procedures. The comparisons do not show any significant difference (0.4% in the calculation of vertical load and 0.6% for moment calculations) in either set of results i.e. from load case 5. By contrast, Bell (1991) reported a quite significant difference in the computed stresses in his two-dimensional cohesive interface element. The finite element analysis results in the

in the figures here show that the Hansen (1970) results are quite conservative, as also found by Bell (1991). (The three-dimensional finite element analysis of a partially penetrated spudcan (conical) footing presented in Chapter 8 also confirms that Hansen's (1970) solution gives conservative estimates of bearing capacity of surface footings subjected to vertical and lateral loading.) Although the finite element analysis results cannot be truly accurate due to the close proximity of the zero displacement boundaries in the finite element mesh and to the coarse discretisation of the soil continuum, the over estimation of results is nevertheless within acceptable limits. The interface element model has produced satisfactory results in modelling the rigid footing-soil contact problem. In Chapter 5 it will be used for interface analysis of a rigid circular disc in cohesive soils.

APPENDIX 4A

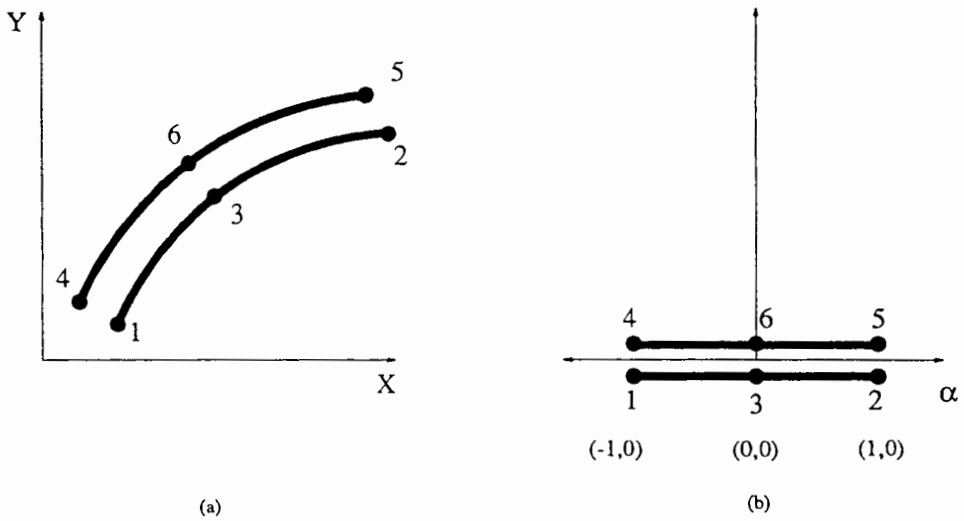

Figure 4A-1: Mapping for the six-noded plane strain interface element

Figure 4A-1 shows the isoparametric mapping between the parent and the reference elements for the six-noded interface element.

The vectors $\underset{\sim}{x}$ and $\underset{\sim}{X}$, that are related by equation (4.1), are defined as:

$$\underset{\sim}{x}^T = [x_a \; y_a \; x_b \; y_b] \tag{4A.1}$$

$$\underset{\sim}{X}^T = [X_1 \; Y_1 \; X_2 \; Y_2 \; \ldots \; X_6 \; Y_6] \tag{4A.2}$$

Where X_i , Y_i are the global co-ordinates of the i^{th} node. The shape function matrix, which

is required to keep the co-ordinates (x_a , y_a) and (x_b , y_b) congruent, is of the form:

$$[N] = \begin{bmatrix} f_1 & 0 & f_2 & 0 & f_3 & 0 & 0 & 0 & 0 & 0 & 0 & 0 \\ 0 & f_1 & 0 & f_2 & 0 & f_3 & 0 & 0 & 0 & 0 & 0 & 0 \\ 0 & 0 & 0 & 0 & 0 & 0 & f_1 & 0 & f_2 & 0 & f_3 & 0 \\ 0 & 0 & 0 & 0 & 0 & 0 & 0 & f_1 & 0 & f_2 & 0 & f_3 \end{bmatrix} \tag{4A.3}$$

where:

$$f_1 = \frac{\alpha(\alpha - 1)}{2} \tag{4A.4}$$

$$f_2 = 1 - \alpha^2 \tag{4A.5}$$

$$f_3 = \frac{\alpha(\alpha + 1)}{2} \tag{4A.6}$$

The matrix $[B]$ of equation (4.2) is given by:

$$[B] = \frac{1}{J} \begin{bmatrix} -f_1x' & -f_1y' & -f_2x' & -f_2y' & -f_3x' & -f_3y' & f_1x' & f_1y' & f_2x' & f_2y' & f_3x' & f_3y' \\ f_1y' & -f_1x' & f_2y' & -f_2x' & f_3y' & -f_3x' & -f_1y' & f_1x' & -f_2y' & f_2x' & -f_3y' & f_3x' \end{bmatrix} \tag{4A.7}$$

where

$$x' = \frac{dx}{d\alpha}$$

$$y' = \frac{dy}{d\alpha}$$

$$J = \left[\left(\frac{dx}{d\alpha}\right)^2 + \left(\frac{dy}{d\alpha}\right)^2\right]^{\frac{1}{2}}$$

CHAPTER 5

ANALYSIS OF SINGLE PILES UNDER LATERAL LOADING

5.1 Introduction

The determination of the ultimate lateral soil resistance is essential in the design of laterally loaded piles. In practice, such design is often done using *p-y* curve analysis with *p-y* curves derived empirically (see above, Section 2.3). An alternative, the use of numerical methods to evaluate a *p-y* curve, is explored in this chapter. It contains a description of plane strain finite element analyses that were carried out to predict the ultimate soil resistance when a circular pile is loaded laterally in a cohesive soil. It is shown that with the help of these analyses, not only is the ultimate soil resistance predicted accurately but also a theoretical *p-y* curve can be derived which match closely with the *p-y* curve proposed by Matlock (1970). (Frictional soils are dealt with in Chapter 7.) In these analyses, the assumption is made that the depth is sufficiently large for behaviour around the pile to be modelled adequately using a plane strain finite element formulation i.e. when the soil at failure moves round the pile in one plane (Fleming, Weltman, Randolph and Elson (1985)). Numerical analysis of pile groups follows in Chapter 6.

The ultimate soil resistance which develops along the laterally loaded pile in a cohesive soil can be calculated by means of the theory of plasticity, assuming failure of soil takes place along plane or spiral slip surfaces and according to Broms (1964a) hypothesis, at a depth of approximately 3.0 times pile diameter below the surface where plane strain conditions hold.

Randolph and Houlsby (1984) presented an exact solution using the method of characteristics in which they match both upper and lower bound solutions for a rigid circular pile loaded laterally in a purely cohesive soil. This analysis, excellent as it is, does not provide any information at all about the size of the actual displacements: it gives only the ultimate lateral load (p_u=11.94$S_u d$ for a rough pile-soil interface and p_u=9.14$S_u d$ for a smooth interface). But when designing a pile foundation, it is necessary to have as precise an idea as possible about how far the foundation may move before the ultimate load point is reached. If such displacements can be satisfactorily calculated it is possible to design the foundation accordingly. A plane strain finite element analysis does provide information on both the ultimate lateral load *and* the required displacements i.e. a *p-y* curve. Although, it provides a theoretical *p-y* curve which is more reliable than the empirically constructed curve, there is a problem regarding the size of the mesh required to capture displacements exactly. The analytical solution for a laterally loaded rigid circular disc in an ideal elastic soil medium given by Baguelin *et al.* (1977) (reported in Chapter 2) suggests that for an infinite elastic medium the displacements are infinite i.e. with the increasing size of the finite element meshes the displacements will not converge to a single value but will be continuously increasing with the mesh size. If we find the solution to be correct then the problem is how to model the infinite domain or far-field behaviour of the soil. The important question is whether we really need to do it when the main interest lies within the near-field. This problem is addressed in detail, in the following Section 5.4.

In what follows, two out of the three pile loading phases, namely the pile installation phase and the phase after the soil recovery period i.e. after soil equilibration or consolidation phase when external load is applied, are investigated in respect of how the pile and the soil interact and affect the ultimate soil resistance. First: it is assumed that there are no initial stresses present in the soil; then the effect of initial stresses which are due to the self weight of the soil and after that the effect of initial stresses caused by pile installation are taken into account. The ultimate soil resistance in both the cases is compared. Secondly: after the end

of the consolidation phase, when excess pore pressures developed during installation phase dissipate and the soil recovers, its strength increases as well as the *in situ* stresses in the soil; the effect of both the *in situ* stresses and the increase in shear strength on the ultimate lateral soil resistance is studied. In all the calculations, the soil is assumed to be elastic perfectly cohesive material. However, the possibility of using a non-linear elastic perfectly cohesive soil model is also explored (see Section 5.2). Finally: pile-soil interaction is studied using the cohesive interface element developed in Chapter 4. The possibility of loss of contact of soil at the back of the pile (near the ground surface) is modelled using the interface element. (The ultimate lateral reaction in frictional soils is discussed in Chapter 7.)

5.2 Choice of material constitutive behaviour

The most common constitutive law for modelling undrained clay is the linear elastic perfectly plastic Tresca model (Calladine (1985)). However, under axi-symmetric conditions, singularities (i.e. the yield function is not differentiable) are encountered at the corners of the yield function (Sloan (1981)). Even though corrections can be made for these special cases, the alternative von Mises plasticity yield criterion (Calladine (1985)), shown in Figure 5.1 is used to model the cohesive soil.

The figure shows the yield criterion in the π plane - a section through the yield locus in the (q-p) stress space. Where q is the difference of maximum and minimum principal stresses and p is the volumetric stress. The plastic strain rates are derived from a fully associated flow rule which gives zero plastic dilation rate and is therefore suitable for the modelling of undrained clay behaviour as discussed by Wroth and Houlsby (1985). A fully associated flow rule requires that the plastic potential and the von Mises yield functions are exactly identical when plotted together using consistent axes, and the plastic strains are then normal to the yield surface.

In elasto-plastic soil models, it is assumed that yield surfaces exist which bound the region of stress space which can be reached by a soil without incurring irrecoverable deformations.

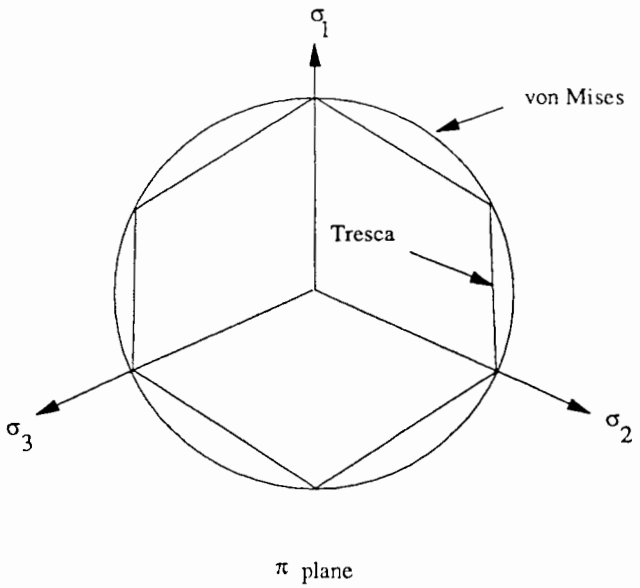

Figure 5.1: Yield criterion in the π plane (after Burd (1986))

Within the yield surface, deformations are entirely recoverable and elastic. It has been common practice to evaluate soil moduli in the form of an equivalent linear elastic response over a wide range of strains. With the recent advancements in laboratory strain measuring techniques/methods, it is possible to measure soil stiffness more accurately. Evidence from laboratory tests demonstrates that the pre-yield soil behaviour is inelastic throughout loading except at very small strains (Atkinson (1993)). Real soils show more gradual yielding process. Their response is highly non-linear and influenced by many variables such as mineralogy, fabric, structure, stress state, loading and drainage conditions. It is revealed that the characteristic soil stiffness-strain curve resembles S-shape (see Figure 5.2). Three characteristic regions of soil stiffness can be identified. There is a region where the behaviour is elastic but this corresponds to very small strains (usually less than about 0.001%). There is a region of large strains, greater than about 1%, where the behaviour is inelastic and there are large irrecoverable plastic strains. Between these there is a region where the stiffness decreases with strain and the behaviour is highly non-linear. Figure 5.2 shows that soil is only linear and elastic within the range of very small strains corresponding to changes of stress of a few kPa. At large strains, soil is yielding and high proportions of the total strains is

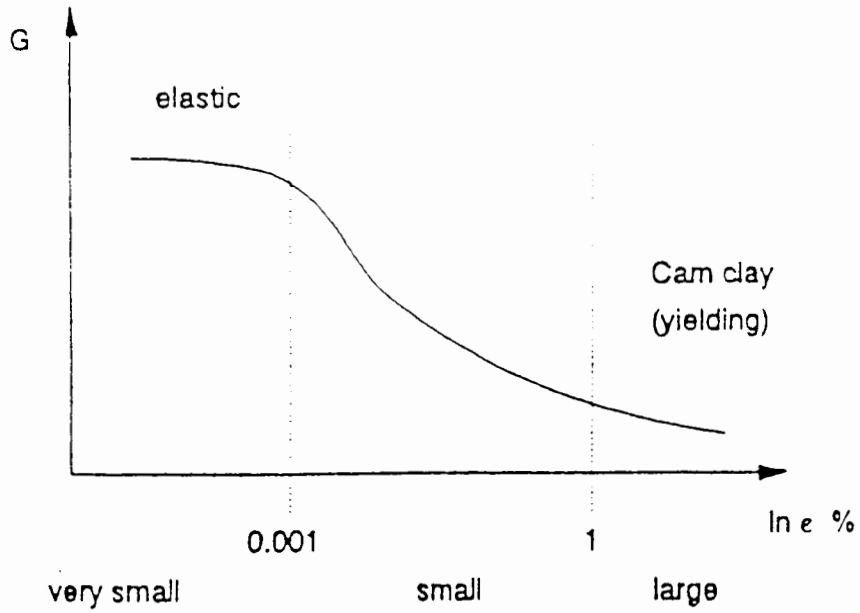

Figure 5.2: The 'S-shaped curve' relating stiffness to magnitude of strain (after Atkinson (1993))

inelastic. The question then arises as to the nature of the straining within the intermediate, small strain region. One possibility is to regard this as essentially elastic, but non-linear and to use curve fitting techniques to obtain an empirical expression relating shear modulus to strain. This is the approach followed by Duncan and Chang (1970) and Jardine *et al.* (1991); the method requires complex laboratory tests in which stress paths mimic the *in situ* paths and numerical analyses which should start and restart at each change in the direction of a stress path. An alternative approach is to regard soil behaviour in the small strain region as inelastic with yielding and hardening with kinematic surfaces inside the yield surface. The simplest approach seems to be to adapt the Cam clay models by including additional surfaces (e.g. Mroz *et al.* (1979); Al-Tabbaa and Wood (1989); Atkinson and Stallebrass (1991). A similar model is proposed by Houlsby and Chow (1994) and is explored in this chapter in addition to the linear elastic plastic model. Although Simpson (1993) presented a novel idea of expressing non-linearity with an analogue of bricks on strings pulled by a man. The man was taken to represent the point in the strain space of a small element. Each brick represented a proportion of the element. Movement of a brick represented plastic strain and the elastic strain is given by the difference between the movement of the man and the sum of the movement

of the bricks, each weighted by the proportion of the soil it represented. Thus the S-shaped curve can be modelled in a stepwise fashion.

5.3 Choice of the finite element

The difficulty of using the finite element method to do deformation analysis at constant volume - collapse load calculations (under vertical loading) incompressible or nearly incompressible materials) - is widely acknowledged. The difficulty arises from the imposition of additional kinematic constraints on the nodal velocities by the incompressibility condition. The condition reduces the number of degrees-of-freedom in the finite element mesh. As a result, the finite element method produces an over-stiff response and predicts the exact collapse load with an error margin which may be unacceptable. The same difficulty arises when the finite element method is used to determine the response of laterally loaded single-piles in soft clay - because the incompressibility condition again applies, producing the same over-stiffness and unacceptable error margin.

The incompressibility condition also affects calculation of stress field in a solid body. The result, when the finite element method is used, is spurious variation of stresses across each element in the finite element mesh. These inaccuracies in the predicted stresses are confined to the mean normal stresses, the deviatoric stresses being relatively unaffected (see Naylor (1974)).

There are several methods of dealing with the incompressibility condition in the finite element calculations. An excellent review of these methods by Burd and Houlsby (1990) can be summarised as follows:

1) Quadrilateral element with reduced integration. This is adopted to evaluate the element stiffness matrices. The eight-noded quadrilateral element with four-Gauss point integration

rule is normally recommended (Kooijman (1989)).

2) A variant is quadrilateral element with full integration for deviatoric strain terms. Reduced integration scheme is used only for the volumetric strain terms (only they are affected by the incompressibility condition).

3) 'Mixed methods'. In this approach, the primary variables in the formulation of the finite element are not all of the same type. Herrmann (1965) described a variational formulation in which mean pressure is taken as an additional variable. This was discussed further by Nagtegaal *et al.* (1974).

4) The hybrid method is an alternative form of 'mixed method' in which stresses as well as displacements are used as primary variables.

It has been shown that the variants of the finite element method based on reduced integration or mixed method approaches are essentially equivalent (see Zienkiewicz *et al.* (1983) which has a good review of the application of mixed methods to incompressible analysis).

A quite different way of approaching the application of the finite element method to problems involving material incompressibility is described by Sloan and Randolph (1982). They showed that, as the order of polynomials used to describe the strains within an element is increased, the rate of increase of incompressibility is less than the increase in degrees-of-freedom introduced by the additional nodes. If the total number of degrees-of-freedom in a finite element mesh is held constant, therefore, the total number of constraints may be reduced by using higher order elements. A satisfactory finite element solution should, therefore, be possible without having to resort to reduced integration. This hypothesis had been confirmed by Sloan (1981) who performed a series of small strain collapse load calculations using 15-noded triangular elements.

A similar study was carried out by Bell (1991) in which he defined a new parameter, namely 'free degrees-of-freedom', to explore the suitability of three-dimensional finite elements for collapse load calculations.

According to Sloan and Randolph (1982) and, later, Bell (1991), a linear strain triangular element is quite suitable for performing collapse load calculations. The appropriateness of the element for the prediction of the ultimate lateral resistance is tested in this and the following chapter. As we shall see in Section 5.4, a very fine discretisation within one pile diameter around the pile is required. To predict the lateral resistance accurately, the minimum number of free degrees-of-freedom are found to be 1000 (see Table 5.1). If this number is held constant, fewer higher order elements are required i.e. mesh can be less fine.

The reduced-integration approach has been tried elsewhere (see Kooijman (1989)), and the mixed variable approach, as Zienkiewicz *et al.* (1983) showed, is equivalent in practice. But there are other reasons than novelty in favour of the choice of a triangular element:

1) The mathematical functions defining the displacements within the element are complete polynomials unlike other finite elements.

2) Aspect ratio of the element is not as important as in quadrilateral elements where high aspect ratios cause problems in the numerical solution.

3) The reduced-integration approach is of course inadequate in large displacement problems where geometric non-linear effects have to be considered (Burd (1986), Brocklehurst (1993)). While the problem we are considering is *not* a large displacement problem, as soon as a gap opens up at the back of the pile between it and the soil, large displacements occur but without causing large strains i.e. strains remain infinitesimal.

5.4 Finite element analysis of a single-pile

A rigid disc approximation of a single-pile is adopted in the finite element analyses for the prediction of limit loads for elastic, perfectly plastic soil behaviour. The finite element meshes used in the analyses are shown in Figures 5.3-8.

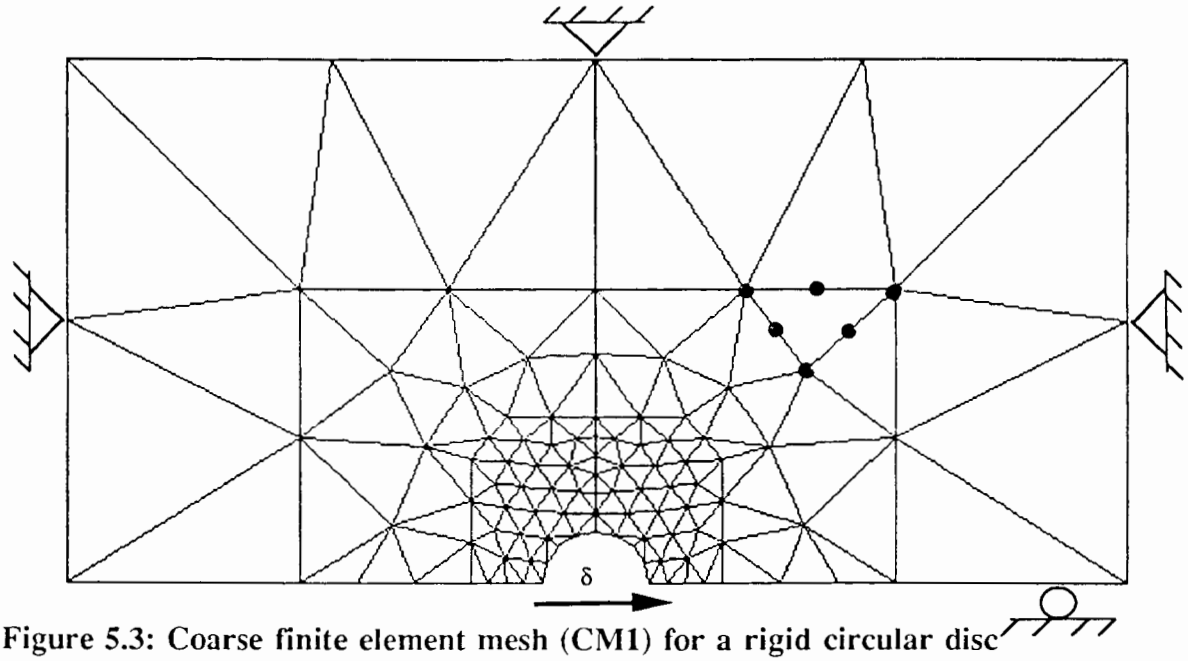

Figure 5.3: Coarse finite element mesh (CM1) for a rigid circular disc

Figure 5.3 and Figure 5.4 show coarse finite element meshes whereas Figures 5.5 to 5.8 show some refined meshes. Since the problem is symmetric, it is only necessary to analyse one half of the disc and indeed the consideration of anti-symmetry allows the analysis to be reduced to a quarter of the disc.

Six-noded linear strain triangular elements are used. (The suitability of these elements for the prediction of collapse loads for incompressible materials was demonstrated by Sloan *et al.* (1982) and later by Bell (1991).) When performing limit analysis or collapse load calculations, the incompressibility condition imposes additional kinematic constraints on the nodal velocities which reduce the number of degrees-of-freedom in the finite element mesh. Choosing the mesh dimensions is an important consideration in a finite element analysis, especially when modelling an incompressible material behaviour. The close proximity of the

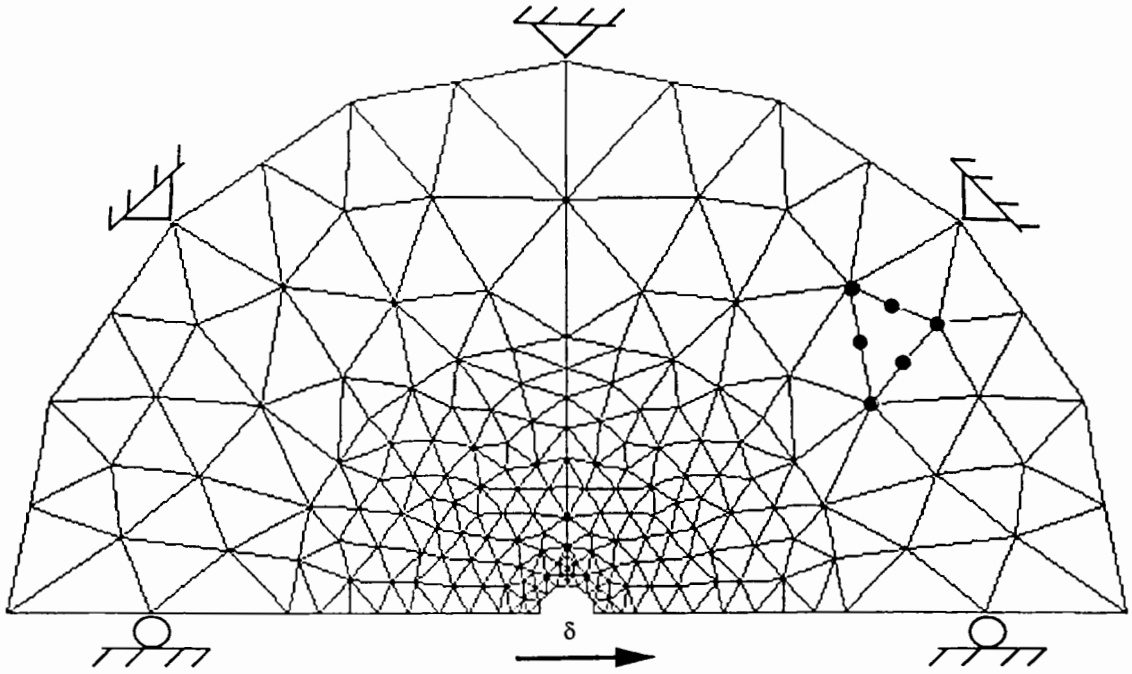

Figure 5.4: Coarse finite element mesh (CM2) for a rigid circular disc

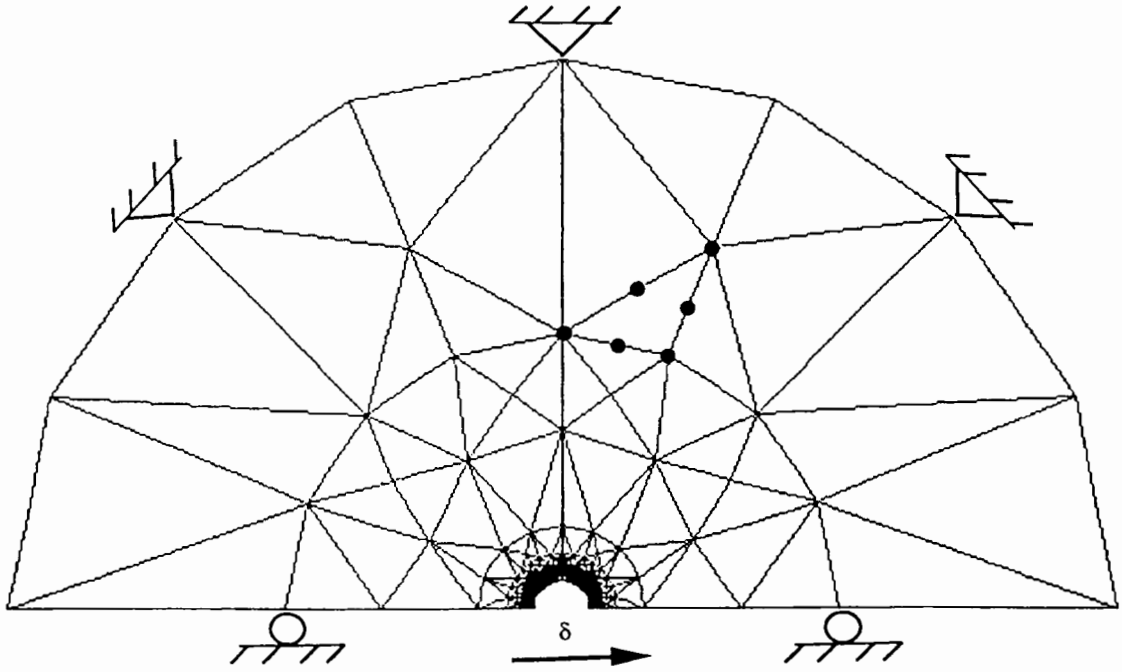

Figure 5.5: Refined finite element mesh (RM1) for a rigid disc

mesh boundaries results in fewer degrees-of-freedom compared to total number of constraints in a finite element mesh. This severely hampers the quality of the finite element solution. Error in the finite element solution arises not only because of the closeness of the mesh

boundaries to the loaded area but also because of incompressibility constraints (discussed earlier, Section 5.3), and because of coarse discretisation of the mesh. In such circumstances the finite element solution often overestimates the exact collapse load by an unacceptably large amount (Nagtegaal *et al.* (1974); Sloan (1981); Sloan *et al.* (1982)). (For a detailed review of the methods of dealing with the condition of incompressibility in finite element analyses for the prediction of collapse loads, see Burd and Houlsby (1990).)

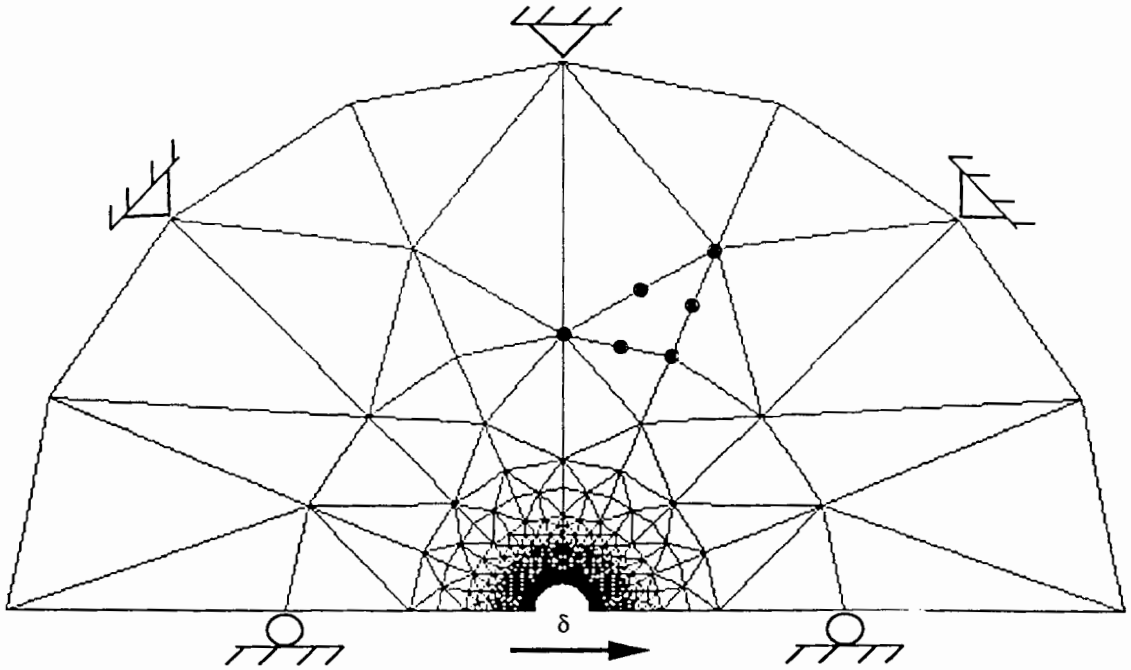

Figure 5.6: Refined finite element mesh (RM2) for a rigid circular disc

The most obvious way to get degrees-of-freedom in a finite element mesh sufficient to predict collapse loads with reasonable accuracy, is to set the boundaries far apart from the loaded area and thus increasing the number of elements.

In order to find the optimum distance to set the outer boundaries, the finite element analysis needs to be repeated by varying the distance of the outer fixed boundary each time. Otherwise, the finite element mesh becomes very large for the computer to process and a large computer memory space is required, even for a simple problem. The optimum dimension of the outer boundary is decided by setting an acceptable percentage error in the finite element solution when compared to the closed form solution (if one is available), and

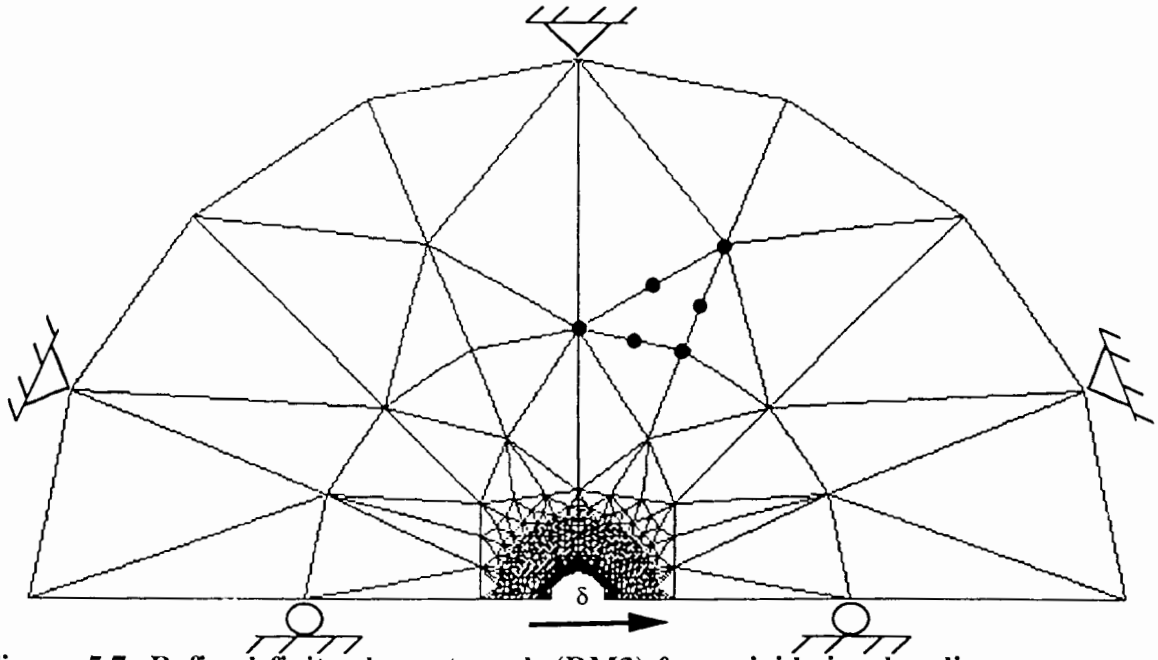

Figure 5.7: Refined finite element mesh (RM3) for a rigid circular disc

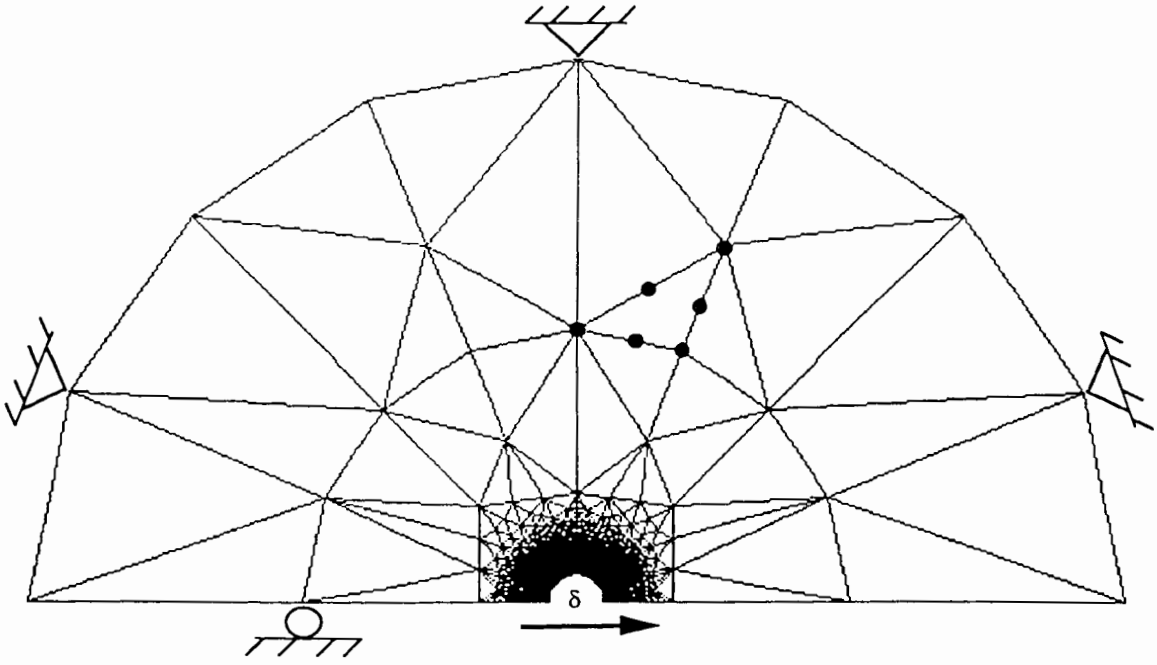

Figure 5.8: Refined finite element mesh (RM4) for a rigid circular disc

bearing in mind that the available closed form solutions (lower bound) are for infinite soil domain. Based on such numerical experiments, Yegian *et al.* (1973) suggested that the radius of the zone of the pile influence needs to be approximately eight times the pile diameter. The

zone of influence depends very much on the type of calculation. For an elastic calculation we need quite a large area however, there is a question mark how large? (The elasticity solution given by Baguelin *et al.* (1977) (reported in Chapter 2) suggests that displacements increase monotonically with the increase in zone of influence.) and for a plasticity calculation we need much smaller area (Randolph and Houlsby (1984)). Another way of avoiding these boundary effects is to couple the finite element mesh to external boundary elements. The main drawback of this approach however, is that, the boundary element matrices are fully populated representing coupling of all the nodes on the boundary as a result the coefficients of the stiffness matrix are altered: the whole matrix is disturbed and its banded nature is lost which loss reduces the efficiency of the analysis. Neither this possibility nor the possibility of combining infinite elements around the finite element mesh (e.g. Chen and Poulos (1993)) was explored for the current problem. As mentioned earlier, we have to answer the question - do we really need to model infinite boundaries for this problem? The problem under consideration is not a conventional finite element problem in which it is necessary to discount the boundary effects from the calculated solution. This problem is peculiar in the sense that the elastic solution given by Baguelin *et al.* (1977) suggests that before focusing our attention on modelling infinite boundaries we need to think about the choice of material constitutive behaviour. In this situation, initially it was thought that in order to predict reasonably accurate limiting loads and to prevent the finite elements from being locked-up we need to have a softer layer around the finite element mesh. (Since the use of a softer layer in the analysis of a large displacement cavity expansion problem has been quite successful (Burd and Houlsby (1990)), there will be an added advantage in setting up correct initial stresses in the finite element mesh that would be generated due to pile installation.) Therefore, an outer soft (correcting) layer around the soil was introduced as was done in the analysis of a single-pile under axial loading (see Section 3.5). For the current problem, it was difficult to calculate the parameters of the outer soft layer. The parameters were chosen arbitrarily to be half those used for the inner soil layer. (The analytical solution for a rigid circular disc loaded laterally in an ideal elastic soil medium given by Baguelin *et al.* (1977) was considered in order to

determine the soil parameters for the outer soft layer in a manner similar to the one used by Burd and Houlsby (1990) to determine the soil parameters of the soft layer in the analysis of a large displacement cavity expansion problem. It was found that the elastic solution given by Baguelin *et al.* (1977) is unreliable for the reason that, it gives infinite displacements for a rigid disc loaded laterally in an infinite medium, which is physically not right. In order to check the reliability of the solution, a series of plane strain finite element analysis for purely elastic material constitutive behaviour with increasing mesh sizes (with position of outer boundary varying from $20r_o$-$120r_o$, where r_o is the radius of the circular disc.) were carried out. The results are shown below in Figure 5.9 which seems to confirm the solution given by

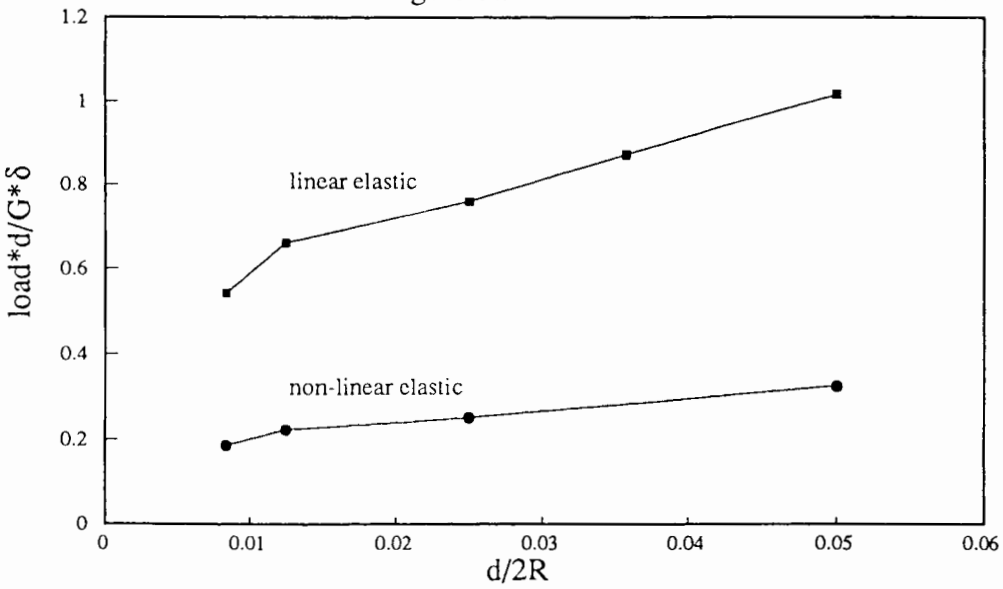

Figure 5.9: Effect of mesh boundaries on the initial elastic stiffness

Baguelin *et al.* (1977). The solution appears to suggest that we can choose an infinite number of outer boundaries where displacements are zero and there is no unique zero-displacement boundary. The choice of each boundary will give a different value of initial stiffness i.e. variable initial response of the problem. The initial stiffness will decay gradually to zero as the boundary will move outward to infinity. The introduction of an outer soft layer, therefore, can in no way discount the boundary effects leaving the initial response less certain. Its ability to prevent locking up of the finite element meshes and help in accurately predicting the ultimate load in an incompressible material for the particular problem under consideration was

also investigated. Figure 5.10 below shows two curves one with an outer soft layer and other

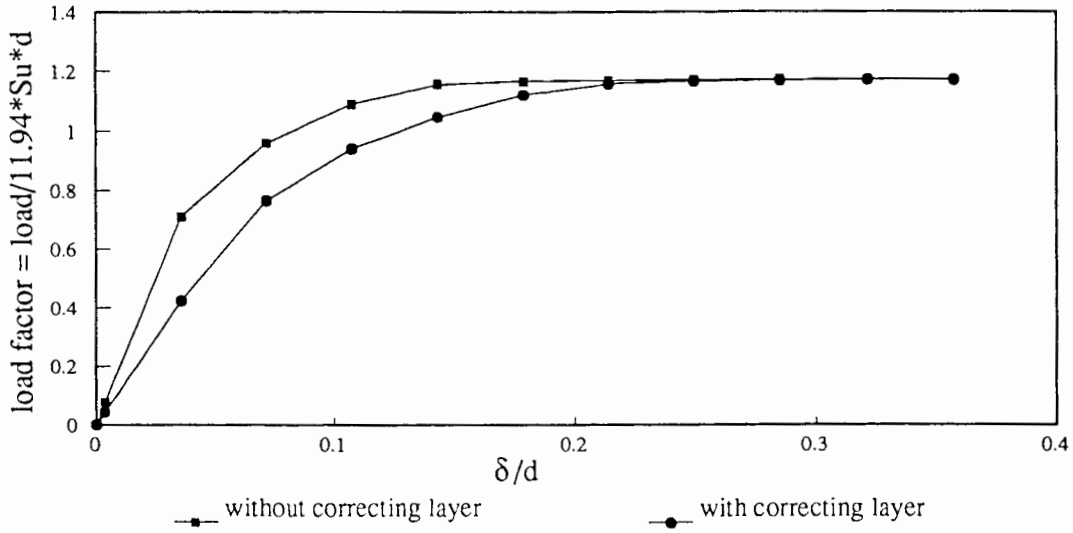

Figure 5.10: Effect of correcting layer on the pre-yield response

without a soft layer. It was found that the outer soft layer did not help in achieving a better accuracy in the predicted ultimate soil reaction but it had a detrimental effect on the elastic stiffness (i.e. stiffness was not the same as given by the elastic analytical solution given by Baguelin *et al.* (1977)). (We shall see later in this chapter that the density of elements around the disc and mesh grading are rather more important for the accurate prediction of the ultimate load.) This simple investigation suggested perhaps it is not possible to decide on the limit of the mesh size using elastic perfectly plastic model and it was decided to repeat the above analyses with varying mesh sizes using non-linear elastic plastic model developed by Houlsby and Chow (1994). These results are also shown in Figure 5.9 and we can see this model is also unable to help solving this particular problem. Although the material model is non-linear elastic, the problem arises due to the tiny part of elasticity which it has got right at the start of the analysis. Figure 5.9 also shows that it is certainly better to use a non-linear elastic model with an initial high stiffness and then decaying stiffness with increased strain levels but there is no analytical solution available to-date to validate the finite element results. It was therefore decided to keep the soil model simple (as suggested by Wroth (1984)) and use elasto-plastic model in the following analyses in such a way that it gives us realistic solutions. Mesh boundaries can be chosen such that the initial stiffness is representative of

a particular soil deposit and at the same time match with Baguelin *et al.* (1977) solution. Perhaps, it is not always possible to apply complex elasto-plastic soil models with features like kinematic hardening to every geotechnical problem. We shall see in the later Section 5.8 on lateral loading of rigid disc at the end of the consolidation phase that our choice of mesh boundaries and soil model turned out to be quite successful. The *p-y* curve obtained from this analysis (a loading case close to real field conditions) shows a surprising close match with the *p-y* curve suggested by Matlock (1970).

Although the present analysis is of a different nature to vertical collapse load calculations: collapse load calculations for lateral loading. The dimensions of the mesh on either side are taken as ten times the radius of the disc, following Sloan (1981) and Burd (1986) for two-dimensional finite element meshes used in collapse load calculations for vertical loading. A correcting layer of the same dimensions was then added round the mesh, thus setting the fixed boundaries at a distance of twenty times the radius from the centre of the disc. Later, we found that there is no advantage in having a correcting layer round the finite element mesh even though keeping the outer fixed boundaries at the same distance ($20r_o$ on either side) from the centre of the disc. A complete rough contact between pile and the soil was assumed, with full interface tension behind the pile (no loss of contact of soil with the pile). The soil (soft clay) had a rigidity index, I_r (where $I_r = G/S_u$) of 50, $S_u = 30kPa$ and Poisson's ratio of 0.499, representing a nearly incompressible material. A series of displacement controlled finite element analyses for the different meshes shown earlier (Figures 5.3-8), were done using the finite element program 'OXFEM', developed by the Civil Engineering Group, Department of Engineering Science, the University of Oxford. A full description of the program can be found in Burd (1986), Yu (1990) and Chow (1994). A displacement finite element approach was adopted. Although, OXFEM was specifically designed to conduct large displacement, large strain calculations for both the plane strain and axi-symmetric analyses of geotechnical problems, it is an added feature of this program that it can also perform small

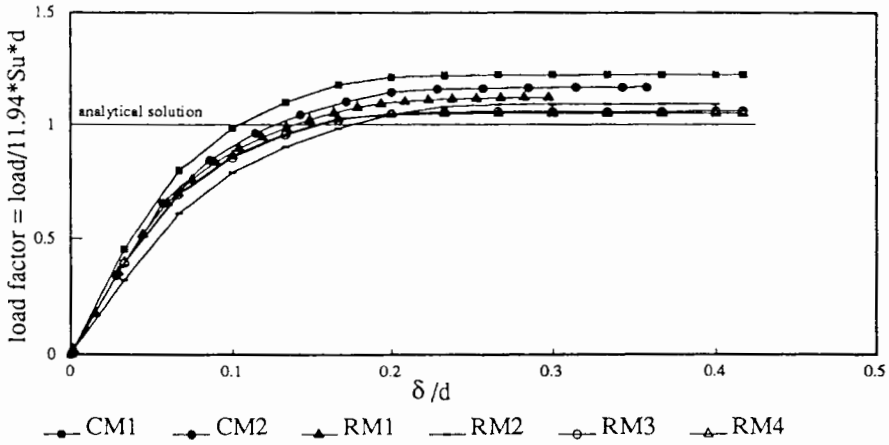

Figure 5.11: Load factor displacement curves

displacement, small strain analyses. The results are shown in Figure 5.11. The predicted limiting load is non-dimensionalised by the analytical solution given by Randolph and Houlsby (1984) and is termed as load factor. Each curve in the figure shows an over-estimation in the predicted limiting load. The percent over-estimation is given below in Table 5.1.

Table 5.1: Summary of finite element analyses

Mesh No.	Number of Elements	Total number of degrees of freedom	Geometric constraints	Incompressibi-lity constraints	Total number of free degrees of freedom	Poisson's ratio	%age over-estimation
CM1	174	762	98	522	142	.49	22.56
CM2	348	1494	150	1044	300	.49	17.5
RM1	432	1842	178	1296	368	.49	12.23
RM2	860	3590	230	2580	780	.49	9.03
RM3	696	2906	186	2088	632	.49	6.13
RM4	1376	5642	202	4128	1312	.499	4.5

The solution obtained by using mesh RM3 is superior than mesh RM2 despite the fact that

it has less number of free degrees of freedom than mesh RM2. This superiority is due to the mesh density as greater number of elements are packed near the pile. A further (40%) increase in the mesh dimensions of RM4 did not show any improvement in the results. A small change in the value of Poisson's ratio ν from .49 to .499 greatly improved the numerical solution. The result is shown as the curve corresponding to mesh *RM4* in Figure 5.11 (also see Table 5.1).

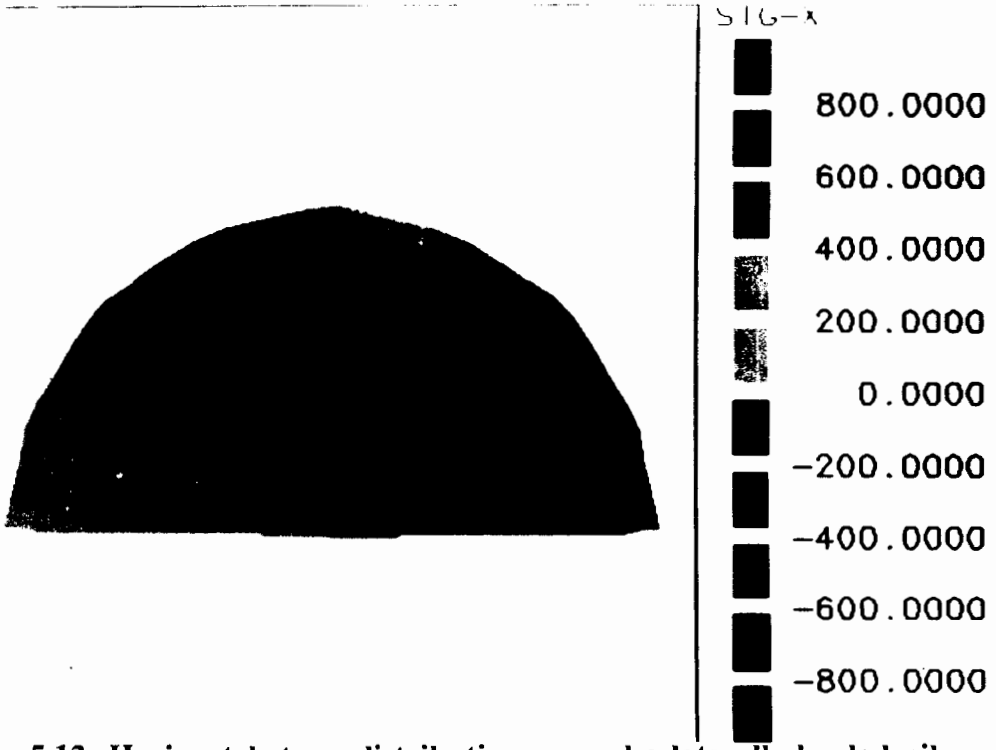

Figure 5.12: Horizontal stress distribution around a laterally loaded pile

Figure 5.12 shows the horizontal stress (kN/m^2) distribution in x-direction around a laterally loaded pile. The horizontal stresses are high close to the pile and decay very rapidly within a radial distance of one pile diameter from the face of the pile. Figure 5.13 shows the soil yielded zone around a laterally loaded pile. (The figure shows various zones between 0-1 representing elastic and yielded zones respectively.) The extent of this yielded zone do match very well with the characteristics mesh adopted by Randolph and Houlsby (1984) in the determination of upper bound solution for a laterally loaded pile in a cohesive soil using plasticity theory. The prediction of small scattered yielded pockets in addition to the main yielded zone around the pile is a result of coarse finite element discretisation of the problem

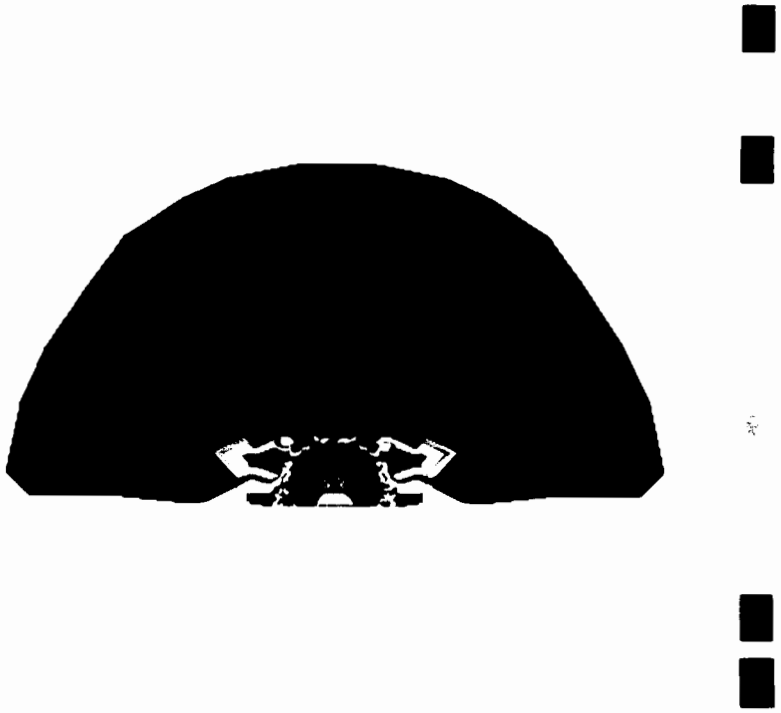

Figure 5.13: Yielded zone of soil around a laterally loaded pile

and inability to model accurately a completely incompressible material behaviour in a finite element analysis. A vector plot of displacements around a laterally loaded pile is shown in Figure 5.14.

5.5 Effect of mesh density on solution quality

It has been observed that the problem of a rigid disc moving laterally in a cohesive material is highly constrained near the disc. The quality of the results is dependent on the mesh grading and element density within the area adjacent to the disc. A significant over-estimation of the analytical limit load (Randolph and Houlsby (1984)) was obtained when the meshes were coarse. Subsequent analyses, using refined finite element meshes, revealed that a very high density of elements is required within a distance of one diameter on either side of the disc in order to obtain a good solution with an acceptable level of error. In the mesh refinement process, each mesh fulfilled the criteria for the two-dimensional collapse load

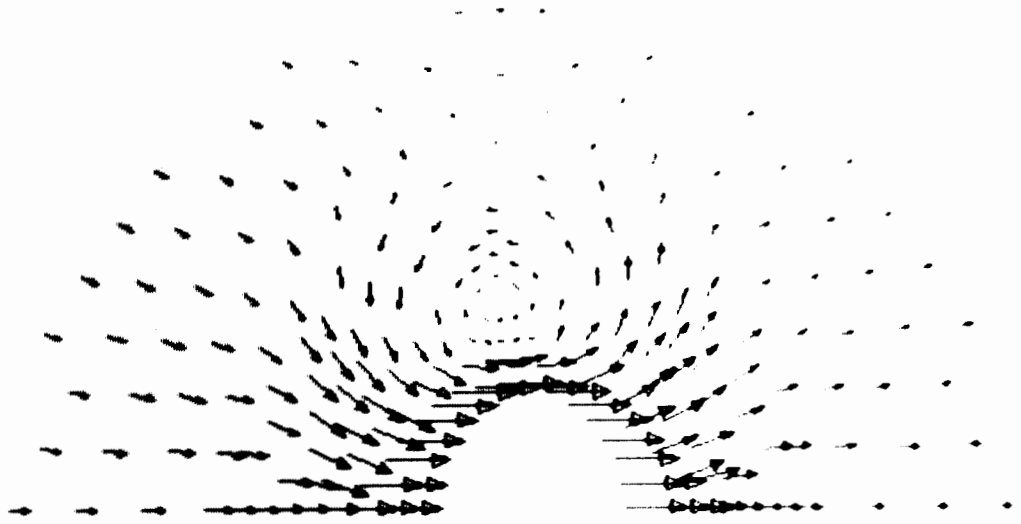

Figure 5.14: Vector plot of displacements (at the end of the analysis) around a laterally loaded pile (RM4)

calculations put forward by Sloan *et al.* (1982) and later modified by Bell (1991), namely that the number of degrees-of-freedom should be greater than the number of constraints in a finite element mesh consisting of a particular type of element. During the mesh refinement process, it was found that a stage is reached when further mesh refinements do not improve the solution. This is due to the fact that the shape functions used in the finite element do not capture accurately the strain fields around the disc (Burd and Houlsby (1992)). (In his thesis, Sloan (1981) had also made a similar emphasis that, for the accurate prediction of collapse load in a fairly refined mesh, it is necessary not only that the ratio of the number of degrees-of-freedom to the number of constraints (including the incompressibility ones) should be greater than or at least equal to unity, but also other criteria (such as ability to match strain gradients correctly) should be taken into consideration when choosing a finite element mesh.) Mesh refinement beyond the stage when any further refinement did not improve the solution quality, was pointless because this would have made the problem unnecessarily large, occupying too much computer memory space.

5.6 Effect of varying soil parameters

The soil parameters involved in the finite element plane strain analyses are undrained shear strength of the soil S_u, shear modulus G and Poisson's ratio ν. The analyses carried out by varying the rigidity index, I_r show that the higher the rigidity index, the stiffer the response and vice versa. But the non-dimensionalised load factor remains unaffected. This means that if we have soil from two different locations with the same rigidity index but one is stiffer than the other, the load factor-displacement response curves for the two locations will overlap on the same plot but the limiting loads p_u will be different. The soil with a higher shear strength will have a higher limiting load. This result confirms the Randolph and Houlsby (1984) solution for p_u which is independent of the value of G.

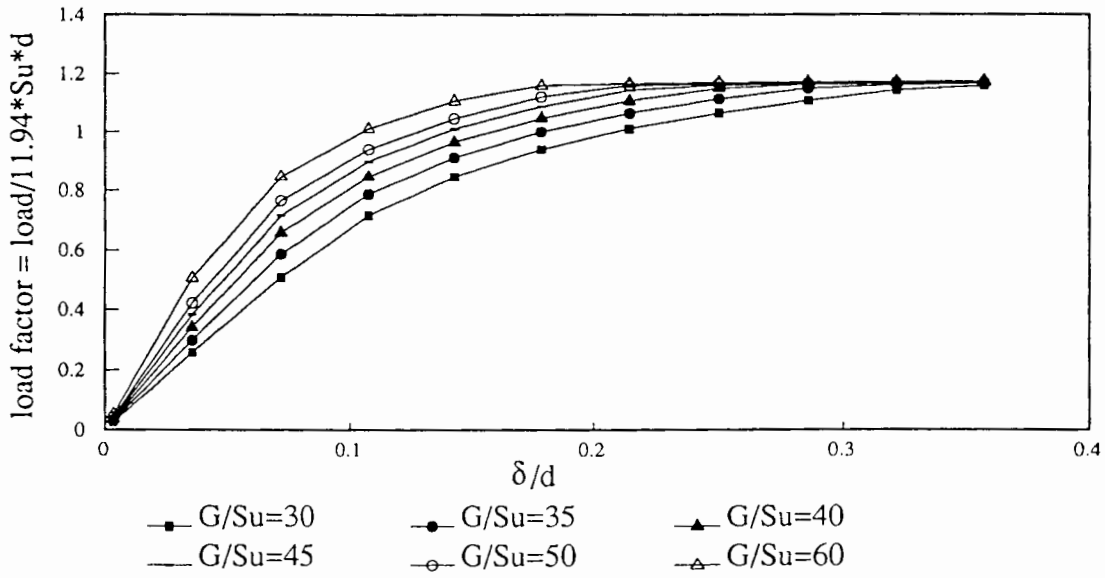

Figure 5.15: Load factor displacement curves (variable rigidity index)

Thus, curves with variable rigidity index shown in Figure 5.15 provide initial non-linear response of the soil prior to reaching the ultimate load. If we non-dimensionalise the horizontal scale in Figure 5.15 by I_r, the curves in the figure overlap (as shown in Figure 5.16) which is another indication that the ultimate lateral load is independent of shear

stiffness. A similar observation was made by Chen and Poulos (1993), namely that shear stiffness of the soil has little effect on the limiting load: in their analyses, there was a tendency in the stiffer soils to achieve slightly greater value for p_u.

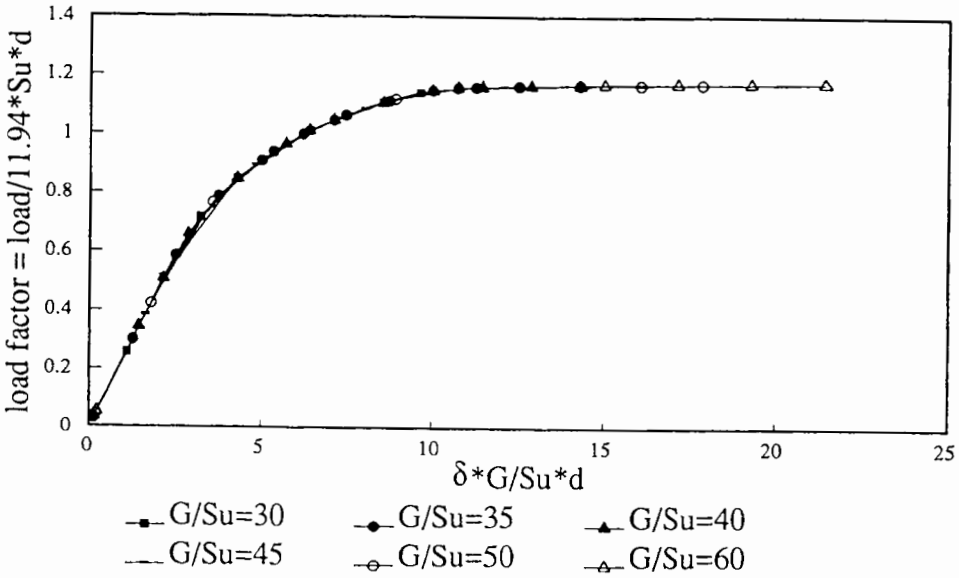

Figure 5.16: Non-dimensionalised load factor displacement curves

5.7 Analysis of a single-pile assuming initial cavity expansion to model installation

A complete static analysis of piles comprises three phases. The first one is the pile installation phase, when the pile is driven into the ground. The process of pile installation is difficult to consider theoretically as the problem is indeterminate to an extreme degree. As a preliminary to this study, arbitrary stresses were generated in the mesh by prescribing radial displacements prior to lateral ones to the inner boundary nodes of the mesh (representing the circular disc). The effect of initial stresses in the ground on the ultimate lateral soil reaction is shown in Figure 5.17. There are three load displacement curves. The curves with initial stresses (representing different K_o values) have a flexible initial response compared to the third curve without initial stresses, and they reach the same limiting load as for zero initial stresses but require higher displacements. The negligible difference between the peaks of these three

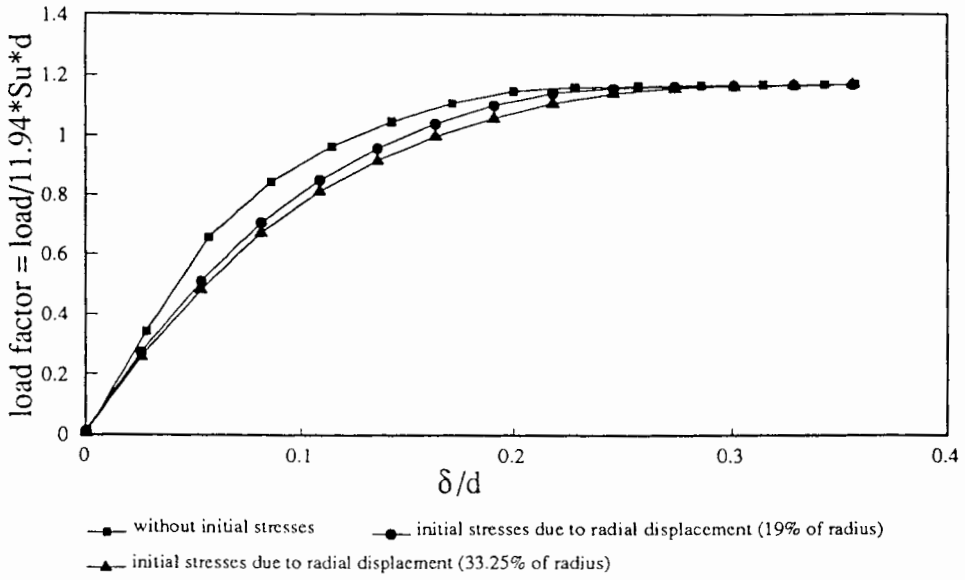

Figure 5.17: Effect of initial stresses on the load factor

curves is due to finite element discretisation and the approximations inherent in the finite element method. A similar observation was made by Brown and Shie (1991) in their finite element analyses by varying K_o values in their three dimensional analyses. Although, the presence of initial stresses do not effect the ultimate lateral resistance but they have an effect on the initial response of the pile i.e. at loads less than ultimate loads. The stresses in the soil will depend on the past loading history of the ground. As the pile is driven, these stresses are altered. Theory derived from an analogy with the monotonic expansion of a cylindrical cavity (to model stresses in the ground due to pile installation) was proposed by Carter *et al.* (1979). More recently two-dimensional strain path solution have been developed by Baligh (1986). We will not discuss the strain path method in this section and will use the former theory as its suits computationally to the plane strain finite element analyses described in this Chapter. (However, some recent studies reported in the literature seems to support the strain path method e.g. Jardine and Potts (1988) and Bond and Jardine (1991).) Carter *et al.* (1979) showed that these stresses can be taken as stresses caused by expanding a cylindrical cavity from a zero initial radius. (In contrast to this real situation, axi-symmetric numerical calculations need to begin with a finite cavity radius to avoid infinite circumferential strain

that would occur for an initial cavity radius of zero.) Hill (1950) has presented closed form solution for the creation of a cavity from zero initial cavity radius in a rigid plastic material which follows Tresca's yield criterion (Calladine (1985)). Hill (1950) has shown that limit cavity pressure is reached immediately, before any displacement occurs. Gibson and Anderson (1961) has presented the closed form solution in an elastic-perfectly plastic Tresca material. Carter *et al.* (1979) has shown that Gibson and Anderson's (1961) solution approaches Hill's (1950) solution at larger radii. The authors have found that the doubling of cavity radius is adequate (to generate stresses in the soil which are created by expanding a cavity from zero radius) and expanding beyond twice the cavity radius is simply to cause a further growth of annular region of yielded soil. Carter *et al.* (1979) have also shown that the final stresses are independent of the initial overconsolidation ratio OCR. The effect of these initial stresses, after the expansion of the cavity, on the limiting lateral resistance of the soil subjected to the applied lateral load is studied in this section. The problem of cylindrical cavity expansion in incompressible material (material under consideration in this chapter) has also been studied by Sagaseta (1984) for an elastic-perfectly plastic von Mises material using large strain analysis and presented close form solutions for the stresses. In order to model the effect of installation stresses on the lateral response of a rigid disc, the stresses (see Figure 5.18) given by Sagaseta (1984) are set up in the finite element mesh by expanding a cavity by a ratio of 4 before loading the disc laterally. Although, there is a yielded soil around the pile due to cavity expansion which seems to suggest that there will be zero incremental stiffness upon loading the pile laterally soon after installation. Figure 5.19 shows a finite value of stiffness i.e. there is still an initial elastic response before reaching the value of ultimate lateral reaction. This elastic stiffness perhaps arises from the elastic region bounding the plastic zone and due to change in stress path (i.e. once the cavity is expanded) which soil particles have to follow in order to mobilise a collapse mechanism to achieve the ultimate lateral reaction. The analytical solution of Randolph and Houlsby (1984) for a rigid disc is an exact solution whereby both lower bound and upper bound solutions match. In the derivation of the analytical solution, a complete tension at the back of the disc and a complete adhesion all

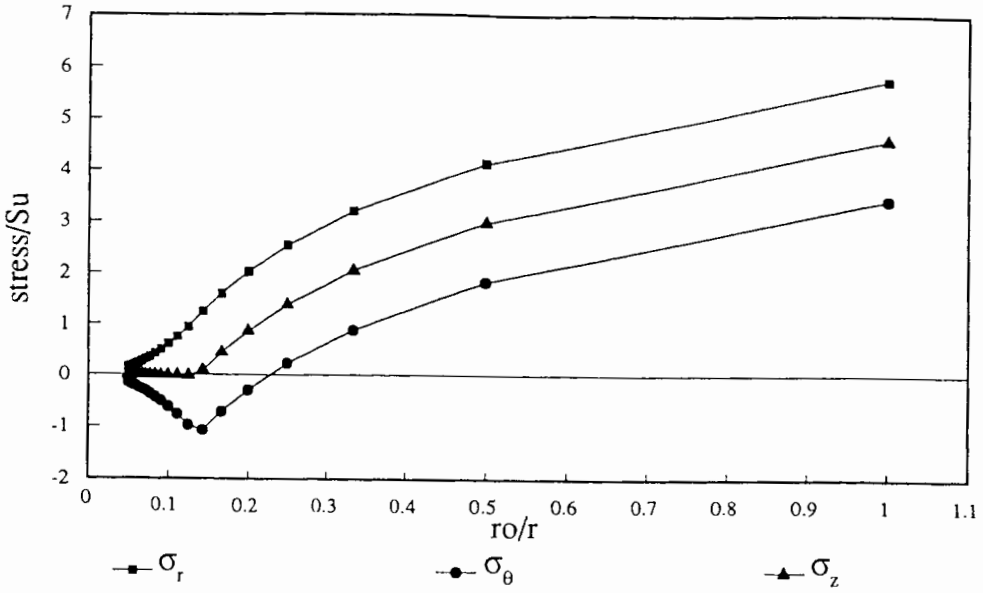

Figure 5.18: Distribution of stresses after pile installation

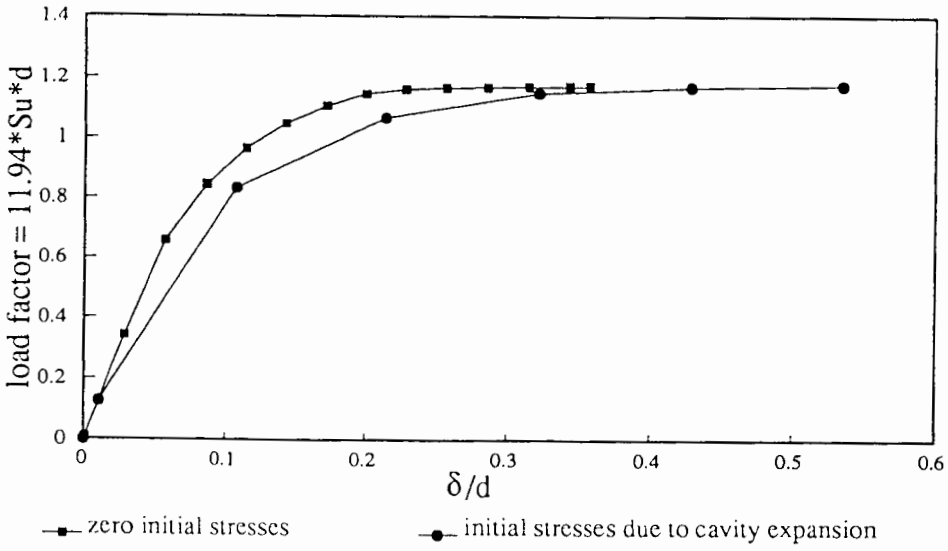

Figure 5.19: Effect of installation stresses on the load factor

around, are assumed. The presence of initial stresses due to installation, which are assumed to arise from the expansion of a cylindrical cavity in an elasto-plastic material, is supposed to relieve some of the tension at the back of the disc. It seems that the stresses arising from the cylindrical cavity expansion are not sufficient for complete tension relief at the back of the pile but do result in a partial tension relief, which is compensated by the increased friction

at the sides of the disc. Thus, no effect of the initial stresses on the limiting load is observed in Figure 5.17. Figure 5.19 shows that when the disc is displaced laterally after expansion of the cavity, the cavity expansion stresses have negligible effect on the soil limiting resistance. However, pre-yield behaviour is affected by the presence of initial stress and plastic flow around the pile. The numerical results of this section confirm the Randolph and Houlsby (1984) solution which is derived as independent of the current (total) stress level. It is important to note here that (according to Baguelin *et al.* (1977) elasticity solution) these displacements are also affected by the choice of zero-displacement boundary in the finite element mesh. As shown earlier, the strong dependency of displacements on zero-displacement boundary can be reduced by adopting a non-linear soil model as described earlier in Section 5.4 (see Figure 5.9).

5.8 Analysis of a single-pile assuming radial variation of soil strength around the pile

The subsequent phase following installation is soil consolidation around the pile. The excess pore pressures generated in the previous phase dissipate over time increasing the effective stresses around the pile. Along with this rise in stresses, the undrained shear strength of the soil within the plastic zone also increases over time compared to the rest of the surrounding soil (see Figure 5.20). This constitutes a radial inhomogeneity of the soil. The shear strength increase with radial distance from the face of the pile, after the end of the consolidation phase can be given by a logarithmic distribution, which was presented by Randolph, Carter and Wroth (1979).

The third and final phase, after consolidation, is the actual loading stage when the soil has completely recovered from all the initial disturbances and regained strength to carry the applied loads. This situation is modelled by setting up the stresses and the increase in strength, after the end of the consolidation phase obtained from Randolph, Carter and Wroth (1979), in the mesh. In the present study, the logarithmic strength increase was, as suggested

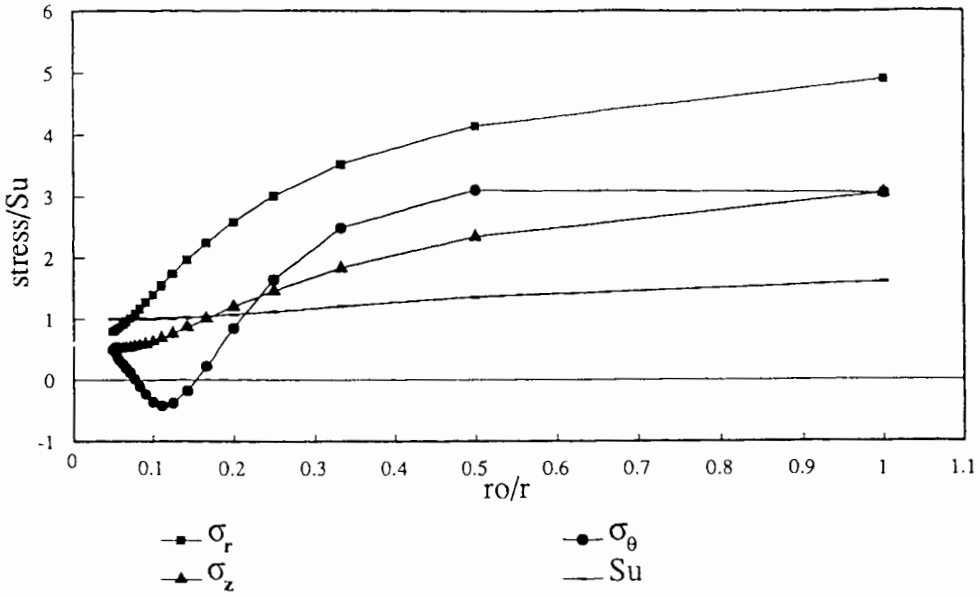

Figure 5.20: Distribution of stresses after the end of consolidation

by Randolph, Carter and Wroth (1979), incorporated to begin with, in the finite element mesh by dividing it into various sub-regions and specifying the new shear strength values in a stepwise fashion (obtained from the logarithmic curve at the end of consolidation, as mentioned above - see Figure 5.22) of these regions. However, a more appropriate way to achieve this variation in shear strength with radial distance was to do consolidation analysis using a work-hardening soil model (the Modified Cam-Clay model) before running any lateral load analysis. Studying the effect of the shear strength increase on the limiting lateral resistance of the soil in this way, there was found to be a 35% increase in the latter. The finite element mesh is shown as Figure 5.21. There are 396 linear strain triangles with 348 free degrees of freedom. Variable shear strength used in the analysis and the results are shown in Figures 5.22-23 respectively. (The shear strength at the end of consolidation is denoted by (^). The pile radius is r_o and r is the radial distance from the centre of the disc.)

The results in Figure 5.23 show that if the pore water in the soil around the pile is allowed to drain, a higher load is required for failure than otherwise. This implies that pile groups would also require higher loads at which the plastic zones around the individual piles will

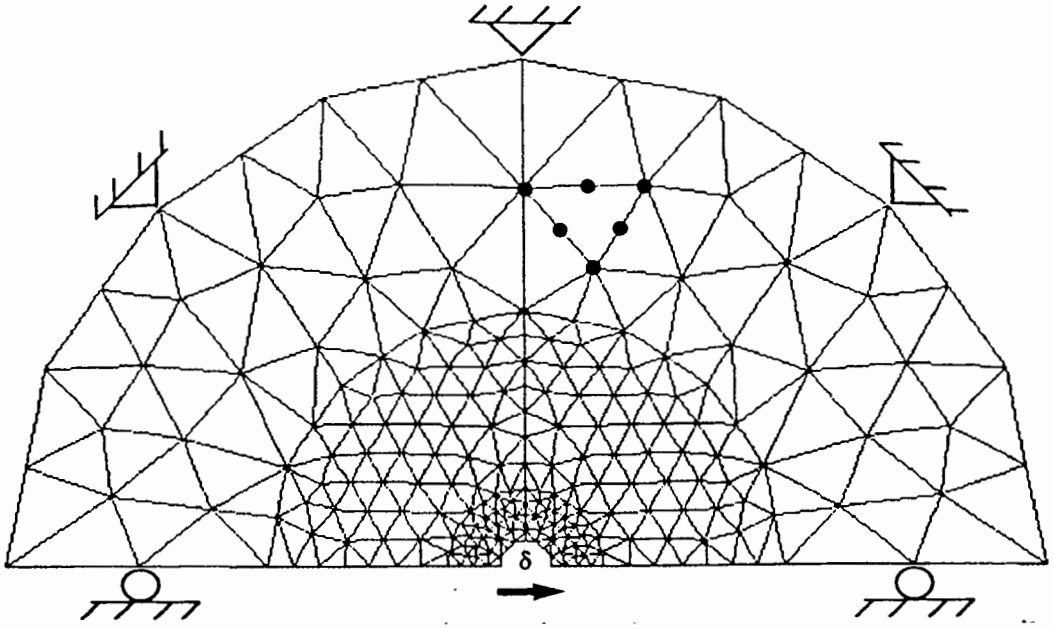

Figure 5.21: Finite element mesh with variable shear strength around the pile

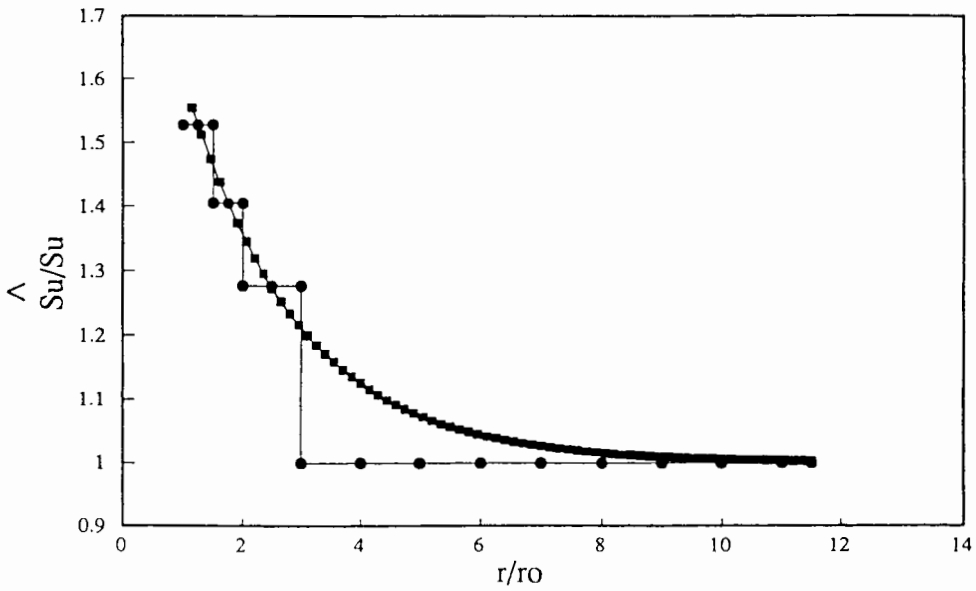

Figure 5.22: Variation of shear strength around the pile

start to overlap causing greater pile-soil-pile interaction. Later on a simplified analysis was performed in which the logarithmic variation of shear strength and the initial stresses after consolidation were incorporated in the finite element program. This modelling was achieved by fitting mathematical expressions to the stresses and the increase in shear strength predicted by Randolph, Carter and Wroth (1979) and then implementing in the finite element solution. Thus radial inhomogeneity was duly accounted for in the analysis. (Another approach to

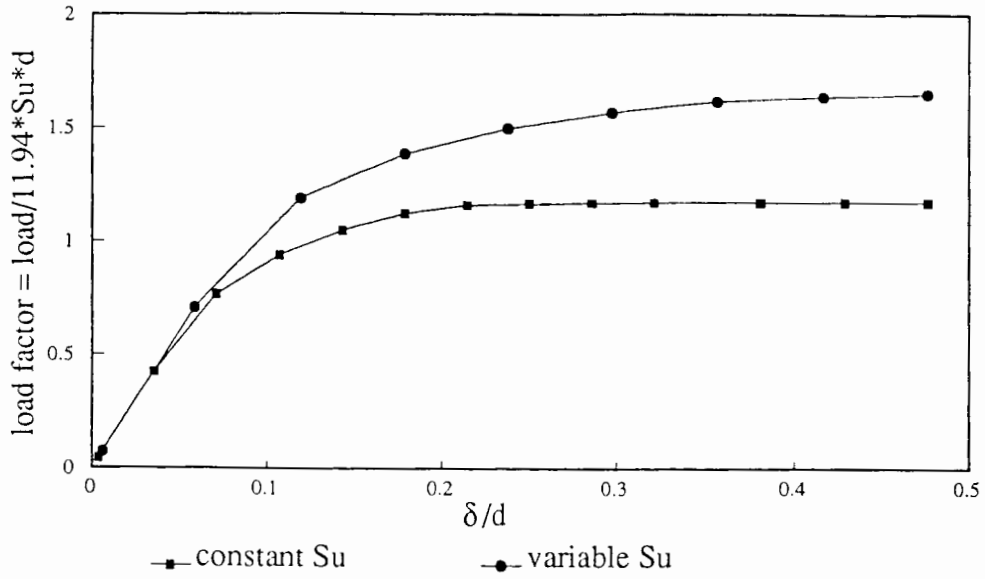

Figure 5.23: Load factor displacement curves (variable shear strength)

model radial variation of the soil shear strength is to relate it with the change in the hydrostatic pressure in the soil as the finite element proceeds. Randolph, Carter and Wroth

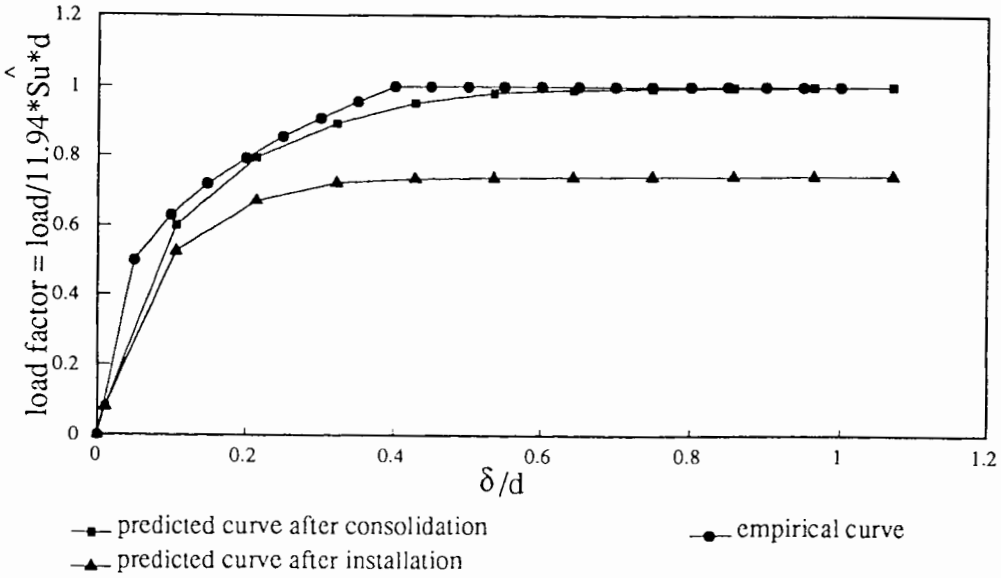

Figure 5.24: Comparison of *p-y* curves

(1979) suggested an approximate relationship between the change in the hydrostatic pressure and the soil shear strength at the end of the consolidation phase. This relationship when implemented in the finite element analysis provides a more realistic response of laterally loaded single-piles as well as pile groups.) The mesh dimensions were kept at $20r_o$ from the

centre of the pile (see Figure 5.21). The results are shown in Figure 5.24. The figure shows that the *p-y* curve obtained numerically match closely with the *p-y* curve proposed by Matlock (1970). Thus this pilot study shows that better *p-y* curves can be derived using plane strain finite element analysis. Although a non-linear model seems more appropriate in this case, as we can see that after the end of the consolidation, soil has undergone a loading-unloading cycle, and its behaviour will tend to be strongly non-linear rather than linear upon re-loading. (The strain response on unloading and reloading is hysteretic. There is no longer one to one relationship between stress and strain in the region. The soil stiffness is influenced by the recent stress history. Therefore, nested yield loci model (Houlsby and Chow (1994)) seems to be more suitable to model soil behaviour at the end of the consolidation phase.) Finally, Figure 5.24 compares the load displacement responses both immediately after installing the pile and after the end of the consolidation phase. The figure shows that the pile capacity immediately after installation is almost half of that at the end of consolidation phase.

In the analysis of Randolph, Carter and Wroth (1979), the choice of shear modulus G in the soil model adopted, influences the generation of excess pore pressures. They pointed out that if the shear modulus was tied to current effective stress level (rather than to the past maximum stress level) then lower pore pressures were generated. They did not recommend that shear modulus be linked with current *in situ* stresses which results in low values of I_r at high values of OCR. This seems to suggest that the initial effective stresses in the soil may affect the resulting shear strength increase after the end of consolidation around the pile and in turn the ultimate limiting soil resistance of the soil. Another point made by Randolph, Carter and Wroth (1979) about their analysis concerns taking account of the assumption of plane strain conditions and ignoring the shear stresses in the vertical plane (***r-z*** planes). Shear stresses will be present not only due to residual driving stresses but also to balance the high total vertical stresses which occur during pile driving. Field measurements have shown that excess pore pressures, greater than the existing effective overburden stresses, are generated during pile installation. The resulting changes of total vertical stress must be balanced by shear stresses in the soil around the pile in order to maintain vertical equilibrium. The effect

on the resulting increase in soil shear strength around the pile of the presence of these shear stresses, and the resulting out of plane (vertical) soil movement, has yet to be investigated.

5.9 Interface analysis

A purely cohesive interface, zero thickness element with some allowable tension cut-off value, developed in Chapter 4, is used here to model pile-soil interaction. The need to use this type of element arises for the following reasons. Firstly, it is capable of capturing the deformations close to the pile where there are very high stress concentrations and strain gradients i.e. it smooths stresses at the discontinuous boundary. Secondly, it is capable of studying tension at the back of the pile. Thirdly, it is possible to vary the adhesion between the soil and the pile. Although this possibility was not tried out. It was found that even a coarse finite element mesh with a layer of interface elements next to the pile predicted the exact limiting load given by Randolph and Houlsby (1984). Earlier, Kooijman (1989) also showed that the predicted limiting lateral load using a refined finite element mesh was the same as from a coarse mesh with the addition of a thin layer of continuum elements or interface elements to model the pile-soil interface. In the analysis of a rigid disc displaced laterally in a cohesive soil, the soil is highly constrained next to the rigid disc so does the mesh close to the rigid disc, which explains the over-stiff response in the absence of an interface element. In the absence of an interface element, the number of free degrees-of-freedom are not enough in the coarse mesh to predict an exact collapse load, which results in a gross over-estimation of the limit load (see Section 5.4). The presence of the cohesive interface elements provides additional degrees-of-freedom in the coarse mesh without any increase in the incompressibility constraints, and so corrects the over-prediction by eliminating the over-stiff response. The finite element mesh used in the analysis is shown in Figure 5.25. The use of interface elements need a careful choice of interface stiffnesses. Choice of lower stiffnesses makes the interface flexible and the predicted limiting load remains lower than the exact limiting load given by Randolph and Houlsby (1984). A predicted lower value for the limiting load should not mean that the finite

element method under-predicts the limiting lateral load (which can not be right). The under-prediction can be improved (though not completely) by using a higher order integration scheme for the interface elements i.e. by over integrating the stiffness matrix or with the choice of appropriate interface stiffnesses as is the case for the analysis described in this section. Interface shear and normal stiffnesses used in the present analysis are *71500 kN/m* and *143000 kN/m* respectively. Sometimes the choice of interface stiffnesses makes the interface stiffer than required which brings ill-conditioning in the calculations and instabilities in the final solution.

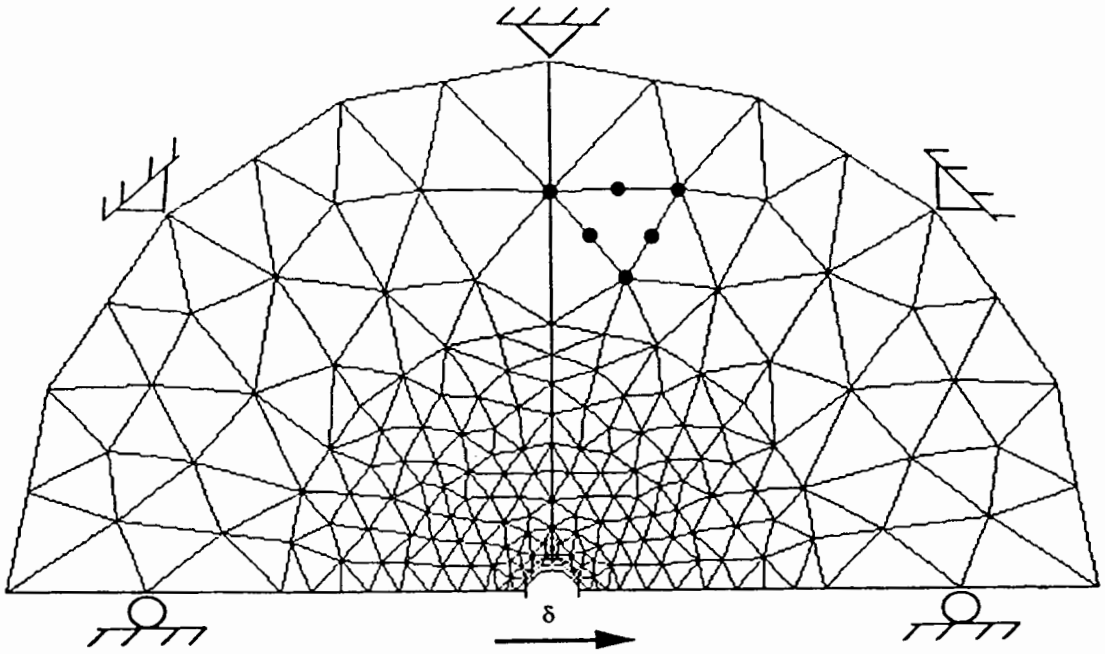

Figure 5.25: Finite element mesh with a layer of interface elements around the rigid pile

The load displacement curve with full tension at the back of the pile is shown in Figure 5.26.

5.10 Effect of no-tension behaviour of pile-soil interface

As the lateral load on the pile increases, the strength of the soil at the back of the pile is

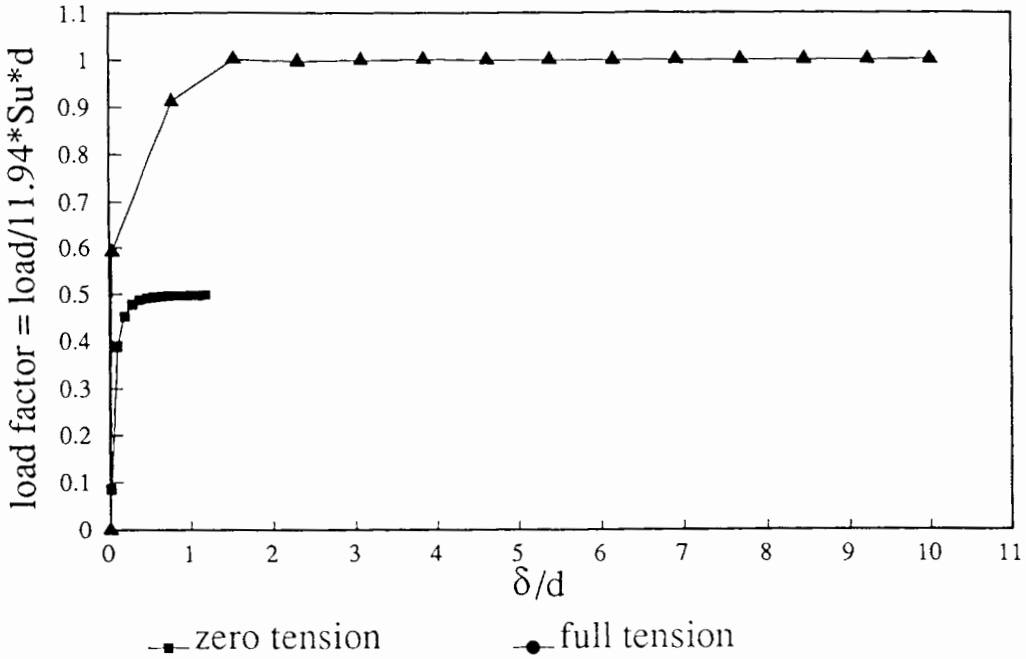

Figure 5.26: Interface analysis for a single rigid pile

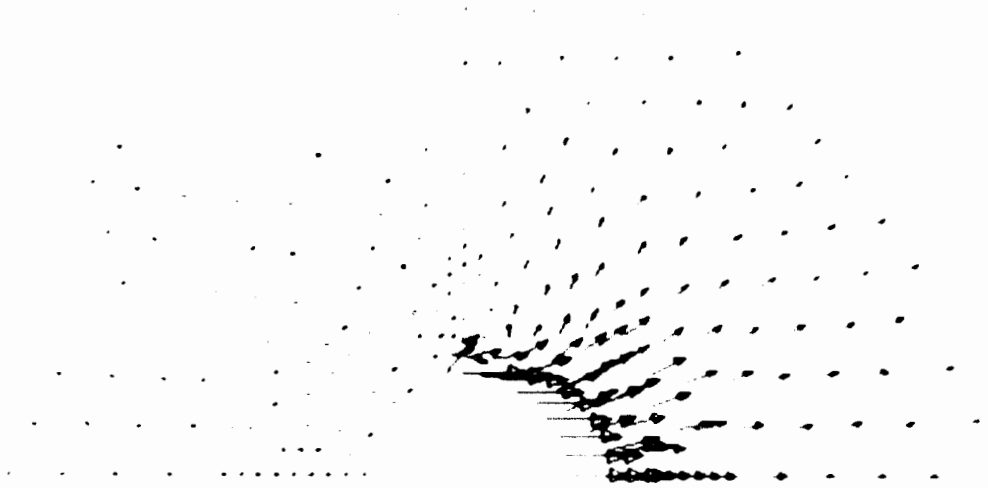

Figure 5.27: Vector plot of displacements when a gap opens up at the back of a laterally loaded pile

exhausted and unable to take any further tension. At this stage of tension cut-off, a gap between the pile and the soil opens up with a sudden decrease in the lateral load capacity of the pile. (A vector plot of displacements when a gap between the pile and the soil opens up

is shown in Figure 5.27.) The interface element predicts the limiting soil reaction which matches with Randolph and Houlsby's (1984) solution (see Figure 5.26) and if there is a tension cut-off, the value of limiting soil reaction reduces to half of its value with full tension i.e. as in the exact solution given by Randolph and Houlsby (1984). The tension cut-off value specified in the analysis is *250 kPa*. The adhesion between the soil and pile can easily be varied by changing the value of the shear strength of the interface.

CHAPTER 6

PLANE STRAIN ANALYSIS OF PILE GROUPS

6.1 Introduction

Groups of piles are generally arranged in square/rectangular grids, or in concentric circles, with the spacing of the piles determining the size of the foundation. A pile group may contain battered piles and may be subject to simultaneous axial, lateral, moment and possibly, torsional loads. In this chapter we will be dealing with laterally loaded pile groups only. In the absence of analytically derived solutions for the ultimate soil resistance in a laterally loaded pile group, the focus will be mainly on the numerical methods currently in use. These methods can be categorised into three main types as described below.

In Type 'one' methods, the piles are treated as beams and the soil is represented by non-linear springs. The characteristics of the springs may be determined by empirical rules e.g. the *p-y* curves proposed by Matlock (1970) for saturated soft clays or by plane strain calculations as described in this chapter.

Type 'two' methods treat both the pile and the soil as a 'continuum'. The behaviour of the piles grouped in this case may be determined by any suitable method e.g. the integral equation/boundary element method or the finite element method. (Generally speaking the boundary element method is most appropriate for elastic soil behaviour and the finite element method is most appropriate for cases where non-linear soil models are assumed. Detailed

discussion of previous work on these methods is given in Chapter 3. The obvious problem with these methods is that the amount of computation required is immense in any multi-pile group. Therefore, it is usual to perform the calculations for two piles and to work out the interaction factor α between them. The analysis of a two-pile group is then extended to any number of piles in a group as proposed by Poulos and Davis (1980) and is known as elastic interaction approach for the prediction of pile head displacements.) To model elasto-plastic soil behaviour, the finite element method is the best among those available, although it too has limitations. Its limitations derive from the problem of knowing where to fix a 'boundary' to the soil continuum, and from the problem of knowing which of the soil models will give the best results in any given situation. It follows from these limitations that care need to be taken in applying this method. But does it matter whether the finite element analysis is done for three-dimensions or only for two-dimensions? Three-dimensional analysis is prohibitively expensive in terms of volume of calculations and corresponding computer memory involved. However, the technology is developing all the time and it may be possible to run a three-dimensional analysis more economically in the not-too-distant future. Until a new generation of fast high memory computers becomes available, a two-dimensional analysis is clearly preferable.

Type 'three' methods use interaction factors to describe the interactions between the piles in a group. It is assumed that an interaction factor is valid for any two neighbouring piles in the group regardless of their position in the group and regardless of the total number of piles. Interaction factors may be computed using a type 'two' method. The interaction factor approach is certainly applicable at the pile cap level (pile head). That is good enough insofar as it provides the vertical settlement and lateral deflection of the pile head. However, it ignores the variation in deflection and bending moment along the length of the piles. Piles have to be considered as having a constant cross-section, and the pile head restraints have to be either fully fixed (i.e. no rotation) or fully free (i.e. no bending moment). The basic

assumption is that all piles in the group behave identically i.e. the piles are spaced equally around a circumference of a circle, each pile displaces equally and carries equal load (a symmetrical group) and the principle of superposition is valid. The limitations of the elastic approach to pile interaction under lateral loading were exposed by the model pile tests carried out on a centrifuge by Barton (1982). These tests showed that the leading piles of groups embedded in sand carry a higher proportion of overall applied load than the trailing piles even at load levels lower than the failure load. For pairs of piles at close spacing (s/d=2), Barton found that at a lateral displacement of 0.2d, the applied load was shared 60% to the front piles and 40% to the rear piles. By contrast, Matlock *et al.* (1980) had reported results of tests on pile groups in clay, in which applied load was found to be shared quite uniformly. Clearly, the adequacy of the interaction factor approach depends on a number of factors such as load level, soil type, and most importantly pile spacing. The assumption that the interaction factor between the piles remains elastic, and the principle of superposition applies, is not valid at all for closely spaced pile groups: the elastic interaction approach works well at small displacement levels. (We shall see in the following Sections 6.2-3 (Figure 6.5 and Figure 6.11) that at close spacings, the load shared by individual piles in a 2-pile group and a 2x2 pile group is equal only at small displacements.) Such simplification of the problem, together with the other assumptions and approximations entailed, means that the resulting solutions based on elastic interaction approach are not reliably accurate.

Chapter 5 analysed pile-soil interaction for a single-pile and demonstrated that a two-dimensional idealisation corresponds very well with real behaviour beyond a depth of 3.0 times the pile diameter below the surface (Broms (1964a)), and when the mesh boundaries are more than 10 times the pile diameter from the centre of the pile. The same conditions should apply in the finite element analyses of pile-soil interaction for pile groups. It is the aim of this chapter to test whether that is the case.

The chapter is divided into five further sections as follows: Section 6.2 describes the finite element analyses of 2-pile groups under two loading conditions - when the load acts in a

direction parallel and perpendicular to the line joining the pile centres of the 2-pile group. A comparison is made between soil resistance around a single-pile and a 2-pile group in order to determine the most effective spacing to meet the specified loading conditions. Analytical expressions are also suggested as a way of comparing and checking results from the finite element method. Section 6.3 presents plane strain analysis for a 2x2 pile group, and it confirms the conclusions drawn from Section 6.2. Section 6.4 describes interaction factors between piles where the effective pile spacing (Figure 6.7, Sections 6.2 and 6.3) is not possible. It is found that the inter-relationships between the piles spaced otherwise is not linear at all, rather it is highly non-linear. An iterative analysis procedure is proposed to predict load-displacement response of a symmetrical pile group. The analysis procedure makes use of non-linear interaction factors determined in Section 6.4. Section 6.5 describes plane strain analyses of pile groups to obtain theoretical *p-y* curves which take account of non-linear pile-soil-pile interactions. Section 6.6 tries to explain theoretically why certain results obtained from field tests carried out on a 5-pile group and a 10-pile group drift from what is theoretically predicted by others. The methods of back analysis that have been tried to date were discussed in Chapter 2 and the difficulties with them pointed out. The numerical approach used here enables us to quantify the interaction attributed to the overlapping plastic zones around the piles. Section 6.6 also suggests an alternative method in the absence of the ideal three-dimensional finite element analysis. A two-dimensional finite element analysis combined with the *p-y* curve analysis enables the engineer, particularly one designing pile foundations for offshore structures, to design with a greater assurance that the foundation will be sound and economical.

6.2 Plane strain analysis of 2-pile groups

The limiting load for a pile in a rigid 2-pile group where both piles undergo equal displacements could be higher or lower than that for a single-pile depending upon the

direction of loading. In the discussion following, a 2-pile group is analysed for two loading conditions - when the applied load is parallel to the centre line of the pile group and when it is perpendicular to the centre line. The finite element meshes used in the analysis are shown in Figures 6.1 and 6.2. The symmetrical nature of the problem means that only half of the geometry needs to be discretised.

The mesh dimensions are chosen in a way similar to that adopted for the single-pile analysed in the preceding chapter. The element type, the boundary conditions and the material properties are also the same.

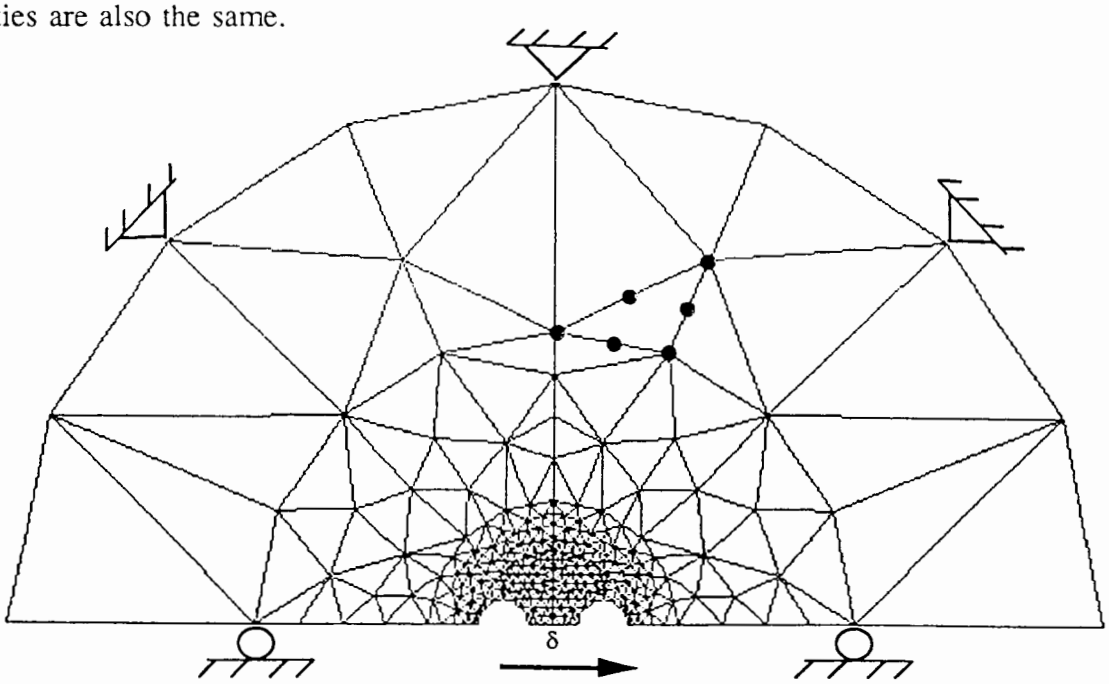

Figure 6.1: Finite element mesh for a 2-pile group (loading parallel to the centre line of the pile group)

The curve for the single-pile in Figure 6.3 shows some considerable discrepancy (%error = 14) with respect to the analytical solution given by Randolph and Houlsby (1984). This is due to the coarse discretisation of the mesh used in the analysis. A mesh of similar density is used in the analysis of the two-pile group. Therefore, a comparable error does exist in the curve for the two-pile group. The errors are also due in part to the particular type of finite element chosen for the analyses. Six-noded triangular elements are quite suitable for the collapse load calculations in nearly incompressible materials (i.e. undrained clays with which we have been

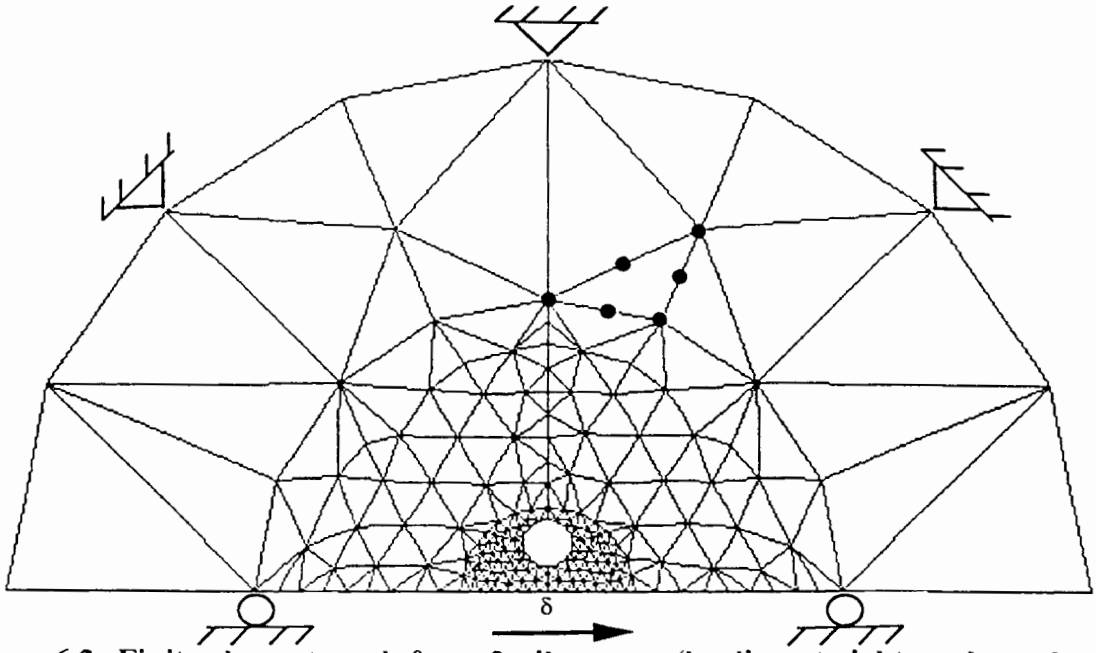

Figure 6.2: Finite element mesh for a 2-pile group (loading at right angle to the centre line of the pile group)

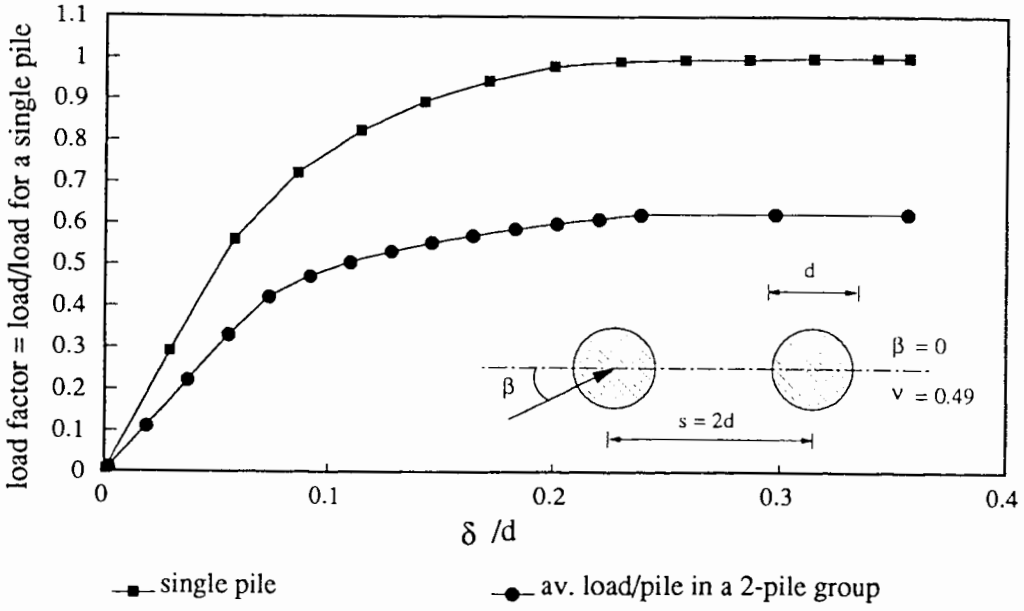

Figure 6.3: Load displacement curves (2-pile group; ß=0)

dealing), and have the additional advantage (as compared to the quadrilateral family of elements) that the polynomial functions defining the displacements within the element are complete. However, they fail to capture the strain fields around the piles and need finer

discretisation to do so. At a centre-to-centre pile spacing of two pile diameters (see Figure 6.3), if the loading is parallel to the centre line of the pile group, the limiting load for a pile in a group is nearly half that for a single-pile as described in Chapter 5. The reduction is due to the overlapping plastic zones between the two piles which modifies the stiffness of the soil. Randolph and Houlsby (1984) showed that the expected plastic zone in front of a laterally loaded pile extends to a distance of one diameter from the face of the pile. This means that there will be a complete overlap of plastic zones at a centre-to-centre pile spacing of two pile diameters (see Figure 6.4). At a spacing of three pile diameters the boundaries of the plastic zones will be just touching each other; they move further apart until, at a spacing of about six pile diameters, the lateral reaction approaches that of a single-pile. (The pile spacing at 7d is derived analytically: see below, equation (6.1) and Appendix 6A.)

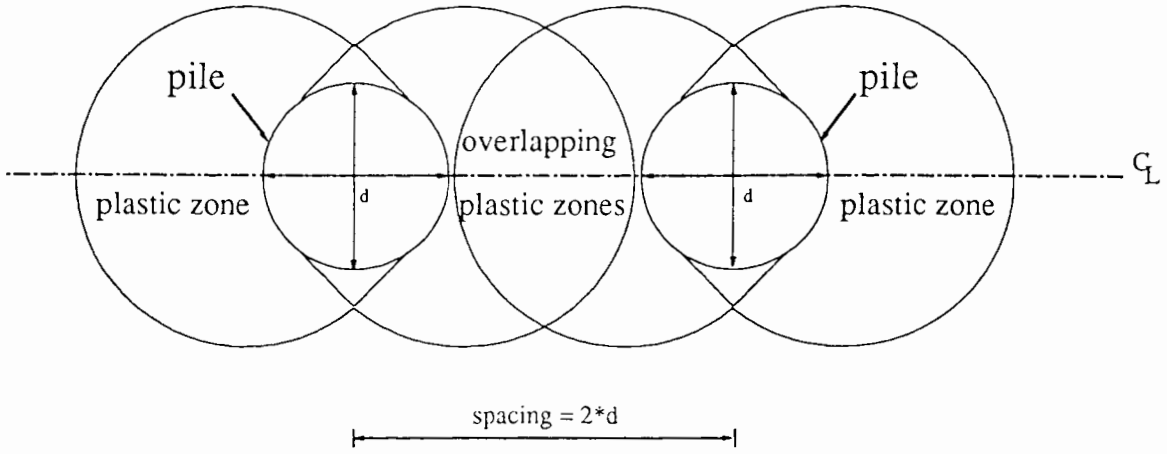

Figure 6.4: Overlapping plastic zones in 2-pile group (loading parallel to the centre -line)

The load shared by the individual piles in a 2-pile group (spacing = 2d; loading parallel to the centre line of the pile group) is shown in Figure 6.5. Load shared by each pile is uniform at small displacement levels.

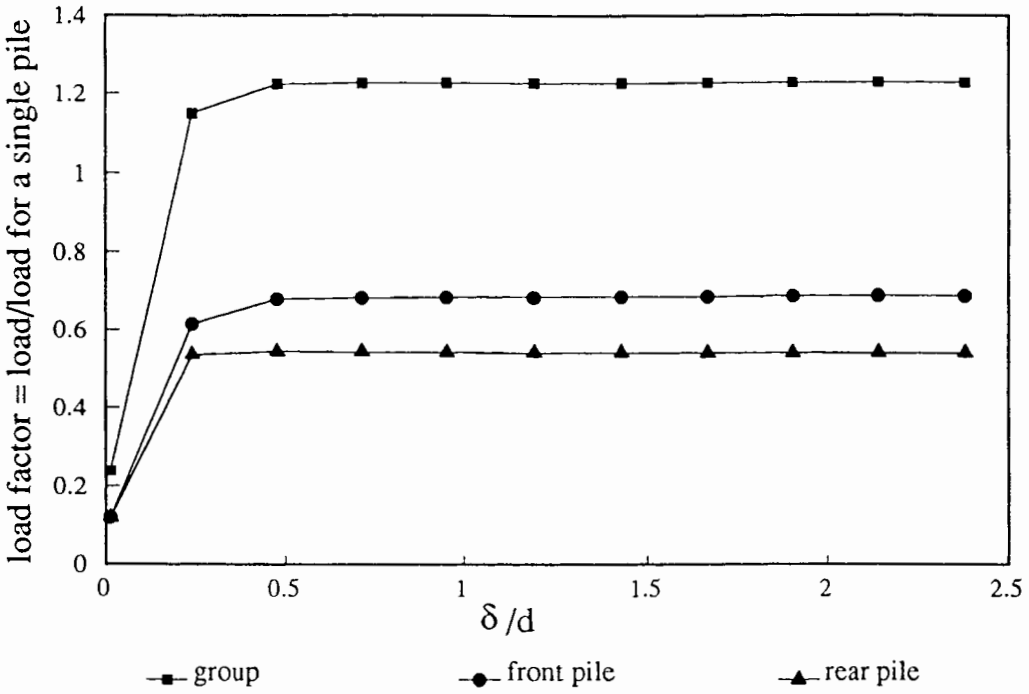

Figure 6.5: Load distribution among the piles in 2-pile group (spacing = 2d)

The limiting load for a pile in a group may be higher than that for a single-pile, if the loading is perpendicular to the centre line of the pile group. The increase is due to the mobilisation of a larger plastic zone around the pile group which behaves like a large diameter single-pile instead of two piles in a group. This is shown in Figure 6.6 where angle β is the direction of loading. Figure 6.7 shows the results for variable pile spacing up to 10 diameters. Besides the finite element analyses, two simple analytical expressions can be used (with reservations to be explained below) to work out the spacing at which the pile group will attain the limiting load for a single-pile. The two expressions, when the load is in line with (parallel to) the pile group centre line and when it is perpendicular to that line are, respectively:

$$P = \frac{s}{d} + \frac{11.94}{\sqrt{3}} \tag{6.1}$$

and

$$P = \frac{11.94}{\sqrt{3}}(1+\frac{s}{d}). \qquad (6.2)$$

In both cases s is the pile spacing and, d is the diameter of the pile. (For details, see Appendix 6A.)

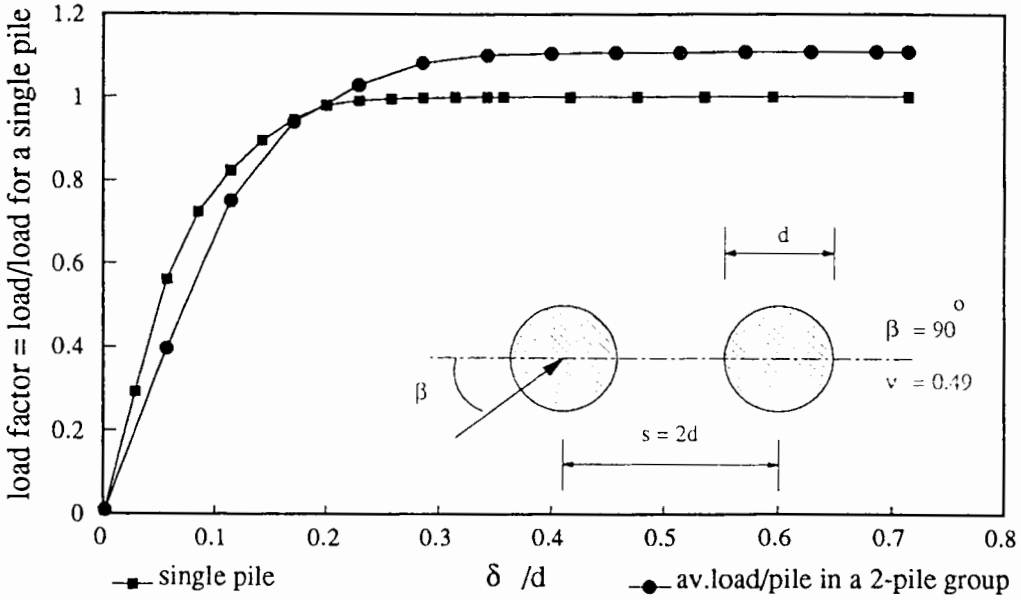

Figure 6.6: Load displacement curves (2-pile group; ß =90)

Whereas expression 6.1 is quite successful in that it suggests that at a pile spacing of approximately 7 times the pile diameter, the pile group attains the limiting load for single-pile, expression 6.2 is not so successful. Possibly, as the expression is derived on the basis of size of a plastic zone for a single-pile whereas in reality we have two piles and their interaction will effect the size of the plastic zone. It predicts higher limiting loads; and it does not fully trace the variation of the limiting load with the pile spacing. It works only as far as $s/d = 3$, at which point the limiting load drops abruptly to the value for a single-pile.

The results show that when the load is applied in line with the two piles, the limiting load decreases with closer spacing; as the spacing is increased, the value of the limiting load gradually reaches that for a single-pile. The reason for this is that plastic zones around each pile move further apart as spacing increases. The converse is the case when the load is

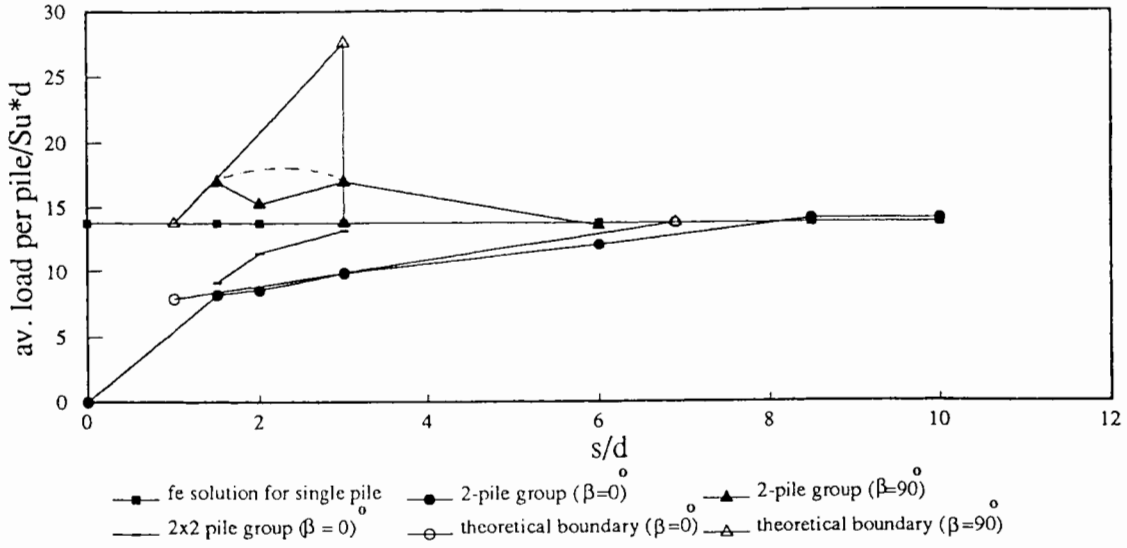

Figure 6.7: Variation of ultimate lateral reaction with variable pile spacing

perpendicular to the centre line of the pile group: i.e. the limiting load increases at closer spacings - the piles tend to act as a large diameter single-pile - and decreases gradually to the value of a limiting load for a single-pile at wider spacings. Note that the 2-pile group is stiffer for the loading case when $\beta=90°$ than the one when $\beta=0°$.

The dotted line in Figure 6.7 showing a possible curve for the 2-pile group when $\beta = 90°$. The spurious data point falling below this curve is due to numerical scatter: as explained earlier, the discretisation of the meshes used was too coarse to give ideal results. It is quite certain from the analytical solution (6.2) shown in Figure 6.7 that at pile spacing of three pile diameters, there can be no overlapping of plastic zones (see Figure 6.8) and therefore the limiting load must be the same as for a single-pile. In other words, the numerical results (using (6.2)) are sound on this point.

There is also non-convergence between the results for a single-pile and those for the pile group loaded parallel to the centre line. As shown in Figure 6.7, this non-convergence is very small.

The results summarized in Figure 6.7 clearly imply that the pile group is much stronger when

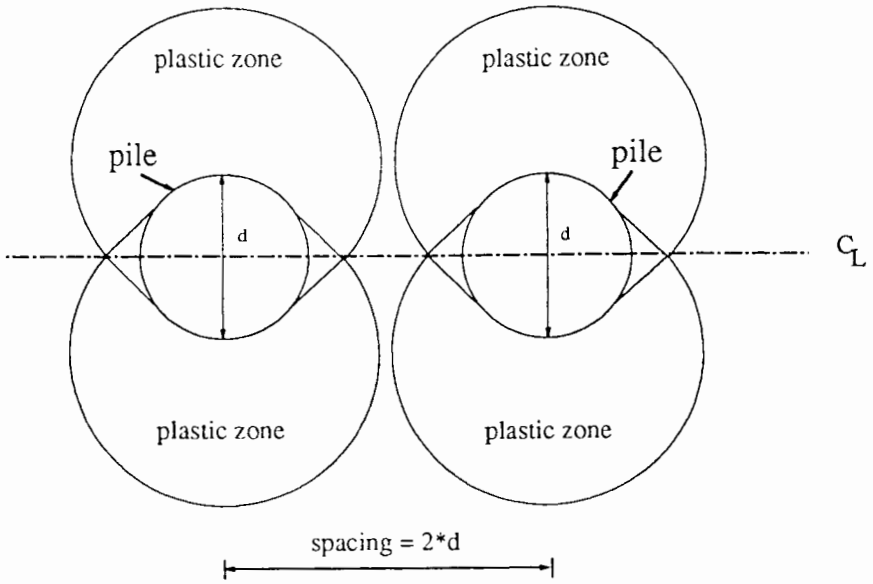

Figure 6.8: Plastic zones in a 2-pile group (loading perpendicular to the centre-line)

the applied load is at right angles to the centre line. It follows that for pile groups in rectangular patterns, where piles cannot be spaced far apart, there will be weakness on one side of the pile system. In this situation, and assuming spacing at more than two pile diameters, a circular arrangement of piles avoids this potential weakness. Returning to the results in Figure 6.7: ideally, piles should be arranged in a circle of diameter 6 times the pile diameter with a centre-to-centre spacing of 3 times the pile diameter.

6.3 Plane strain analysis of a closely spaced 2x2 pile group

Plane strain analysis of a 2x2 pile group confirms the danger, alluded to above, of block failure when piles are closely spaced. The finite element mesh for loading parallel to the centre line of 2x2 group is shown in Figure 6.9. As before, the mesh dimensions are fixed as in Chapter 5: the finite element type, boundary conditions and the material properties are the same as calculation in previous section. The results are summarised in the three curves in

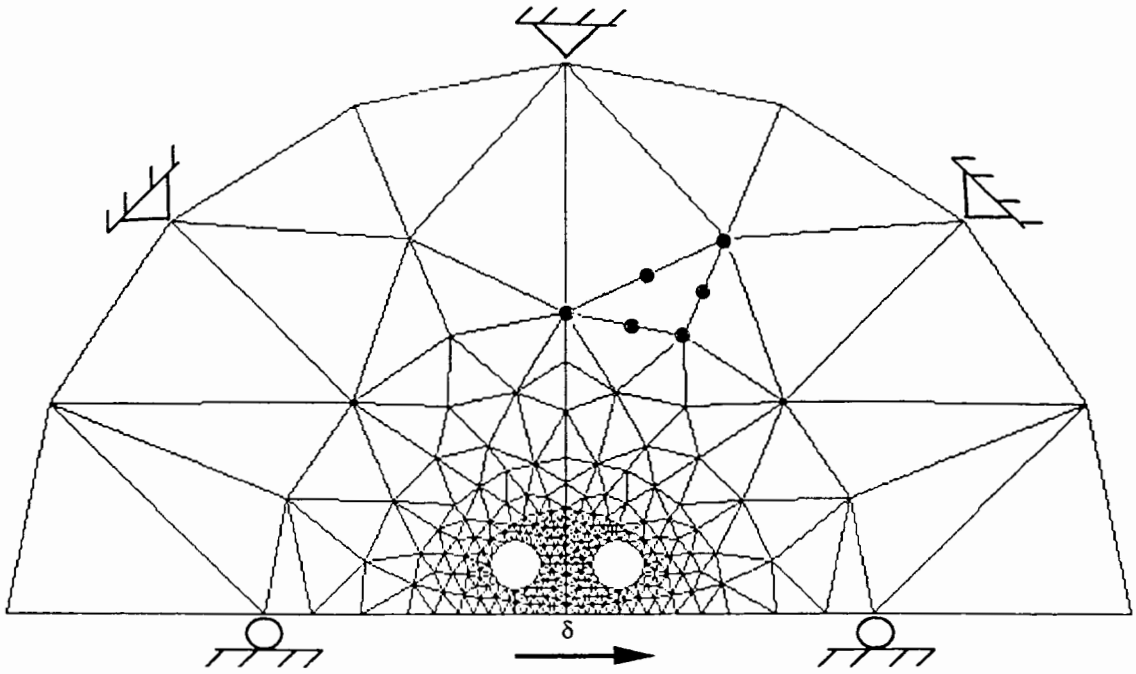

Figure 6.9: finite element mesh for a 2x2 pile group

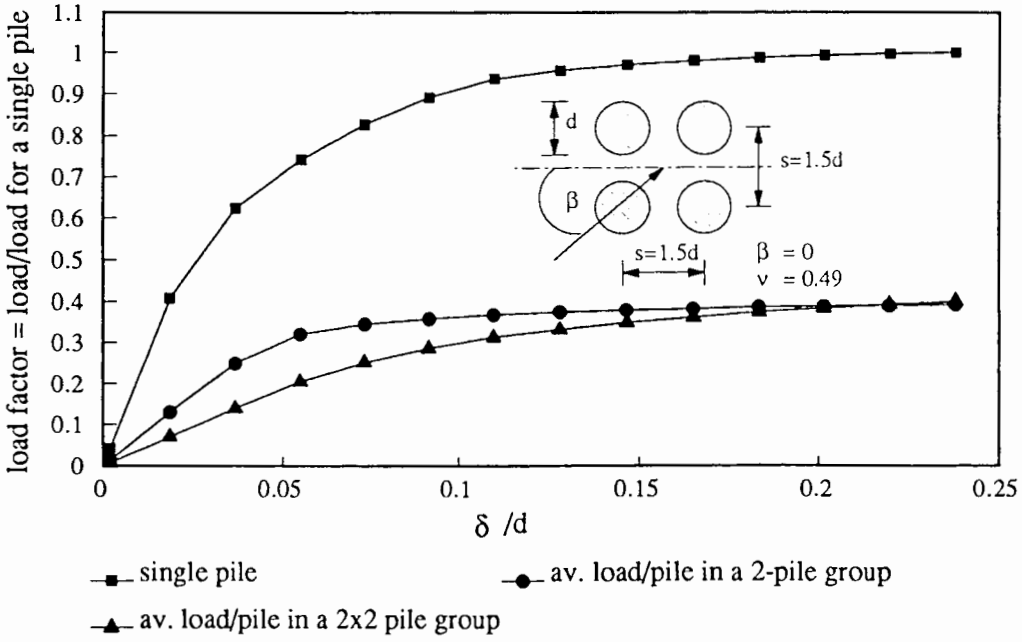

Figure 6.10: Load displacement curves (2x2 pile group)

Figure 6.10. As mentioned earlier, the curve for the single-pile shows a significant error of about 14% in the predicted limiting load; so a comparable error does exist as well for the

curves for the 2-pile and 2x2 pile group. In both groups the piles are spaced at 1.5 times pile diameter, centre-to-centre. Each pile develops a plastic zone which, at this spacing, overlaps with the plastic zones of the others. The results clearly show that the 2-pile and 2x2 pile group reach the same limiting load per pile, which is less than half the load for a single-pile. If we accept the error in the finite element results and assume that it could be reduced to acceptable limits (see above, Section 5.2) by using a finer mesh, then the results tell us that in the case of a rigid 2x2 pile group, the interaction between any two piles in line with the applied load is more significant than the interaction between any two piles whose centre line is at right angles to the applied load. The results also show that, initially, i.e. when the displacements are smaller, the response of each pile in the 2x2 pile group is more flexible than the one in the 2-pile group. Taken together, the results imply that in large square/rectangular pile groups where piles are arranged in longitudinal and transverse rows, the interaction between the piles in individual pile rows parallel to the direction of loading is going to be critical in the design of the foundation. Therefore centre-to-centre pile spacing should not be so small as to provoke block failure. The load shared by individual piles in a 2x2 pile group (spacing = 2d) is shown in Figure 6.11. The load distribution among the piles is uniform at small displacement levels.

6.4 Determination of pile-soil-pile interaction factors

In this section, non-linear pile-soil-pile interaction factors are discussed. A single plane strain finite element analysis of a pile represented as a rigid circular disc proved remarkably helpful in determining the interaction factors for variable pile spacings and for lateral loading at various departure angles (β).

Figure 6.12 shows the finite element mesh used. As before, half of the geometrical arrangement is enough for the analysis because of symmetry. A very fine discretisation of the mesh is necessary close to the pile due to high concentration of stresses. The numerical over-

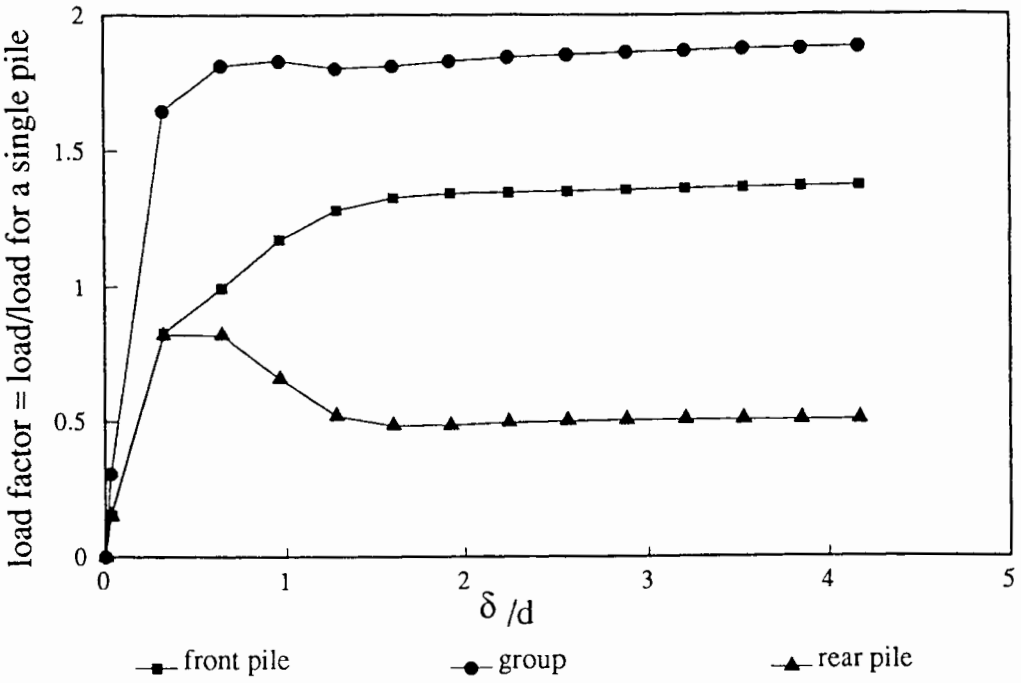

Figure 6.11: Load distribution among the piles in a 2x2 pile group (spacing = 2d)

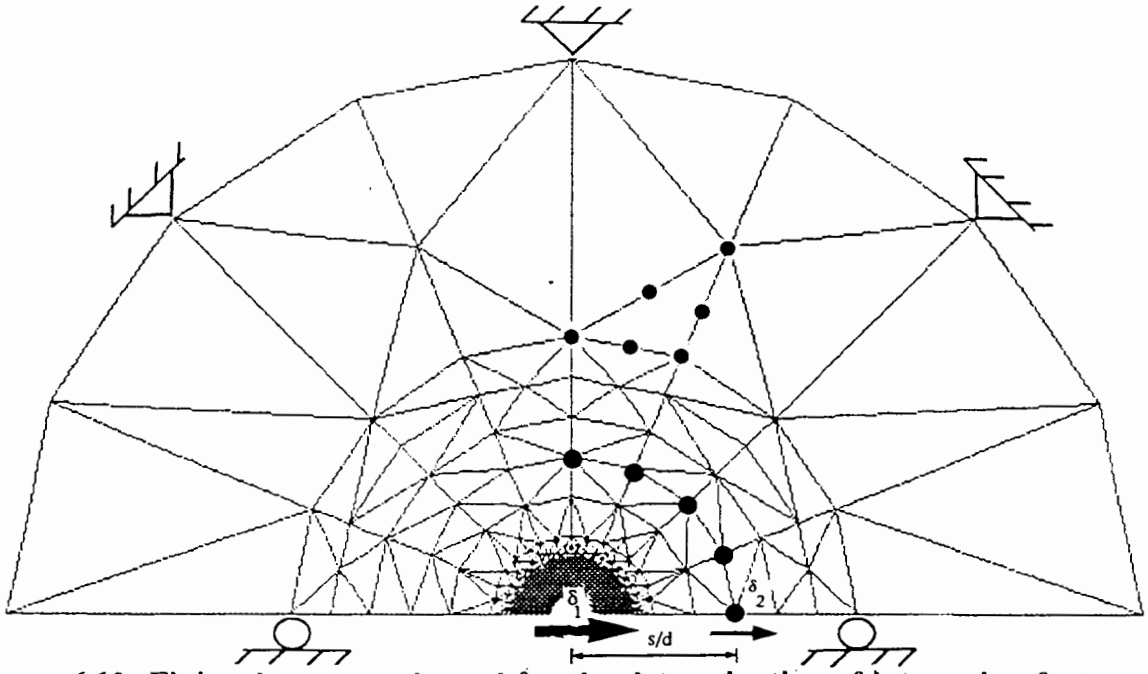

Figure 6.12: Finite element mesh used for the determination of interaction factors

estimation of the limiting load as determined by analytical method is below 5% i.e., the adopted mesh is better than the one used in the previous chapter. (The load displacement curve obtained from the finite element analysis using this mesh is shown in Figure 6.13.)

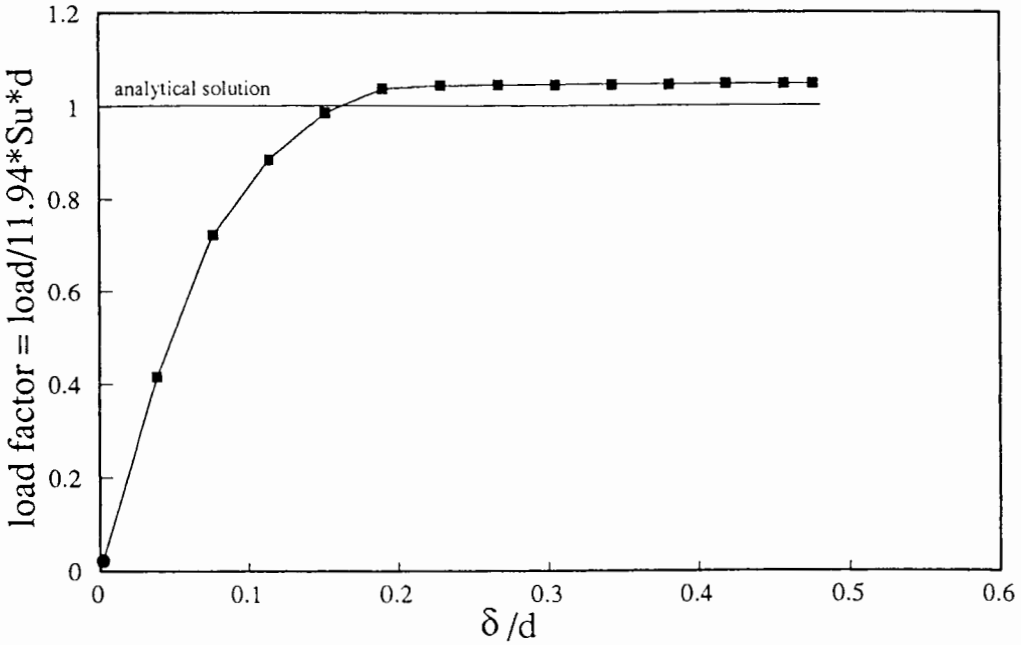

Figure 6.13: Load displacement curve

Variable centre to centre pile spacing in Figure 6.12 is represented by establishing nodal points in radial directions at departure angles (β) of 0, 22.5, 45, 67.5, 90 degrees. These nodal points represent pile spacings of up to 10 pile diameters.

When the 'disc' is moved laterally, it induces lateral movements in the same direction in the established nodal points. These lateral movements are in addition to movements which occur as a result of other loads (if any) acting on those points. An interaction factor can therefore be defined as the ratio of the additional displacement caused by an adjacent pile to the displacement caused by its own loading. This type of interaction has been studied by Mandolini and Viggiani (1992) for the case of a pair of axially loaded vertical piles.

Figure 6.14 shows interaction curves for loading at various departure angles, at a spacing of 1.5 times the diameter of the pile (similar curves can be drawn for other spacings). As we can see, the interaction factors are linear for small displacements (i.e. elastic interactions for small load levels) and after that increase non-linearly with the applied displacement/load. In other words, the figure shows that the interaction factors are not unique for all load levels. Curves for departure angles (β)= 0°, 22.5° converge toward the same level of ultimate interaction.

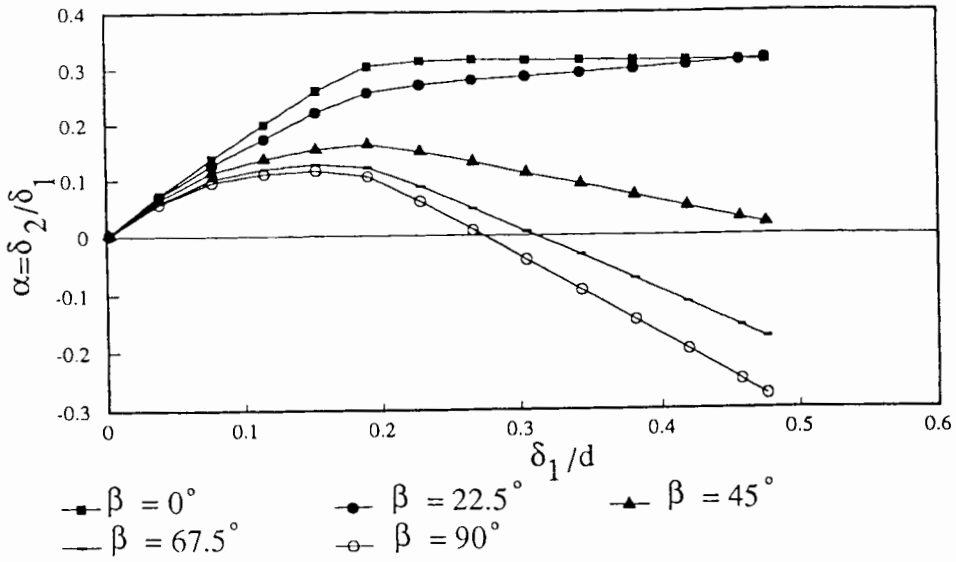

Figure 6.14: Interaction curves

Interactions with (β) = 45°, 67.5°, 90° reach a maximum value which is lower than the interaction values for (β)= 0°, 22.5° which diminish as the load increases. The diminishing values for departure angles (β)= 67.5°, 90° become negative and reach maximum negative value. This trend is as might be expected. When the lateral load approaches a limiting value, the soil tends to flow round the piles which causes them to move in a direction opposite to the applied load. This trend explains why side-by-side pile groups are stiffer. The movement of each of the piles impedes the other.

The results suggest that, in order to keep the effect of pile-soil-pile interaction to a minimum, the optimum angular pile spacing is 45°.

The non-linear variations of interaction factors with variable pile spacing for lateral loading for various departure angles are shown in Figure 6.15. These factors correspond to δ_1/d=20%, the value at which the soil starts yielding. The elastic interaction factors given by Poulos and Davis (1980) are also shown for comparison.

The diminishing trend is striking and it can be seen from the figure that, for departure angles

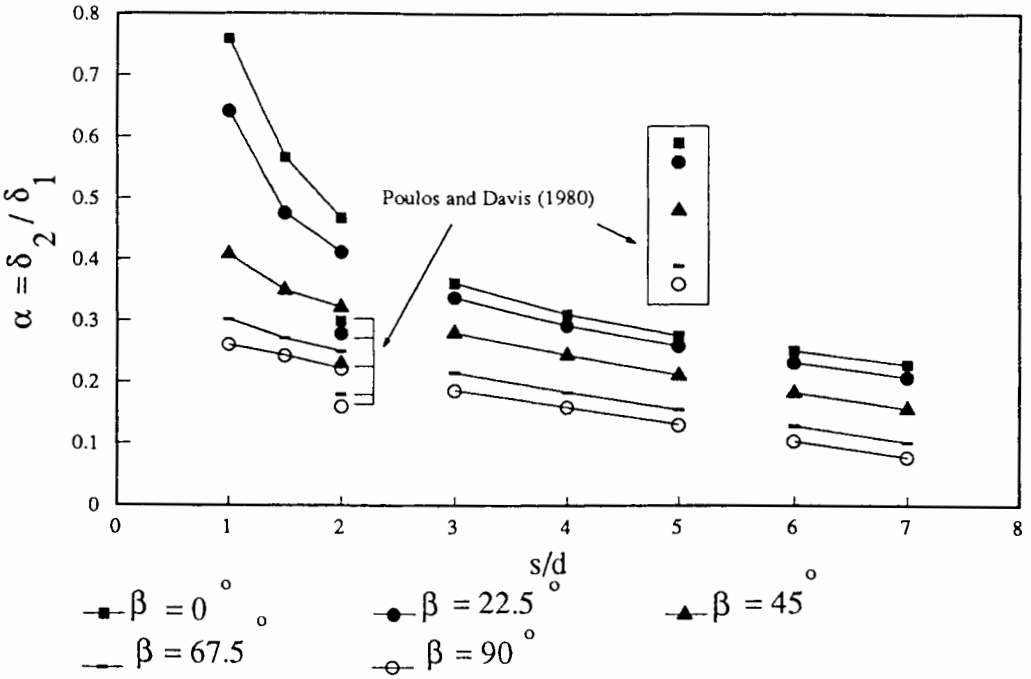

Figure 6.15: Interaction factors

(β) = 0°, 22.5°, the response of a pile is still about 10% more flexible than a single-pile, even at a spacing as large as seven pile diameters. This flexibility occurs when only one pile is loaded in the pile group; if all the piles are loaded at the same time, the response will be even more flexible.

The results taken together show the complex nature of the interactions among closely spaced piles in a pile group: the assumptions of the interaction factor approach (type 3 methods, see Section 6.1 above) are not applicable in this situation. However, for a fixed headed pile group in which all the piles displace equally, the method proposed by Poulos and Davis (1980) for the analysis of a general pile group can be used to determine the load displacement curve of a circular pile group adopting an iterative procedure (Section 6.4.1), using the non-linear interaction factors given Figures 6.14-15.

6.4.1 Approximate prediction of load-displacement curve for circular pile groups

In this sub-section we will describe how non-linear interaction factors derived above can be

used to construct an approximate load displacement curve at pile cap level of a rigid circular pile group in which piles are located only at the periphery of a circle and displace equally. We will make use of the following expression proposed by Poulos and Davis (1980):

$$\delta_k = \bar{\delta}\left[\sum_{\substack{j=1 \\ j\neq k}}^{n}(H_j \bullet \alpha_{kj}) + H_k\right] \tag{6.3}$$

where

$\bar{\delta}$ is the displacement of a single-pile under unit horizontal load

δ_k is the displacement of pile k

H_j is the load on pile j

α_{kj} is the interaction factor between piles k and j

and the total load on the group is H_G given by:

$$H_G = \sum_{j=1}^{n} H_j \tag{6.4}$$

In the case of equal displacements, the n equations from the above expression together with the equilibrium equation may be solved for the unknown loads and the group displacement. If we use interaction factors at failure given in Figure 6.15 we can find out the ultimate lateral load taken by the group. The ratio of average load per pile in the group to the ultimate load of a single-pile will give us the capacity reduction factor for that particular group. Applying this capacity reduction factor to the load-displacement curve of the single-pile will give us a new load displacement curve (modified p-y curve). (The derivation of p-y curves using the finite element method is described in Chapter 5). Now, a load displacement curve can be constructed for the pile group following an incremental procedure in which for each value of

incremental displacement, an average load per pile in the group is obtained from the above expressions 6.3-4, using the appropriate interaction factors for that particular displacement from Figure 6.14. (Mathematical expressions to the interaction curves shown in Figure 6.14 can be fitted and appropriate values of interaction factors will be calculated directly from these expressions during the analysis.) But in order to have the correct stiffness each calculated load-displacement couplet will be matched iteratively with the modified *p-y* curve obtained above. Validation of this method is left to future work. In the following Section 6.6, we back analyse (using the same concept) field tests carried out by Matlock *et al.* (1980) on two circular pile groups using the *p-y* curve analysis. The *p-y* curves used in this analysis take account of elasto-plastic pile-soil-pile interactions within the pile groups. Section 6.5 describes how these curves are obtained using the finite element method.

6.5 Plane strain analysis of multiple pile groups

The results from the preceding Section 6.4 suggest that any analysis which does not consider the non-linear pile-soil-pile interactions among closely spaced pile groups is liable to predict pile group response inaccurately. Many methods currently in practice fail in this respect, except the finite element method. In this section, plane strain finite element analyses of multiple pile groups are described. Plane strain idealisation is made on the basis that in the event of horizontal displacement of the pile, any vertical displacements will be negligible by comparison. However, plane strain idealisation is not valid for the whole length of the pile but only after a certain depth (approx. 3d). Theoretical *p-y* curves are obtained from these analyses which take account of non-linear pile-soil-pile interactions within the pile groups. The effect of pile-soil-pile interaction can be incorporated by introducing a strength modification factor to the undrained shear strength of the soil to make up the reduction in the soil resistance in a pile group. Strength modification factors are obtained through plane strain finite element analyses described in Section 6.5.1-2. Although, we have discovered in the

previous chapter that we do not require a soft layer for the analysis of a single laterally loaded pile, we have used a correcting layer in these analyses used for the determination of strength modification factors. A correcting layer is not going to affect these factors.

Field lateral load tests on two pile groups of 5 and 10 piles, arranged in a circle in both cases, carried out by Matlock *et al.* (1980) are chosen here for analysis. In these tests, all piles were of steel, 13.4m long, with an external diameter of 168mm, and a wall thickness of 7.1mm. They were driven to a penetration depth of 11.6m below the bottom of an excavated pit. The pile centre line spacing were 3.4 and 1.8 pile diameters for the 5-pile and 10-pile groups respectively. In order to simulate pile head restraints typical of an offshore platform, pile head deflections were enforced at two elevations, one just above the groundline, and the other near the pile top to simulate head restraint of a pile cap. During the loading tests, pile group deflections at two supports above the groundline and the total group load, as well as individual pile head shear and bending moments along the individual pile shaft, were measured at various load levels.

In the plane strain finite element analysis which follows, static monotonic loading is considered and the soil properties (S_u = 21kPa; G = 2070kPa) are taken from the paper by Matlock *et al.* (1980). A nearly incompressible material behaviour is assumed for the soil (undrained soft clay) by taking Poisson's ratio of the soil to be 0.49.

6.5.1 Plane strain analysis of 5-pile group

In this section, a 5-pile group is analysed as a two-dimensional problem to obtain a strength modification factor for the group. The finite element mesh used in the analysis is shown in Figure 6.16. The lateral soil reaction in the 5-pile group is shown in Figure 6.17.

Exploiting, as before, the symmetry of the problem, half of the geometry is discretised. Boundary conditions and direction of loading are also shown in the figure. The average response of a pile in a group is flexible compared to the isolated single-pile. This is due to

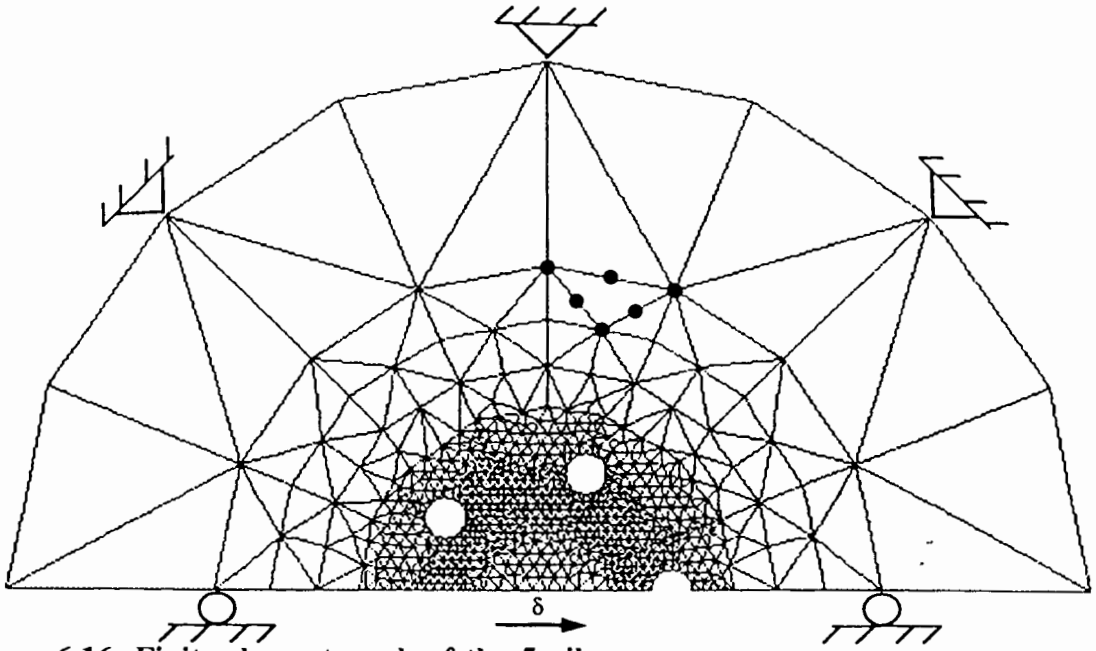

Figure 6.16: Finite element mesh of the 5-pile group

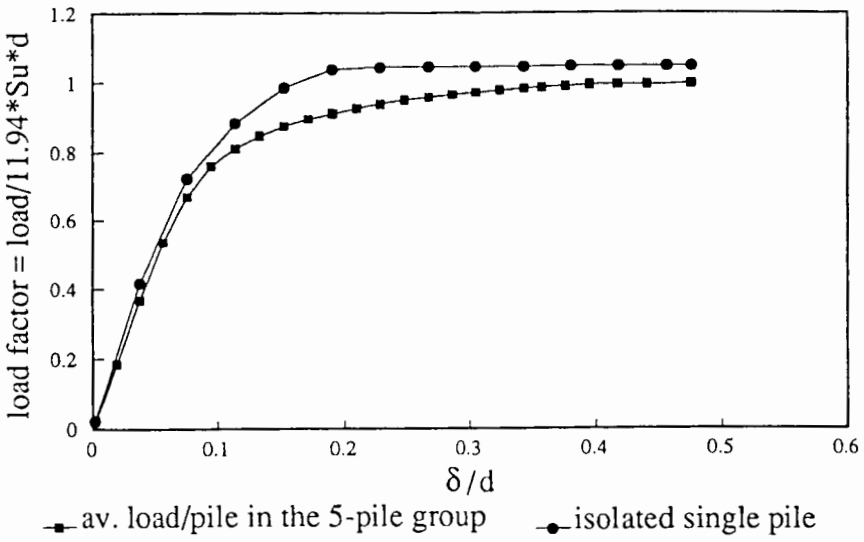

Figure 6.17: Average lateral soil reaction in a pile group

the interaction of plastic zones around individual piles which tend to overlap and the ultimate resistance offered by the soil is reduced. Figure 6.17 shows the flexible response of a pile in the group, whereas Figure 6.18 shows that, if the soil strength is modified by 5%, the average soil reaction in the group is the same as for a single-pile. In other words if we apply a

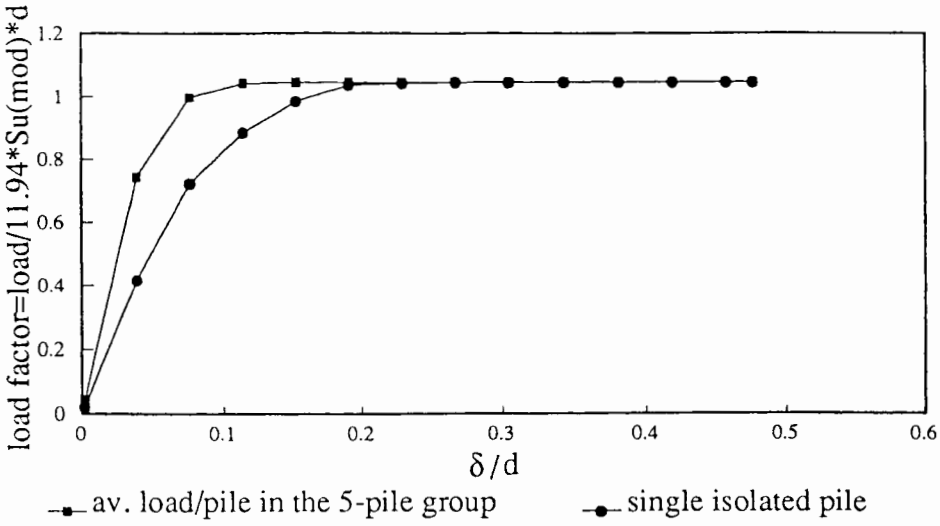

Figure 6.18: Load displacement curve (modified shear strength)

capacity reduction factor of 0.95 to the ultimate resistance of a single isolated pile we can obtain an average soil resistance of a pile group.

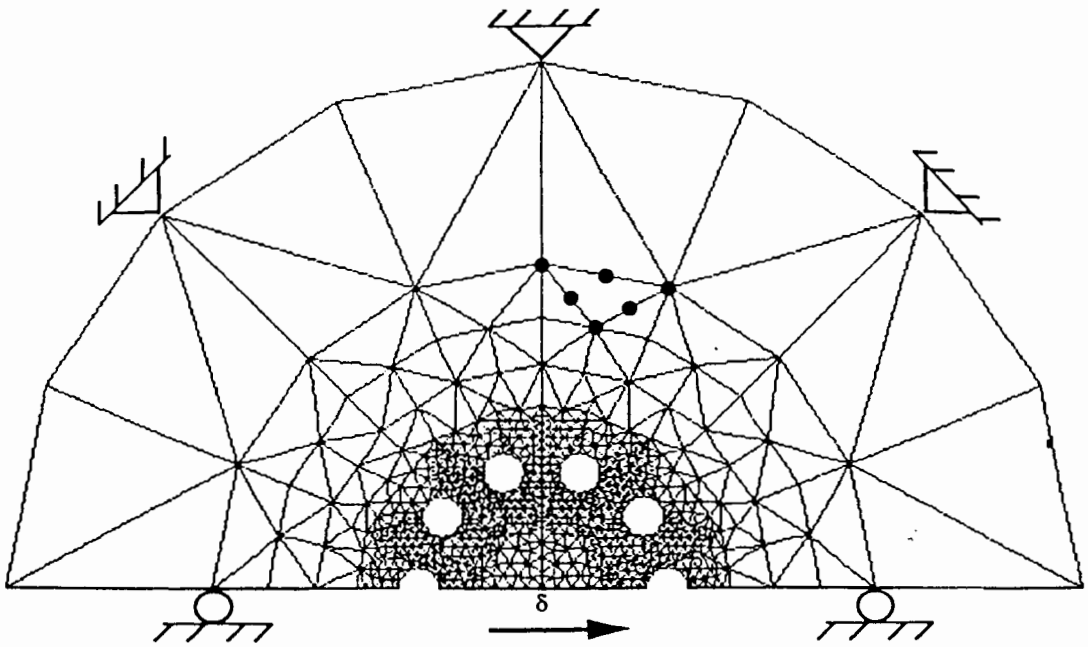

Figure 6.19: Finite element mesh for the 10-pile group

6.5.2 Plane strain analysis of 10-pile group

The finite element mesh of a 10-pile group is shown in Figure 6.19. Again, half of the discretised geometry; and boundary conditions and direction of loading are shown. A behaviour similar to the 5-pile group is observed. The ultimate soil resistance developed in this group is shown in Figure 6.20. The response 'as expected' is much more flexible than the 5-pile group since the pile spacing is 1.8 times pile diameter causing overlap of soil flow around the piles. Figure 6.21 shows that if the soil strength is modified by 38%, the average soil reaction in the group is the same as for a single isolated pile.

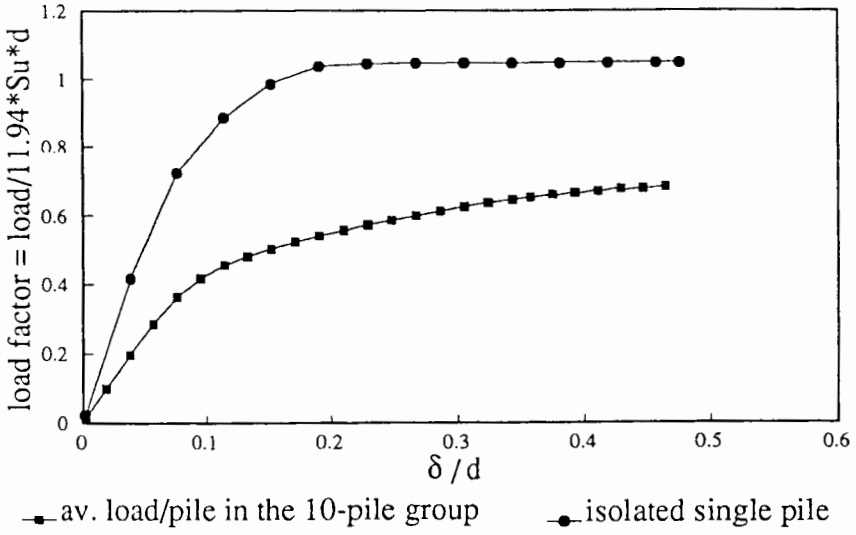

Figure 6.20: Average lateral soil reaction in a pile group

6.6 Back analysis of field tests

Back analysis of the field load tests done by Matlock *et al.* (1980) on a single-pile and two pile groups (5-pile and 10-pile) in soft clays, is presented in this section. Various attempts have been made to back analyse these tests using methods with different degrees of rigour e.g. Leung and Chow (1987) and Kooijman (1988) described in Chapter 2.

In this section a simplified approach to back analyse field tests using plane strain finite

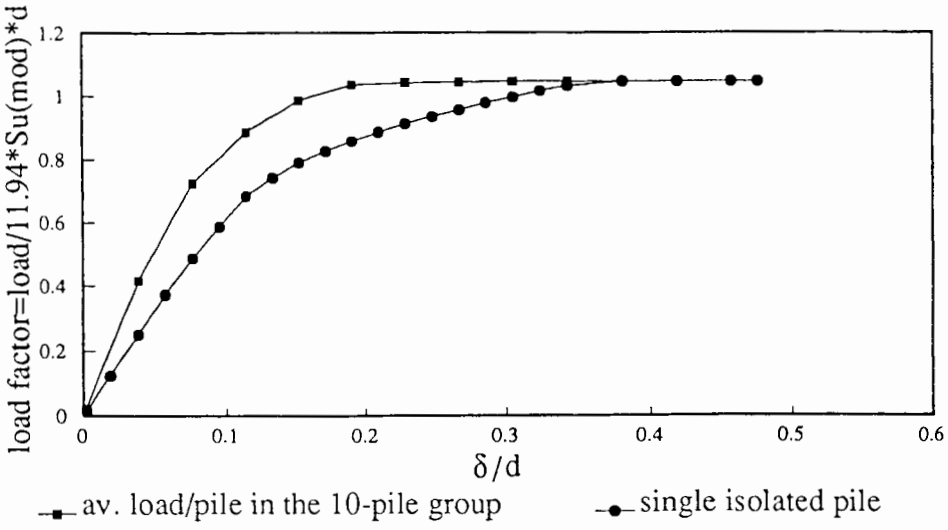

Figure 6.21: Load displacement curve (modified shear strength)

element analysis is presented. It is shown how the *p-y* curve analysis can be used to mimic the response of a pile group. (The variation of *in situ* stresses, soil stiffness and shear strength with depth is duly accounted for in the analysis). A single plane strain analysis is found to be sufficient to obtain a series of *p-y* curves along the length of the pile. In this section, a *p-y* curve analysis was performed independently to model these tests. Soil parameters are taken from the paper by Matlock *et al.* (1980). The undrained shear strength S_u of the soil at the groundline was taken as 13.1kPa, increasing to 23.31kPa at a depth of 0.4m, and thereafter increasing with depth at a rate of 2.258kPa per metre. Based on the above information and using a rigidity index, I_r (where $I_r = G/S_u$) equal to 100 for soft clay, an approximate linearly increasing shear modulus profile was used. The self weight of soil, γ, was taken 20kPa per metre depth and earth pressure coefficient at rest, K_o, was unity.

It was not necessary to carry out a series of plane strain finite element analyses at every metre depth along the length of the pile group to obtain theoretical *p-y* curves. We have shown in the previous chapter (Section 5.6) that the variation of I_r can be represented by a single curve

if the horizontal axis (abscissa) of the load-displacement curve is non-dimensionalised with I_r. It is further revealed in this section that load-displacement curves with variable K_o values can also be non-dimensionalised in a similar way. Figure 6.22 shows such a curve and a series of *p-y* curves are obtained from this single curve. Appropriate strength modification factor (strength modification factors as determined in sections 6.5.1-2) is then applied to these *p-y* curves. Thus single plane strain analysis yields theoretical *p-y* curves which become input

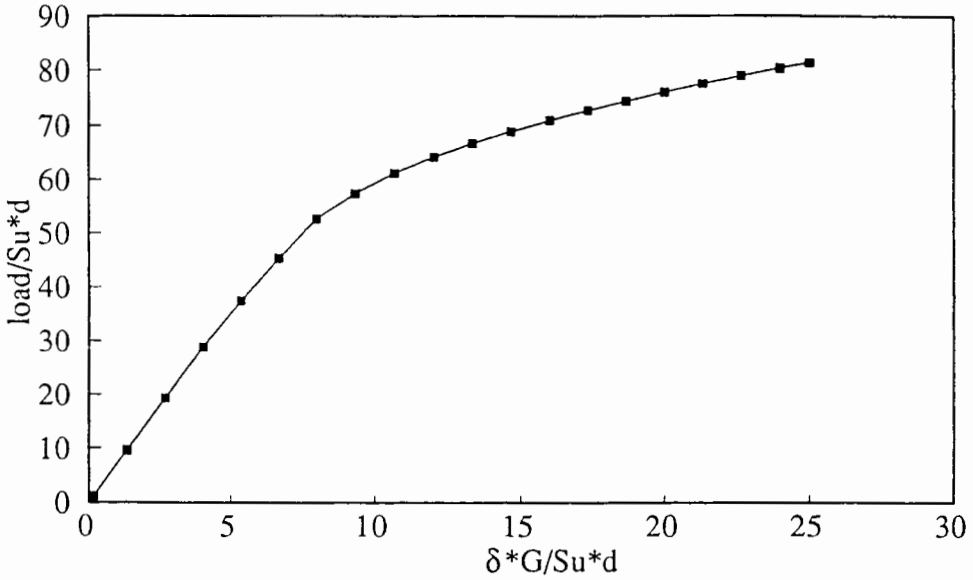

Figure 6.22: Non-dimensionalised *p-y* curve

for a standard non-linear beam-column equation which is solved numerically using iterative solution procedure. This was done and the results are shown in Figures 6.23, 6.24 and 6.25. (This method is similar to the one proposed by Kooijman (1989). Although, the method suggested by Kooijman (1989) is more integrated than the one described in this section, the *p-y* curves used in the former method are not as reliable as being used in the present method. The theoretical response curves obtained by *p-y* curve analysis were then compared with the field results. The *p-y* curve response is seen to be more flexible than the field results. The obvious reason for this behaviour is the invalidity of plane strain assumption in the upper regions of the pile.

In the absence of a complete three-dimensional finite element analysis of multiple pile groups,

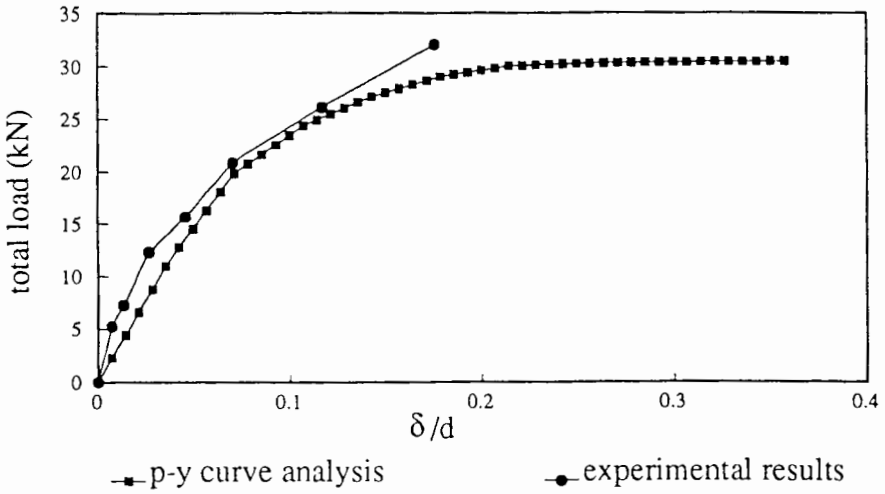

Figure 6.23: *p-y* curve analysis of a single-pile group

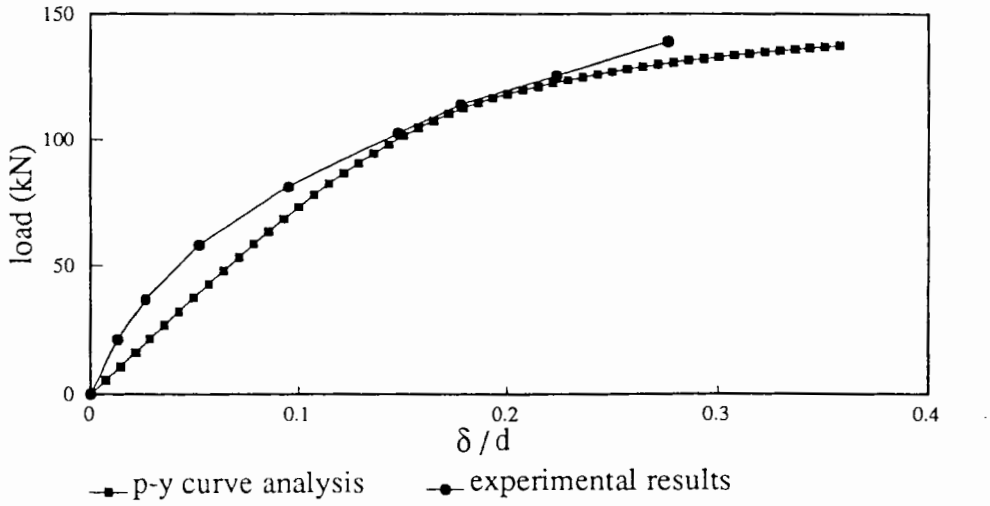

Figure 6.24: *p-y* curve analysis of 5-pile group

the analysis presented here is a viable and useful way of working out lateral load capacity of multiple-pile groups. Plane strain analysis enables a designer, from the predicted ultimate lateral load capacity of the pile group, to optimise his design rather than designing over-conservatively. Similarly, the modified *p-y* curve analysis proposed here enables a designer

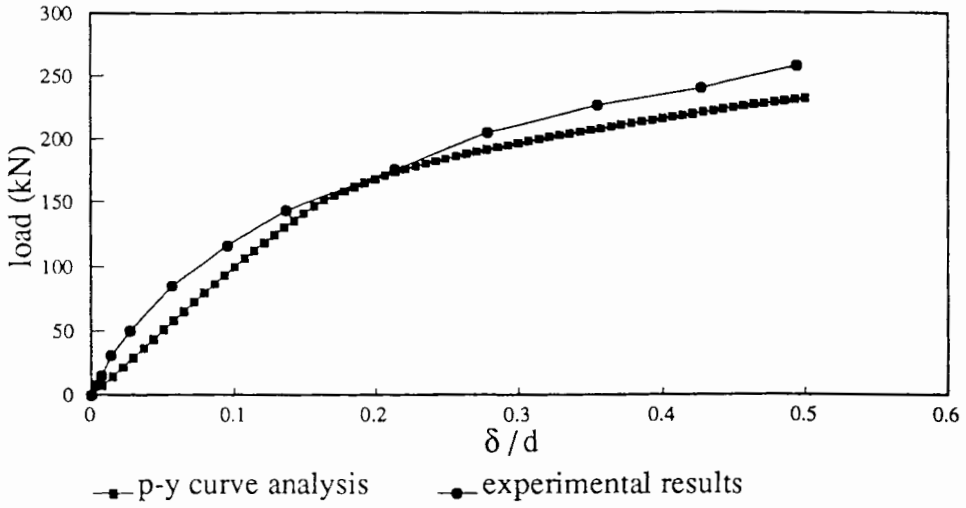

Figure 6.25: *p-y* curve analysis of 10-pile group

to work out flexural stiffness of the individual piles in a group. Three-dimensional finite element analysis is inherently more economical than full scale field tests on pile groups, and it allows for soil parameters to be varied which, plainly, is hardly practicable in the field. Thus three-dimensional finite element analysis has much to recommend it. The drawback, as we have stated, is that it is simply too bulky and too expensive in computing time to do at present: the necessary improvements in computer technology are still some way off. Two-dimensional plane strain analysis, with the reservations we have expressed above, is a present, practicable alternative to both three-dimensional finite element analysis and field tests. It is worth remembering that even when (if) the technology allows for three-dimensional analysis of the 5 to 10 pile pile-groups usual in offshore applications, the two-dimensional alternative will remain relevant for pile groups with more than 10 piles, usual in on-shore/inland pile foundations.

APPENDIX 6A

Analytical solutions for a 2-pile group

Pile-soil-pile interaction in a multi-pile group is a very complex phenomenon. It is difficult to quantify analytically the influence of this interaction on the response of a multi-pile group. A simplified analytical approach is here presented to study the behaviour of a 2-pile group. We consider two loading cases: loading parallel to the centre line of the group and loading perpendicular to the centre line.

Loading parallel to the centre line

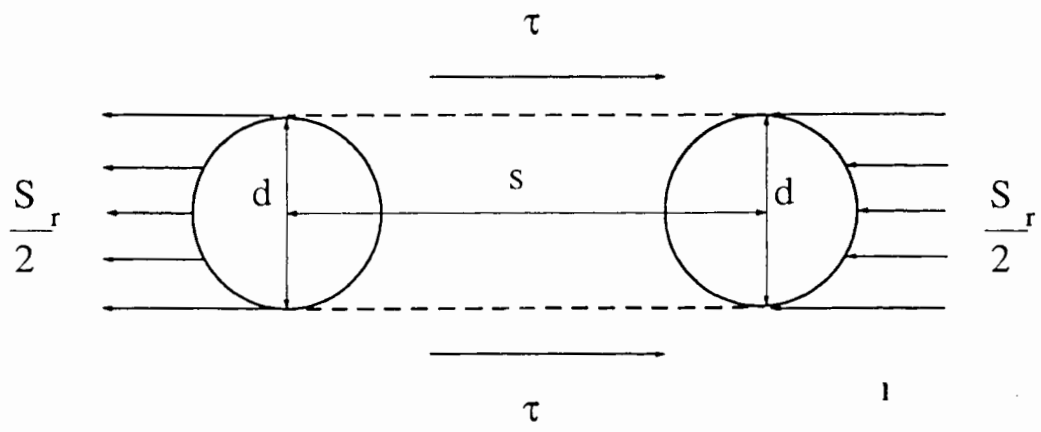

Figure 6A.1: 2-pile group (loading parallel to the centre line)

Consider a group of two rigidly connnected circular discs of diameter d shown in Figure

6A.1. Both the discs are pushed laterally by an equal amount parallel to the centreline of the group. The two discs are located at a distance s apart.

It is assumed that at failure, the discs and the soil between them will move together as a whole block. The forces acting on this whole block are shown in Figure 6A.1.

Considering the horizontal equilibrium of the forces, the net force F acting on the group will be:

$$F = 2\tau s + S_r$$

where

$$\tau = S_u$$

and

$$S_r = \frac{2}{\sqrt{3}} * 11.94 * S_u d.$$

The horizontal equilibrium equation can be rearranged as:

$$\frac{F}{2S_u d} = \frac{s}{d} + \frac{11.94}{\sqrt{3}}$$

or

$$P = \frac{s}{d} + \frac{11.94}{\sqrt{3}}.$$

In the above expression P is the ultimate load taken by the group. It is clear from the above expression that P depends upon the spacing between the piles. The group response will be more flexible than the response of a single-pile at close spacings and will become equal to that of a single-pile at a spacing of *6.89d*.

Loading normal to the centre line

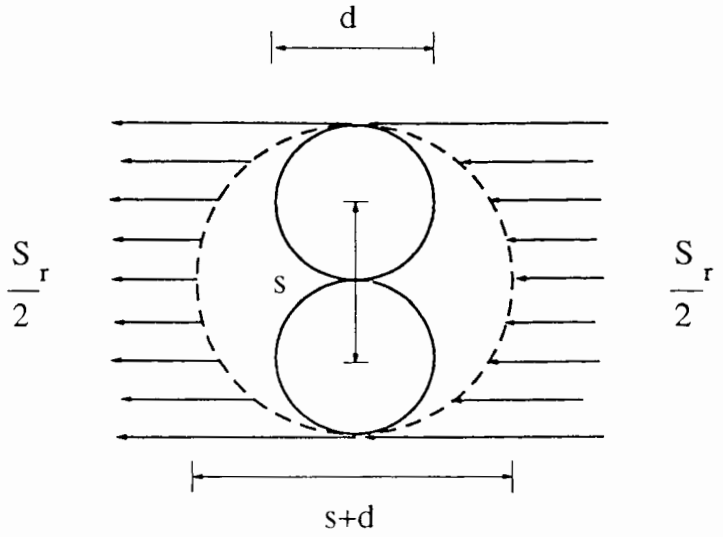

Figure 6A.2: 2-pile group (loading perpendicular to the centre line)

The arrangement of the 2-pile group is shown in Figure 6A.2. In this situation, when the two piles are too close to each other, a block failure is unlikely and the piles tend to behave as a single larger diameter pile. Considering the equilibrium of horizontal forces acting on the group (see Figure 6A.2), the net force F acting on the group will be:

$$F = S_r$$

where

$$S_r = 11.94 * \frac{2}{\sqrt{3}} * S_u(s+d).$$

The horizontal equilibrium equation can be rearranged as:

$$\frac{F}{2S_u d} = \frac{11.94}{\sqrt{3}}\left(1+\frac{s}{d}\right)$$

or

$$P = \frac{11.94}{\sqrt{3}}(1+\frac{s}{d}).$$

The above expression shows that the response of a 2-pile group will be more stiff than the response of a single pile at close spacings in contrast to a 2-pile group with loading parallel to the centre line of the group.

ANALYSIS OF LATERALLY LOADED PILES IN FRICTIONAL SOILS

7.1 Introduction

In order to proceed with the analysis of laterally loaded piles in frictional soils, we need to determine the ultimate lateral soil reaction as discussed in Chapters 5 and 6. It is difficult to determine the ultimate lateral reaction in a frictional soil due to dilatancy effects. When the pile is pushed laterally, the soil in front of the pile tends to dilate and as a result, both the normal stress and the shear stress in the soil continues to increase indefinitely. Likewise, the lateral reaction of the soil also continues to increase due to increase in volume. In this situation, the ultimate reaction cannot be defined and, in the absence of any analytical solution available for frictional soils, there is no absolute certainty about the ultimate lateral reaction. (It is not right, however, to assume that the volumetric strains will continue to increase indefinitely, since dilation gradually diminishes with the increase in mean effective stress and decrease in initial density.) This problem has not received much attention in the past. However, Lane and Griffiths (1988) carried out a series of finite element analysis of laterally loaded single piles in frictional soils using the Mohr-Coulomb model to represent the soil constitutive behaviour. They adopted a non-associated flow rule (i.e. plastic strain increments are not normal to the yield surface) with zero dilation as they found that dilation caused 'locking' of the meshes and an over-stiff, over-strong response at high pressures. Although they did carry out parametric studies taking into consideration both rough and smooth pile-soil

contact, these results cannot be validated in the absence of an analytical solution or experimental data. Lane and Griffiths (1988) also considered no-tension criteria (by inclusion to the Mohr-Coulomb model) and showed the interesting result that a pile with zero tension at the back of the pile had stiffer response compared to the one with full tension, and that there is no well-defined ultimate lateral reaction. They explained that no-tension criterion causes stress redistribution away from the back of the pile and this increases the apparent stiffness of the soil in front of the pile, leading to its increased load response. As briefly mentioned earlier in Chapter 5, the result seems to confirm our view that once the gap between pile and soil opens up at the back of the pile, the problem of a laterally loaded pile is no longer a problem of small displacement but one of a large displacement. (Large and small displacement problems generally refer to geometric effects. This, however, is not strictly a large displacement effect.)

In this chapter the ultimate lateral soil reaction is calculated using the Matsuoka (1976) model to represent material constitutive behaviour of frictional soils, having considered both the associated (plastic strain increment is normal to the yield surface) and the non-associated flow rules. The finite element calculations are carried out for both constant as well as variable friction and dilation angles. For the case of variable friction and dilation angles, the dilatancy of frictional soils is considered to be a function of relative density I_D and mean effective stress as proposed by Bolton (1986). The dilation of the soil gradually decreases with increasing stress levels and reducing I_D during the analysis. The model captures successfully, the post peak behaviour of the soil and tackles the problem of 'mesh locking'.

7.2 Background

In order to understand the subtle stress-strain behaviour of frictional soils, it is necessary to define the angles of friction ϕ' and dilation ψ. The angle of friction ϕ' describes the strength of the soil and is expressed as the ratio of a shear stress to a normal stress:

$$\sin\phi' = \frac{\sigma_1' - \sigma_3'}{\sigma_1' + \sigma_3'}$$

where σ_1, σ_3 are the maximum and minimum principal stresses. The superscript (′) is used to show that these are 'effective' and not 'total' stresses. However, in fully drained analyses (i.e. pore pressures are zero) as is the case here in this chapter, 'total' stresses are equal to 'effective' stresses.

The angle of dilation ψ is expressed as the ratio of a volumetric strain rate to a shear strain rate:

$$\sin\psi = \frac{-(\dot{\varepsilon}_1 + \dot{\varepsilon}_3)}{\dot{\varepsilon}_1 - \dot{\varepsilon}_3}$$

in the case of plane strain ($\varepsilon_2 = 0$), where $\varepsilon_1, \varepsilon_3$ are the maximum and minimum principal strains. The superior (.) represents strain rates. The term *rate* is used in the same sense as in plasticity theory, in which the time increment is artificial. The (-) sign arises simply from the convention that compressive stresses and strains are taken as positive in soil mechanics.

The angle of dilation is related to the density of the soil as dense soils have large dilation angles. If we perform a simple shear test on a dense sand, the sand usually dilates i.e. expands in volume as the test proceeds. The dilation usually takes place after a small initial compression and denser samples have the tendency to expand more rapidly. A peak is usually observed in the stress-strain curve followed by a reduction in shear stress at large strain. The corresponding peak and large strain friction angles are denoted by ϕ_p' and ϕ_{cv}' respectively. The subscript '*cv*' indicates that the shearing takes place at constant volume i.e. no dilation occurs.

If the same test is carried out at a number of normal stress levels, the angle of peak friction decreases with increasing stress level. The peak friction angle approaches the large strain friction angle ϕ'_{cv} at very high stress levels. Barden *et al.* (1969) showed from drained, plane strain compression tests on sand at the same density that the angle of peak friction and the

angle of dilation were significantly affected by the confining stress. Similarly, Stroud (1971) carried out simple shear tests on sands. These tests, covering a range of initial stresses and densities show that denser soils exhibit higher friction angles but for a given density, the angle of friction reduces slightly with increasing stress level. These test results suggest that the angles of friction and dilation, density and stress levels are inter-related.

Various sophisticated theories explaining the relationship between the friction and dilation angles include those given by Taylor (1948), Schofield and Wroth (1968), Rowe (1962) and de Josselin de Jong (1971, 1988). The broad basis of these theories is the sawtooth model in that the friction angle is the sum of the angle of friction at constant volume and the angle of dilation. Bolton (1986) presented a comprehensive review of the experimental data on friction and dilation angles, and suggested a very simple empirical fit to the data. This empirical expression is given by:

$$\phi'_p = \phi'_{cv} + 0.8\psi_{max}$$

where ψ_{max} is the peak angle of dilation.

Bolton showed that the above expression agrees well with the stress dilatancy relationship of Rowe (1962). (A detailed discussion on these theories is given by Houlsby (1991).)

Similarly, the link between the angle of dilation, density and pressure has also been explored. Based on the Critical State concept, Wroth and Bassett (1965) suggested that the rate of dilation is a function of specific volume and pressure. Wroth (1990), as reported by Houlsby (1991), replotted shear tests data obtained by Stroud (1971) and suggested simple expression for the variation of the angle of dilation with distance from the critical state line:

$$\sin\psi = \alpha(\Gamma - V_\lambda) \tag{7.1}$$

where

$$V_\lambda = V + \lambda \ln\left(\frac{p'}{p_a}\right),$$

V = specific volume,

λ = slope of the Critical State Line whose position is fixed by Γ,

Γ = value of specific volume at some reference pressure p_a.

The value of α was found to be typically near unity.

Recently, Wroth's concept is further elaborated in terms of relative density I_D rather than specific volume by Houlsby (1991):

$$\sin\psi = \alpha(\Gamma - V_{max}) + \alpha(V_{max} - V_{min})I_D - \alpha\lambda\ln\left(\frac{p'}{p_a}\right) \tag{7.2}$$

where

$$I_D = \frac{e_{max} - e}{e_{max} - e_{min}},$$

e = current void ratio,

e_{max}, e_{min} = maximum and minimum void ratios.

Expression (7.2) can be simplified as:

$$\sin\psi = A + BI_D - C\ln\left(\frac{p'}{p_a}\right)$$

where A, B and C are simple functions of well-defined properties of the soil.

Earlier, Bolton (1986) presented the following empirical expression in which he combined the relative density and pressure into a relative dilatancy index I_R.

$$\phi'_p - \phi'_{cv} = 3I_R$$

where

$$I_R = I_D(10 - \ln p') - 1.$$

The correlation is found to be applicable within the range $0 < I_R < 4$. Bolton's (1986) empirical

expressions can be combined to derive the following expression for the angle of dilation (plane strain) in radians:

$$\psi = -0.11+0.59I_D-0.11I_D\ln\left(\frac{p'}{p_a}\right). \qquad (7.3)$$

Both Bolton's (1986) expression (7.3) and the theoretical expression (7.2) based on Wroth's concept, given by Houlsby (1991) fit well with the range of experimental data available on sands. Although, theoretical expression (7.2) is equally convenient and axial capacity of piles in frictional soils has been determined by Houlsby (1991). The finite element calculations, presented in this chapter using Matsuoka model for variable friction and dilation angles, make use of Bolton's empirical expressions to relate dilation angle as a function of pressure and density. (Similar finite element calculations have been carried by Nutt (1993) to show the influence of the variable friction and dilation angles on the cone pressuremeter tests in carbonate sands.)

In order to carry out the finite element calculations based on the variable friction and dilation angles defining the Matsuoka yield surface, it is necessary first to calculate appropriate material stiffness matrix and update (Gauss point) stresses during the course of analysis, as the analysis is usually performed by dividing the applied loads or displacements or both into a number of steps. New subroutines are added to the finite element code 'OXFEM' to carry out these tasks without altering the structure of the program.

7.3 Material stiffness matrix

In this section, we will describe how the material stiffness matrices are derived for the Matsuoka (1976) model. In the following Section 7.4, we can see some important parts of the stress updating procedures which are adopted in the finite element analyses presented in this chapter.

7.3.1 The Matsuoka yield surface - constant friction and dilation angle (model 1)

As explained by Burd (1986), the Mohr-Coulomb yield surface contains singularities at the corners of the yield surface i.e. yield function is not differentiable at the corner points. It is therefore preferable to choose the Matsuoka surface in which the yield function is

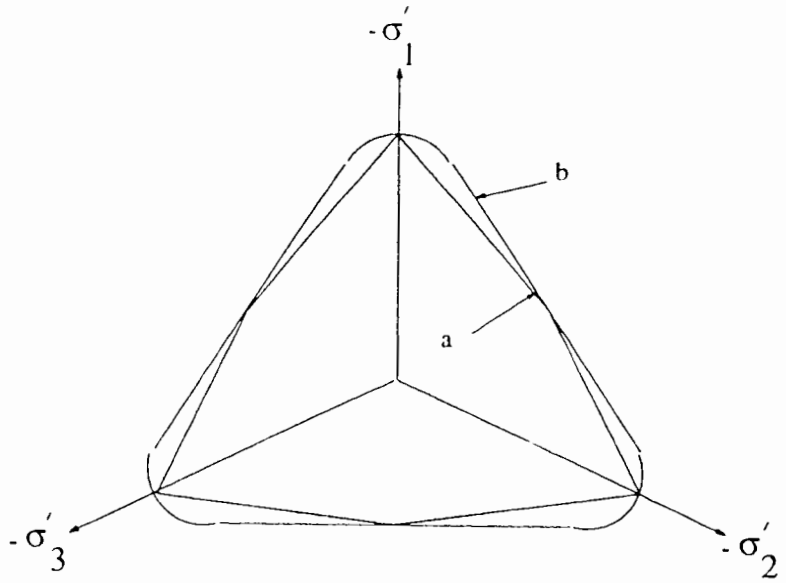

a - Mohr-Coulomb
b - Matsuoka

Figure 7.1: Yield surfaces in the ' π' plane

differentiable everywhere. Both these surfaces are shown in Figure 7.1

The Matsuoka yield function, in terms of stress invariants, can be defined as:

$$f(\underset{\sim}{\sigma'}) = I_1 I_2 - I_3 \zeta$$

where

$$I_1 = \sigma'_x + \sigma'_y + \sigma'_z,$$

$$I_2 = \sigma'_x \sigma'_y + \sigma'_y \sigma'_z + \sigma'_x \sigma'_z - \tau_{xy}^2,$$

$$I_3 = \sigma'_z (\sigma'_x \sigma'_y - \tau_{xy}^2),$$

$$\zeta = 9+8\tan^2\phi'_{tc}.$$

ϕ'_{tc} is the triaxial compression friction angle.

A material is said to have yielded when the stresses satisfy the yield criterion:

$$f(\underset{\sim}{\sigma'}) = 0.$$

From the normality of the plasticity theory, originally developed for metals, the plastic strain increments are in the direction normal to the yield surface defined by f so that:

$$d\underset{\sim}{\varepsilon}^p = \frac{\partial f}{\partial \underset{\sim}{\sigma'}}.$$

A component of the normal to this yield surface is given by:

$$\frac{\partial f}{\partial \sigma'_x} = I_2+I_1(\sigma'_y+\sigma'_z)-(9+8\tan^2\phi'_{tc})\sigma'_y\sigma'_z.$$

and similarly other components can also be derived.

For granular soil behaviour, however, it is more appropriate to use a separate function $g(\underset{\sim}{\sigma'})$ termed as plastic potential is used to describe incremental plastic strain:

$$d\underset{\sim}{\varepsilon}^p = \frac{\partial g}{\partial \underset{\sim}{\sigma'}}$$

When a dilation angle ψ is specified, the plastic potential g can be calculated from the yield function f. This can be done using one of the two following approaches. In Figure 7.2, the yield function f is shown in $\tau : \sigma$ space where τ is the shear stress with a constant friction angle ϕ. Full association occurs when the plastic strain increment $\partial g/\partial \underset{\sim}{\sigma'}$ coincides with the normal to the yield surface f for a particular stress level. Zero association, which results in zero volume change, occurs when the plastic strain increment is vertical. Following the

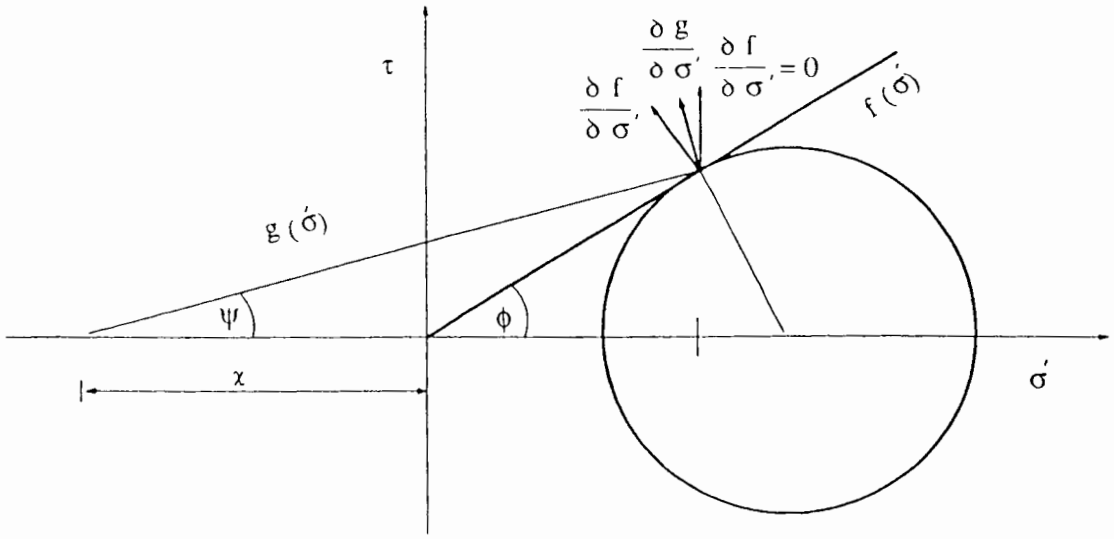

Figure 7.2: Yield function and plastic potential in ' τ-σ ' stress space

approach proposed by Burd (1986), the plastic strain increment can be calculated from linear interpolation between the full and zero association cases. In an alternative approach, proposed by Yu (1990), an assumption is made that the plastic potential function g is similar to the yield function f but ϕ'_{tc} is replaced by ψ_{tc}. Since f and g must intersect at the current stress state, the apex of surface g is shifted from the origin by a distance $-\chi$ so that:

$$g(\sigma^*) = I_1^* I_2^* - I_3^* \zeta^*$$

where

$$\sigma^* = \sigma' + \chi I,$$

$$\zeta^* = 9 + 8\tan^2\psi_{tc}.$$

and I is the unit vector. This condition is used to derive a cubic equation in terms of the principal stresses from which χ can be solved. (The approach proposed by Yu (1990) is adopted in the finite element calculations (Section 7.5) involving the Matsuoka yield criterion with variable friction and dilation angles (Section 7.3.2).)

Once the plastic strain increments are derived, the plastic stiffness matrix $[D]^P$ defined in

equation (4.10) can be calculated. The stress changes can then be related to the strain changes by an elastic-plastic stiffness matrix defined as:

$$[D]^{EP} = [D]^{E} - \frac{[D]^{E}\left[\frac{\partial g}{\partial \underset{\sim}{\sigma}'}\right]\left[\frac{\partial f}{\partial \underset{\sim}{\sigma}'}\right]^{T}[D]^{E}}{\left[\frac{\partial f}{\partial \underset{\sim}{\sigma}'}\right]^{T}[D]^{E}\left[\frac{\partial g}{\partial \underset{\sim}{\sigma}'}\right]}$$

where $[D]^{E}$ is a symmetric matrix of elastic constants: bulk modulus K and shear modulus G.

$$[D]^{E} = \begin{bmatrix} K+\frac{4G}{3} & K-\frac{2G}{3} & K-\frac{2G}{3} & 0 \\ K-\frac{2G}{3} & K+\frac{4G}{3} & K-\frac{2G}{3} & 0 \\ K-\frac{2G}{3} & K-\frac{2G}{3} & K+\frac{4G}{3} & 0 \\ 0 & 0 & 0 & G \end{bmatrix}$$

The friction angle ϕ'_{tc} and dilation angle ψ_{tc} remain constant throughout the analysis and hence the yield surface continues to extend indefinitely with increasing mean effective stress.

7.3.1.1 Finite element analysis of a single-pile

In the finite element analyses described in this section, a rigid disc approximation of a single-pile is adopted as it has been done earlier in Chapters 5 and 6. The lateral response of a rigid disc in a frictional soil is calculated using displacement controlled finite element analyses. A

constant friction angle ϕ'_{tc} of 32° with dilation angle ψ of 0°,5°,10°,15° is used in the analyses. The soil has a Poisson's ratio ν of 0.3 and G/p_o' ratio of 300 (where p_o' is an initial compressive stress).

Since the problem is symmetric, it is only necessary to analyse one half of the disc. Six-noded linear strain triangular elements are used. A complete rough contact between the pile-soil is assumed. The finite element mesh is shown in Figure 7.3. The outer boundaries of the mesh are fixed at a distance of $20r_o$ from the centre of the disc; where r_o is the radius of the disc. The fixed boundaries are thought to be far enough to have no detrimental effect on the load displacement response.

Using the material model described in Section 7.3.1, the lateral response of a single disc in frictional soils is calculated and the results are shown in Figures 7.4 and 7.5.

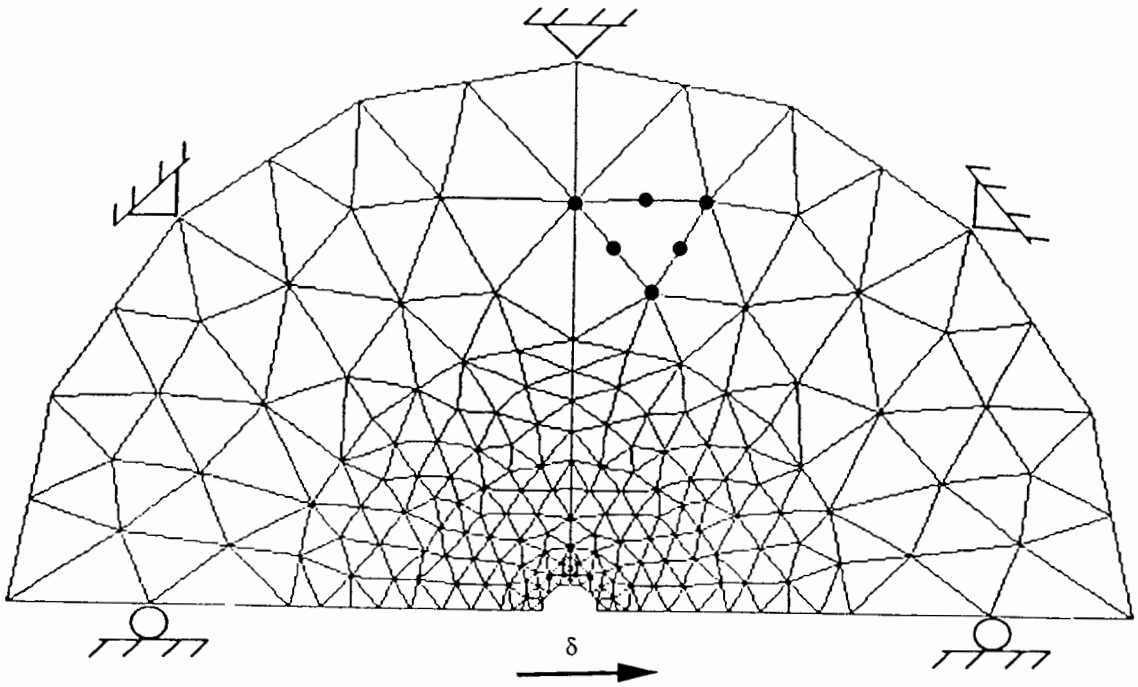

Figure 7.3: The finite element mesh for a rigid circular disc

The results in Figures 7.4 and 7.5 involve the calculation of plastic potential as proposed by Burd (1986) and Yu (1990) respectively. Burd's (1986) approach considers dilation as a degree of association and is denoted by 'γ'. (The material properties considered are the same

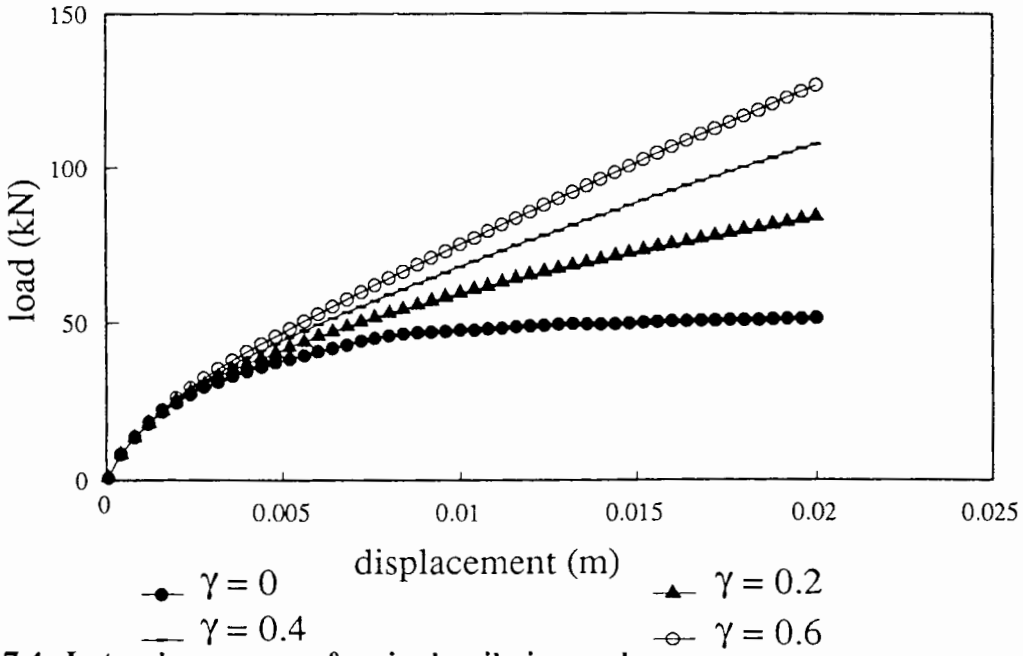

Figure 7.4: Lateral response of a single-pile in sand

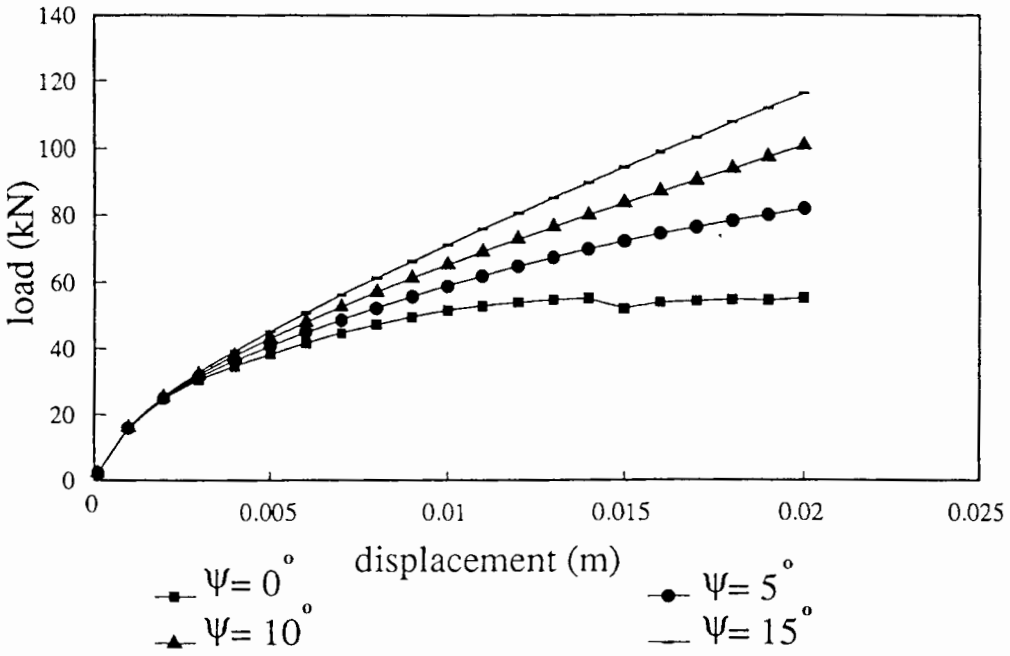

Figure 7.5: Lateral response of a single-pile in sand

as mentioned above except that instead of using dilation angles, an equivalent degree of association γ of 0, 0.2 0.4 0.6 is used in the analyses.) It can be seen that using a non-associated flow rule, the ultimate lateral load is obtained only when the dilation angle is zero. However, Lane and Griffiths (1988) have reported 'mesh locking' for this case using the Mohr-Coulomb model. In case of dilation, plastic volumetric strains continue to increase and

it appears that the ultimate lateral load cannot be achieved.

7.3.2 The Matsuoka model - variable friction and dilation angles (model 2)

It is unrealistic to assume that the peak friction angle remains constant in frictional soils at increasingly high normal stresses, or that volumetric strains continue indefinitely. As was mentioned earlier (see Section 7.2) dense frictional materials have higher rates of dilation but for a given density, the angle of dilation reduces with increasing stress levels. The relationships between $\phi'_p - \phi'_{cv}$, I_R and ψ_{max} as defined earlier in Section 7.2, are used here with the Matsuoka yield function (Section 7.3.1) to model a more realistic yield surface as shown in Figure 7.6. The failure surface remains unbounded, and any increase beyond a critical stress level, the friction angle remains constant at ϕ'_{cv} and the dilation is zero. Variations in ϕ' and ψ are accounted for in the model by specifying $\phi'_{cv}, V_{max}, V_{min}$ and initial I_D, denoted by I_D^o where I_D is continually updated during the calculation. An

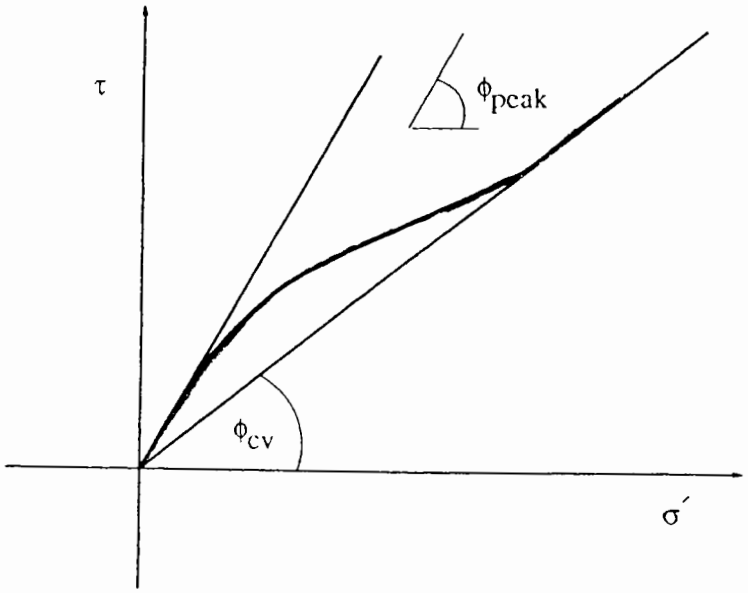

Figure 7.6: Curved yield surface in ' τ-σ ' stress space

additional term is also necessary in determining the normal to the failure surface $\partial f/\partial \underset{\sim}{\sigma}'$ given above because of dependency of ϕ' on σ'. This term is given by:

$$\frac{\partial f}{\partial \phi'}\cdot\frac{\partial \phi'}{\partial p'}\cdot\frac{\partial p'}{\partial \underset{\sim}{\sigma}'} = \frac{I_3 16\tan\phi'}{\cos^2\phi'}\cdot\frac{-3I_D}{p'}\cdot\frac{1}{3}$$

$$= \frac{48 I_3 I_D \tan\phi'}{I_1 \cos^2\phi'}$$

where

$$I_D = \frac{V_{max} - \left[\left(V_{max} - I_D^o (V_{max} - V_{min})\right)(1+\varepsilon_v)\right]}{V_{max} - V_{min}}$$

ε_v are the current volumetric strains.

7.4 Stress update calculations

An important feature of the finite element program 'OXFEM' is the numerical solution scheme (Modified Euler scheme (Burd (1986)). It requires an equilibrium check at the end of each load step. The equilibrium is maintained by making sure that the work done by the internal stresses is equal to the applied load which is done by evaluating an integral of the form:

$$P = \int_v [B]^T \sigma dV$$

where $[B]$ is obtained by appropriate differentiation of the shape functions of the element. This feature of the program 'OXFEM' requires accurate stress updating at the end of each load step. As described by Burd (1986), three separate operations, in general are needed to

calculate the updated Gauss point stresses. Firstly, it is necessary to calculate the strain rates $\dot{\underset{\sim}{\varepsilon}}$ which when integrated over the time step, are compatible with the incremental displacements. The second stage is to obtain the incremental Gauss point stresses by integrating the constitutive equations. In some cases, updated stresses may be obtained from a closed form solution (e.g. elastic behaviour, and von Mises plasticity excluding the Jaumann terms) but for the Matsuoka model it is necessary to use a numerical integration scheme. An 'error control' algorithm is used, based on a Runge-Kutta scheme in which the updated stresses are evaluated by dividing the calculation step into a number of 'sub-increments'. In order to improve the efficiency of this calculation, a procedure is used in which the size of the 'sub-increments' are varied automatically in order to perform the integration at each of the Gauss points to a specified accuracy. In this algorithm, which is described by Sloan (1984), an estimate is made of the errors occurring at each 'sub-increment'. The magnitude of the error is then used to determine the size of the following 'sub-increment', or, if the error is unacceptable, the size of the sub-increment is reduced, and the calculation repeated. The third and the final stage of the 'stress update' calculation is to correct the stresses back to the yield surface, as a numerical scheme has been used to integrate the constitutive law.

7.4.1 Calculation of yield surface intersection

As we have seen in Chapter 4 that if the material becomes plastic during the calculation step, it is necessary to find the point in the increment at which the yield surface intersection occurs (see Figure 7.7). The increment is then split into two parts and the 'stress update' calculation for the elastic and plastic parts performed independently.

For the case of Matsuoka yield surface defined by a constant friction angle, a cubic equation of the form:

$$t^3+a_1t^2+a_2t+a_3=0$$

is derived (see Burd (1986)) and solved for the appropriate root. The coefficients a_1, a_2 and a_3

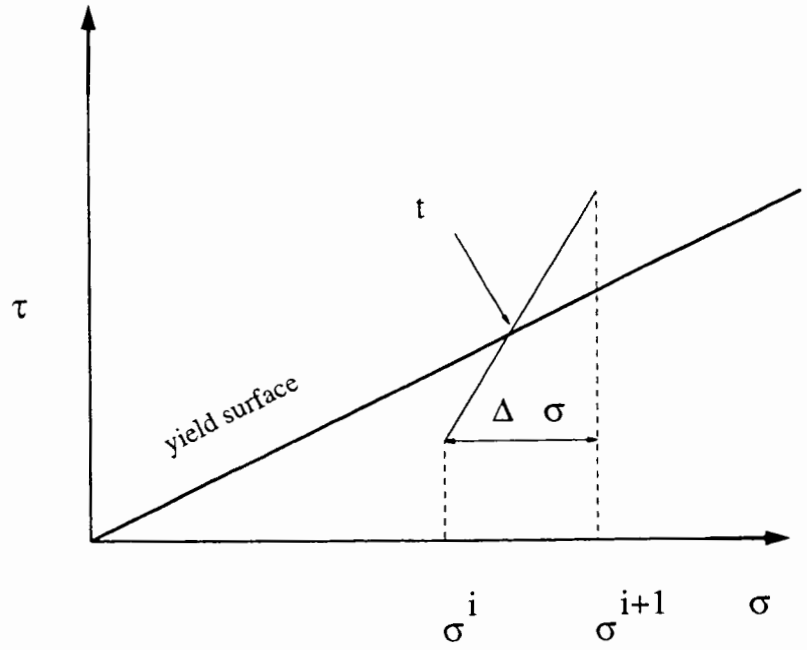

Figure 7.7: Yield surface intersection

involve the calculation of the constant ζ defined earlier. For the case of Matsuoka model with variable friction angle, the value of ζ varies with the angle of friction. The angle of friction varies with time and is a function of logarithm of hydrostatic pressure which is also a function of time.

$$\phi = 3I_D(10-\ln p')-1+\phi_{cv}$$

where

$$p'^3 = t^3+c_1t^2+c_2t+c_3.$$

The coefficients c_1, c_2 and c_3 are defined in Burd (1986). As we can see that the cubic equation initially derived by Burd (1986) to calculate yield surface intersection, now takes a much more complex form due to the dependence of the angle of friction on pressure and relative density. Therefore, we need to resort to numerical methods to calculate yield surface intersection. An interpolation method (false position method) is used to calculate the intersection. The rest of the stress update procedures i.e. integration of the constitutive equations and the yield surface correction are the same as described by Burd (1986).

7.5 Verification of the Matsuoka model (2)

7.5.1 Plane strain analysis of a unit square soil element

In this test problem a square element is given initial isotropic compressive stresses and is sheared by imposing additional tensile forces in the x-direction. The boundary conditions and the applied loading on the element are depicted in Figure 7.8. The material properties used

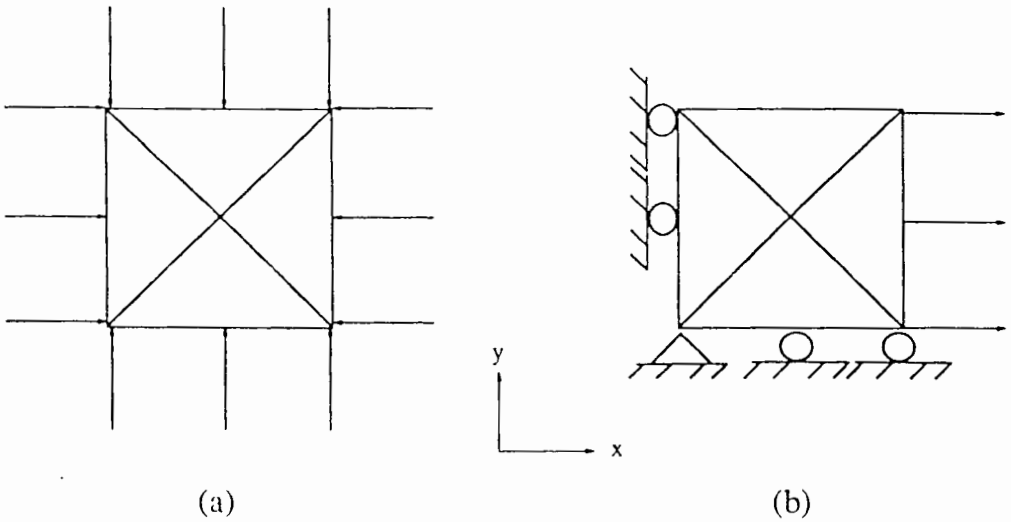

Figure 7.8: Unit square soil element

in the analysis are: G = 10000kPa; p_o' = 800kPa; Poisson's ratio ν = 0.3; I_D^o = 0.9; V_{max} = 2.79 and V_{min} = 2.49. The validation of the model is carried out by plotting out variation of the friction and dilation angles during the analysis (see Figures 7.9-10).

As we have seen in the formulation of the Matsuoka model, the yield surface is defined by the triaxial friction angle. Therefore, in order to carry out the plane strain analyses using this model, we need to find out the equivalent plane strain friction angle. Burd (1986) presented such correlations for the zero and full association of the plastic potential. We have used the correlation for the zero association (i.e. no dilation) to see that the plane strain friction angle

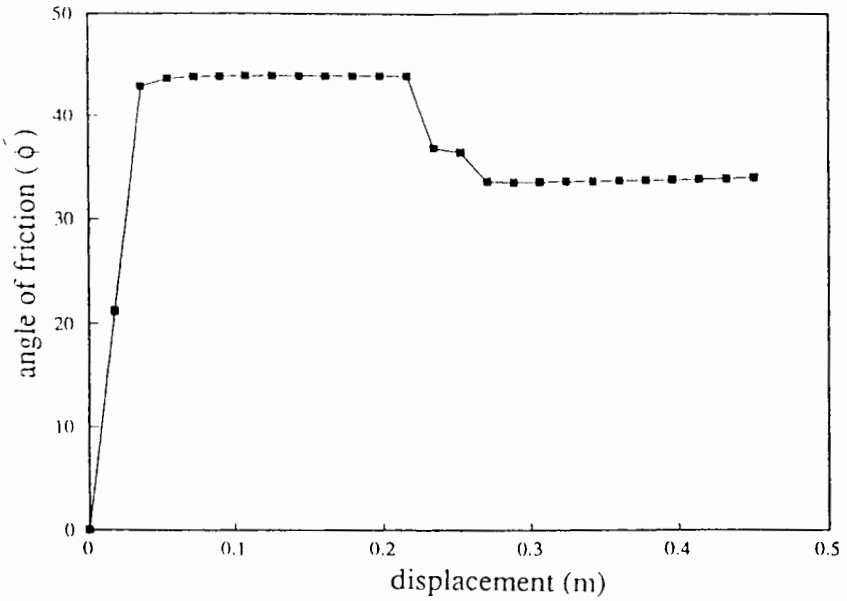

Figure 7.9: Variation of friction angle

calculated from the correlation, matches with the critical state friction angle at the end of the analysis. A triaxial critical state friction angle ϕ'_{cv} equal to $31.04°$ is used in the analysis. The corresponding plane strain critical state friction angle is worked out to be of $34°$. The friction angle at large displacement, shown in Figure 7.9, matches exactly with this value.

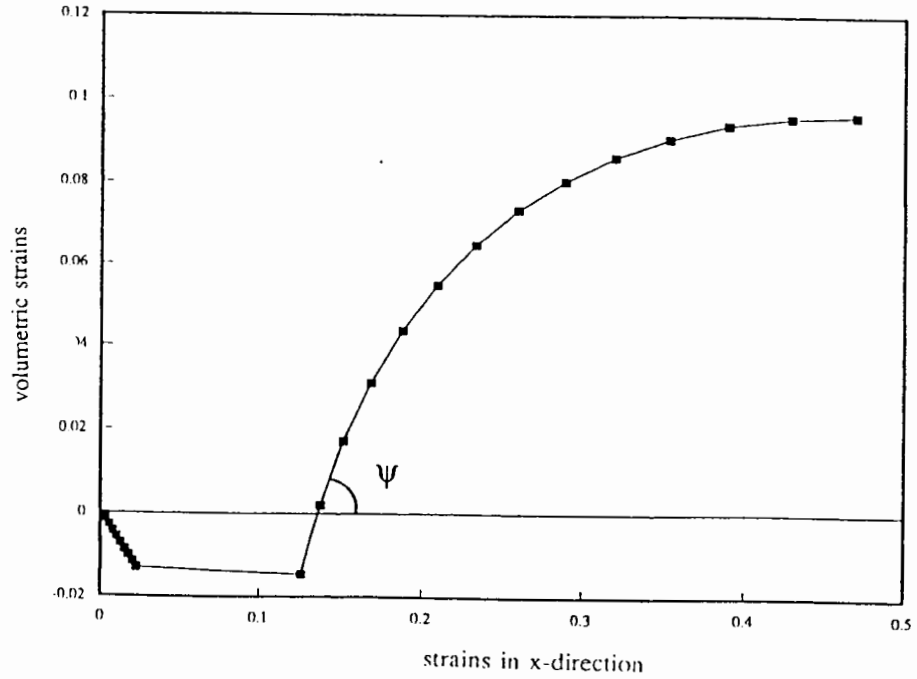

Figure 7.10: Variation of volumetric strains

Figure 7.10 shows the variation of volumetric strain ε_v with the strain in the x-direction obtained from a force controlled finite element analysis. We can see from the figure that the square element after having an initial compression tends to dilate and as the stresses increase and the relative density decreases during the analysis by the application of further tensile force, dilation gradually disappears.

7.5.2 Laterally loaded single-pile (after Lane and Griffiths (1988))

In this section, the analysis for a laterally loaded rigid disc analysis is carried out using the Matsuoka model (2). The finite element mesh used in the analysis is the same as described in Section 7.3.1.1. A similar analysis, using Mohr-Coulomb model, was carried out by Lane and Griffiths (1988). In their analysis, the soil had a friction angle ϕ' of 30°, cohesion c of 10kPa and Poisson's ratio of 0.3. The load displacement response is shown in Figure 7.11. The figure shows that the ultimate load value is not well-defined. The load displacement curve obtained, using the Matsuoka model (2), is also shown in Figure 7.11. The following

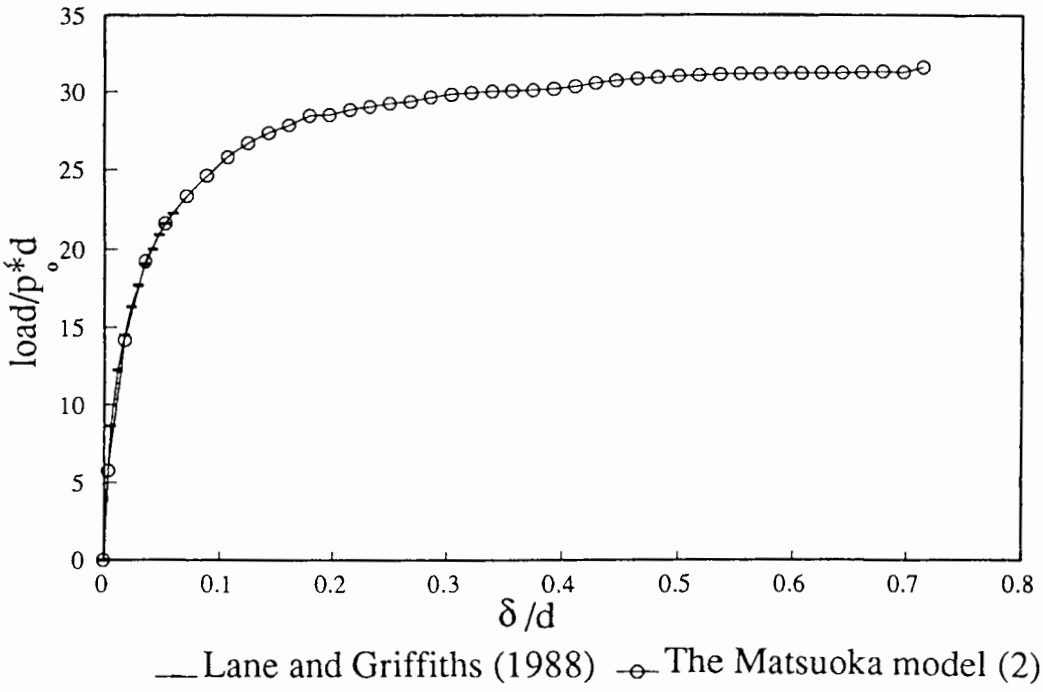

Figure 7.11: Comparison of load displacement response

material parameters are used in this analysis: the initial relative density I_D^o of 0.3, G/p_o' ratio of 1000, the initial and final void ratios of 1.49 and 1.79 respectively. The model not only traces back exactly Lane and Griffiths's (1988) curve but also gives a value for the ultimate lateral load.

7.6 Laterally loaded single-pile - the effect of initial relative density I_D^o

In this section the analyses described in Section 7.3.1.1 are repeated using the Matsuoka model (2). The finite element mesh and the material properties are the same as given in Section 7.3.1.1. The analyses are carried out for values of initial relative density I_D^o = 0.33 and 0.9 representing relatively loose and dense soils. The results are plotted in Figures 7.12-13. It is shown in Figure 7.12 that loose sands do not dilate and the Matsuoka model (2) can reproduce the obtained curve using the Matsuoka model (1) with zero dilation. However, if the soil is initially too loose then it may cause the friction angle at first to drop down below ϕ'_{cv}

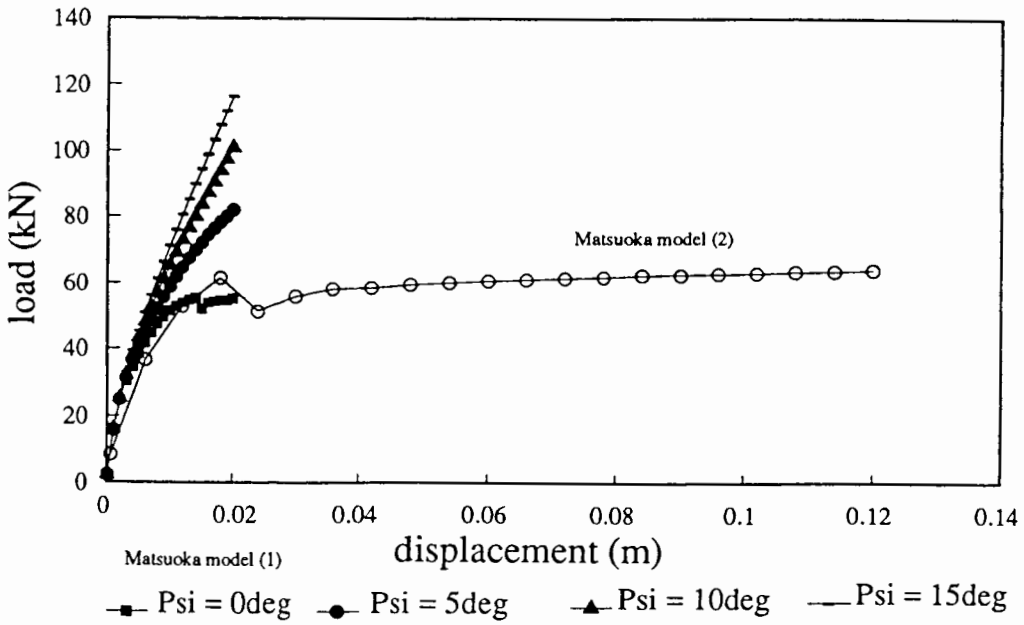

Figure 7.12: Load displacement response (I_D^o = 0.33)

and then recovering back to ϕ'_{cv} during the course of the analysis. On the contrary, dense sands dilate and the Matsuoka model (2) is capable of predicting the ultimate lateral load in a dilating sand using non-associated flow rule (see Figure 7.13). However, in the absence of an analytical solution, it is difficult to validate these results.

7.7 Conclusions

The Matsuoka model (2) is a more realistic model to predict the response of laterally loaded piles in sands. The finite element analysis can be used to predict the load displacement response (a theoretical *p-y* curve). The theoretical *p-y* curve captures the non-linear soil

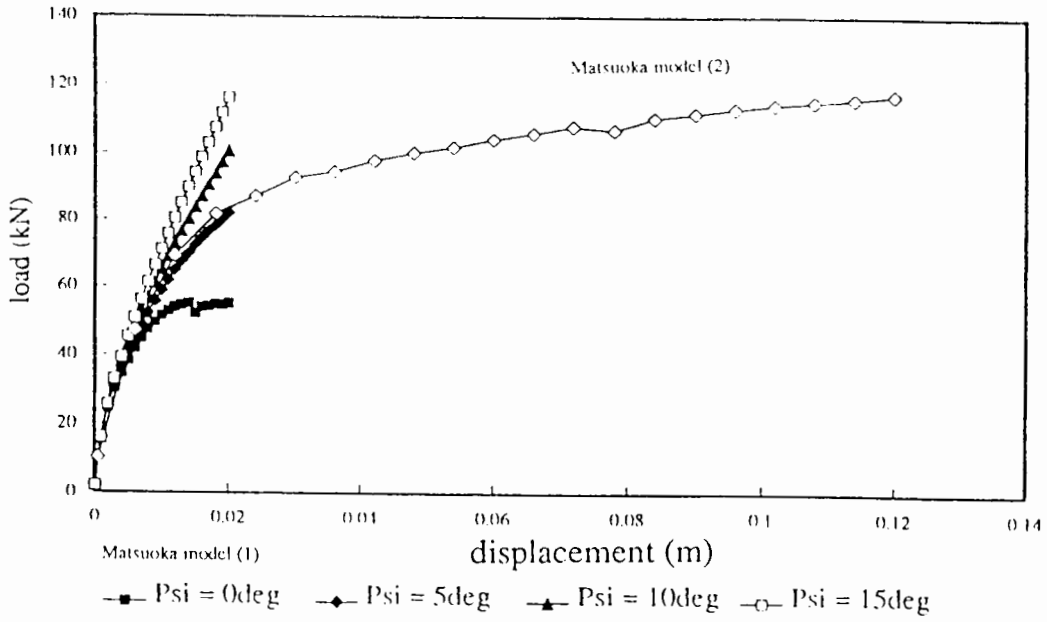

Figure 7.13: Load displacement response ($I_D{}^o$ = 0.9)

behaviour and seems more reliable than the empirically constructed *p-y* curve proposed by Reese *et al.* (1974) which is essentially a bilinear curve based on a constant friction angle (Yan and Byrne (1992)). The theoretical *p-y* curve can be non-dimensionalised as shown in Figure 7.14 and a series of *p-y* curves along the length of the pile can be obtained by a single finite element analysis. These curves can then be used as inputs to the standard subgrade

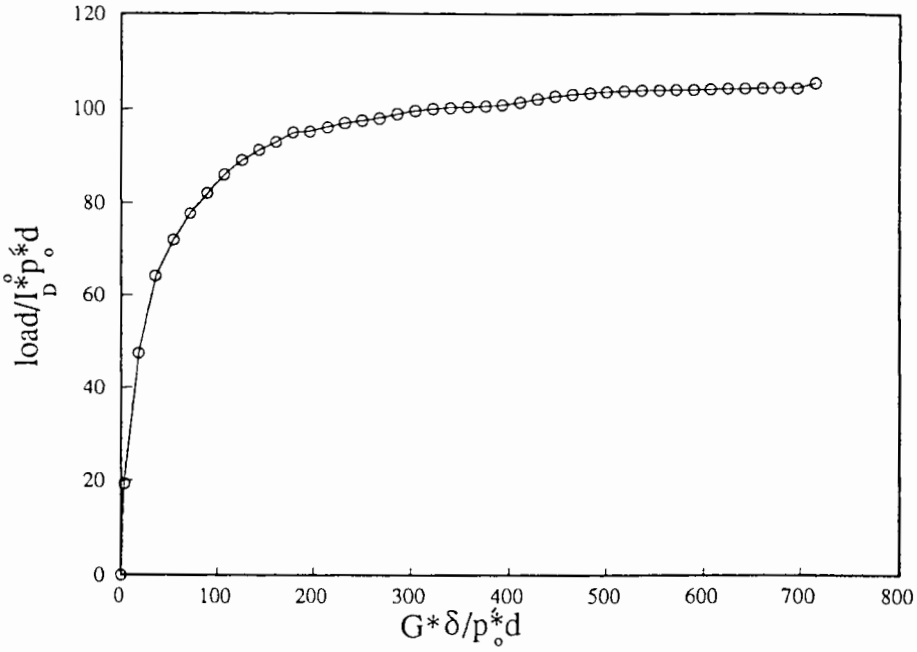

Figure 7.14: A theoretical *p-y* curve

reaction analysis (see Chapters 5-6) to predict the pile head displacement of a single-pile as well as pile groups. A further work similar to that carried out in Chapters 5-6 is accordingly, proposed in this direction.

CHAPTER 8

BEARING CAPACITY OF A JACKUP SPUDCAN FOOTING

8.1 Introduction

The ultimate bearing capacity of a flat surface footing, as briefly discussed in Chapter 4, is dependent on the footing-soil interaction under vertical, horizontal and moment loading which governs the stability of the footing. In this Chapter we shall consider the stability of a jackup spudcan footing and calculate its ultimate bearing capacity using the finite element method, though without pursuing the detailed interface analysis undertaken for a flat footing.

The growing use of mobile jackup units on spudcan footings in deep offshore waters has raised a great deal of concern about the overall stability of a jackup unit in hostile environmental forces. The stability of a jackup unit is greatly influenced by the performance of a typical spudcan footing under storm loading conditions. Therefore, as a result, much research has been focused towards the study of a spudcan footing behaviour subjected to combined vertical, horizontal and moment loading. Recently, over a period of several years, a Joint Industry Study coordinated by Noble Denton Associates (NDA) has been considering many aspects of jackup stability including the soil-structure interaction (see Osborne, Trickey, Houlsby and James (1991)).

Mobile jackup units consist of a floatable drilling platform, supported on three or more legs which can be raised or lowered (see Figure 8.1). A detailed description of the installation procedure is given by Tan (1990). The platform legs can either be supported separately as shown in Figure 8.1a or they can be supported on a single shared mat (Arnesen *et al.* (1988)).

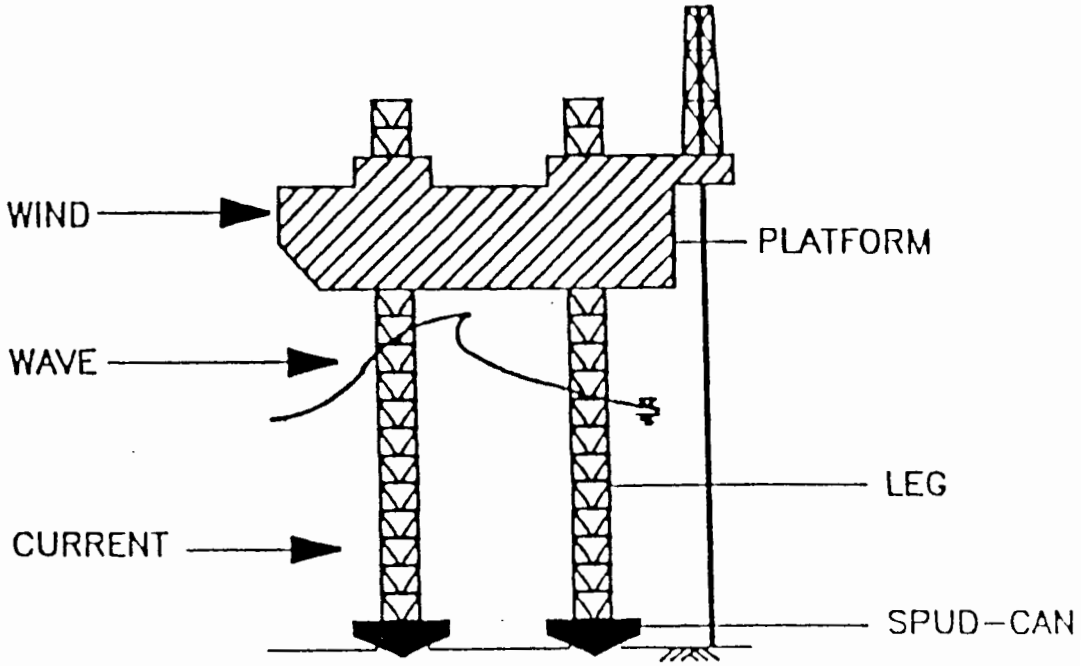

(a)

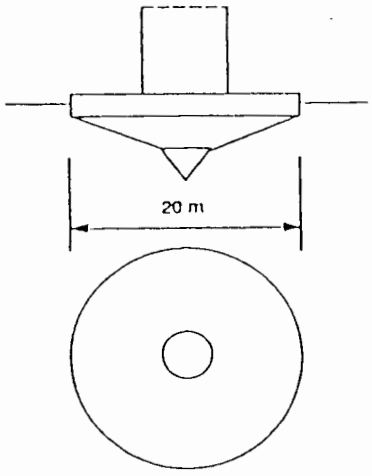

(b)

Figure 8.1: (a) Jack-up platform and environmental loads (after Tan (1990))
(b) Spudcan footing

Most modern jackup platforms are of the former type and have approximately conical shaped footings with a protruding tip at the centre. These are commonly referred to as 'spudcan' footings (see Figure 8.1b).

The mobility of jackup units allows for relocation and re-use of the platform. Before actual oil and gas exploration activity begins, the legs of the platform are preloaded to almost twice the working load. During this loading operation, spudcan footings move into the seabed to a depth of almost twice their diameter. In soft clays, a 30m penetration of a 15m diameter spudcan is not uncommon. The bearing capacity of spudcan footings increases with the depth of penetration below the seabed. The increase of bearing capacity with footing embedment is an important factor, since even a small embedment can significantly increase the bearing capacity of such offshore footings (Houlsby and Martin (1993)). However, this is not usually the case in coarse materials as penetration depths are typically very small (see e.g. Dean *et al.* (1993)).

In addition to the vertical load of the jackup structure, a spudcan footing is also subjected to large horizontal forces due to severe environmental conditions reaching, in stormy weather, up to 30% of the total vertical load and thereby producing a correspondingly large moment (Poulos (1988)). However, moment loading will not be pursued further here. Environmental loads, as mentioned elsewhere in this thesis (see Chapter 1) are cyclic in nature and are beyond the scope of this thesis.

In this chapter we are making a conventional assumption, that a jackup leg is pinned at the foundation level and that therefore a spudcan footing offers no moment restraint to the leg (see Figure 8.2a). This means that, only the interaction between horizontal and vertical loading needs to be studied. Although, in recent studies moment restraint at the footing has also been considered which would reduce the bending moment in the lower leg guide (see Figure 8.2b), which is often a critical feature of the structure in extreme loading conditions: a full interaction between vertical, horizontal and moment loading has been studied by e.g. Houlsby and Martin (1993) for clays, and by Dean *et al.* (1993) for sands.

We discuss here the ultimate bearing capacity of a partially penetrated spudcan footing

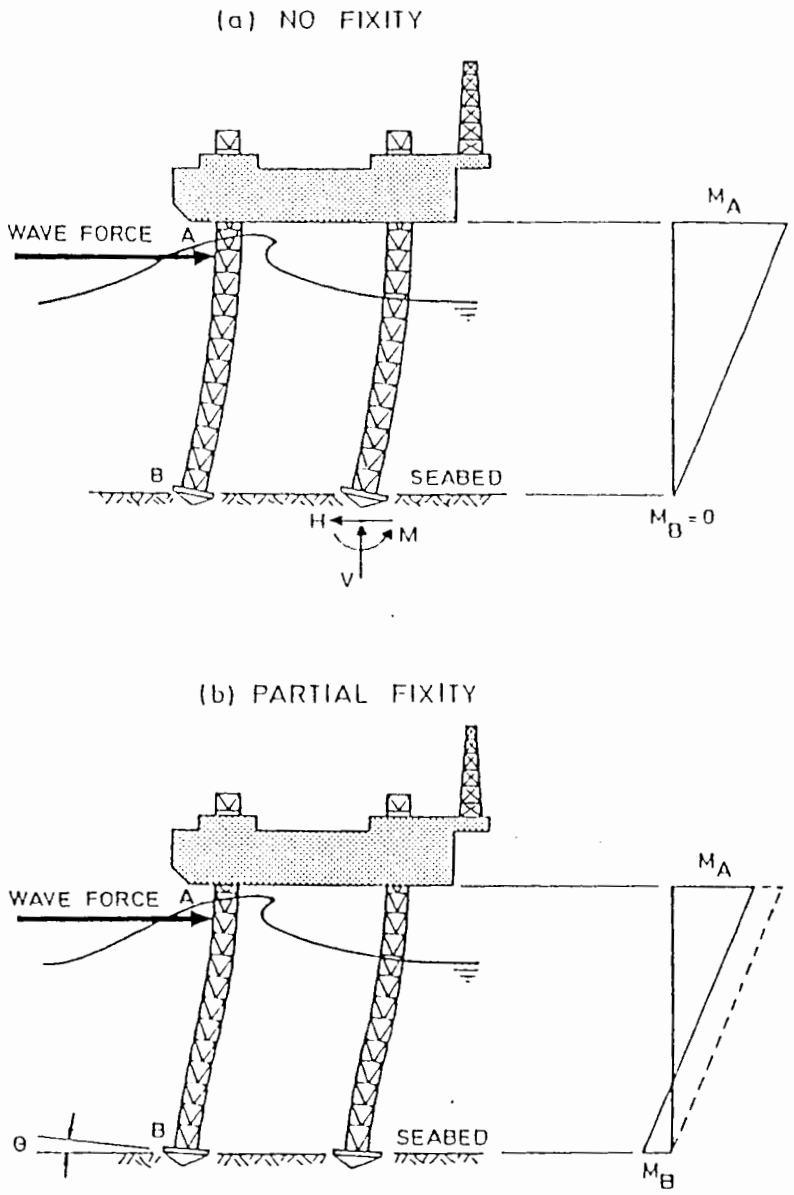

Figure 8.2: Bending moments in the legs of Jack-up units (after de Santa Maria (1988))

subjected to combined vertical and horizontal loading, and describe a three-dimensional finite element analysis of the footing. (Although, in the preceding chapters we preclude the use of a complete three-dimensional analysis for deep foundations due to the enormous amount of computational effort involved. The same is true here for a surface footing but the size of the problem is not as large as a multi-pile group foundation.) The aim of the analysis was to carry out an independent investigation of the behaviour of the spudcan footing under combined vertical and horizontal loading, and compare the results with the existing theories. A parallel laboratory investigation of the same geometry is described by Hambly (1992).

8.2 Background

The bearing capacity solutions of Meyerhof (1953), Hansen (1970) and Vesic (1975) are commonly used to determine the ultimate bearing capacity of plane strain footings. These solutions are modified by introducing shape factors to cover circular geometries (see e.g. Hambly (1992), Dean *et al.* (1993)). In the case of spudcan footings, their embedded circular area in plan (i.e. plan area at ground surface) is used for the bearing capacity calculations. In order to investigate the applicability of the bearing capacity solutions to spudcan footings, theoretical and experimental studies of conical shaped footings (based on centrifuge model tests) have been undertaken by Cambridge University Engineering Department (CUED) and Andrew N. Schofield and Associates (ANS&A) over a period of several years. Work has been reported in various publications including M.Phil and Ph.D thesis. One such extensive study, carried out by Tan (1990) is reported in Dean *et al.* (1993). In this study, a series of tests of cones of angles 0° (flat), 13°, 25°, 45° and 60° was conducted on sand at 28.3mm diameter model footings at 56.6g, representing 1.6m prototypes in the drum centrifuge. It is shown in the study that spudcan footings can be treated as equivalent cones enclosing the same volume. The load displacement response of a spudcan footing and an equal volume cone is almost identical. The ultimate bearing capacity of these footings for vertical loading only, combined horizontal - vertical (inclined) loading, vertical - moment (eccentric) loading and

lateral - moment loading has been determined. The results are compared with existing bearing capacity theories and analytical solutions where possible. The study shows that the vertical bearing capacity does not vary much for cone angles between $0°-20°$. However, for flat circular footings under combined vertical - horizontal loading (referred as shear sideswipe tests at constant penetration), most of the experimental data lies outside the curves proposed by Meyerhof (1953), Hansen (1970) and Dean *et al.* (1993).

Hambly (1992) carried out laboratory tests in sands on two model footings - flat and spudcan. The purpose of this investigation was to compare the ultimate bearing capacity of flat and spudcan footings. In the series of tests performed by Hambly (1992), the footings were preloaded until the penetration for the flat footing was 10% of its diameter (Vesic (1975)) and for the spudcan footing, a penetration of its bearing area at the ground surface equivalent to the bearing area of the flat footing. Hambly (1992) found that the preload force that mobilized the ultimate bearing capacity of the sand under the flat circular footing was insufficient to mobilize the ultimate bearing capacity of the sand under the spudcan footing. Hambly (1992) showed that the ultimate bearing capacity of a partially penetrated spudcan footing is twice the preload force required for the flat footing. He obtained enhanced sliding resistance of the spudcan footing using twice the preload force for the flat footing with Hansen's (1970) theory. He attributed the difference between the preload force and the ultimate bearing capacity to the much greater volume of sand displaced by a flat footing mobilising ultimate bearing resistance, as compared to the volume displaced by the partially penetrated cone of the spudcan. He suggested 'partial penetration factors' to determine the ultimate bearing capacity from the vertical preload force. He concluded in his study that a further laboratory investigation is needed to validate his results. Although, in the absence of such an investigation it is difficult to comprehend Hambly's (1992) results, the experimental results described by Tan (1990) resembles more closely the actual preload operation of the spudcan footing. The footing penetrates into the seabed as the load is applied and continues to penetrate until there is no further penetration i.e. the footing is locked vertically. The final value of the load, thus, represents the ultimate bearing capacity of the footing.

The three-dimensional finite element analysis of the spudcan footing here described was done using the commercial finite element code 'ABAQUS'. For the given penetration depth of the spudcan footing (i.e. the depth at which the ground surface bearing area of the spudcan footing became equal to the bearing area of the flat footing), the finite element analysis predicts a vertical preload which is the ultimate bearing capacity of the partially penetrated spudcan footing i.e. theoretically equal to the ultimate bearing capacity of the flat footing of the equivalent bearing area. The numerical results obtained from the finite element analysis (which can also be found elsewhere: Burd (1991)) compares well with Hambly's (1992) laboratory results for both the flat footing and the spudcan footing with a partial penetration factor of 2. A comparison with the results from Hansen's (1970) solution showed the latter (as mentioned earlier: see Section 4.4.3) to give rather conservative estimates of the bearing capacity of such offshore footings.

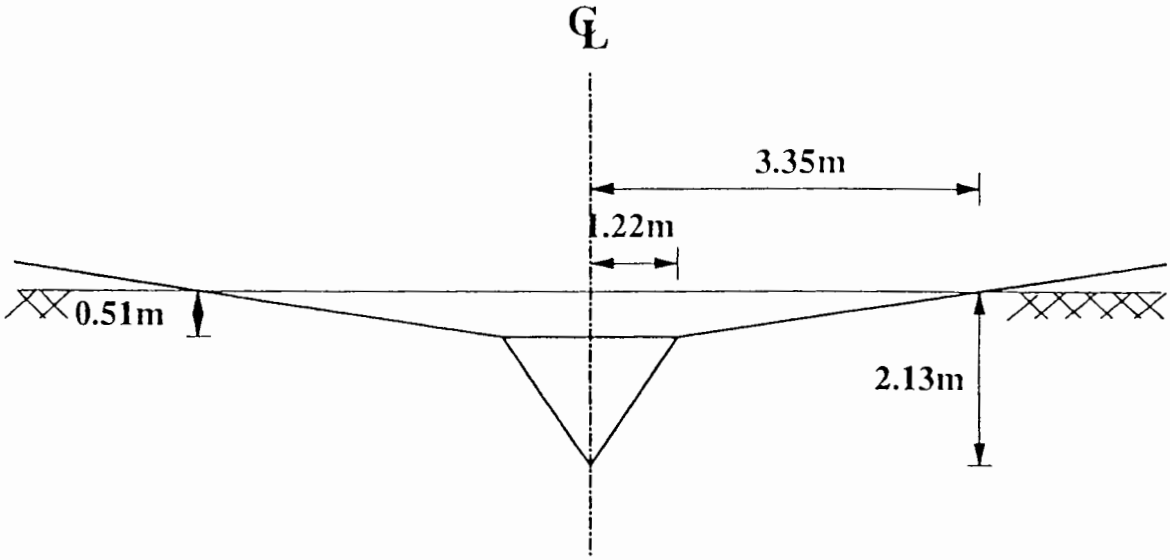

Figure 8.3: Spudcan geometry

8.3 Description of the problem

The dimensions of the spudcan footing (the 'cone' and its protruding central tip) assumed in the finite element calculations are shown in Figure 8.3. The face of the 'cone' is inclined at

an angle of 13.46° to the horizontal (later in the text referred as cone angle 'Ω') with an apex angle of 152.7°. The dimensions of the central tip are also shown in Figure 8.3. The spudcan is partially embedded (depth=2.13m) in dense sand with a bearing area diameter equal to 6.71m. The following load paths are analysed:

1) Initial vertical loading to determine the preload, for the given penetration depth.

2) Reduction of vertical load with increase in horizontal load to cause yielding in dense sand

3) A further reduction of vertical load followed by further increase in horizontal and vertical loads.

In each of these load paths, as indicated above, moment loading is not taken into account.

8.4 Choice of material constitutive behaviour

The finite element analyses were carried out using a linear elastic, perfectly plastic soil model in which failure is defined by the Drucker-Prager (1952) failure criterion. The failure surface is circular when viewed in the π plane, as shown in Figure 8.4a. The Drucker-Prager model is an inaccurate theoretical representation of granular material behaviour. The failure surface can either be inner matching or outer matching to the Mohr-Coulomb irregular hexagon shown in Figure 8.4a. In Figure 8.4b, the Mohr-Coulomb and the Drucker-Prager yield criterion are plotted in a stress (q-p) space. The figure shows that for an inner matching circle, the Drucker-Prager yield line matches well with the Mohr-Coulomb yield line for that part of the stress space which represents the stress states as they are in a triaxial extension test (i.e. in the fourth quadrant) . Similarly, for an outer matching circle, the Drucker-Prager yield line

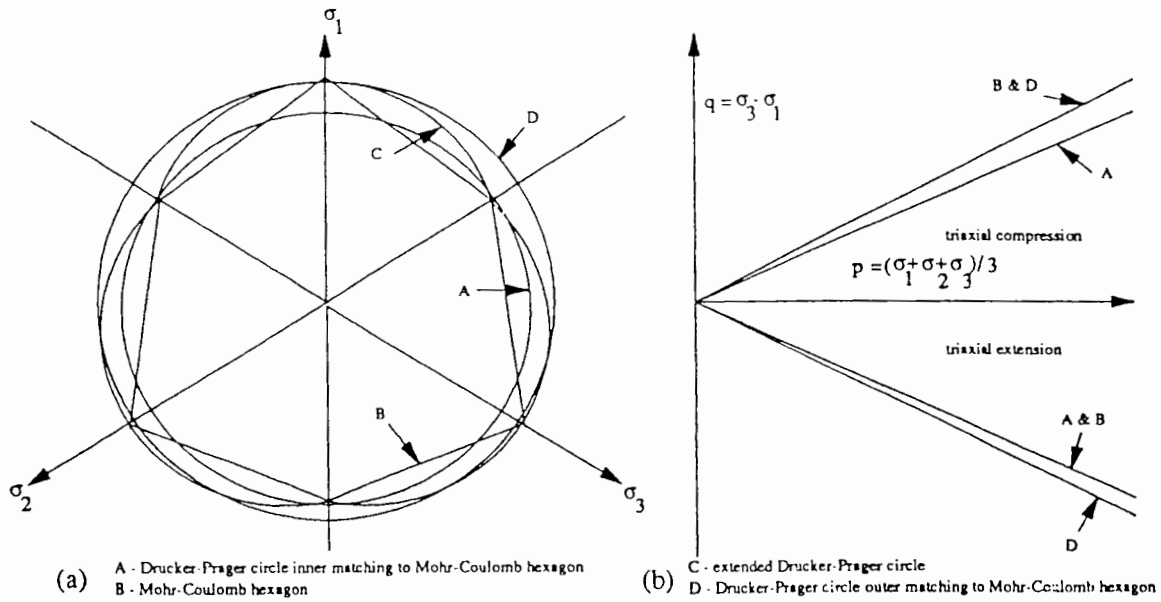

Figure 8.4: (a) Yield surfaces in 'π' plane (after ABAQUS manual)
(b) Yield surfaces in (q-p) stress space

matches with the Mohr-Coulomb yield line for the stress states as they are in a triaxial compression test (i.e. in the first quadrant). The Drucker-Prager model does not yield a unique match for both the Mohr-Coulomb yield lines in the stress space. It was difficult to choose parameters for the Drucker-Prager model to depict a given Mohr-Coulomb friction angle, as the parameter that determines the inner matching circle to a given Mohr-Coulomb hexagon does not yield the same outer matching Mohr-Coulomb hexagon that one would expect from an inner matching Drucker-Prager circle, i.e. it does not yield the same (chosen) Mohr-Coulomb friction angle, and the difference between these two Mohr-Coulomb angles is quite substantial (see Figure 8.5a). It seems to suggest that if the failure condition is described by triaxial extension tests, the consequence is that the angle of friction in compression tests is smaller than the angle of friction in extension tests (see Atkinson and Bransby (1978)). Similarly, with the outer matching Drucker-Prager circle to a given Mohr-Coulomb hexagon, the parameter leads to a non-existent inner matching hexagon for the chosen outer matching Drucker-Prager circle, which cannot be right. (This situation is depicted in Figure 8.5b.) We need to have a plasticity model which provides a smooth approximation to the Mohr-Coulomb surface. The Matsuoka (1976) model shown in Figure 8.5c, by contrast, more accurately

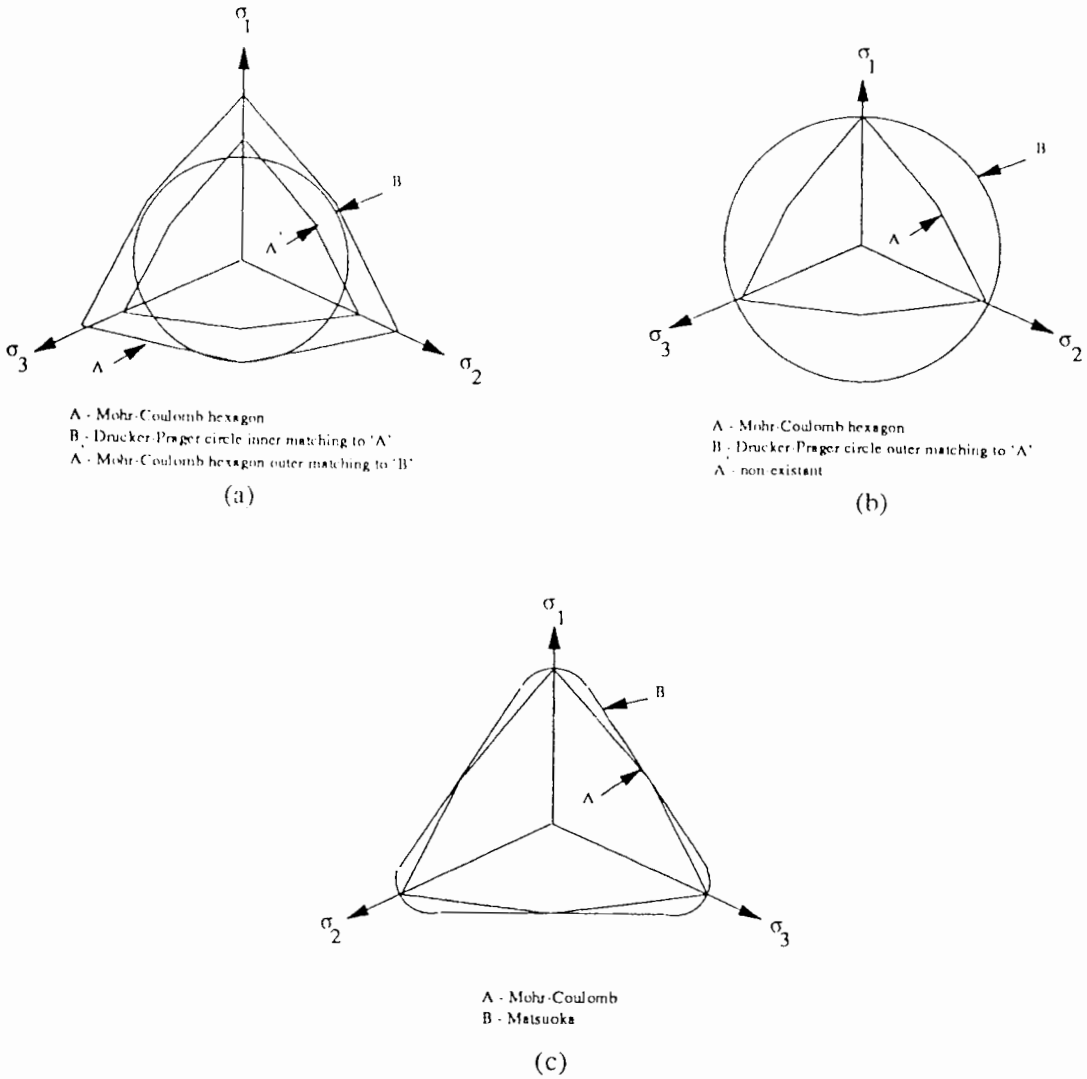

Figure 8.5: Yield surfaces in 'π' plane

represents granular material behaviour and resembles the shape of the Mohr-Coulomb hexagon in the π plane. This model, however, is not available in 'ABAQUS'. It was therefore necessary to determine appropriate parameters for the Drucker-Prager model to represent an equivalent Mohr-Coulomb friction angle for the soil. In all of the finite element calculations, the results of which follow, the parameters of the failure surface were chosen in such a way that the surface coincides with the triaxial extension points (inner matching circle) of the Mohr-Coulomb envelope for a Mohr-Coulomb friction angle of 37.5°. That

surface corresponds to Curve (B) on Figure 8.5. An inner matching Drucker-Prager circle was deliberately chosen since it was more likely that the stresses inside the soil underneath the spudcan footing would reach a stress state which is better represented by a triaxial extension test, i.e. the horizontal load is dominant to the applied vertical load on the spudcan footing. We will see later in this chapter that this choice (inner matching Drucker-Prager circle) turned out to be quite successful in predicting the failure load for the spudcan footing under consideration. The predicted failure load is close to the one estimated analytically. The plasticity model is fully associated, i.e. the angle of dilation is set as equal to the angle of friction. In order to avoid numerical problems in the analysis procedures, it is necessary to include a small amount of cohesion in the soil model: a value of 2.5 kPa is adopted in all of the calculations here.

8.5 Finite element model

As we have already seen in the preceding Chapters 3,5-7, it is difficult to model rigid boundaries in a finite element analysis. The presence of rigid boundaries in close proximity to the loaded area has a detrimental effect on the quality of the resulting solution. Moreover, the sheer volume of computations involved in a three dimensional analysis is too costly in computer time. It is therefore necessary, in order to contain the bulk of the problem, to nominate an appropriate location for the rigid boundaries in the finite element model.

Theoretical calculations of bearing capacity were carried out for this purpose by Houlsby (1991), using an axi-symmetric method of characteristics analysis, described in Houlsby (1982), Houlsby and Wroth (1982, 1983). This method gives a lower bound solution to the incremental collapse problem. (Various different stress fields (characteristics) can be studied which satisfy the conditions for a lower bound solution but the only stress field that gives a true lower bound is the one which can be extended throughout the whole soil mass.) The theoretical extent of the failure zone was determined and the rigid boundaries in the finite element model were then set sufficiently far beyond this zone. In the axi-symmetric analysis

done here, the footing is modelled as a simple cone, assumed to be fully rough, and a Mohr-Coulomb friction angle ϕ of 37.5° is assumed for the soil. The mesh of characteristics obtained from this analysis is shown in Figure 8.6. It indicates that the zone of failure, for

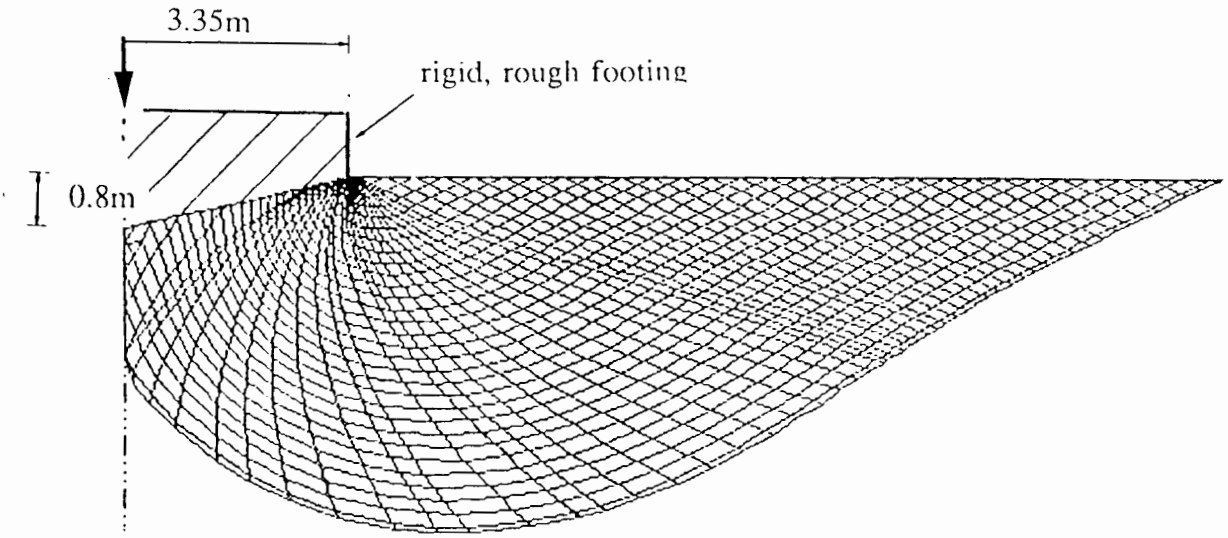

Figure 8.6: Characteristics mesh for vertical loading (after Houlsby (1992))

the case of vertical loading (load path 1), extends to a depth of about 5m and to a radius of about 16m. The rigid boundaries in the finite element mesh were therefore set at a radius of 20m from the centre of the footing and 7m below the ground surface. The linear dimensions, at which the boundaries are set, are, respectively, 25% and 40% greater than the corresponding dimensions of the theoretical failure zone. The elastic parameters used in the model have a Young's modulus of 500 MPa and a Poisson's ratio of 0.2.

8.6 Finite element analyses

In this section, the finite element analyses for the load paths (mentioned in Section 8.3) are described. Load path 1 determines the vertical bearing capacity of a spudcan footing in the

absence of any horizontal loading. Load paths 2 and 3 are complementary and determine the ultimate bearing capacity of a spudcan footing subjected to combined vertical and horizontal loading.

8.6.1 Vertical bearing capacity of a spudcan footing (vertical preload to cause yield)

In this section, the vertical bearing capacity of a spudcan footing is determined using the axi-symmetric and the three-dimensional finite element analyses and the results are compared with Hansen's (1970) bearing capacity solution. We describe first Hansen's solution and then the finite element analyses.

8.6.1.1 Vertical bearing capacity solution

The bearing capacity solution for a circular footing, given by Hansen (1970) can be simplified (for vertical loading only), and written as presented by Dean *et al.* (1993):

$$V = A_p \cdot \left(\frac{1}{2} \cdot N_\gamma \cdot \gamma' \cdot B_p \right) \tag{8.1}$$

where B_p is the penetrated diameter, A_p is the plan contact area, γ' is the soil effective (buoyant) unit weight, and N_γ is an axi-symmetric self-weight bearing capacity factor. B_p can be written in terms of penetration depth D_p as:

$$B_p = 2D_p \cot\Omega$$

where Ω is the cone angle (see Figure 8.7a).

Substituting B_p in the bearing capacity solution (equation 8.1), we get the following equation:

$$V = \pi N_\gamma \gamma' \cot^3\Omega D_p^3$$

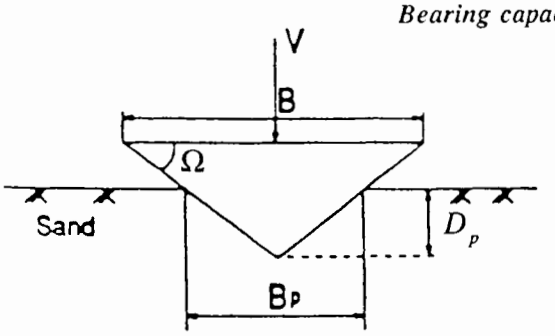

(a) **Conical footing at partial penetration** p

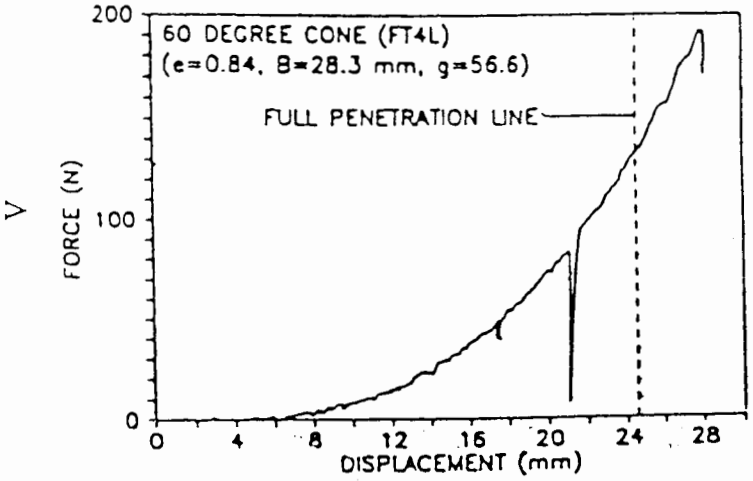

(b) **Initial cubic nature of curve before full penetration** (after Tan (1990))

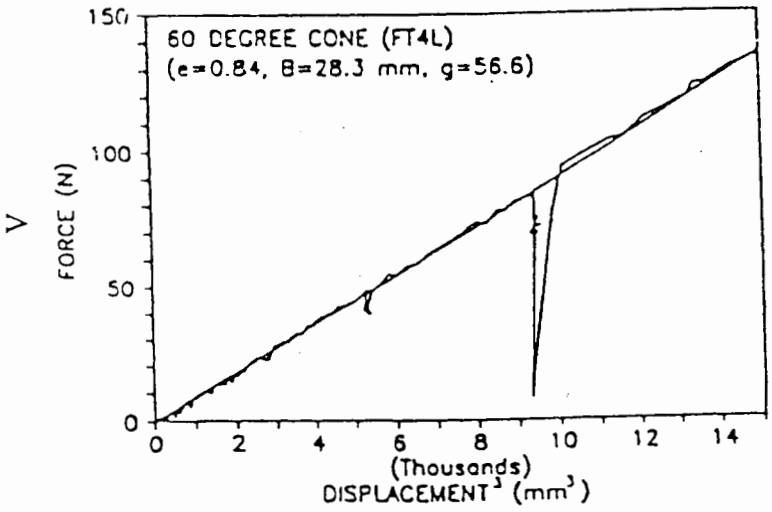

Figure 8.7: (c) Plot of force against the cube of displacement

(after Tan (1990))

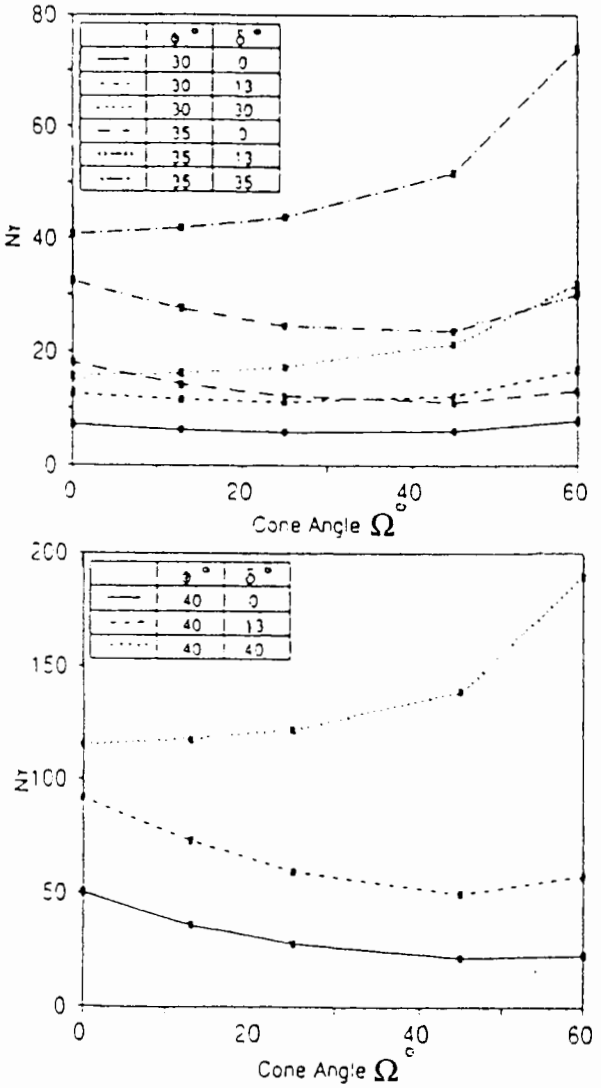

Figure 8.8a: Theoretical axisymmetric N_γ values for cones on cohesionless soil (after Tan (1990))

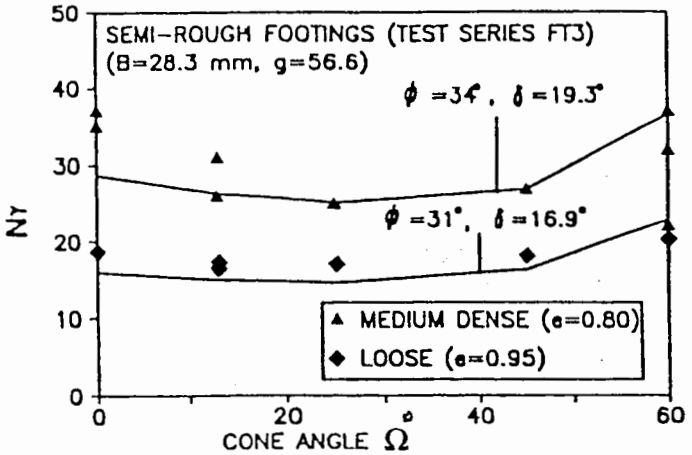

Figure 8.8b: Effect of cone angle on N_γ of semi-rough footings; theoretical and experimental comparison (after Tan, 1990)

Thus for a given cone angle Ω, V is directly related to the D_p^3, if N_γ is approximately constant then V and D_p^3 relationship is a straight line. Such a straight line relationship is shown in Figure 8.7c for a 60° cone (Tan 1990) on fine Leighton Buzzard sand tested in the drum centrifuge at 56.6g. However, for a given depth of penetration, the value of N_γ varies with the cone angle and the variation depends on the surface roughness of the footing. The theoretical variation of N_γ with the cone angle using the method of characteristics is shown in Figures 8.8a . Figure 8.8b shows the same variation of N_γ with the cone angle calculated from the centrifuge test results using equation (8.1) and the comparison with the theoretical results. The results agree well in the region ϕ=31° and δ=17° for loose sand (void ratio 0.95) and ϕ=34° and δ=19° for medium dense sand (void ratio 0.8). (In these figures ϕ is the friction angle and δ represents the degree of roughness of the cone.) It can be seen from the Figures 8.8a that for a fully rough footing (as is the case here in this chapter) the value of N_γ stays almost the same for cone angles between 0°-20°. But for cone angles greater than 25° there is a significant increase in the value of N_γ. These results show that a conical footing with cone angle Ω=13.46° has a slightly higher ultimate load compared to a footing with Ω=0° (flat). But there is a need for further experimental investigation in order to prove that the load is 100% higher as we learn from Hambly (1992).

8.6.1.2 Finite element analyses results (load path 1)

A preliminary analysis was carried out using the axi-symmetric mesh shown in Figure 8.9. The overall dimensions of the mesh were set at 20m radius and 7m depth. The mesh consists of a total of 21 'reduced-integration' 8-noded quadrilateral elements. The footing is taken to be perfectly rough. The analysis consisted of two stages. In the first stage, the appropriate self weight stresses were applied to the model, using a soil unit weight of 10.2 kPa/m (submerged)

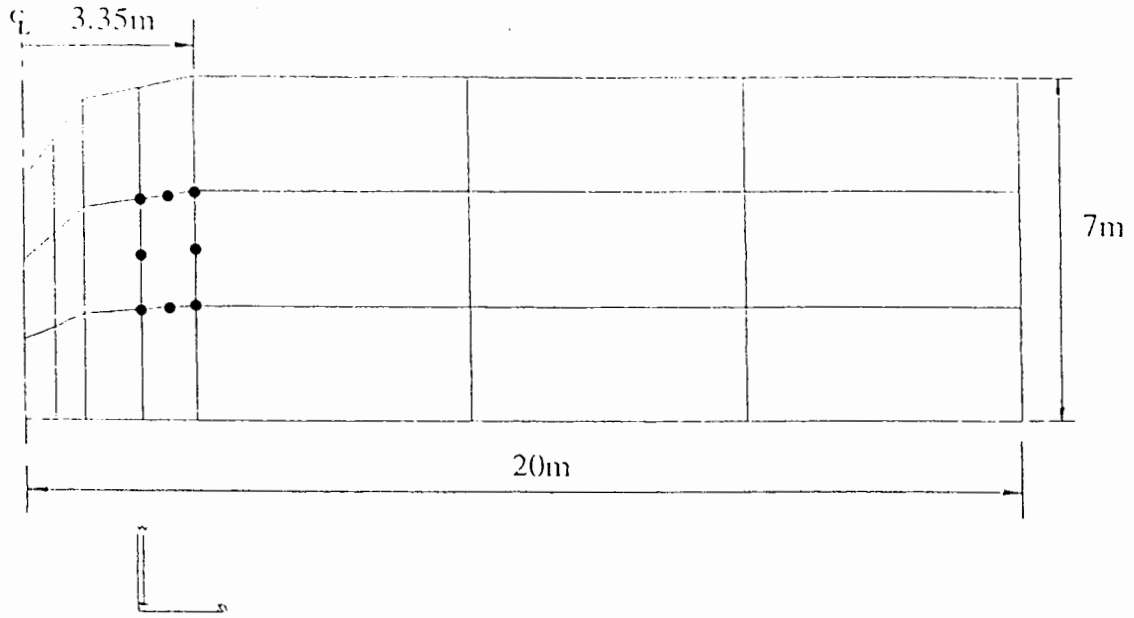

Figure 8.9: Axi-symmetric finite element mesh

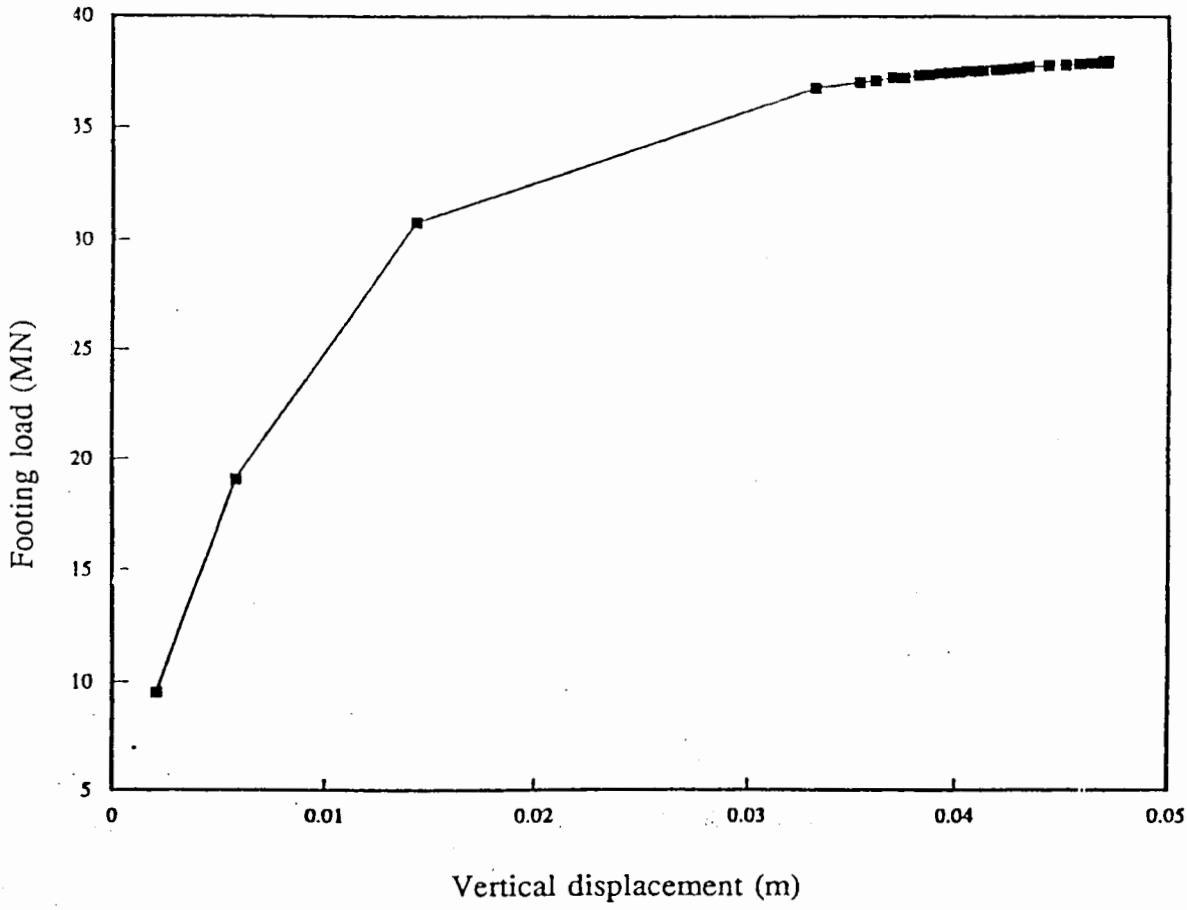

Figure 8.10: Vertical load-displacement curve (axi-symmetric analysis)

and a K_o value of 1.0. In the second stage, a set of vertical prescribed displacements were

applied to the footing.

A plot of the footing load-displacement curve obtained from this analysis is given in Figure 8.10. The footing load at the end of the calculation is 38 MN, with the vertical displacements reaching 47mm.

A further analysis of the vertical failure load was studied using the three-dimensional mesh shown in Figure 8.11. This mesh has roughly the same dimensions as the axi-symmetric mesh shown in Figure 8.9 and consists of a total of 120, 20-noded 'reduced-integration' hexahedral elements with a total of 719 nodes.

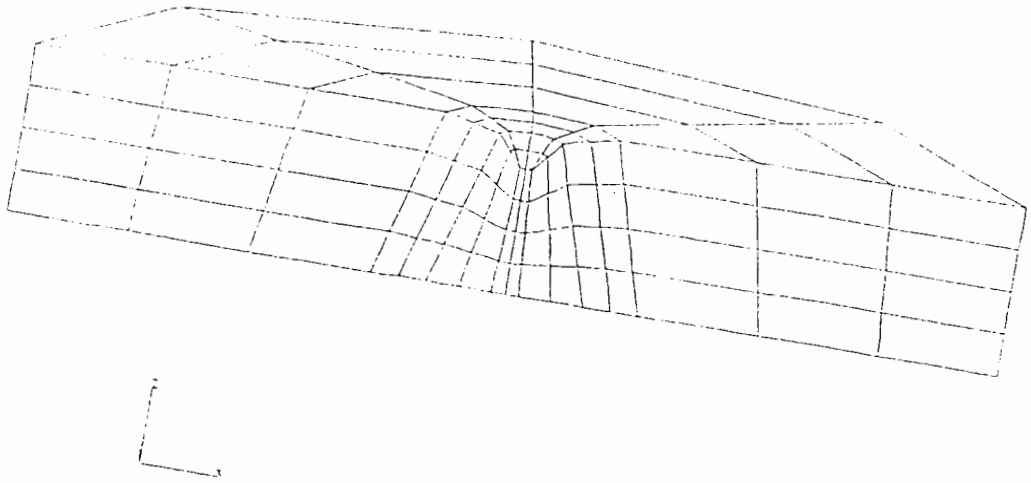

Figure 8.11: Three-dimensional finite element mesh

In this mesh it proved necessary to flatten the apex on the axis of symmetry of the footing in order to allow the mesh to be built entirely from the hexahedral elements. (An earlier analysis based on the unmodified footing geometry and a mesh consisting of a mixture of hexahedral elements and wedge elements had been unsuccessful.)

When viewed from above, the mesh is seen to be built up of a set of concentric half octagons. The footing is therefore, implicitly, assumed to be octagonal in plan. The geometry of the mesh is set up so that the actual vertical area of the footing is equal to the area of the

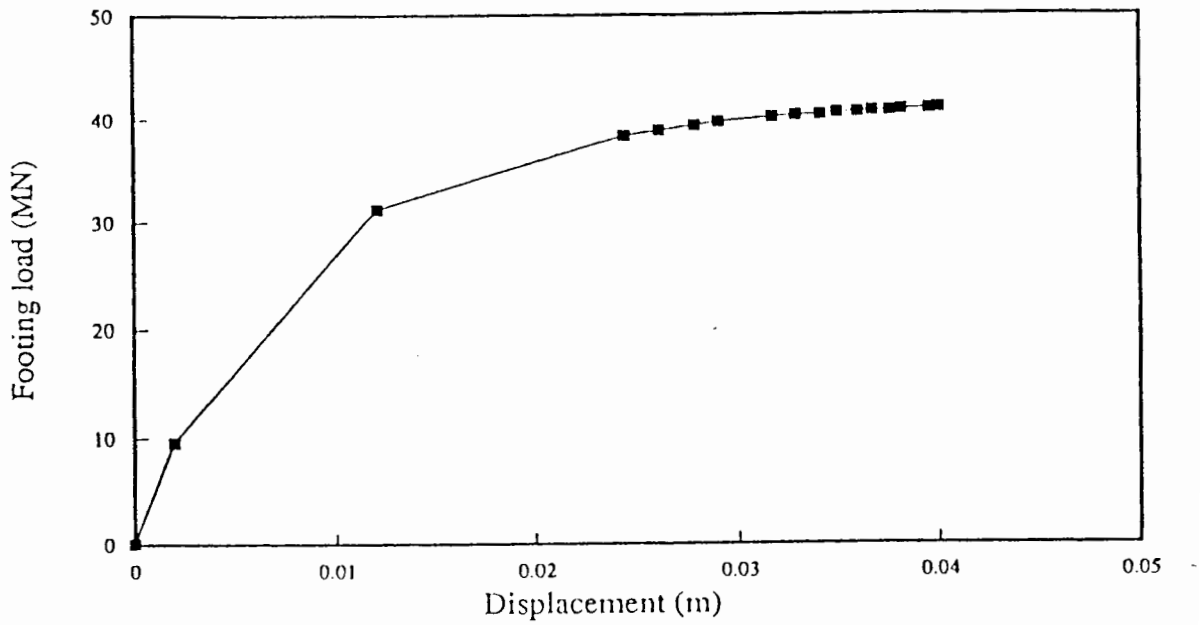

Figure 8.12: Vertical load-displacement curve (three dimensional analysis)

corresponding octagon.

The load-displacement curve obtained from this analysis is shown in Figure 8.12. It indicates a final load of 41 MN, with the vertical displacements reaching 40mm.

The value of bearing capacity factor N_γ for the current problem is worked out to be 52 using equation 8.1. The value corresponds to a friction angle of 36° which is quite close to the friction angle of 37.5°, used in the current finite element analyses. The discrepancy is below 5% which may be a result of the choice of soil model which is unable to model sand behaviour accurately (see Section 8.4). The finite element analyses seem to confirm validity of Hansen's (1970) equation to calculate the vertical bearing capacity of spudcan footings.

8.6.2 Reduction of vertical load (vertical unloading) with increase of horizontal load to cause yield

The bearing capacity solutions and the finite element calculations described in this and the following sub-section are regarding the bearing capacity of the spudcan footing subjected to combined vertical - horizontal loading.

8.6.2.1 Bearing capacity solutions

Various empirical equations to calculate bearing capacity include equations proposed by Meyerhof (1953) and Hansen (1970) for plane strain surface footings which are modified for circular footings by the introduction of a shape factor. These equations are equally applicable to spudcan footings since area of the footing in plan is used in the bearing capacity calculations.

Meyerhof's equation:
$$\frac{H}{V_M}=\frac{V}{V_M}\tan\left[\left(1-\left(\frac{V}{V_M}\right)^{0.5}\right)\phi\right] \tag{8.2}$$

Hansen's equation:
$$\frac{H}{V_M}=\frac{V}{V_M}\left[1-\left(\frac{V}{V_M}\right)^{0.25}\right] \tag{8.3}$$

where $V_M=A\left(\frac{1}{2}N_\gamma\gamma' B\right)$.

It is possible to obtain an interaction diagram in terms of (H/V_M) and (V/V_M). These interaction loci are shown in Figure 8.13. Also shown is an interaction locus based upon the empirical equation given by Dean *et al.* (1993):

$$\frac{H}{V_M} = \left(\frac{\alpha}{\beta}\right)\left(\frac{V}{V_M}\right)\left(1 - \frac{V}{V_M}\right)$$

where the constant (α/β) is taken as 0.56. It can be seen that the Meyerhof and Hansen loci are in general conservative in relation to available 1g data for strip and circular foundations (Ingra and Baecker (1983)). Also plotted in Figure 8.13 there is data for test FT2K obtained

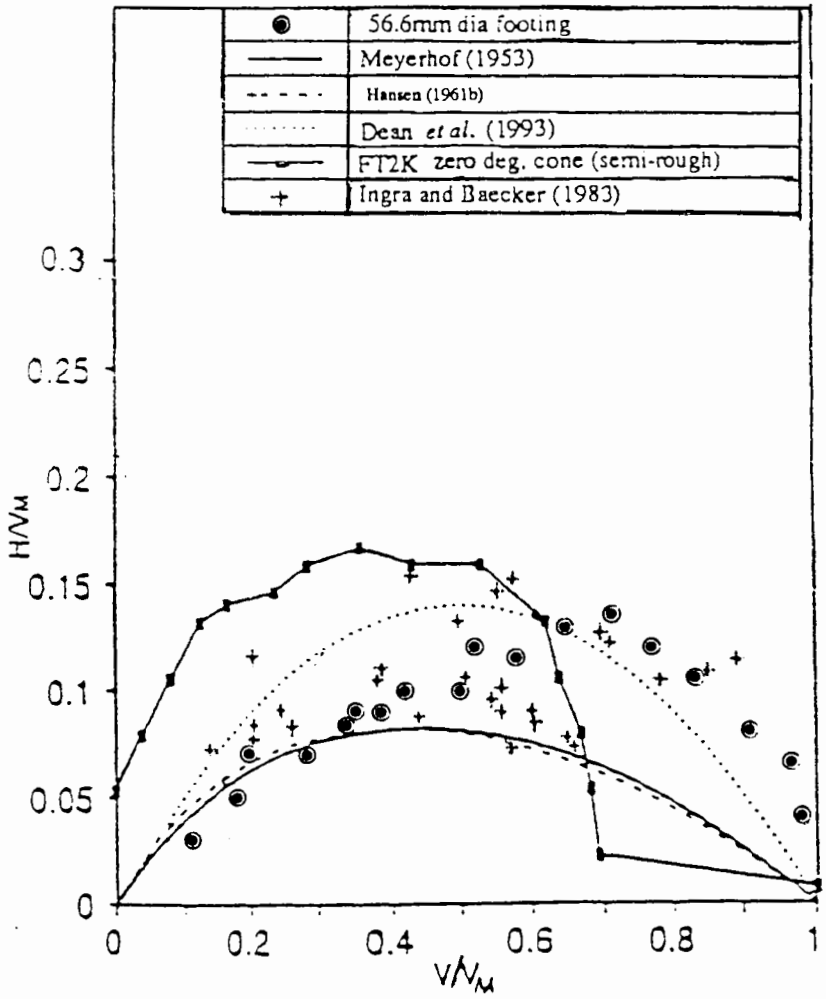

Figure 8.13: Interaction loci for surface footings with inclined load (after Dean *et al.* (1993))

from a drum centrifuge which stands alone from the rest of the data. This is a special test

known as sideswipe test in which the footing is allowed to penetrate vertically until it is locked and there is no further penetration. It is then displaced laterally to bring the sand to collapse. The bearing capacity calculations described in the next sub-section do not represent sideswipe tests but depict the bearing capacity of a spudcan footing at working loads.

As mentioned earlier that V_M is influenced by the depth of penetration D_p. It implies that D_p will also have an affect on H/V_M (see Figure 8.14a where H_P is the peak lateral resistance). Figure 8.14b shows the variation of H_P/V_M with wedge angles. In the absence of satisfactory method of calculation for the axi-symmetric case, this figure shows a series of stress field calculations for the lateral loading of plane wedges. The variation of H_P/V_M with wedge angle and experimental results corrected for penetration are shown in Figure 8.14c. Figure 8.14b implies that the peak lateral resistance does not vary significantly for wedge angles less than 30° which seems to match with experimental observations for conical footings for cone angles up to 30° (Figure 8.14c). However, for cone angles greater than 30° there is a significant increase in lateral capacity. In the light of these theoretical and experimental results, it is difficult to confirm that a spudcan footing of cone angle 13.46° will have more sliding resistance compared to an equivalent area flat footing unless some future research will show otherwise. (We shall see later in Figure 8.23 that the results of the current finite element analyses for the spudcan footing match quite well with Hambly's (1992) results for the flat footing and the spudcan footing with a partial penetration factor of 2. This agreement between the two results, also seems to confirm what we learn from Figure 8.14a i.e. the ultimate lateral capacity of a spudcan footing with a cone angle Ω=13.46° is almost the same as for an equivalent bearing area flat footing.)

8.6.2.2 Finite element analysis result (load path 2)

One of the limitations of the 'ABAQUS' package is that it is not possible to unload from the

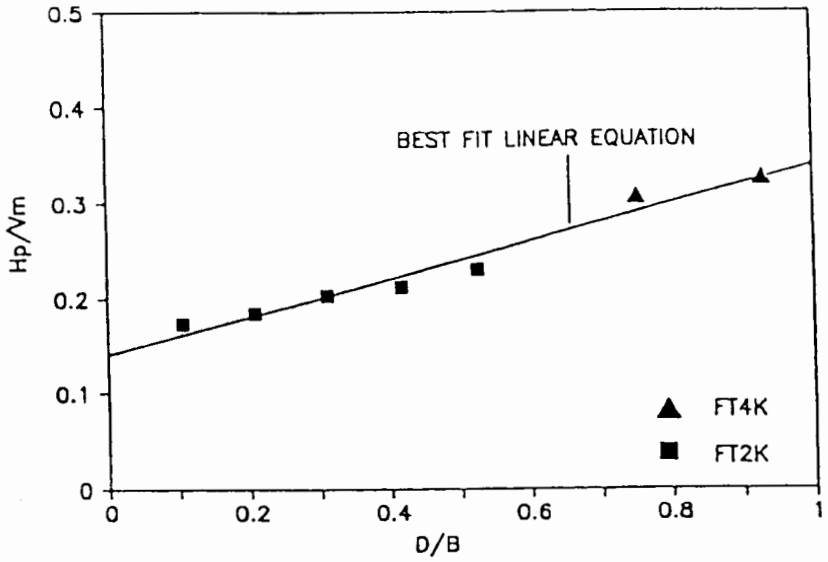

Figure 8.14a: Effect of depth of overburden on H_p/V_m (after Tan 1990))

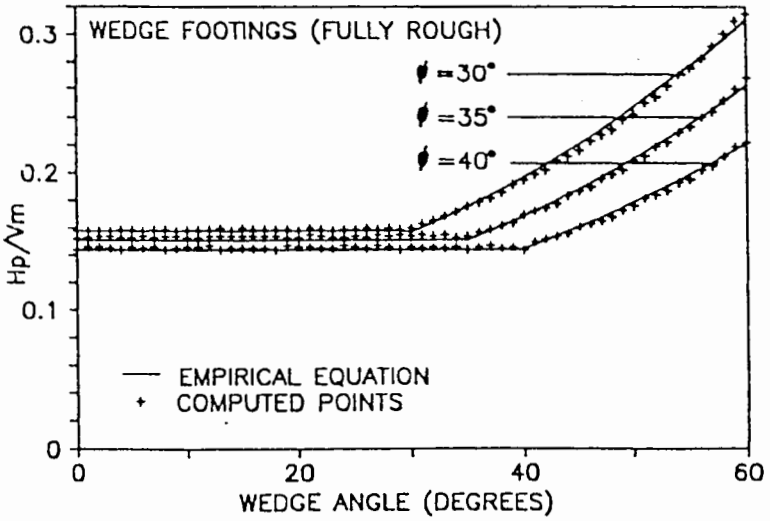

Figure 8.14b: Effect of wedge angle on peak of interaction locus (after Tan, 1990)

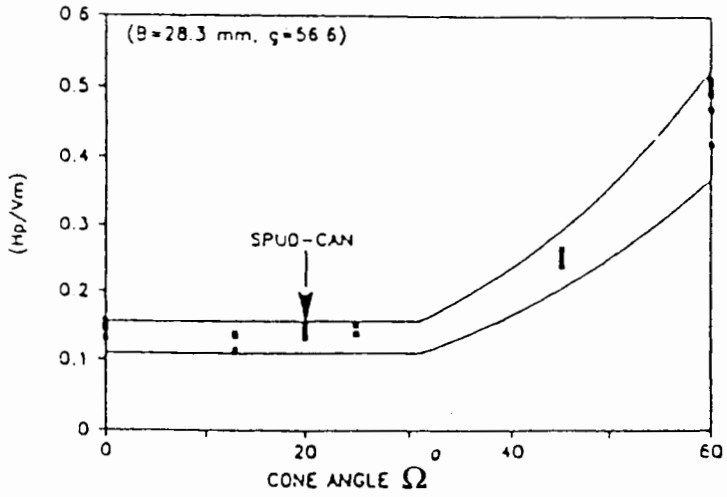

Figure 8.14c: Effect of cone angle on 'corrected' (H_p/V_M) (after Tan (1990))

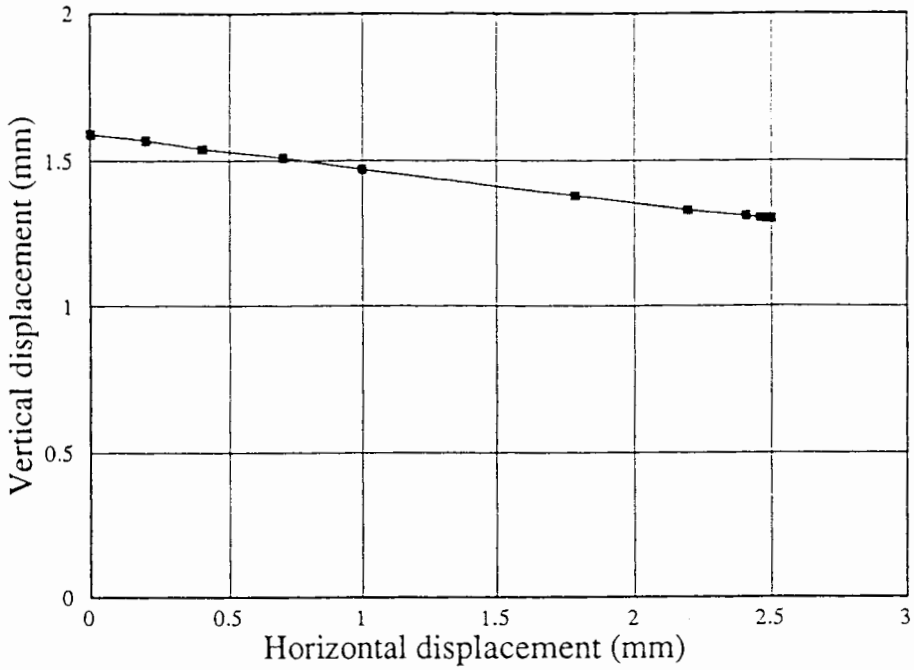

Figure 8.15: Vertical-horizontal displacement curve

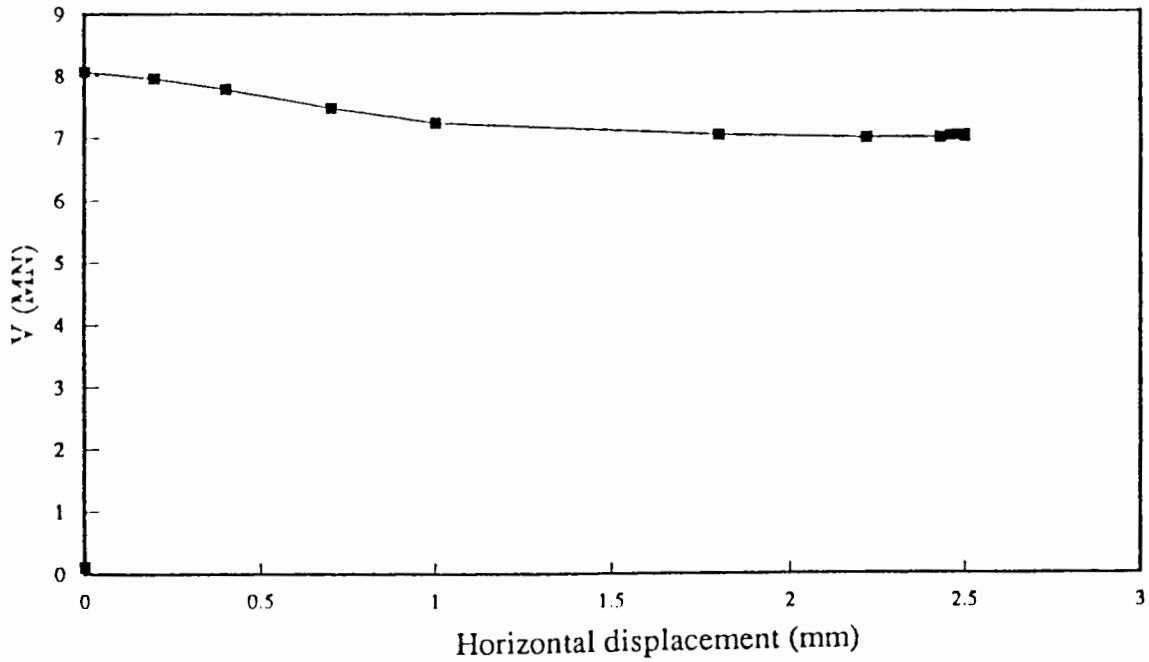

Figure 8.16: Vertical load-horizontal displacement curve

preload described in load path 1. In order to proceed to the analysis of load path 2, therefore, it was necessary to apply a vertical load lower than the preload and then apply suitable horizontal loads. In fact a vertical displacement of 1.59mm was followed by a horizontal

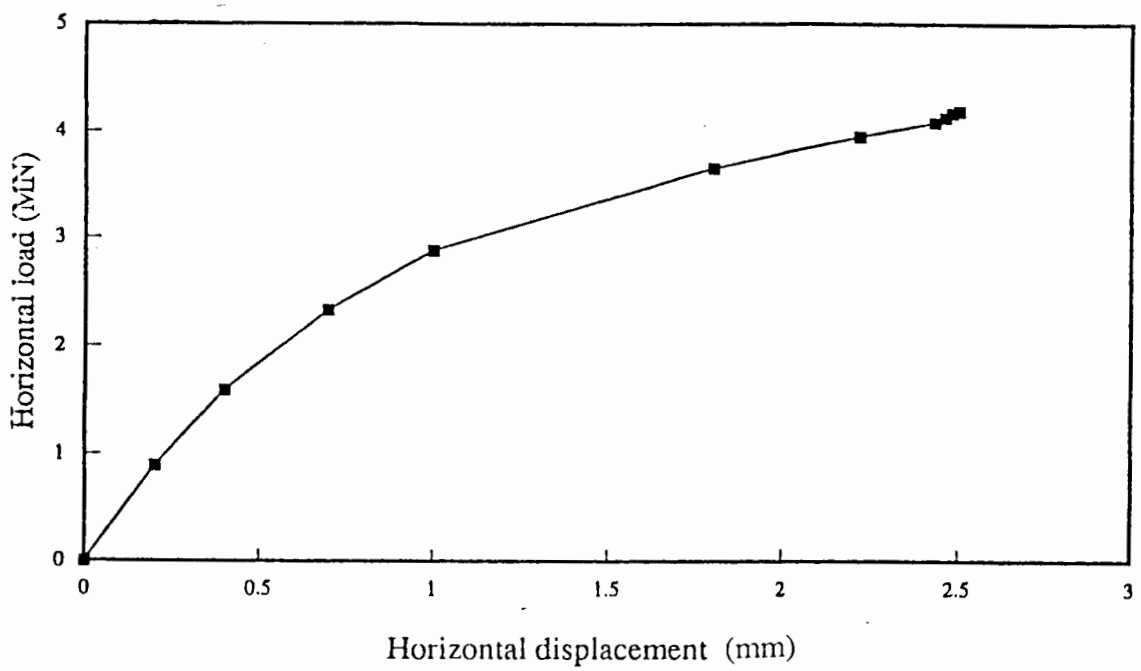

Figure 8.17: Horizontal load-horizontal displacement curve

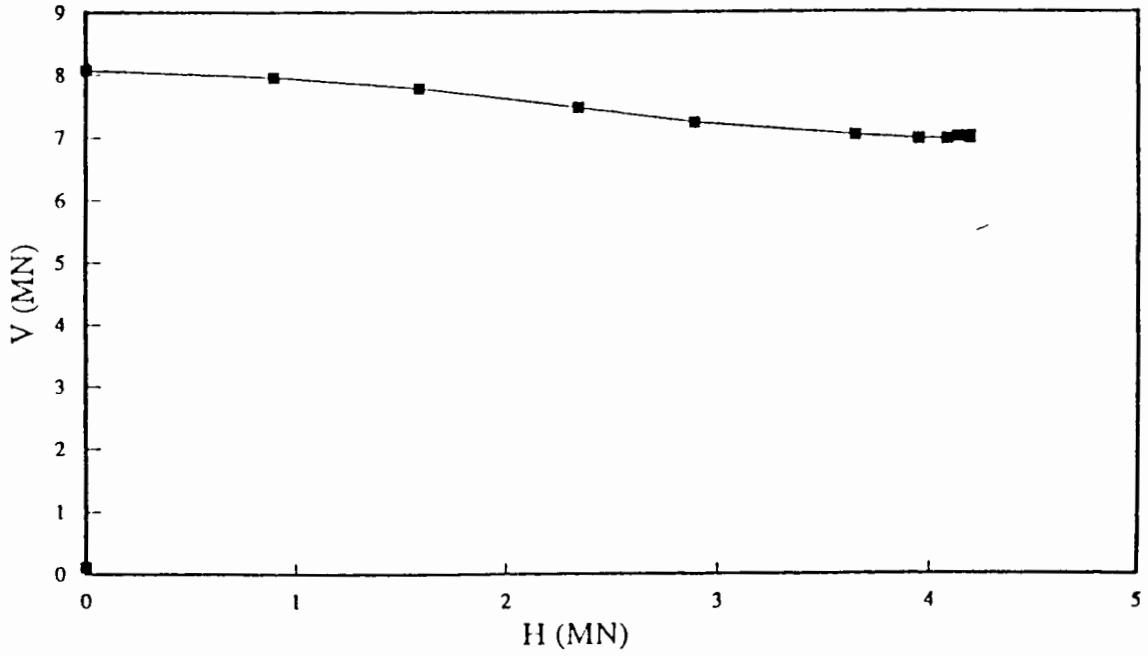

Figure 8.18: Vertical-horizontal load curve

displacement of 2.5mm (see Figure 8.15).

The vertical load response during this loading path is plotted against horizontal displacement

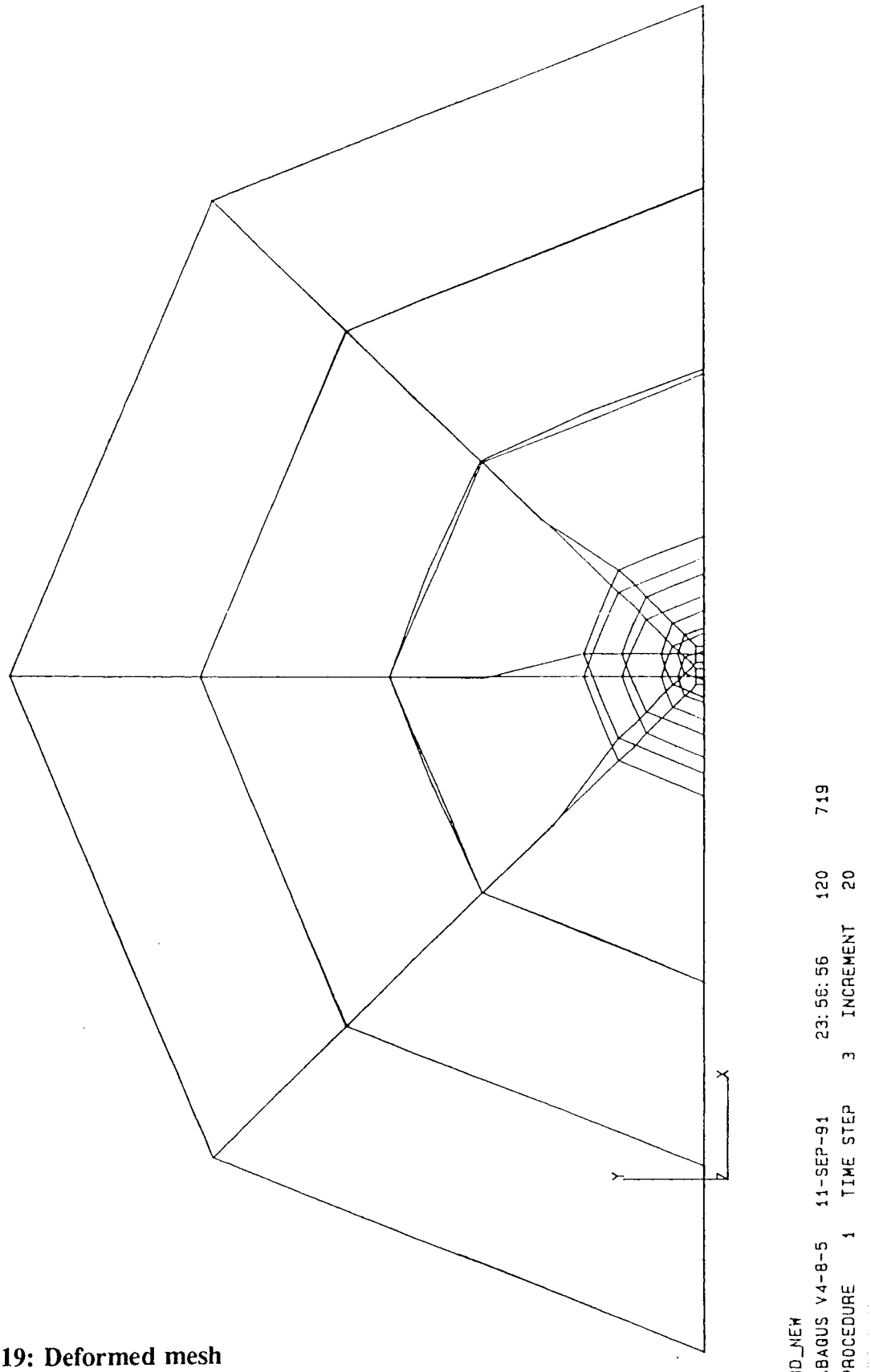

Figure 8.19: Deformed mesh

in Figure 8.16. At zero lateral displacement, the vertical load is 8.1 MN (i.e. 19.8% of the maximum vertical load indicated in Figure 8.12) and this is reduced to 7.0 MN as the horizontal displacements are increased. The variation of horizontal load with horizontal displacement is shown in Figure 8.17. The horizontal load increases monotonically until a value of 4.2 MN is reached. A plot of vertical versus horizontal load is given in Figure 8.18. (The final values of vertical and horizontal load from Figure 8.18, which represent the failure loads for the spudcan footing, are non-dimensionalised by the preload force obtained in Section 8.6.1.2, and are plotted in Figure 8.23. It can be seen that the results lie quite close to Hansen's (1970) curve for a flat circular footing.)

A plot of the deformed mesh at the end of the analysis, viewed from above, is shown in Figure 8.19.

8.6.2.3 A further reduction of vertical load followed by further increase in horizontal and vertical loads (load path 3)

A further calculation was carried out in which a vertical displacement of 0.66mm was prescribed to the footing followed by further vertical and horizontal displacements as shown in Figure 8.20. The calculated horizontal and vertical loads are shown in Figures 8.21 and 8.22. (The final values of vertical and horizontal load from Figure 8.22, which represent the failure loads for the spudcan footing, are non-dimensionalised by the preload force obtained in Section 8.6.1.2, and are plotted in Figure 8.23. It can be seen that, again, the results lie quite close to Hansen's (1970) curve for a flat circular footing.)

8.7 Comparison of results

Figure 8.23 shows Hansen's (1970) solution for flat circular footings, in the form of a parabolic curve in a vertical load versus horizontal load space (interaction diagram). Both the finite element and Hambly's (1992) laboratory test results are also plotted in this figure. As

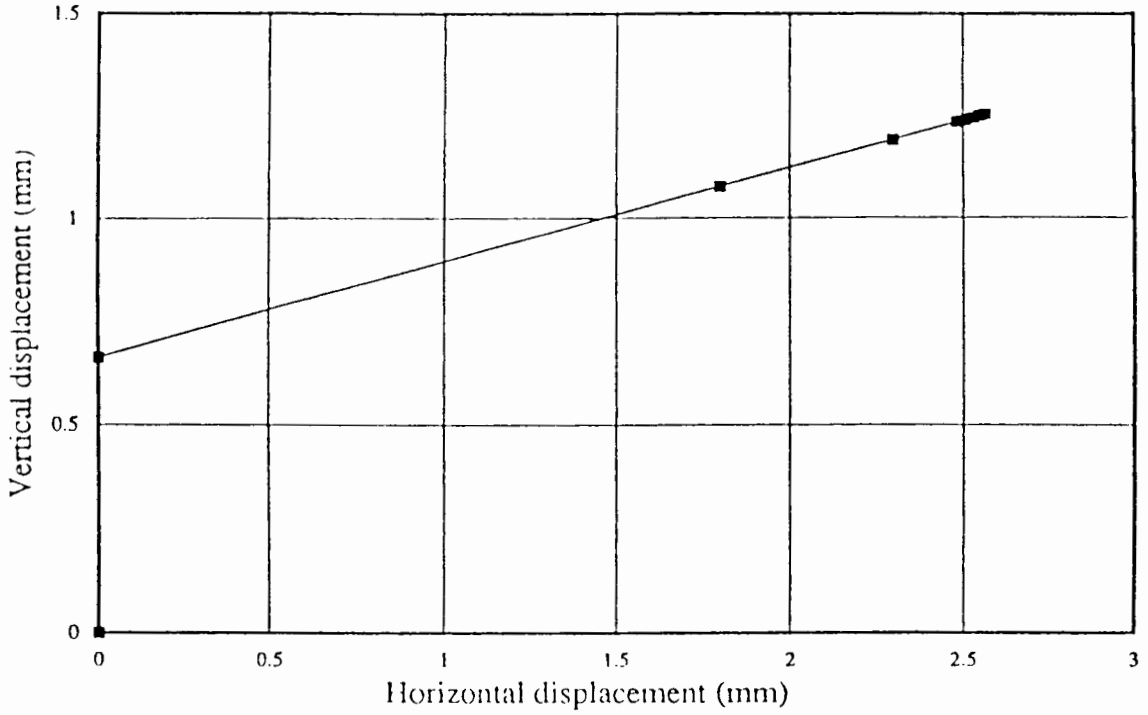

Figure 8.20: Vertical-horizontal displacement curve

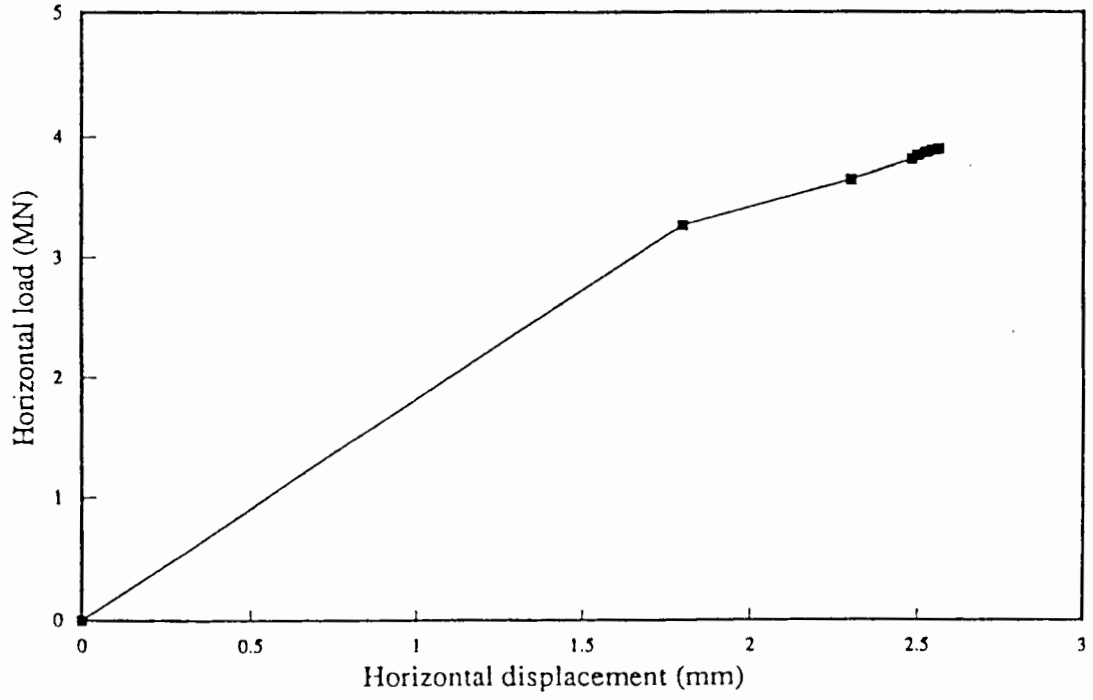

Figure 8.21: Horizontal load-horizontal displacement curve

we can see, the results match reasonably well, which confirms what the finite element analysis predicts: a vertical preload which is the precise ultimate bearing capacity of the

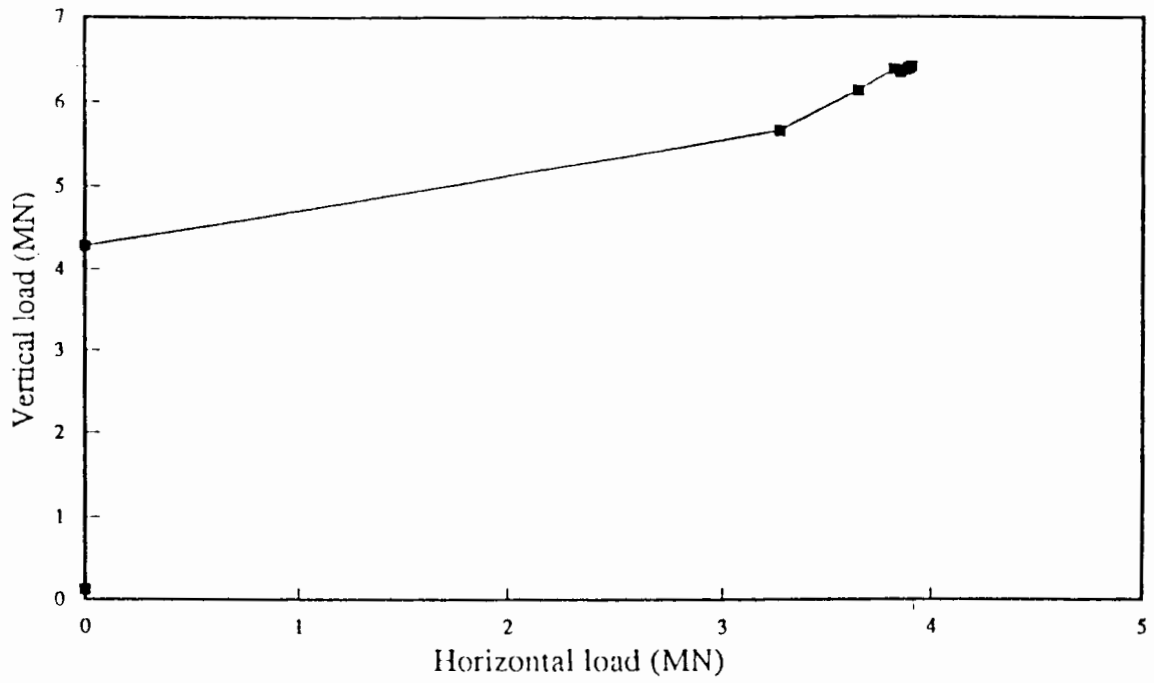

Figure 8.22: Vertical-horizontal load curve

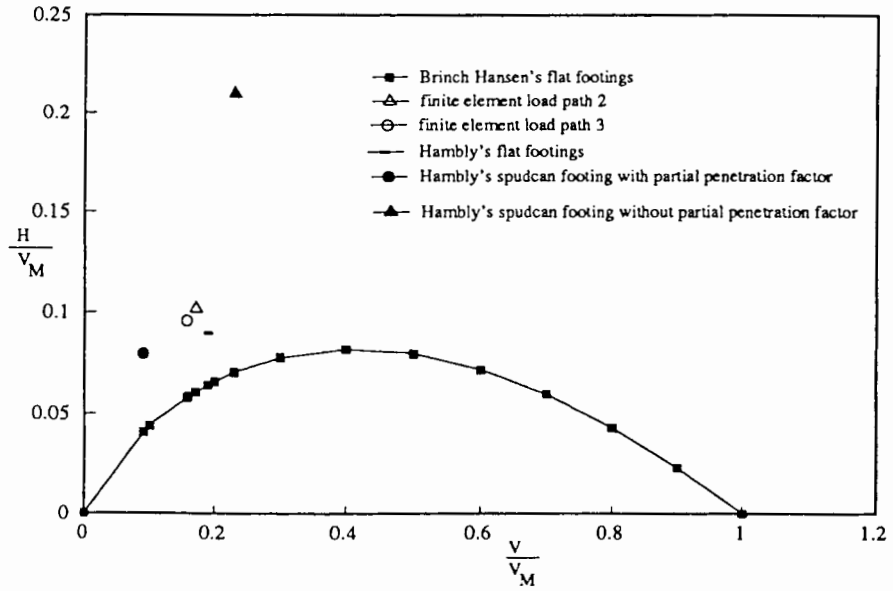

Figure 8.23: Horizontal-vertical load interaction curve

spudcan footing (i.e. equal to the bearing capacity of a flat footing of equivalent bearing area). The figure also shows that Hansen's solution gives conservative estimates of the bearing

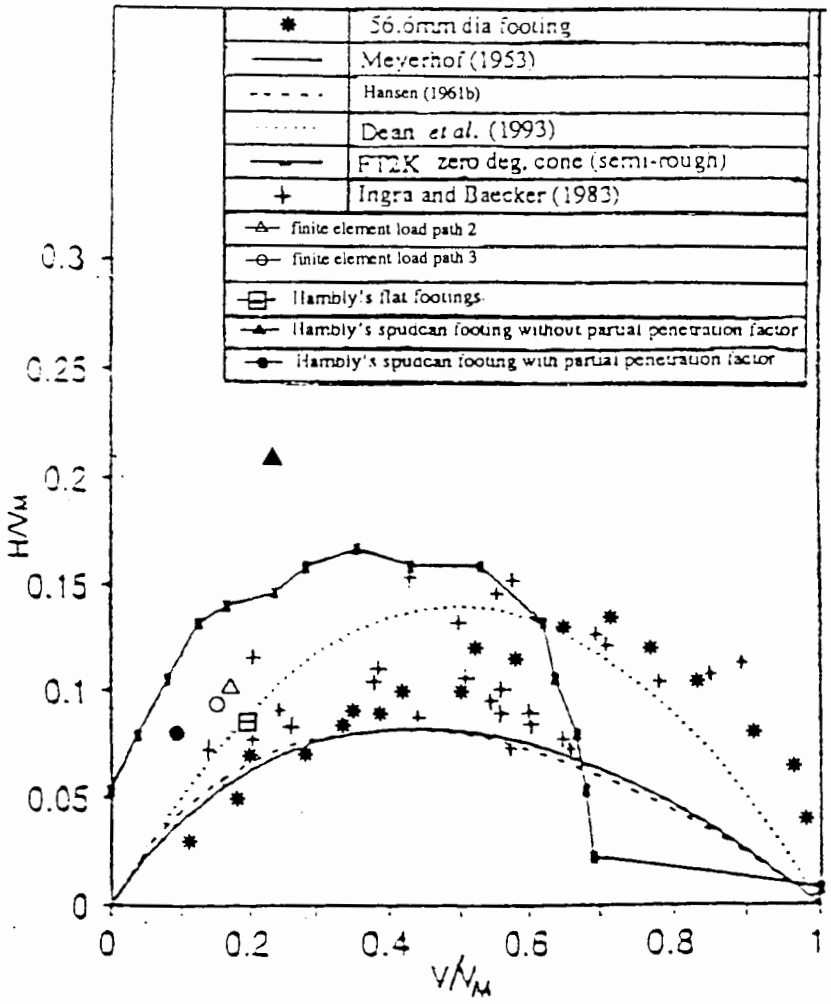

Figure 8.24: Interaction loci for surface footings (after Dean *et al.* (1993))

capacity of such offshore footings. The finite element analysis results do not match with Hambly's (1992) laboratory result for spudcan footing without a partial penetration factor. Both the current finite element and Hambly's (1992) laboratory results are replotted on another interaction diagram containing data from other sources (see Figure 8.24 which is actually the same Figure 8.13 with additional data points). It can be seen that Hambly's test result for a spudcan footing lies far away from the rest of the data points. This inconsistency is resolved by Hambly (1992) with the introduction of partial penetration factors. However,

the validity of these partial penetration factors need further experimental evidence.

8.8 Conclusions

The finite element method predicts a vertical preload force which is the ultimate bearing capacity of a spudcan footing and match with Hambly's (1992) laboratory result for model flat circular footing and the result for the spudcan footing, using a partial penetration factor of 2. (Although, further investigations to validate partial penetration factors suggested by Hambly'(1992), are proposed.)

The finite element results fits well within the centrifuge test data reported by Dean *et al.* (1993). However, Hansen's (1970) theory gives conservative estimates of the sliding/bearing resistance of a spudcan footing on sand.

CHAPTER 9

CONCLUSIONS

9.1 Concluding remarks

Most offshore oil extraction platforms are pile supported fixed structures. Groups of closely spaced piles around each of the four columns of the structure pin it to the sea-bed. Careful study of pile-soil-pile interactions in these pile groups is necessary in order to predict their behaviour under severe gravity and environmental (lateral) loads. The analysis of a pile foundation involves the solution of a three-dimensional problem in which two different materials act together to withstand the external applied loads. Each of these materials exhibits different stress-strain characteristics. It is difficult to put together an analysis procedure able to capture closely the combined behaviour of the two materials and so determine the true response of a pile foundation. Various idealisations and possible approximations need to be made in order to represent the material constitutive behaviour and the geometry of the problem. The methods that have been developed since around 1967 have different degrees of rigour depending upon the approximations involved in the analysis. In addition to these approximations, numerous other factors exist which can significantly affect the pile foundation response. These include: the sequence of loading, involving initial disturbance of the soil in close proximity to the pile due to installation, and subsequent re-consolidation of the soil in the intermediate time of recovery prior to actual loading; non-linearity and inhomogeneity of the soil; plastic deformations in the soil around the pile; relative slip between the pile and the soil at their interface under axial loading; tension and gap formation at the back of the pile

under lateral loading. The only sufficiently versatile analysis method, capable of considering all these factors satisfactorily, is the finite element method. Of course a full, three-dimensional finite element analysis requires a huge amount of computational effort; nevertheless, it is quite economical compared to full scale field experiments on pile groups. Given the present impracticability of either a full three-dimensional analysis or comprehensive field experiments, an alternative was presented in Chapter 6.

The objective of the thesis was to investigate a suitable method for the analysis and design of pile foundations. To this end the integral equation method/quasi boundary element method was formulated in order to compare its performance with the finite element method. Although, when considering elastic soil behaviour, it is clearly superior, in terms of computational effort required, over the finite element method, it does not give complete stress distribution inside the soil medium. If adapted to meet this demand, it starts to function in a way similar to the finite element method. It also becomes less efficient than the finite element method when a more refined (i.e. elasto-plastic) soil behaviour needs to be considered. It was not deemed worthwhile to try to develop the quasi boundary element method into a general two-dimensional boundary element method combined with elasto-plastic soil modelling - the finite element method was already available to do this. However, it was necessary to find a new, computationally efficient approach for performing the finite element calculations. The new approach, presented in Chapter 3, also models the rigid or infinite boundaries in the finite element mesh.

It was found, further, that a two-dimensional idealisation of single-piles and pile groups subject to lateral loading is quite successful in predicting their response, just as it is for the case of axial loading.

Three mains areas of single-pile and pile group behaviour were studied in this thesis. These are: axial load capacity and axial response of piles (9.2); interface analysis (9.3); and lateral

load capacity and response of single-piles and pile groups (9.4).

9.2 Axial load capacity and axial response of piles

Chapter 3 of this thesis demonstrated that, for the preliminary estimation of vertical settlement of piles, the analytical approach presented by Randolph and Wroth (1979) is very practicable and useful. The axial capacity cannot be predicted accurately unless the distribution of shear stress (skin friction) along the pile-soil interface is precisely known. Neither the subgrade reaction approach/load transfer method (t-z curve analysis), nor the elastic boundary element, can determine this with sufficient accuracy. Only the finite element method is competent to deal with the complex pile-soil interface behaviour and predict the axial load capacity with a high degree of accuracy. A new approach to deal with the size of the finite element mesh and the infinite boundaries was also presented in this chapter. With this new approach it is possible to study the behaviour of closely spaced pile groups in which, in reality, the pile-soil-pile interactions are non-linear.

9.3 Interface analysis

After highlighting the importance of pile-soil interface behaviour in Chapter 3, a cohesive interface element was developed in Chapter 4 to determine the stress distribution at the pile-soil interface. This element offers an easy way to vary the pile roughness. It models small relative pile-soil movement (slip), tension at the back of the pile when the pile is loaded laterally, and the formation of a gap once the limiting tension exceeds some prescribed value. The interface element was also quite successful in the stability analysis of surface footings. Surprisingly, and in contrast to some of the earlier work done in this area (reported in Chapter 4), no numerical instabilities were found. In addition to the interface analysis, three-dimensional finite element analysis was carried out to predict the ultimate bearing capacity

of a partially penetrated spudcan footing (Chapter 8). The analysis results help to explain the applicability of the existing bearing capacity theories to conical footings.

9.4 Lateral load carrying capacity and response of single piles and pile groups

In Chapters 5, 6 and 7, it was demonstrated that two-dimensional idealisation of a laterally loaded pile or a pile group was quite suitable for studying the lateral reaction mechanisms in both cohesive and frictional soils. The new material model introduced (in Chapter 7) to represent the constitutive behaviour of the frictional soils successfully models dilation and the post-peak behaviour of the soils. The simplification (two-dimensional idealisation) of the problem was adopted to study pile-soil-pile interactions in closely spaced offshore pile groups. It adds significantly to our understanding of the overlapping plastic zones within the group.

A method of pile group analysis was then suggested which combines plane strain finite element analysis for predicting the pile head response with a *p-y* curve approach for determining the bending moments and deflections along the piles. The *p-y* curves used are theoretical curves obtained by a single plane strain finite element analyses along the length of the piles.

9.5 Future research

The research work undertaken in this thesis is related to undrained loading of soils. As demonstrated and described in Chapter 5, a significant amount of saving in the design of pile foundations can be made if an effective stress design approach is followed. The consolidation analysis performed in Chapter 5, in which the increase in shear strength of the soil around the pile (taken from the logarithmic distribution of the shear strength after consolidation

obtained by Randolph *et al.* (1979)) was approximately incorporated in the finite element analysis based on the Cam-Clay model (Roscoe and Schofield (1963)), is not sufficiently refined. The deficiency could be made up by doing a two-dimensional large displacement coupled consolidation analysis using a sophisticated work hardening soil model (modified Cam-Clay model (Roscoe and Burland (1968)). This would be a significant leap forward towards the development of effective stress analysis and economical design of pile foundations.

Since, for the present, a complete three-dimensional analysis is prohibitively expensive, a new versatile analysis approach is suggested in Chapter 6. However, another approach for pile groups whose one dimension is significantly larger than the other, is to carry out a single two-dimensional finite element analysis by developing a two-dimensional beam element compatible with the soil element to represent the piles. The problem of rigid boundaries in the finite element mesh could be resolved by developing an infinite element. In this case we would have to compromise on the effect of the stiffness of the pile element and, instead, look for a balanced out pile-soil stiffness representing the whole group, as for example suggested by Stewart *et al.* (1993). Interface analysis could be helpful in determining active and passive soil pressures around the piles. Large displacement formulations could also be useful since, once a gap has opened up at the back of the pile, a small displacement is unlikely. Consolidation analysis could also be coupled together. This approach, too, we can see as an approximation of what is in reality a three-dimensional problem. It would not be possible to capture the true collapse mechanism in the soil using this approach, simply because of its inability to model overlapping plastic zones around individual piles in a group.

Another possibility would be to make use of the axial symmetry of the problem in the finite element analysis and apply the loading in terms of Fourier harmonics in order to study the lateral response of single piles and pile groups. This work too could be extended to coupled consolidation analysis, as mentioned earlier.

An immediate work, as proposed in Chapter 7 is to carry out work similar to the one described in Chapters 5 and 6, using the Matsuoka model (2) presented in Chapter 7.

BIBLIOGRAPHY

Aldridge, T.R. and Erbrich, C. (1990)
"*A new method for the prediction of lateral pile group behaviour - FUGROUP*",
Proc. 2nd European Conf. on Numerical Methods in Geotechnical Engineering, Santander: pp 349-353

Al Tabbaa, A. and Wood, D.M. (1989)
"*An experimentally based 'bubble' model for clay*",
Proc. 3rd Int. Symposium on Numerical Models in Geomechanics, Niagra, Canada: pp 91-99

Arnesen, K., Dahlberg, R., Helge, K. and Carlsen, C.A. (1988)
"*Soil-structure-interaction aspects for jackup platforms*",
BOSS, Trondheim

Atkinson, J.H. and Bransby, P.L. (1982)
"*The Mechanics of Soils*",
The McGraw-Hill Publishing Company Ltd., London, UK: pp 310-312

Atkinson, J.H. and Stallebrass, S.E. (1991)
"*A model for recent history and non-linearity in the stress-strain behaviour of overconsolidated soil*",
Proc. 7th Int. Conf. of the Int. Association for Computer Methods and Advances in Geomechanics, Cairns, Queensland, Australia: pp 555-560

Atkinson, J.H. (1993)
"*A note on modelling small strain stiffness in Cam Clay*",
Proc. Wroth Memorial Symposium, Oxford, UK: pp 628-643

Baguelin, F., Frank, R. and Said, Y.H. (1977)
"*Theoretical study of lateral reaction mechanism of piles*",
Geotechnique, Vol. 27, No. 3: pp 405-434

Baguelin, F. and Frank, R. (1980)
"*Theoretical studies of piles using the finite element method*",
Proc. Inst. Civ. Engrs. Conf. on Numerical Methods in Offshore Piling, London: Paper No. 11

Baligh, M.M. (1986)
"*Undrained deep penetration, I: shear stresses (and) II: pore pressures*",
Geotechnique, Vol. 36, No. 4: pp 471-502

Banerjee, P.K. and Driscoll, P.M. (1976)
"*Three dimensional analysis of raked pile groups*",
Proc. Inst. Civ. Engrs. Part 2, Vol. 61: pp 653-671

Banerjee, P.K. and Davies, T.G. (1978)
"*The behaviour of axially and laterally loaded single piles embedded in non-homogeneous soils*",
Geotechnique, Vol. 28, No. 3: pp 309-326

Banerjee, P.K. and Mustoe, G.G.W. (1978)
"*The boundary element method for two-dimensional problems of elasto-plasticity*",
Proc. Int. Conf. on Recent Advances in Boundary Element Method, Pentech Press London: pp 309-326

Banerjee, P.K. and Davies, T.G. (1980)
"*Analysis of some reported case histories of laterally loaded pile groups*",
Proc. Inst. Civ. Engrs. Conf. on Numerical Methods in Offshore Piling, London: pp 83-91

Banerjee, P.K. and Butterfield, R. (1980)
"*Boundary element methods in engineering science*",
McGraw-Hill, London, UK

Banerjee, P.K. and Dargush, G.F. (1988)
"*Progress in BEM applications in geomechanics via examples*",
Proc. Conf. on Numerical Methods in Geomechanics, Innsbruck: pp 13-22

Barden, L. Ismail, H. and Tong, P. (1969)
"*Plane strain deformation of granular material at low and high pressures*",
Geotechnique, Vol. 19, No. 4: pp 441-452

Barton, Y.O. (1982)
"*Laterally loaded model piles in sand: centrifuge tests and finite element analyses*",
Ph.D Thesis submitted to the Department of Engineering, University of Cambridge.

Bell, R.W. (1991)
"*The analysis of offshore foundations subjected to combined loading*",
M.Sc. Thesis, University of Oxford, UK

Bettes, P. (1977)
"*Infinite elements*",
Int. Journal for Numerical Methods in Engineering, Vol. 11: pp 53-64

Bogard, D. and Matlock, H. (1983)
"*Procedures for analysis of laterally loaded pile groups*",
Proc. Conf. on Geotechnical Practice in Offshore Engineering, Austin, Texas: pp 499-535

Bolton, M.D. (1979)
"*A guide to soil mechanics*",
The Macmillan Press Ltd., London, UK

Bolton, M.D. (1986)
"*The strength and dilatancy of sands*",
Geotechnique, Vol. 36, No. 1: pp 65-78

Bond, A.J. and Jardine, R.J. (1991)
"*Effects of installing displacement piles in a high OCR clay*",
Geotechnique, Vol. 41, No. 3: pp 341-363

Brocklehurst, C.J. (1993)
"*Finite element studies of reinforced and unreinforced two-layer soil systems*",
D.Phil. Thesis, University of Oxford, U.K.

Broms, B.B. (1964a)
"*Lateral resistance of piles in cohesive soils*",
Proc. ASCE, Journal of the Soil Mechanics and Foundation Engineering Division, 90 (SM3): pp 27-63

Broms, B.B. (1964b)
"*Lateral resistance of piles in cohesionless soils*",
Proc. ASCE, Journal of the Soil Mechanics and Foundation Engineering Division, 90 (SM3): pp 123-156

Brown, D.A. and Shie, C.-F. (1990a)
"*Numerical experiments into group effects on the response of piles to lateral loading*",
Computers and Geotechnics, Vol 10: pp 211-230

Brown, D.A. and Shie, C.-F. (1990b)
"*Three dimensional finite element model of laterally loaded piles*",
Computers and Geotechnics, Vol 10: pp 59-79

Burd, H.J. (1986)
"*A large displacement finite element analysis of a reinforced unpaved road*",
D.Phil. Thesis, University of Oxford, UK

Burd, H.J. and Houlsby, G.T. (1990)
"*Finite element analysis of two cylindrical expansion problems involving nearly incompressible material behaviour*",
Int. Journal for Numerical and Analytical Methods in Geomechanics, Vol. 14: pp 351-366

Burd, H.J. (1991)
"*Report submitted to Edmund Hambly Ltd*"

Burd, H.J. and Brocklehurst, C.J. (1991)
"*Parametric studies of a soil reinforcement problem using finite element analysis*",
Proc. 7th Int. Conf. of the Int. Association for Computer Methods and Advances in Geomechanics, Cairns, Queensland, Australia, Vol. 3: pp 1783-1788

Burd, H.J. and Houlsby, G.T. (1992)
"*Personal communication*"

Butterfield, R. and Banerjee, P.K. (1971)
"*The elastic analysis of compressible piles and pile groups*",
Geotechnique, Vol. 21, No. 3: pp 43-60

Burland, J.B. (1973)
"*Shaft friction of piles in clay - a simple fundamental approach*",
Ground Engineering, Vol. 6, No. 3: pp 30-34

Calladine, C.R. (1985)
"*Plasticity for Engineers*",
Ellis Horwood Ltd., Chichester, West Sussex, UK

Carter, J.P., Randolph, M.F. and Wroth, C.P. (1979)
"*Stress and pore pressure changes in clay during and after the expansion of a cylindrical cavity*",
Int. Journal for Numerical and Analytical Methods in Geomechanics, Vol. 3: pp 305-322

Chen and Poulos (1993)
"*Analysis of pile-soil interaction under lateral loading using infinite and finite elements*",
Computers and Geotechnics, Vol. 15: pp 189-220

Cheung, Y.K., Tham, L.G. and Guo, D.J. (1988)
"*Analysis of pile group by infinite layer method*",
Geotechnique, Vol. 38, No. 3: pp 415-431

Cheung, Y.K., Lee, P.K.K. and Zhao, W.B. (1991)
"*Elastoplastic analysis of soil-pile interaction*",
Computers and Geotechnics, Vol. 12: pp 115-132

Chow, Y.K. (1986)
"*Analysis of vertically loaded pile groups*",
Int. Journal for Numerical and Analytical Methods in Geomechanics, Vol. 10, No. 1: pp 59-72

Chow, Y.K. (1987)
"*Three dimensional analysis of pile groups*",
Proc. ASCE, Journal of the Geotechnical Engineering Division, 113 (GT6): pp 637-651

Chow, L. (1994)
"*The prediction of surface settlements due to tunnelling in soft ground*",
M.Sc. Thesis, University of Oxford, UK

Clausen, C.S.F., Aas, P.M. and Hasle, E. (1984)
"*SPLICE - a computer program for analysing structure/pile/soil interaction programs*",
Norwegian Geotechnical Institute Publication 152 Oslo

Coop, M.R. and Wroth, C.P. (1989)
"*Field studies of an instrumented model pile in clay*",
Geotechnique, Vol. 39, No. 4: pp 679-696

Coyle, H.M. and Reese, L.C. (1966)
"*Load transfer for axially loaded piles in clay*",
Proc. ASCE, Journal of the Soil Mechanics and Foundation Engineering Division, 92 (SM2): pp 1-26

Dean, E.T.R., James, R.G., Schofield, A.N., Tan, F.S.C. and Tsukamoto, Y. (1993)
"*The bearing capacity of conical footings on sand in relation to the behaviour of spudcan footings of jackups*",
Proc. Wroth Memorial Symposium, Oxford, UK: pp 140-150

De Borst, R. and Vermeer, P.A. (1984)
"*Possibilities and limitations of finite elements for limit analysis*",
Geotechnique, Vol. 34, No. 2: pp 199-210

De Josselin de Jong, G. (1971)
"*The double sliding free rotating model for granular assemblies*",
Geotechnique, Vol. 21: pp 155-163

De Josselin de Jong, G. (1988)
"*Elastic-plastic version of the double sliding model in undrained simple shear tests*",
Geotechnique, Vol. 38, No. 4: pp 533-555

Desai, C.S., Zaman, M.M., Lightner, J.G. and Siriwardane, H.J. (1984)
"*Thin-layer elements for interfaces and joints*",
Int. Journal for Numerical and Analytical Methods in Geomechanics, Vol. 8: pp 19-43

De Santa Maria, P.E.L. (1988)
"*Behaviour of footings for offshore structures under combined loads*",
D.Phil. Thesis, University of Oxford, UK

Drucker, D.C. and Prager, W. (1952)
"*Soil mechanics and plastic analysis or limit design*",
Quarterly Journal of Applied Mathematics, Vol. 10, No. 2: pp 157-165

Duncan, J.M. and Chang, C.Y. (1970)
"*Nonlinear analysis of stress and strain in soils*",
Proc. ASCE, Journal of the Soil Mechanics and Foundation Engineering Division, 96 (SM5): pp 1629-1653

Evangelista, A. and Viggiani, C. (1976)
"*Accuracy of numerical solutions for laterally loaded piles in elastic half space*",
Proc. 2nd Int. Conf. Numerical methods in Geomechanics, Blacksburg, Vol 3: pp 1367-1370

Fleming, W.G.K., Weltman, A.J., Randolph, M.F. and Elson, W.K. (1992)
"*Piling Engineering*",
Chapman and Hall, Glasgow, 2nd edition.

Frank, R., Guenot, A. and Humbert, P. (1982)
"*Numerical analysis of contacts in geomechanics*",
Proc. 4th Int. Conf. on Numerical Methods in Geomechanics, Edmonton, Canada, Vol. 1: pp 37-45

Gens, A., Carol, I. and Alonso, E.E. (1989)
"*An interface element formulation for the analysis of soil-reinforcement interaction*",
Computers and Geotechnics, Vol. 7, No 1-2: pp 133-151

Georgiadis, M. and Butterfield, R. (1982)
"*Laterally loaded pile behaviour*",
Proc. ASCE, Journal of the Geotechnical Engineering Division, 108 (GT1): pp 155-165

Ghaboussi, J., Wilson, E.L. and Isenberg, J. (1973)
"*Finite element for rock joints and interfaces*",
Proc. ASCE, Journal of the Soil Mechanics and Foundation Engineering Division, 99 (SM10): pp 833-848

Gibson, R.E. and Anderson, W.F. (1961)
"*In situ measurement of soil properties with the pressuremeter*",
Civil Engineering and Public Works Review, Vol. 56, No. 658: pp 615-618

Goodman, R.E., Taylor, R.L. and Brekke, T.L. (1968)
"*A model for the mechanics of jointed rock*",
Proc. ASCE, Journal of the Soil Mechanics and Foundation Engineering Division, 94 (SM3): pp 637-659

Griffiths, D.V. (1985)
"*Numerical modelling of interfaces using conventional finite elements*",
Proc. 5th Int. Conf. on Numerical methods in Geomechanics, Nagoya, Japan: pp 837-844

Guo, D.J., Tham, L.G. and Cheung, Y.K. (1987)
"*Infinite layer for the analysis of a single pile*",
Computers and Geotechnics, Vol. 3, No. 4: pp 229-249

Hambly, E.C. (1992)
"*Jackup spudcan sliding/bearing resistance on sand*",
BOSS, London

Handel, E., Schweiger, H.F. and Yeo, K.C. (1990)
"*A simple thin-layer element to model soil-geotextile interaction*",
Int. Conf. on Reinforced Soil, Strathclyde, UK: pp 10-12

Hansen, J.B. (1961a)
"*The ultimate resistance of rigid piles against transversal forces*",
Geoteknisk Institut. Bull. No. 12, Copenhagen.

Hansen, J.B. (1961b)
"*A general formula for bearing capacity*",
Danish Geotechnical Institute, Copenhagen, Bull. No. 11

Hansen, J.B. (1970)
"*A revised and extended formula for bearing capacity*",
Danish Geotechnical Institute, Copenhagen, Bull. No. 28: pp 38-46

Herrmann, L.R. (1965)
"*Elasticity equation for incompressible and nearly incompressible materials by a variational theorem*",
Journal of American Institute of Aeronautics and Astronautics, 3, 1896-1900

Herrmann, L.R. (1978)
"*Finite element analysis of contact problems*",
Proc. ASCE, Journal of the Engineering Mechanics Division, 104 (EM5): pp 1043-1057

Hetenyi, M. (1946)
"*Beams on elastic foundations*",
Univ. of Michigan Press, Michigan.

Heydinger, A.G. and O'Neil, M.W. (1986)
"*Analysis of axial pile-soil interaction in clay*",
Int. Journal for Numerical and Analytical Methods in Geomechanics, Vol. 11: pp 367-381

Hibbit, Karlsson and Sorensen (1989)
"*ABAQUS - Theory Manual, version 4.8*"

Hill, R. (1950)
"*The Mathematical Theory of Plasticity*",
Oxford University Press, London

Houlsby, G.T. (1982)
"*Theoretical analysis of the fall cone test*",
Geotechnique, Vol. 32, No. 2: pp 111-118

Houlsby, G.T. and Wroth, C.P. (1982)
"*Direct solution of plasticity problems in soils by the method of characteristics*",
Proc. 4th Int. Conf. on Numerical Methods in Geomechanics, Edmonton, Canada, Vol. 3: pp 1059-1071

Houlsby, G.T. and Wroth, C.P. (1983)
"*Calculations of stresses on shallow penetrometers and footings*",
Proc. Int. Union of Theoretical and Applied Mechanics/Int. Union of Geodesy and Geophysics Symposium on Seabed Mechanics, Newcastle upon Tyne, pp 107-112

Houlsby, G.T. (1992)
"*Personal communication*"

Houlsby, G.T. (1991)
"*How the dilatancy of soils affects their behaviour*",
Report No. OUEL 1888/91, Engineering Science Department, University of Oxford, UK

Houlsby, G.T. (1993)
"*Personal communication*"

Houlsby, G.T. and Martin, C.M. (1993)
"*Modelling of the behaviour of foundations of jackup units on clay*",
Proc. Wroth Memorial Symposium, Oxford, UK: pp 235-253

Houlsby, G.T. and Chow, L. (1994)
"*Modelling the variable stiffness of undrained clay using multiple yield surfaces*",
Report No. OUEL 2024/94, Engineering Science Department, University of Oxford, UK

Ingra, T.S. and Baecker, G.B. (1983)
"*Uncertainty in bearing capacity of sands*",
Proc. ASCE, Journal of the Geotechnical Engineering Division, 109 (GT7): pp 899-914

Jardine, R.J. and Potts, D.M. (1988)
"*Hutton tension leg platform foundations: prediction of driven pile behaviour*",
Geotechnique, Vol. 38, No. 2: pp 231-252

Jardine, R.J., Potts, D.M., St. John, H.D. and Hight, D.W. (1991)
"*Some applications of a non-linear ground model*",
Proc. 10th European Conf. on Soil Mechanics and Foundation Engineering, Florence, Vol. 1: pp 223-228

Katona, M.G. (1983)
"*A simple contact-friction interface element with applications to buried culverts*",
Int. Journal for Numerical and Analytical Methods in Geomechanics, Vol. 7, No. 3: pp 371-384

Kodikara, J.K. and Moore, I.D. (1991)
"*A versatile interaction analysis for nonlinear bodies*",
Proc. 7th Int. Conf. of the Int. Association for Computer Methods and Advances in Geomechanics, Cairns, Queensland, Australia, Vol 2: pp 1171-1176

Kraft, L.M., Jr., Ray, R.P. and Kagawa, T. (1981)
"*Theoretical t-z curves*",
Proc. ASCE, Journal of the Geotechnical Engineering Division, 197 (GT11): pp 1543-1561

Kooijman, A.P. and Vermeer, P.A. (1988)
"*Elasto-plastic analysis of laterally loaded piles*",
Proc. Conf. on Numerical Methods in Geomechanics, Innsbruck: pp 1033-1042

Kooijman, A.P. (1989)
"*Comparison of an elasto-plastic Quasi three dimensional model for laterally loaded piles with field tests*",
Proc. 3rd. Int. Symposium on Numerical Models in Geomechanics, Niagara, Canada: pp 675-682

Kuhlemeyer, R.L. (1979)
"*Static and dynamic laterally loaded floating piles*",
Proc. ASCE, Journal of the Geotechnical Engineering Division, 105 (GT2): pp 289-304

Lane, P.A. and Griffiths, D.V. (1988)
"*Computation of the ultimate pressure of a laterally loaded pile in frictional soil*",
Proc. Conf. on Numerical Methods in Geomechanics, Innsbruck: pp 1025-1031

Langen, H. and Vermeer, P.A. (1990)
"*Finite element analysis of a pile penetration problem in clay*",
Proc. 2nd European Conf. on Numerical Methods in Geotechnical Engineering, Santander: pp 18-20

Leung, C.F. and Chow, Y.K. (1987)
"*Response of pile groups subjected to lateral loads*",
Int. Journal for Numerical and Analytical Methods in Geomechanics, Vol. 11, No. 3: pp 307-314

Mandolini, A. and Viggiani, C. (1993)
"*Settlement predictions for piled foundations from loading tests on single piles*",
Proc. Wroth Memorial Symposium, Oxford, UK: pp 464-482

Matlock, H. and Reese, L.C. (1960)
"*Generalised solutions for laterally loaded piles*",
Proc. ASCE, Journal of the Soil Mechanics and Foundation Engineering Division, 86 (SM5): pp 63-91

Matlock, H. (1970)
"*Correlation for design of laterally loaded piles in soft clay*",
Proc. 2nd Offshore Technology Conf., Houston, Vol 1: pp 577-594

Matlock, H., Ingram, W.B., Kelly, A.E. and Bogard, D. (1980)
"*Field tests on the lateral behaviour of pile groups in soft clay*",
Proc. 12th Offshore Technology Conf., Houston, Vol 1: pp 163-174

Matsuoka, H. (1976)
"*On the significance of the spatial mobilised plane*",
Soils and Foundations, Vol. 16, No. 1: pp 91-100

Mattes, N.S. (1969)
"*The influence of radial displacement compatibility on pile settlements*",
Geotechnique, Vol. 19: pp 157-159

Mattes, N.S. and Poulos, H.G. (1969)
"*Settlement of single compressible pile*",
Proc. ASCE, Journal of the Soil Mechanics and Foundation Engineering Division, 95 (SM1): pp 189-207

Medina, F. (1981)
"*An axisymmetric infinite element*",
Int. Journal for Numerical Methods in Engineering, Vol. 17: pp 1177-1185

Meyerhof, G.G. (1953)
"*The bearing capacity of foundations under eccentric and inclined loads*",
Proc. 3rd Int. Conference on Soil Mechanics, Zurich, Vol 1: pp 440-445

Mindlin, R.D. (1936)
"*Force at a point in the interior of a semi-infinite solid*",
Physics, Vol 7: pp 195-202

Moore, I.D. and Booker, J.R. (1989)
"*Geometrically non-linear analysis of buried cylinders*",
Proc. 3rd Int. Symposium on Numerical Models in Geomechanics, Niagra, Canada: pp 716-723

Mroz, Z., Norris, V.A. and Zienkiewicz, O.C. (1979)
"*Application of an anisotropic hardening model in the analysis of elasto-plastic deformation of soils*",
Geotechnique, Vol. 29, No. 1: pp 1-34

Muqtadir, A. and Desai, C.S. (1986)
"*Three-dimensional analysis of pile group foundation*",
Int. Journal for Numerical and Analytical Methods in Geomechanics, Vol. 10: pp 41-58

Nagtegaal, J.C., Parks, D.M. and Rice, J.R. (1974)
"*On numerically accurate finite element solutions in the fully plastic range*",
Computer Methods in Applied Mechanics and Engineering, Vol. 4: pp 153-177

Naylor, D.J. (1974)
"*Stresses in nearly incompressible materials by finite elements with application to the calculation of excess pore pressures*",
Int. Journal for Numerical Methods in Engineering, Vol. 8: pp 443-460

Nutt, N.R.F. (1993)
"*Development of the cone pressuremeter*",
D.Phil. Thesis, University of Oxford, UK

O'Neill, M.W., Ghazzaly, O.I. and Ha, H.B. (1977)
"*Analysis of three dimensional pile groups with non-linear soil response and pile-soil-pile interaction*",
Proc. 9th Offshore Technology Conf, Houston, Texas, Vol 2: pp 245-256

Osborne, J.J., Trickey, J.C., Houlsby, G.T. and James, R.G. (1991)
"*Findings from a joint industry study on foundation fixity of jackup units*",
Offshore Technology Conf, Houston, Texas: paper OTC6615

Ottaviani, M. (1975)
"*Three dimensional finite element analysis of vertically loaded pile groups*",
Geotechnique, Vol. 25, No. 2: pp 159-174

Pasternak, P.L. (1954)
"*On a new method of analysis of an elastic foundation by means of two foundation constants*",
Moscow: Gos.Izd.Lit.Po Stroit-i-Arch (Russian).

Potts, D.M. and Martin, J.P. (1982)
"*The shaft resistance of axially loaded piles in clay*",
Geotechnique, Vol. 32, No. 4: pp 369-386

Poulos, H.G. and Davis, E.H. (1968)
"*The settlement behaviour of single axially loaded incompressible piles and piers*",
Geotechnique, Vol 18: pp 351-371

Poulos, H.G. (1971a)
"*Behaviour of laterally loaded piles: I-Single piles*",
Proc. ASCE, Journal of the Soil Mechanics and Foundation Engineering Division, 97 (SM5): pp 711-731

Poulos, H.G. (1971b)
"*Behaviour of laterally loaded piles: II-Pile Groups*",
Proc. ASCE, Journal of the Soil Mechanics and Foundation Engineering Division, 97 (SM5): pp 733-751

Poulos, H.G. and Davis, E.H. (1974)
"*Elastic Solutions for Soil and Rock Mechanics*",
Wiley: New York

Poulos, H.G. (1976)
"*Behaviour of laterally loaded piles near a cut or slope*",
Journal of Australian Geomechanics, Vol. G6, No. 1: pp 6-12

Poulos, H.G. (1980)
"*An approach for the analysis of Offshore pile groups*",
Proc. Inst. Civ. Engrs. Conf. on Numerical Methods in Offshore Piling, London: pp 119-126

Poulos, H.G. (1980)
"*User's guide to DEFPIG - deformation analysis of pile group*",
School of Civil Engineering, University of Sydney

Poulos, H.G. and Davis, E.H. (1980)
"*Pile foundation analysis and design*",
Wiley New York.

Poulos, H.G. (1988)
"*Marine Geotechnics*",
Unwin Hyman, London, UK

Poulos, H.G. (1989)
"*Pile behaviour - theory and application*",
Geotechnique, Vol. 39, No. 3: pp 365-415

Randolph, M.F. (1977)
"*A theoretical study of the performance of the piles*",
Ph.D Thesis submitted to the Department of Engineering, University of Cambridge.

Randolph, M.F. and Wroth, C.P. (1978)
"*Analysis of deformation of vertically loaded piles*",
Proc. ASCE, Journal of the Geotechnical Engineering Division, 104 (GT12): pp 1465-1488

Randolph, M.F. and Wroth, C.P. (1979a)
"*An analysis of the vertical deformation of pile groups*",
Geotechnique, Vol. 29, No. 4: pp 423-439

Randolph, M.F. and Wroth, C.P. (1979b)
"*An analytical solution for the consolidation around a driven pile*",
Int. Journal for Numerical and Analytical Methods in Geomechanics, Vol. 3, No. 3: pp 217-229

Randolph, M.F., Carter, J.P. and Wroth, C.P. (1979)
"*Driven piles in clay - The effects of installation and subsequent consolidation*",
Geotechnique, Vol. 29, No. 4: pp 361-393

Randolph, M.F. (1980)
"*PIGLET, a computer program for the analysis and design of piles under general loading conditions*",
Cambridge University Research Report, CUED/D-Soils TR91

Randolph, M.F. (1981)
"*The response of flexible piles to lateral loading*",
Geotechnique, Vol. 31, No. 2: pp 247-259

Randolph, M.F. and Houlsby, G.T. (1984)
"*The limiting pressure on circular pile loaded laterally on cohesive soil*",
Geotechnique, Vol. 34, No. 4: pp 613-623

Randolph, M.F. (1986)
"*RATZ - load transfer analysis of axially loaded piles*",
Rep. No. Geo 86033, Perth: Dept. Civil Engineering, University of Western Australia

Randolph, M.F. and Springman, S.M. (1991)
"*Analysis of pile response due to external loads and soil movement*",
Proc. 10th European Conf. on Soil Mechanics and Foundation Engineering, Florence.

Reese, L.C., Cox, W.R. and Koop, F.D. (1974)
"*Analysis of laterally loaded piles in sand*",
Proc. 6th Offshore Tech. Conf., Houston, Texas, paper OTC 2080: pp 473-483

Reese, L.C., Cox, W.R. and Koop, F.D. (1975)
"*Field testing and analysis of laterally loaded piles in stiff clay*",
Proc. 7th Offshore Tech. Conf., Houston, Texas, paper OTC 2312: pp 671-690

Reese, L.C. (1975)
"*Laterally loaded piles*",
Proc. ASCE, Geotech. Group and Continuing Education Committee, San Francisco section, Univ. of Calif., Berkeley

Reese, L.C. (1977)
"*Laterally loaded piles: Program Documentation*",
Proc. ASCE, Journal of the Geotechnical Engineering Division, 103 (GT4): pp 287-305

Roscoe, K.H. and Schofield, A.N. (1963)
"*Mechanical behaviour of an idealised 'wet clay'*",
Proc. 2nd European Conf. Soil Mechanics, Wiesbaden, Vol. 1: pp 47-54

Roscoe, K.H. and Burland, J.B. (1968)
"*On the generalised stress-strain behaviour of 'wet clay'*",
Engineering Plasticity, Cambridge University Press: pp 535-609

Rowe, P.W. (1962)
"*The stress-dilatancy relation for static equilibrium of an assembly of particles in contact*",
Proc. Roy. Soc., Series A, Vol. 269: pp 500-527

Sagaseta, C. (1984)
"*Quasi-static undrained expansion of a cylindrical cavity in clay in the presence of shaft friction and anisotropic initial stresses*",
Unpublished Research Report, Engineering Science Department, University of Oxford, UK

Schofield, A.N. and Wroth, C.P. (1968)
"*Critical State Soil Mechanics*",
The McGraw-Hill Publishing Company Ltd., London, UK: pp 32-37

Scott, R.F. (1981)
"*Foundation Analysis*",
Prentice-Hall, London, UK

Selnes, P.B. (1982)
"*Geotechnical problems in offshore earthquake engineering*",
Norwegian Geotechnical Institute Publication 140 Oslo

Simpson, B. (1993)
"*Development and application of a new soil model for prediction of soil movements*",
Proc. Wroth Memorial Symposium, Oxford, UK: pp 628-643

Sloan, S.W. (1981)
"*Numerical analysis of incompressible and plastic solids using finite elements*",
Ph.D. Thesis, University of Cambridge, UK

Sloan, S.W. and Randolph, M.F. (1982)
"*Numerical prediction of collapse loads using finite element methods*",
Int. Journal for Numerical and Analytical Methods in Geomechanics, Vol. 6: pp 47-76

Smith, I.M. and Griffiths, D.V. (1988)
"*Programming the Finite Element Method*",
John Wiley and Sons, Chichester, New York, 2nd edition.

Springman, S.M. (1984)
"*Lateral loading on piles due to embankment construction*",
M.Phil. Thesis, University of Cambridge, UK

Springman, S.M. (1989)
"*Lateral loading of piles due to simulated embankment construction*",
Ph.D. Thesis, University of Cambridge, UK

Stroud, M.A. (1971)
"*The behaviour of sand at low stress levels in the simple shear apparatus*",
Ph.D. Thesis, University of Cambridge, UK

Sullivan, W. R., Reese, L. C. and Fenske, C. W. (1980)
"*Unified method for analysis of laterally loaded piles in Clay*",
Proc. Inst. Civ. Engrs. Conf. on Numerical Methods in Offshore Piling, London: pp 135-146

Swedlow, J.L. and Cruse, T.A. (1971)
"*Formulation of Boundary Integral Equations for three-dimensional Elasto-plastic flow*",
Int. Journal for Solids and Structures, Vol. 7: pp 1673-1683

Tan, F.S.C. (1990)
"*Centrifuge and theoretical modelling of conical footings on sand*",
Ph.D. Thesis, University of Cambridge, UK

Taylor, D.W. (1948)
"*Fundamentals of Soil Mechanics*",
Wiley, New York

Telles, J.C.F. and Brebbia, C.A. (1981)
"*New Developments in Elasto-plastic Analysis*",
Proceedings of the Third International Seminar, Irvine, California: pp 350-370

Timoshenko, S.P. and Goodier, J.N. (1970)
"*Theory of Elasticity*",
The McGraw-Hill Book Company, Inc., New York

Verruijt, A. and Kooijman, A.P. (1989)
"*Laterally loaded piles in a layered elastic medium*",
Geotechnique, Vol. 39, No. 1: pp 39-46

Vesic, A.S. (1975)
"*Bearing capacity of shallow foundations*",
"Foundation Engineering Handbook", Ed. by H. F. Winterkorn and H. Y. Fang, Van Nostrand Reinhold, New York, USA: pp 121-147

Vlasov, V. Z., and Leontiev, N.N. (1966)
"*Beams, plates, shells on elastic foundations*",
translated from Russian by Israel Program for Scientific translations, NTIS No. N67-14238.

Wroth, C.P. and Bassett, R.H. (1965)
"*A stress-strain relationship for the shearing behaviour of sand*",
Geotechnique, Vol. 15, No. 1: pp 32-56

Wroth, C.P. and Houlsby, G.T. (1985)
"*Soil mechanics - property characterization and analysis procedures*",
Proc. 11th Int. Conf. on Soil Mechanics and Foundation Engineering, San Francisco, USA, Vol. 1: pp 1-57

Yan, L. and Byrne, P.M. (1992)
"*Lateral pile response to monotonic pile head loading*",
Canadian Geotechnical Journal, Vol. 29: pp 955-970

Yegian, M. and Wright, S.G. (1973)
"*Lateral soil resistance - displacement relationships for pile foundations in soft clays*",
Proc. 5th Annual Offshore Technology Conference, Paper OTC1893, Vol. 2: pp 663-676

Yu, H-S. (1990)
"*Cavity expansion theory and its application to the analysis of pressuremeters*",
D.Phil. Thesis, University of Oxford, UK

Zaman, M.M. (1985)
"*Evaluation of 'thin layer element' and modelling of interface behaviour in soil-structure interaction*",
Proc. 5th Int. Conf. on Numerical methods in Geomechanics, Nagoya, Japan: pp 1797-1803

Zienkiewicz, O.C., Best, B., Dullage, C. and Stagg, K.G. (1970)
"*Analysis of non-linear problems in rock mechanics with particular reference to jointed rock systems*",
Proc. 2nd Int. Cong. on Rock Mechanics, Belgrade, Vol. 2: pp 501-509

Zienkiewicz, O.C. (1977)
"*The finite element method*",
Third edition, McGraw-Hill, London, UK